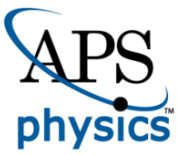

Nonequilibrium physics in biology

Xiaona Fang, Karsten Kruse, Ting Lu, and Jin Wang

Rev. Mod. Phys. **91**, 045004 — Published 20 December 2019

DOI: 10.1103/RevModPhys.91.045004

Nonequilibrium Physics in Biology

Xiaona Fang

State Key Laboratory of Electroanalytical Chemistry,
Changchun Institute of Applied Chemistry,
Changchun, Jilin 130022,
China

Karsten Kruse

NCCR Chemical Biology,
Department of Biochemistry and Department of Theoretical Physics,
University of Geneva,
30 quai Ernest-Ansermet, 1211 Geneva 4,
Switzerland

Ting Lu

Department of Bioengineering,
University of Illinois at Urbana-Champaign,
Urbana, IL 61801,
USA

Jin Wang

Department of Chemistry and Physics,
State University of New York, Stony Brook,
NY 11794 USA.[*]

(Dated: August 23, 2019)

Life is characterized by a myriad of complex dynamic processes allowing organisms to grow, reproduce, and evolve. Physical approaches for describing systems out of thermodynamic equilibrium have been increasingly applied to living systems, which often exhibit phenomena not found in those traditionally studied in physics. Spectacular advances in experimentation during the last decade or two, for example, in microscopy, single cell dynamics, in the reconstruction of sub- and multicellular systems outside of living organisms, and in high throughput data acquisition have yielded an unprecedented wealth of data on cell dynamics, genetic regulation, and organismal development. These data have motivated the development and refinement of concepts and tools to dissect the physical mechanisms underlying biological processes. Notably, landscape and flux theory as well as active hydrodynamic gel theory have proven very useful in this endeavour. Together with concepts and tools developed in other areas of nonequilibrium physics, significant progress has been made in unraveling the principles underlying efficient energy transport in photosynthesis, cellular regulatory networks, cellular movements and organization, embryonic development and cancer, neural network dynamics, population dynamics and ecology, as well as ageing, immune responses and evolution. Here, we review recent advances in nonequilibrium physics and survey their application to biological systems. We expect many of these results to be important cornerstones as the field continues to build our understanding of life.

CONTENTS

[*] To whom correspondence should be addressed. E-mail: jin.wang.1@stonybrook.edu

I. INTRODUCTION

Life is never at equilibrium. The principle of detailed balance defines an equilibrium system as one in which transitions between two states occur on average at equal rates in either direction. Typically, the dynamics of living systems cannot be described in these terms because they continuously exchange matter and energy with their environment in a non-reversible fashion. Living systems take up food that provides the building blocks necessary for growth and proliferation. Food can supply the organism with energy; living systems may also absorb energy from the environment in the form of light or heat. Because living systems continuously exchange matter and energy with their environment, they cannot be described as physical systems relaxing to equilibrium.

On subcellular scales, life seems to be governed exclusively by physical laws (Schrodinger, 1944); explicitly, no natural law unique to biology has been identified as being necessary to explain the dynamics of biomolecules. Energy acquired from the environment drives enzymatic reactions which favor specific molecular changes over others. However, it is currently unclear how this specificity is achieved. Furthermore, large-scale features of living systems such as cell migration and division, consciousness, population organization, or evolution are poorly understood in terms of the molecular components that make up these systems. This stands in stark contrast to the behavior of equilibrium statistical systems, which can be understood in terms of their microscopic components. In this review, we aim to present recent developments in the field of nonequilibrium dynamics and thermodynamics that provide routes toward answering these fundamental questions about living systems. Eventually, they will prove instrumental for identifying features common to a large variety of biological systems and elucidate how mechanics and chemistry act in concert to shape life.

Because living systems regularly showcase phenomena that defy purely molecular explanations, physical analy-

sis is required. Simultaneously, living systems provide a frontier of physical research that is as rewarding as the study of the very small or the very large, with philosophical implications of similar depth. Even if topics such as consciousness are not discussed, living systems provide a plethora of phenomena that are alien to systems of inanimate matter such as spontaneous oscillations or flows. Beyond the detailed description of isolated phenomena, the physics of active matter (Marchetti et al., 2013a; Wang, 2015) aims to develop a framework of concepts and tools that is universally applicable to active, intrinsically nonequilibrium systems and nonliving, equilibrium systems. In this context, matter is referred to as active because it is intrinsically nonequilibrium. That is, instead of being driven by an external field or gradient, the constituents of active matter themselves are driven out of equilibrium. For example, a molecule might undergo conformational changes as a bound molecule of adenosine triphosphate (ATP) loses a phosphate group through hydrolysis and the replacement of adenosine diphosphate (ADP) by ATP restores the original conformation. In presence of an excess of ATP, this will lead to a cycling of the molecule between the two conformations.

To reach the aim of a universal framework, results from various disciplines are exploited, notably nonlinear dynamics, nonequilibrium thermodynamics, and nonequilibrium kinetics (Ao, 2008; Gardiner, 1983; Graham, 1989; Haken, 1987; Hu, 1995; Jackson, 1989; Jiang, 2003; Marchetti et al., 2013a; Nicolis and Prigogine, 1977; Qian, 2009; Sasai and Wolynes, 2003; Schnakenberg, 1976; Van Kampen, 2007; Wang, 2015; Wang et al., 2008), as well as nonequilibrium thermodynamics (Ao, 2008; Assaf et al., 2011; Aurell and Sneppen, 2002; Feng et al., 2010; Feng and Wang, 2011; Feng et al., 2014; Freidlin and Wentzell, 1984; Gardiner, 1983; Gaspard, 1998; Ge and Qian, 2010; Haken, 1987; Hatano and Sasa, 2001; Jiang, 2003; Lv et al., 2014; Maier and Stein, 1997; Nicolas and Prigogine, 1989; Nicolis and Prigogine, 1977; Qian, 2009; Roma et al., 2005; Schnakenberg, 1976; Schuss, 2010; Seifert, 2008; Van and Esposito, 2010; Van Kampen, 2007; Walczak et al., 2005; Wang, 2015; Wang et al., 2006a, 2010c; Zhang et al., 2012; Zhang and Wang, 2014). In this endeavour it has proven particularly useful to start with concepts from equilibrium physics. A central concept is that of a potential or free energy landscape that describes the evolution of a physical system towards equilibrium in terms of gradient descent towards the landscape's minima. This powerful picture has found its way into many other disciplines, notably, into biology (Fisher, 1930; Frauenfelder and Wolynes, 1994; Waddington, 1957; Wright, 1941) via "Waddington's landscape." This landscape is used to illustrate the process of cell differentiation, when a stem cell specializes to become a liver cell, a brain cell, or some other kind of cell with a specific function (Waddington, 1957). Similarly, "fitness landscapes" are used to picture the course of evolution towards more adapted species in response to some environmental constraints(Fisher, 1930; Wright, 1941).

However, the concept of energy landscapes needs to be generalized for nonequilibrium systems to explain the phenomena such as limit cycles. One way to generalize the energy landscape of a system is to first consider its stochastic form. Under very general conditions, the probability distribution asymptotically reaches a steady state even for systems out of equilibrium. Gradients in the steady-state probability landscape drive the deterministic "mean field" dynamics onto one of the possible attractors, for example, a limit-cycle orbit. Typically, a second driving force results from a rotational flux that arises from energy or material input into the system (Xu et al., 2012). This flux drives dynamics such as limit-cycle orbits within an attractor (Wang et al., 2008). Because these rotational fluxes arise from energy or material being pumped into the system, behaviors such as limit-cycle orbits are absent from equilibrium systems. Rotational fluxes driven from sources external to the system are thus tightly linked to entropy production and time-reversal symmetry breaking.

A different generalization of energy landscapes arises in the context of nonequilibrium thermodynamics that is based on the rate of energy dissipation (de Groot and Mazur, 1985). In this framework, one assumes spatially-extended systems are locally at thermodynamic equilibrium, but that these equilibria may differ at different locations. In this way, a "free energy landscape" of "spatially heterogeneous equilibria" can be defined. Together with conservation laws and broken continuous symmetries, this assumption allows for a systematic framework to analyze deviations from thermodynamic equilibrium. For example, this approach yields the Navier-Stokes equation for an isotropic system of a single, conserved molecular species. Generalized hydrodynamics have notably been developed for active matter and applied to various biological systems (Marchetti et al., 2013a). Both the stochastic system and the energy dissipation approaches allow for the distinction between driving forces resulting from thermodynamic equilibrium relaxation and from environmental coupling (Marchetti et al., 2013a; Wang, 2015).

In addition to their applications to biological systems, these approaches are noteworthy because they raise immediate physics questions. How do other equilibrium concepts such as thermodynamic fluctuations, optimal paths, kinetic rates, and the fluctuation-dissipation theorem generalize (Feng and Wang, 2011; Feng et al., 2014; Wang et al., 2010c; Zhang et al., 2012)? The work of Shannon (Sloane and Wyner, 1993) reveals a deep formal connection between concepts from equilibrium physics and information theory, though it is currently still not very clear how this connection extends to nonequilibrium systems. Furthermore, biological systems are often characterized by their function, for example their ability to

"make decisions" in response to stimuli. Can specific phenomena and function be conceptualized and physically quantified, particularly towards understanding population dynamics?

Although physics has been applied to study biological processes for a long time, its popularity for this application is currently surging.Thanks to the sequencing of the genomes of numerous model organisms, the molecular inventory of many biological organisms of interest are now well-known. Many proteins can be isolated and studied in reconstituted systems outside a cell, which allows tests of physical hypotheses in controlled environments. At the same time, proteins can be modified in a variety of ways in living cells to tune biological processes. The addition of fluorescent protein tags to functional proteins allows for researchers to probe their in-vivo behavior. Continuously-advancing fluorescence imaging and electron microscope technology allows for the observation of cellular activities in unprecedented detail. These developments together have led to enormous amounts of data that wait to be analyzed, and new data are continuously added. These experimental advances have a profound impact on expanding the concepts and tools used for describing active matter.

In this review, we describe recent progress in the development of concepts in nonequilibrium physics and their application to biological systems. Since the topic is too vast to be covered fully in the present text, we selected topics that are the focus of current research and have proven to be relevant for understanding vital processes and are the ones these authors are familiar with. We present a brief overview of the current status of concepts from nonequilibrium physics, in which we highlight the nonequilibrium potential and flux approach for dynamics/thermodynamics and the hydrodynamics approach for active matter. We then show how these concepts have been applied to a broad range of biological systems. Then, starting from molecular processes such as enzyme reactions and energy transport, we cover cellular processes. We move up in spatial scales from single-cell processes to multi-cell ensemble behaviors, and then finally to the species and ecological level. Single-cell behaviors we cover are cell fate decision making, cell cycle, differentiation and ageing. Cell ensembles behavior is explored via neural networks, tumors and immunity. Finally, the species and population levels are discussed in terms of ecology, game theory and economy, and evolution. We close with a brief summary and outlook of some current and future directions of the nonequilibrium physics in biology.

II. PHYSICAL CONCEPTS FOR DESCRIBING NONEQUILIBRIUM SYSTEMS

In this section, we review some recently developed physical concepts for describing nonequilibrium dynamics. Special attention is being paid to the landscape and flux theory, which generalizes the notion of potentials to systems out of equilibrium. A more detailed review can be found in (Wang, 2015).

A. Landscape and flux theory for nonequilibrium dynamics

1. Dynamical systems

Consider a dynamical system where a vector $\mathbf{C}$ denotes its variables such as concentrations, momentum, or polar order.When the trajectory of $\mathbf{C}$ evolves deterministically and depends only on its current state, the dynamical equation reads

$$\dot{\mathbf{C}} = \mathbf{F}(\mathbf{C}), \tag{1}$$

where $\mathbf{F}(\mathbf{C})$ is a generalized driving force (Jackson, 1989). This equation describes the evolution of a wide class of systems, for example a series of damped Newtonian oscillators.

Exploration of these equations generally begins by identifying the existence and local stability of fixed points(Jackson, 1989). Global stability needs to be addressed separately, since connections among the steady states are not always known from local analyses; see Sect. II.A.4. For potential systems, the driving force can be expressed as the gradient of a potential (or energy) U, $\mathbf{F} = -\nabla U$, so their dynamic behaviors can be deduced directly from the potential.

2. Nonequilibrium potentials and rotational curl fluxes as the driving forces for dynamics

In general, the driving force cannot be expressed as the gradient of a potential. In this case, it is helpful to explore a stochastic version of the deterministic equation given in (1). The noise term can account for all factors not explicitly described by $\mathbf{F}$ and, if desired, one can eventually take the zero-noise limit (Swain et al., 2002). Stochastic trajectories are determined by the Langevin equation

$$\dot{\mathbf{C}} = \mathbf{F}(\mathbf{C}) + \eta(\mathbf{C}, t). \tag{2}$$

where $\eta(\mathbf{C}, t)$ represents a time-dependent stochastic force. The fluctuation magnitude is measured by the auto-correlation function, $\langle \eta(\mathbf{C}, t) \cdot \eta(\mathbf{C}, t') \rangle = 2D\mathsf{D}\delta(t - t')$, where D represents the fluctuation magnitude and D is the diffusion matrix that describes fluctuation

anisotropies (Van Kampen, 2007). Rather than being described by individual trajectories which are now stochastic and unpredictable, the system evolution is described by a probability distribution P that evolves according to a linear deterministic equation, the Fokker-Planck equation (Van Kampen, 2007)

$$\partial_t P(\mathbf{C},t) + \nabla \cdot \mathbf{J}(\mathbf{C},t) = 0 \tag{3}$$

where $\nabla\cdot$ denotes the divergence in state space and probability conservation is guaranteed. The change of local probability is from the net input. The probability flux $\mathbf{J}$ is given by

$$\mathbf{J}(\mathbf{C},t) = \mathbf{F}(\mathbf{C})P(\mathbf{C},t) - \nabla\cdot[D\mathsf{D}P(\mathbf{C},t)]. \tag{4}$$

where the first term describes an advective flux from the driving force and the next term captures the effects of fluctuations.

Eventually, most systems reach a steady state P^{ss} where $\partial_t P^{ss} = 0$. Consequently, the divergence of the steady state flux vanishes. Potential systems at steady state are in thermodynamic equilibrium; that is, the probability flux vanishes such that detailed balance is obeyed and the probability is given by the Boltzmann distribution. However, the steady state flux generally does not vanish, though it must be purely rotational. The existence of a non-vanishing probability flux at steady state indicates that detailed balance is broken and its magnitude can be used to measure the system's distance from thermodynamic equilibrium.

The driving force can be decomposed into a part that is the negative gradient of a nonequilibrium potential U (or landscape) and a part involving a rotational curl flux (Wang et al., 2008). Explicitly,

$$\mathbf{F} = -D\mathsf{D}\cdot\nabla U + \nabla D\mathsf{D} + \mathbf{J}^{ss}/P^{ss} \tag{5}$$

Here, U is the negative logarithm of the steady state probability, $U = -\ln P^{ss}$. Like its equilibrium analog, the nonequilibrium potential landscape is linked to steady state probability and provides a global quantification of system behavior[1]. However, the nonequilibrium dynamics on the landscape also depends on the rotational curl flux. If one visualizes equilibrium dynamics as charged particles moving in an electric field, nonequilibrium dynamics correspond to charged particles moving in an electric and magnetic field. Note that in contrast to the equilibrium landscape which is given *a priori*, the nonequilibrium potential landscape is associated with the steady state probability that emerges from stochastic dynamics. In turn, the rotational curl flux $\mathbf{J}^{ss}$ is associated with the steady state probability flux from environmental coupling that allows for an exchange of matter, energy, or information (Xu et al., 2012; Zeng and Wang, 2017; Zhang and Wang, 2014). As it does not vanish, it breaks time reversal symmetry and thus creates a time arrow (Feng and Wang, 2011; Li et al., 2011a; Wang et al., 2010c). Furthermore, the rotational curl flux current extends through state space. Hence, unlike in equilibrium systems, the steady state can typically not be described fully by local properties.

There is some freedom in decomposing the driving force into a potential gradient and a rotational curl flux, as one can always add the curl of a vector field to the nonequilibrium potential U. The choice made above is somewhat natural as it leads to the equilibrium case when the flux is zero, and is the closest analog when one wants to describe the relaxation into steady state. It also allows for a generalization of thermodynamics (Feng and Wang, 2011; Ge and Qian, 2010; Seifert, 2005; Van and Esposito, 2010) and of the fluctuation-dissipation relation (Feng and Wang, 2011; Hatano and Sasa, 2001; Seifert, 2008).

There are several other ways of decomposing stochastic dynamics.Some studies focus on finding nonequilibrium potentials (Ao, 2004; Freidlin and Wentzell, 1984; Graham, 1989; Xing, 2010; Zhou et al., 2012) and their associated analytical properties. Others emphasize the role of nonequilibrium curl flux and the nonequilibrium landscape in determining system dynamics (Feng and Wang, 2011; Wang et al., 2008, 2010c; Zhang and Wang, 2014). One approach aimed to find a new type of stochastic dynamics (Ao, 2004), although it may be challenging to obtain numerical solutions. Furthermore, the generality and uniqueness of this approach are still under discussion (Qian, 2014; Zhou and Li, 2016). Another approach, suggested in (Xing, 2010), uses a projection operator to decompose the driving force. A recently-proposed decomposition approach assumed orthogonality between the driving forces, which only works in the deterministic limit (Zhou et al., 2012), reading similar conclusions to those discussed earlier (Feng and Wang, 2011; Wang et al., 2008, 2010c) in the zero fluctuation limit. The force decomposition has been generalized from overdamped to underdamped dynamics (Ge, 2014; Qian, 2014; Risken, 1989; Wu et al., 2018). Another method decomposed discrete Markov chains into two parts: one that preserved and another that broke detailed balance(Luo et al., 2017; Qian and Hou, 1979; Schnakenberg, 1976; Zhang and Wang, 2014; Zia and Schmittmann, 2007).

3. Thermodynamic origin of the rotational flux

The landscape and flux can be obtained as mentioned above once specific dynamics are given, though this statement is rather formal. To gain physical intuition, one can search for the origin of rotational curl flux. For an

[1] Typically, the diffusion coefficient tensor $D\mathsf{D}$ is constant and does not contribute to the driving force, though in general it contributes to the potential landscape.

open system, the flux originates from environmental energy input, which breaks detailed balance. In biology, the energy that drives the system away from equilibrium can be obtained from ATP hydrolysis. For example, the phosphorylation and de-phosphorylation of ATP can provide an energy source for cellular functions, such as cell growth and division. One can couple ATP hydrolysis to specific protein reactions in molecular networks and other cell systems to explicitly quantify the energy input by the chemical potential (voltage) from the ATP/ADP concentration ratio for driving the associated nonequilibrium dynamics (Qian, 2007; Xu et al., 2012). This voltage gives rise to the rotational curl flux. Alternatively, one can phenomenologically couple ATP chemical potential to thermodynamic forces as in the theory of active matter (Kruse et al., 2004; Marchetti et al., 2013a). The quantitative connections from ATP that pump voltage to the flux driving nonequilibrium dynamics and entropy production/free energy cost have been studied in a few examples (Xu et al., 2012).

4. Global stability and Lyapunov function for nonequilibrium systems

The asymptotic dynamics and global stability of a system can be quantified if it admits a Lyapunov function, ϕ, that is monotonically decreasing along the trajectories except in steady state (Jackson, 1989). For a deterministic system, a candidate Lyapunov function can be obtained by calculating the nonequilibrium potential and then taking the zero-noise limit. To see this, consider the WKB ansatz up to leading order in D which solves the Fokker-Planck equation (3), that is, $P \sim \exp[-\phi_0/D]$, where ϕ_0 is the leading-order term of the nonequilibrium potential. We thus arrive at the Hamilton-Jacobian equation (Hu, 1995; Xu et al., 2013, 2014a; Zhang et al., 2012)

$$\mathbf{F} \cdot \nabla\phi_0 + \nabla\phi_0 \cdot \mathsf{D} \cdot \nabla\phi_0 = 0. \tag{6}$$

This equation implies

$$\frac{d\phi_0}{dt} = \mathbf{F} \cdot \nabla\phi_0 = -\nabla\phi_0 \cdot \mathsf{D} \cdot \nabla\phi_0 \leq 0 \tag{7}$$

showing that the nonequilibrium potential is a candidate Lyapunov function.

B. Discrete nonequilibrium dynamics

In a biological context, many systems are characterized by discrete rather than continuous states. For example, gene promoter sites are either occupied or not by transcription factors, molecular motors have discrete binding sites on a cytoskeletal filament, and populations comprise a discrete number of individuals. We will now describe how the approaches described above for continuous systems can be adapted to the discrete case.

1. The Master equation

For a Markovian process in discrete state space, the analog of the Fokker-Planck equation determining the dynamics of the probability distribution P is the Master equation (Gardiner, 1983; Van Kampen, 2007):

$$\frac{dP_i}{dt} = -\sum_j T_{ij}P_i + \sum_j T_{ji}P_j. \tag{8}$$

where P_i is the probability of being in state i and T_{ij} is the transition rate from state i to state j. The master equation reflects that the probability of being in state i decreases through transitions from state i into any other state j and increases through transitions from the other states j into state i. Because a transition to state j from state i is always balanced by a reduction in state i probability, the Master equation implies conservation of probability, $d\sum_i P_i/dt = 0$. Alternatively, we can write Eq. (8) as

$$d\mathbf{P}/dt = \mathsf{M}^T\mathbf{P} \tag{9}$$

with the transition rate matrix M given by $M_{ij} = T_{ij}$ for $i \neq j$ and $M_{ii} = (-1)\sum_j T_{ij}$. One can solve the master equation either directly or by simulating the stochastic evolution of the system dynamics at long times to gain information about steady-state probability P_i^{ss} (Cao et al., 2010; Gillespie, 1976; Krauth, 2006).

In steady state, the flux between two states i and j is $F_{ij}^{ss} = T_{ji}P_j^{(ss)} - T_{ij}P_i^{(ss)}$. Detailed balance is satisfied if $F_{ij}^{ss} = 0$. In that case, the system is in equilibrium and there is a potential V_i such that $P_i^{ss} \propto \exp\{-V_i\}$ (Qian and Hou, 1979; Schnakenberg, 1976; Zia and Schmittmann, 2007). However, $\frac{dP_i}{dt} = 0$ only states that the sum of all fluxes into and out of state i is zero; that is, $\sum_j F_{ij}^{ss} = 0$, but F_{ij}^{ss} is not necessarily zero.

2. Decomposition of the transition matrix

Similar to the flux component in continuous systems, the transition rate matrix can be separated into one part that preserves detailed-balance, D, and one that does not, C. The part that preserves detailed balance is defined by $D_{ij} = \min\{T_{ij}P_i^{ss}, T_{ji}P_j^{ss}\}/P_i^{ss}$, for $i \neq j$ and $D_{ii} = (-1)\sum_j D_{ij}$ (Qian and Hou, 1979; Schnakenberg, 1976). The part that breaks detailed balance is defined by $C_{ij} = \max\{T_{ij}P_i^{ss} - T_{ji}P_j^{ss}, 0\}/P_i^{ss}$ for $i \neq j$ and $C_{ii} = (-1)\sum_j C_{ij}$, and $D_{ij} = \min\{T_{ij}P_i^{ss}, T_{ji}P_j^{ss}\}/P_i^{ss}$, for $i \neq j$ (Qian and Hou, 1979; Schnakenberg, 1976). One can see that $\mathsf{M} = \mathsf{C} + \mathsf{D}$ and $\mathsf{D}^T\mathbf{P}^{ss} = 0$. Because $\mathsf{M}^T\mathbf{P} = (\mathsf{C} + \mathsf{D})^T\mathbf{P}^{ss} = 0$, it follows that $\mathsf{C}^T\mathbf{P}^{ss} = 0$ as well. Whereas D preserves detailed balance, $D_{ij}{P_i}^{ss} = D_{ji}{P_j}^{ss}$, C captures the flux breaking detailed balance and describes irreversible transitions, because $C_{ij}{P_i}^{ss} > 0$ implies $C_{ji}{P_j}^{ss} = 0$ and vice versa.

The steady state fluxes F_{ij}^{ss} resulting from the detailed-balance breaking part of the driving force C can be expressed in terms of fluxes along loops that connect a state with itself, $i \to j \to k \cdots \to n \to i$ (Luo et al., 2017; Qian and Hou, 1979; Schnakenberg, 1976; Zhang and Wang, 2014; Zia and Schmittmann, 2007). In equilibrium, the flux along any loop is the same as for the corresponding reversed loop so that the net flux is zero. The flux loops provide additional information to the probability distribution for describing the nonequilibrium dynamics of a discrete system.

C. Nonequilibrium paths

An alternative formulation for the stochastic dynamic equation (2) describes the dynamical process in terms of a path integral summing over all possible paths $\mathcal{D}\mathbf{C}(t)$ from initial state $\mathbf{C}_{\text{initial}}$ at $t = 0$ to final state $\mathbf{C}_{\text{final}}$ at time t (Aurell and Sneppen, 2002; Feng et al., 2010, 2014; Feynman and Hibbs, 1965; Hunt and Ross, 1981; Li and Wang, 2013, 2014b; Maier and Stein, 1997; Onsager and Machlup, 1953; Roma et al., 2005; Wang et al., 2005, 2006b,c, 2010c, 2011; Wiener, 1964; Zhang and Wolynes, 2014; Zhang et al., 2013). That is,

$$P(\mathbf{C}_{\text{final}}, t, \mathbf{C}_{\text{initial}}, 0) = \int \mathcal{D}\mathbf{C}(t) \exp\{-S[\mathbf{C}(\mathbf{t})]\} \quad (10)$$

integrates over all possible paths between the initial state $\mathbf{C}_{\text{initial}}$ and final state $\mathbf{C}_{\text{final}}$ over time t. The action S is the integral of the Langrangian along the path $\mathbf{C}(t)$; that is, $S[\mathbf{C}(t)] = \int_0^t dt'\, L(\mathbf{C}(t'))$. The Lagrangian L is given by

$$L = \frac{1}{2}\nabla \cdot \mathbf{F} + \frac{1}{4D}\left(\dot{\mathbf{C}} - \mathbf{F}\right) \cdot \mathsf{D}^{-1}\left(\dot{\mathbf{C}} - \mathbf{F}\right) \quad (11)$$

where the first term arises from the deterministic driving force and the second is a consequence of Gaussian fluctuations η.

For a potential system with $F = -D\mathsf{D} \cdot \nabla U$, the cross product terms in the action, $-1/2 \int \frac{1}{\mathbf{D}} \cdot \mathbf{F} \cdot \dot{\mathbf{C}} dt = -1/2 \int \frac{1}{\mathbf{D}} \cdot \mathbf{F} \cdot \mathbf{dC}$, are independent of the path and thus constant, such that they do not contribute to the optimal path equation. However, for non-potential systems they do contribute. In particular, the integral along a loop does not vanish in this case, which is akin to the Aharonov-Bohm effect in quantum mechanics and can be used to classify the underlying topologies of nonequilibrium systems (Feng and Wang, 2011; Wang et al., 2010c).

Often, the integral in Eq. (10) is approximated well by considering only the contribution of the path that minimizes the action, called the optimal path (Feng et al., 2010, 2014; Li and Wang, 2013, 2014b; Wang et al., 2010c, 2011; Zhang et al., 2013). The optimal path of a system is determined by the Euler-Lagrange equation

$$\frac{d}{dt}\frac{\partial L}{\partial \dot{\mathbf{C}}} - \frac{\partial L}{\partial \mathbf{C}} = 0 \quad (12)$$

Since the probabilities (10) can be used to determine the nonequilibrium potential, optimal paths offer a possibility to reduce the computational effort for calculating the landscape from exponential to polynomial (Wang et al., 2010c).

An example of optimal paths connecting two steady states is illustrated in Fig. 1. Due to the curl flux force, optimal paths in general do not follow the landscape gradient and do not pass the saddle point $\hat{\mathbf{C}}$ between the two states' basins of attraction. The example illustrates furthermore that optimal paths in non-potential systems are irreversible.

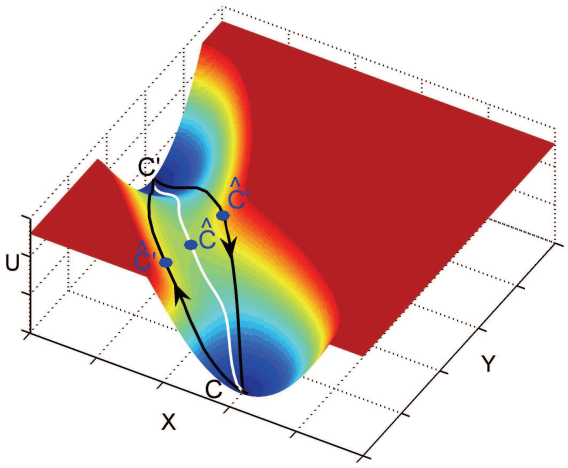

FIG. 1 3D illustration of a nonequilibrium landscape and nonequilibrium paths. The states C and C' are attractors of the system. The black lines indicate the optimal irreversible paths between them, with $\hat{C}'$ denoting the maxima along them. The white line shows the steepest descent gradient path going through the saddle point $\hat{C}$. From (Feng et al., 2014).

It is often very challenging to explicitly solve the Euler-Lagrange equation (12). In practice, the action of each path can be calculated by Monte Carlo methods and the optimal path with minimum action can be obtained through the Hamilton-Jacobi approach. This can reduce the complexity of calculating the action from a multi-dimensional integral to a one dimensional line integral (Elber et al., 1999; Faccioli et al., 2006; Feng et al., 2010, 2014; Li and Wang, 2013, 2014b; Olender and Elber, 1996; Wang et al., 2010c, 2011; Zhang et al., 2013).

D. Nonequilibrium transition state theory

In a stochastic equilibrium system, transitions occur between states associated with landscape minima. The state transfer between the minima follows an optimal path and passes through a "transition state" that is associated with a saddle point of the potential. In the limit of small fluctuations, Kramers calculated the rate to be (Kramers, 1940)

$$r = \frac{D}{2\pi k_b T}\sqrt{U''_{\min}|U''_{\max}|}\exp\left[-\frac{\Delta U}{k_B T}\right]. \tag{13}$$

ΔU is the potential difference between the initial and the transition state, $k_B T$ is the thermal energy, and $U''_{\min}$ and $U''_{\max}$ are the potential curvatures in the initial and the transition state, respectively. The latter are associated with the fluctuations around these states.

For nonequilibrium systems, the optimal paths do not necessarily pass a saddle point unless the fluctuations approach zero. Therefore, the transition state or Kramer's rate theory needs to be modified (Feng et al., 2014; Freidlin and Wentzell, 1984; Maier and Stein, 1997; Schuss, 2010). For small but finite fluctuations (Feng et al., 2014), the rate is written as

$$r = \frac{\lambda_u(\hat{\mathbf{C}})}{2\pi}\sqrt{\frac{\det \mathsf{M}_{\mathsf{fluct}}(\mathbf{C})}{|\det \mathsf{M}_{\mathsf{fluct}}(\hat{\mathbf{C}}')|}}\mathrm{e}^{-S_{\mathrm{HJ}}}. \tag{14}$$

where r is the transition rate from $\mathbf{C}$ to $\mathbf{C}'$, S_{HJ} is the action along the optimal path, $\mathsf{M}_{\mathsf{fluct}}$ is the Hessian of the action, and λ_u is its unstable eigenvalue. Furthermore, $\hat{\mathbf{C}}'$ denotes the point where the optimal path between $\mathbf{C}$ and $\mathbf{C}'$ crosses the line separating the two corresponding basins of attraction, determined by $\mathsf{D}^{-1}\cdot\mathbf{F}=0$ along the optimal path. Similar to the Kramers' rate, the prefactor $\frac{\lambda_u(\hat{\mathbf{C}})}{2\pi}\sqrt{\frac{\det \mathsf{M}_{\mathsf{fluct}}(\mathbf{C})}{|\det \mathsf{M}_{\mathsf{fluct}}(\hat{\mathbf{C}}')|}}$ is associated with fluctuations around $\mathbf{C}$ and $\hat{\mathbf{C}}'$. Note that $\hat{\mathbf{C}}'$ is different for transitions from $\mathbf{C}$ to $\mathbf{C}'$ and back, such that these rates do not obey detailed balance.

E. Nonequilibrium thermodynamics

To develop nonequilibrium thermodynamics, the Shannon entropy is first defined. (Ao, 2008; Feng and Wang, 2011; Ge and Qian, 2010; Nicolis and Prigogine, 1977; Schnakenberg, 1976; Van and Esposito, 2010; Wang et al., 2006a; Zhang et al., 2012)

$$\mathcal{S} = -\int P(\mathbf{C},t)\ln P(\mathbf{C},t)\,d\mathbf{C} \tag{15}$$

The temporal evolution of the entropy can be decomposed into two parts:

$$\dot{\mathcal{S}} = \dot{\mathcal{S}}_t - \dot{\mathcal{S}}_e \tag{16}$$

where

$$\dot{\mathcal{S}}_t = \int (\mathbf{J}\cdot(D\mathsf{D})^{-1}\cdot\mathbf{J})\frac{1}{P}\,d\mathbf{C} \tag{17}$$

represents the entropy production rate or the rate at which the total entropy of the system and the environment change, and

$$\dot{\mathcal{S}}_e = \int (\mathbf{J}\cdot(D\mathsf{D})^{-1}\cdot\mathbf{F}')\,d\mathbf{C} \tag{18}$$

is the entropy flow into or out of the system from the environment. The entropy production rate $\dot{\mathcal{S}}_t$ is directly related to the nonequilibrium flux $\mathbf{J}$ and is always larger than or equal to zero. In the expression of entropy flux $\dot{\mathcal{S}}_e$, the effective force $\mathbf{F}'$ is given by $\mathbf{F}' = \mathbf{F} - D\nabla\cdot\mathsf{D}$. The entropy flux can be positive (reduction of system entropy), which allows for the creation of order in the system as can be observed for living systems. At steady state, the entropy production rate is directly related to the rotational curl steady state probability flux and is equal to the entropy flux or heat dissipation.

Analogs of equilibrium thermodynamic quantities can be defined. If U denotes again the nonequilibrium potential $U = -\ln P^{ss}$, then the nonequilibrium potential energy is given by $\mathcal{U} = D\int U(\mathbf{C})P(\mathbf{C},t)\,d\mathbf{C}$ and the free energy $\mathcal{F}$ by $\mathcal{F} = D\int P(\mathbf{C},t)\ln\left(P(\mathbf{C},t)/P^{ss}(\mathbf{C})\right)\,d\mathbf{C}$. These quantities are related through $\mathcal{F} = \mathcal{U} - D\mathcal{S}$. The negative total entropy $-\mathcal{S}_t$ and the nonequilibrium free energy $\mathcal{F}$ are Lyapunov functions for the evolution of the probability P. Note that the nonequilibrium potential energy and the nonequilibirum free energy, sometimes called relative entropy, are defined in an analogous way to the energy and free energy in equilibrium statistical physics. The amplitude of fluctuations represented by the scale factor D effectively plays the role of temperature; in fact, the physical thermal energy could be involved in D.

Another form of nonequilibrium thermodynamics relates the underlying landscape and flux dynamics from the nonequilibrium fluctuation dissipation relation by evaluating the equal time correlation functions of the flux velocity (Feng and Wang, 2011). The time derivative of the free energy can be written as

$$\dot{\mathcal{F}} = D\left\langle \mathbf{v}\cdot\nabla\ln\left[P/P^{ss}\right]\right\rangle, \tag{19}$$

where $\langle\cdots\rangle$ denotes the average with respect to P and $\mathbf{v} = \mathbf{J}/P$ is the flux velocity. From this,

$$\dot{\mathcal{F}} = \left\langle \mathbf{v}^{ss}\cdot\mathsf{D}^{-1}\cdot\mathbf{v}^{ss}\right\rangle - \left\langle \mathbf{v}\cdot\mathsf{D}^{-1}\cdot\mathbf{v}\right\rangle \tag{20}$$

$$\equiv \dot{Q} - D\dot{\mathcal{S}}_t, \tag{21}$$

where $\dot{Q}$ is the heat flowing out of the system. It follows that the rate of entropy production results from relaxation to the steady state along gradients of the relative potential, $\dot{\mathcal{F}}$, and from a constant exchange of heat

that keeps the system out of equilibrium in steady state, $\dot{Q}$ (Feng and Wang, 2011; Ge and Qian, 2010; Seifert, 2005; Van and Esposito, 2010). Thus the nonequilibrium thermodynamics in this form states that total entropy production is from both non-stationary relaxation to the steady state and housekeeping for maintaining the steady state (Feng and Wang, 2011; Ge and Qian, 2010). At steady state, the entropy production rate is equal to the housekeeping heat for maintaining the steady state. Therefore, it is important to quantify entropy production as the nonequilibrium thermodynamic (or dissipation) cost for maintaining the steady state.

After defining the generalized thermodynamic force as

$$\mathbf{X} = (D\mathsf{D})^{-1} \cdot \mathbf{F}/P \tag{22}$$

one obtains the entropy dissipation

$$\dot{\mathcal{S}}_e = \int \mathbf{J} \cdot \mathbf{X} \, d\mathbf{C}. \tag{23}$$

in terms of the nonequilibrium flux $\mathbf{J}$ and $\mathbf{X}$. Considering the individual components of the scalar product in the integral, on can thus identify pairs of conjugated thermodynamic forces and fluxes. They form the basis of phenomenological, hydrodynamic descriptions of nonequlibrium systems, where the thermodynamic fluxes can be expressed up to linear order in terms of the forces

$$\mathbf{J} = \mathsf{L}\mathbf{X}. \tag{24}$$

The matrix L respects the system symmetries by the Curie principle and contains the phenomenological coupling coefficients, which fulfill the Onsager reciprocal relations (Onsager, 1931).

The above considerations can be also applied to discrete systems. With the transition rate between state i and j again given by T_{ij}, the flux between them is $F_{ij} = T_{ji}P_j - T_{ij}P_i$. We can also introduce the generalized thermodynamic potential $A_{ij} \equiv \ln\left(\frac{T_{ij}P_i}{T_{ji}P_j}\right)$. For the entropy $S = -\sum_i P_i \ln P_i$ one then finds (Schnakenberg, 1976)

$$\dot{S} = \sum_{i,j} F_{ij}A_{ij} = \sum_{i,j} T_{ij}P_i \ln\left[\frac{T_{ij}P_i}{T_{ji}P_j}\right]. \tag{25}$$

Similar to Eq. (23) the change in entropy is thus expressed as a sum of products of conjugated fluxes (F_{ij}) and forces (A_{ij}).

Since changes of entropy are intimately related to the existence of fluxes, the rate of entropy production or change can be used as a measure for how far a system is from equilibrium.

1. Crooks' theorem and the Jarzynski relation

When applying thermodynamics to "small" systems where the number of molecules is on the order of 10^{10} or less, for example on the scale of individual cells (10^4), fluctuations become significant. Consequently, it does not suffice to consider meanfield thermodynamic quantities; distributions must be considered. A number of fluctuation theorems have been derived to relate these distributions to entropy production in case some time-dependent work process is applied to a system (S., 2012). In particular, consider the change of the microstate $\mathbf{C}$ of a system coupled to a heat bath at temperature T. The change occurs along a path $\mathbf{C}(t)$ from $\mathbf{C}(0) = \mathbf{C}_{\text{initial}}$ to $\mathbf{C}(\tau) = \mathbf{C}_{\text{final}}$. Furthermore, let λ denote a time-dependent system parameter. Then the distribution $P\left[\mathbf{C}(t)|\lambda(t)\right]$ of the path and the corresponding distribution for its reverse path $\bar{\mathbf{C}}$ fulfill (Crooks, 1998, 1999)

$$\frac{P\left[\mathbf{C}(t)|\lambda(t)\right]}{P\left[\bar{\mathbf{C}}(\tau-t)|\bar{\lambda}(\tau-t)\right]} = \exp[\Delta S] = \exp[\beta(W-\Delta F)]. \tag{26}$$

Here, ΔS and ΔF denote the differences in entropy and free energy between the initial and the final equilibrium state, whereas W is the work applied to the system and β is inverse temperature. This has been verified experimentally, for example, (Collin et al., 2005; Schuler et al., 2005).

The fluctuation theorem implies the Jarzynski relation, namely that the average exponential of the work performed equals the exponential of the free energy change Jarzynski1, Jarzynski2. Explicitly,

$$\langle \exp[-\beta W] \rangle = \exp[-\beta \Delta F]. \tag{27}$$

This relation implies bounds on the possible paths along which work is extracted from the system by reducing its entropy. From a practical point of view it shows how to measure free energy differences by driving the system in arbitrary ways between two equilibrium states. This has been applied experimentally to conformations of single RNA molecules (Liphardt et al., 2002).

2. Fluctuation-dissipation theorem for intrinsic nonequilibrium systems

The conventional fluctuation dissipation theorem, or FDT, is important in linking the response of the system upon perturbation to equilibrium fluctuations (Kubo, 1966). This is useful for experimental efforts in extracting the equilibrium fluctuations of a system from its response, or vice versa. For nonequilibrium systems with broken detailed balance, a generalization of the FDT is necessary (Cugliandolo et al., 1997; Feng and Wang, 2011; Prost et al., 2009; Seifert, 2005; Seifert and Speck, 2010). In the landscape and flux representation, it takes

the form (Feng and Wang, 2011)

$$R_i^{\Omega}(t-t') = -\langle \Omega(t)\partial_i \ln[P^{ss}(\mathbf{x})]\rangle \tag{28}$$

$$= -\Big[\langle \Omega(t)\tilde{F}_k(t')D_{ik}^{-1}(t')\rangle + \langle \Omega(t)v_k^{ss}(t')D_{ik}^{-1}(t')\rangle\Big], \tag{29}$$

where Ω is an observable and R the response to a perturbation. Furthermore $\tilde{F}_i = F_i - \partial_j D_{ij}$ is again the generalized force and $v^{ss} = J^{ss}/P^{ss}$ is the flux velocity.

The above expression reveals that there are two contributions to the system's response. The first term on the right hand side of Eq. (29) is analogous to the expression for equilibrium systems and results from correlations between observable Ω and their driving force. The second term involves a correlation between the steady state flux velocity and observable Ω, which breaks detailed balance. Thus, this term is absent in equilibrium systems. The general response therefore depends on both steady state fluctuations and curl flux. Equation (29) can be used to experimentally quantify the rotational curl flux by measuring the difference between the response function and the fluctuations around steady state.

F. Nonequilibrium information dynamics

1. Nonequilibrium information landscape and flux, mutual information and entropy production

The physical states of systems and environments can be encoded into bits of information. Information flow is important for cellular signal transduction, development, and brain information processing (Barato et al., 2013; Barato and Seifert, 2014; Bialek, 2012; Levchenko and Nemenman, 2014). Speed and accuracy are crucial for biological information transfer and processing. However, finding phenomena that facilitate fast, efficient, and accurate biological information transfer and processing is challenging. Information dynamics are often stochastic; this can be characterized by probabilistic evolution (Barato et al., 2013; Barato and Seifert, 2014; Hartich et al., 2014; Horowitz and Esposito, 2014).

Information dynamics can be captured by communications among different subsystems enabling information transfer (Sloane and Wyner, 1993). Stochastic information dynamics can be quantified by the probabilistic master equation including, for example, both the whole system Z and its subsystems X and S. (Barato et al., 2013; Barato and Seifert, 2014; Hartich et al., 2014; Horowitz and Esposito, 2014; Zeng and Wang, 2017). The nonequilibrium information system can be globally quantified by its steady state distribution and flux. Weights are assigned to each information state based on the landscape. Both landscape and flux which quantifies the system's distance form equilibrium, determine the information dynamics.(Zeng and Wang, 2017). Shannon's information theory (Sloane and Wyner, 1993) gives a mutual information measure for the capacity of the communications. Explicitly, for a system Z, this is based on the *Mutual Information Rate* (MIR) between its subsystems X and S in steady state. The MIR is defined on the probabilities of all possible time sequences. That is, it depends on the probability of the whole system $P(Z^T)$ and the probabilities of the subsystems X and S given by $P(X^T)$ and $P(S^T)$. The MIR between X and S is explicitly

$$I(X,S) = \lim_{T\to\infty}\frac{1}{n}\sum_{Z^T} P(Z^T)\log\frac{P(Z^T)}{P(X^T)P(S^T)}. \tag{30}$$

which measures the efficient bits of information that X and S exchange with each other in unit time. When $I(X,S)=0$, no information is exchanged between X and S and therefore the subsystems are independent of each other. The general form of mutual information $I(X,S)$ can be decomposed into a time-reversible equilibrium part $I_D(X,S)$ and time-irreversible nonequilibrium part $I_B(X,S)$ directly related to the information flux. This links communication capacity to the driving force of the system's information dynamics (Zeng and Wang, 2017). While the time-reversible part $I_D(X,S)$ operates in both directions without additional energy, the directional flow of information exchange requires energy input and is related to the information flux J_z, one of the two driving forces of the information dynamics. Furthermore, the information communication capacity is associated with the dissipation cost in maintaining it. The detailed balance breaking part of mutual information can be further decomposed into the difference between entropy production rate of the whole system and the individual subsystems (Diana and Esposito, 2014; Zeng and Wang, 2017). Namely,

$$I_B(X,S) = \frac{1}{2}(EPR_z - EPR_x - EPR_s) \tag{31}$$

where, EPR_z, EPR_x, and EPR_s represent the entropy production rate of the whole system Z, and each subsystem X and S respectively. Physically, a system's capacity for irreversible mutual information exchange between its subsystems is related to to the difference between entropy production in the whole system and its subsystems. Efficient mutual information exchange requires an energy input or dissipation cost, which can have direct impacts on the Jarzynski relation and Crooks fluctuation theorem when including information.

2. Fluctuations in information thermodynamics

Thermodynamic fluctuations can significantly alter stochastic information systems. The generalized fluctuation theorem involving information exchange character-

ized by mutual information I is given as (Sagawa, 2013):

$$\frac{P\left[\mathbf{C}(t)|\lambda(t)\right]}{P\left[\bar{\mathbf{C}}(\tau-t)|\bar{\lambda}(\tau-t)\right]}=\exp[\beta(W-\Delta F)+I] \quad (32)$$

This states that the difference in statistical fluctuations forward and backward in time leads to the entropy production given by the difference between the work and the free energy reduction from the mutual information. The generalized Jarzinsky relation (Sagawa, 2013) reads:

$$\langle\exp\left[-\beta W-I\right]\rangle=\exp[-\beta\Delta F]. \quad (33)$$

These relations imply that the effect of information exchange acts as extra work or an effective free energy reduction.

Several studies were carried out on the information and nonequilibrium optimization of biological systems. (Barato et al., 2013; Barato and Seifert, 2014; Bialek, 2012; Levchenko and Nemenman, 2014; Press et al., 2013). Topics examined include maximizing information entropy or max caliber (Press et al., 2013); maximizing mutual information (Bialek, 2012; Levchenko and Nemenman, 2014) for signal transduction and development; uncertainty; sensing; and efficiency of information processing (Barato et al., 2013; Barato and Seifert, 2014; Becker et al., 2015; Lan et al., 2012; Ziv et al., 2007). We expect more applications of the theoretical framework here to the biological information processing.

G. Gauge fields, time reversal symmetry breaking and underlying geometry for nonequilibrium systems

Symmetry is at the heart of many physical laws. Continuous symmetries can be quantitatively described through their associated gauge fields (Peskin and Schroeder, 1995). However, gauge theory can also be applied to nonequilibrium probabilistic dynamics(Feng and Wang, 2011; Polettini, 2012) . Indeed, the Fokker-Plank equation describing probabilistic evolution can be rewritten as

$$\nabla_t P(\mathbf{C},t)=\nabla_i D_{ij}(\mathbf{C})\nabla_j P(\mathbf{C},t), \quad (34)$$

where the covariant derivatives with respect to the system observables and time are defined as

$$\nabla_i=\partial_i+A_i \quad (35)$$
$$\nabla_t=\partial_t+A_t, \quad (36)$$

where $A_i=-\frac{1}{2}D_{ij}^{-1}\tilde{F}_j$ and $A_t=D_{ij}A_iA_j-\partial_i(D_{ij}A_j)$ form the components of an Abelian gauge field.

The components A_i introduce a curvature of the gauge field internal space

$$R_{ij}=2(\partial_iA_j-\partial_jA_i)=\partial_i(D_{jk}^{-1}v_k)-\partial_j(D_{ik}^{-1}v_k), \quad (37)$$

where $\mathbf{v_{ss}}(\mathbf{C})=J_{ss}(\mathbf{C})/P_{ss}(\mathbf{C})$ is the steady state flux velocity. In equilibrium, the steady state flux is zero and the curvature vanishes, which corresponds to $R_{ij}=0$ and thus a flat internal space. Outside of thermodynamic equilibrium, the rotational flux typically does not vanish, therefore $R_{ij}\neq 0$, which yields a curved internal space (Feng and Wang, 2011). Curvature of this internal space is a source of a global topological phase analogous to the quantum Berry phase (Wang et al., 2008, 2010c). The heat dissipated along a closed loop is given by (Feng and Wang, 2011)

$$T\Delta s_m^C=-\oint_C A_i(\mathbf{x})dx_i=-\frac{1}{2}\int_\Sigma d\sigma_{ij}R_{ij}, \quad (38)$$

where Σ is the surface spanned by the closed loop C and $d\sigma_{ij}$ an area element of this surface.

The dissipated heat Δs_m in Eq. (38) is equal to the entropy production at steady state. Through the fluctuation theorem (Crooks, 1998, 1999), time irreversibility emerges when entropy production is non-zero, caused by a flux that breaks detailed balance.(Feng and Wang, 2011; Wang et al., 2010c) Thus, systems with non-zero curvature geometry break detailed balance, showcase the emergence of the flux that explicitly breaks time-reversal symmetry, and generate dissipation.

H. Multiple Landscapes, adiabaticity/non-adiabaticity and curl flux

We have examined nonequilibrium processes with just one underlying landscape. Often, systems have multiple degrees of freedom coupled to each other. In these cases, dividing systems into subsystems and examining their intra- and inter-subsystem dynamics allow for probing the overall system dynamics. In equilibrium systems, each subsystem can be described by a landscape and the whole system is thus considered as multiple coupled landscapes. For example, both the intra-energy nuclear landscape and inter-energy electronic landscape motion determine the dynamics of electron transfer(Marcus, 1964; Morgan and Wolynes, 1987). In equilibrium systems, the coupled landscape approach can be carried out because interaction potential landscapes are known *a priori*. These interaction landscapes are not *a priori* known for nonequilibrium systems, so the conventional equilibrium approach must be extended.

For nonequilibrium systems, both strongly-coupled, adiabatic dynamics and weakly-coupled, non-adiabatic dynamics are important for overall system dynamics. Adiabatic motion is characterized by significantly faster inter-landscape motion while the opposite is true of non-adiabatic motion. Multiple coupled landscapes can be technically challenging to study and visualize because intra-landscape dynamics are often described by continuous variables, whereas inter-landscape dynamics and

coupling are often described by discrete variables. One possible solution is to write all discrete variables in a continuous representation. While the states themselves are discrete, their associated occupation probabilities are continuous. By introducing those additional variables, one can treat systems with coupled discrete and continuous variables as coupled continuous variable systems with extra degrees of freedom using path integrals. Through mathematical transformation, the coupled landscape dynamics can be treated as the dynamics under a single landscape with extended dimensions (Chen et al., 2015a; Zhang et al., 2013). Using this strategy, a unified, global quantification of nonequilibrium multi-landscape dynamics, as determined by landscape gradient and curl flux, can be represented on a single higher-dimensional landscape; details can be found in (Chen et al., 2015a; Zhang et al., 2013) Examples of possible applications for this strategy include the study of molecular motors and gene regulation (Chen et al., 2015a; Jülicher et al., 1997; Zhang et al., 2013).

I. Organization principle of hierarchy and complexity of the dynamical systems at different scales

Complex systems often involve spatial and time scales characterized by different emergent phenomena and dynamics. For example, when we heat up the water for coffee, in principle we can explore the microscopic molecular dynamics and see how the water changes to vapor. However, it is not practical to follow the dynamics of all the molecules involved. In addition, our observation of interest is on a larger scale than individual molecules; we wish to know if the water is boiling or not. The water's state is not determined by any single individual molecule, so it is impossible to determine if the water is boiling or not by examining a single molecule. The boiling behavior is an emergent collective phenomena from the interactions of many individual molecules at microscopic scales.

Large scale behavior emerging from microscopic scales can be very different from small scale behavior. A physical picture and unified quantitative theory is crucial for understanding this organization hierarchy and emergent system complexity (Anderson, 1972; Frauenfelder and Wolynes, 1994; Haken, 2000; Hopfield, 1994; Laughlin et al., 2000; Prigogine and Stengers, 1984; Wolynes, 1996). Emergent behavior is explored using several central concepts, namely, symmetry breaking, bifurcation, phase transition, and emergent rare events. These concepts were integrated to suggest a nonequilibrium landscape framework for mesocopic dynamics derived from the fast, microscopic dynamics at a small scale; intrabasin motions within each state at an intermediate scale; and the slow inter-basin switching with the kinetic rates exponentially dependent on the system size at a larger scale (Qian et al., 2016). This nonequilibirum landscape framework represents microscopic, fast dynamics as a stochastic process and intermediate scale movements using nonlinear dynamics. Multiple attractors from larger scales representing the behavior and function emerge from the interactions of smaller scale systems.

Each inter-basin transition can be described as a dynamic symmetry-break which exhibits catastrophe and a phase transition, breaking ergodicity (Qian et al., 2016), as shown in Fig.2. The dynamics of a nonlinear mesoscopic system at the intermediate scale is stochastic. Therefore, the location and switching between basins of attraction are both emergent phenomena. Stochastic inter-basin dynamics provide the random element for nonlinear dynamics at higher spatial and temporal scales. In fact, the mesoscale landscape and flux emerges from underlying microscale dynamics of the system. At the mesoscopic scale, understanding emergent states in their basins of attraction and how they switch is critical. For example, the water liquid and vapor phase basin dynamics are critical for understanding the boiling system behavior, though individual molecule motion is not as important. The hierarchical structures of protein dynamics at different scales in terms of their associated energy landscapes have been experimentally demonstrated (Frauenfelder and Wolynes, 1994). The nonequilibrium landscape framework discussed here can help to capture the hierarchical structure and emergent complexity of the nonequilibrium biological system organization.

J. Spatial nonequilibrium systems

So far, we have discussed spatially homogeneous systems. However, spatially heterogeneous systems more accurately represent biological phenomena such as organism development, motility, and cell structure. Another example lies in the spatial organization of the neurons in the brain, where the relevant dynamic quantities depend on space (Bray, 2001; Dayan and Abbott, 2001; Getling, 1998; Jaeger et al., 2004; Marchetti et al., 2013a). The dynamics and local stability of such systems have often been studied using deterministic or stochastic partial differential equations. The potential landscape and rotational curl flux approach can be generalized to spatiotemporal nonequilibrium dynamics of such systems (Wu and Wang, 2013a,b, 2014).

1. Landscape and flux decomposition

To identify and quantify the driving force for spatially inhomogeneous nonequilibrium dynamical systems, we first define the system's dynamic variables. These quantities are given by fields that depend on space and time, denoted by $\vec{\phi}(\vec{x},t)$ with components $\phi_a(\vec{x},t)$ representing the different state variables and $\vec{x}$ denoting a point in

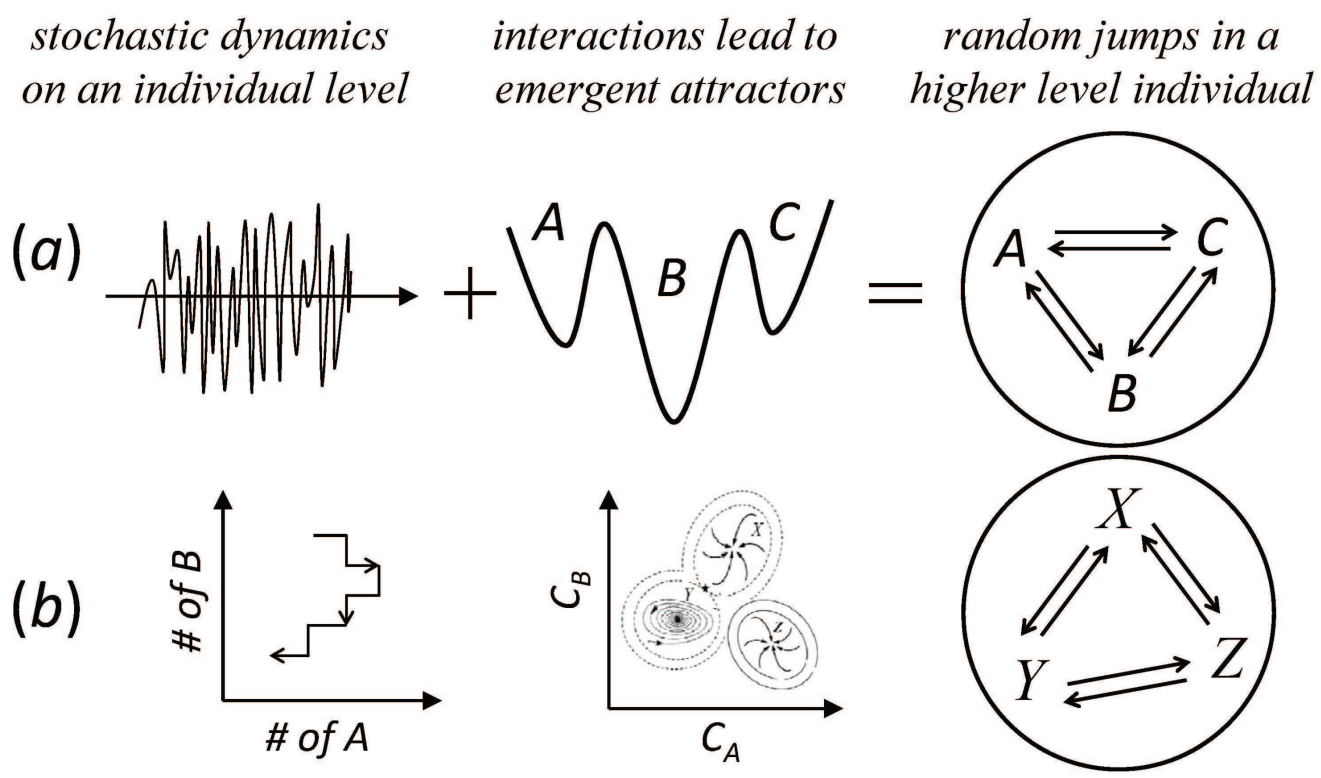

FIG. 2 Illustration of organizational hierarchy and complexity at different scales (a) A schematic showing how rapid solvent-macromolecule collisions, as a source of stochasticity and together with a multi-energy-well landscape, give rise to a kinetic jump process for an individual macromolecule with multiple states (shown within the circle). (b) A level higher, many interacting chemical individuals, each with multiple discrete states,

form mesoscopic nonlinear reaction systems. (from Ref. (Qian et al., 2016)).

space. The Langevin equation for these fields then reads

$$\partial_t \phi_a(\vec{x},t) = F_a[\vec{x};\phi] + \xi_a[\vec{x},t;\vec{\phi}]. \tag{39}$$

where $\vec{F}$ is the deterministic driving force and $\vec{\xi}$ is the stochastic force, defined by

$$\xi_a[\vec{x},t;\vec{\phi}] = \sum_b \int d^3x' G_{ab}[\vec{x},\vec{x}';\vec{\phi}]\zeta_b(\vec{x}',t) \tag{40}$$

where the random fields ζ_a obey

$$\langle \zeta_a(\vec{x},t)\rangle = 0 \tag{41}$$

$$\langle \zeta_a(\vec{x},t)\zeta_b(\vec{x}',t')\rangle = \delta_{ab}\delta^{(3)}(\vec{x}-\vec{x}')\delta(t-t') \tag{42}$$

In the previous equation, $\mathsf{G}[\vec{x},\vec{x}';\vec{\phi}]$ quantifies how the stochastic force field varies in space and by system variable. The stochastic fluctuation strength is characterized by the diffusion tensor D with

$$D_{ab}(x,x';[\phi]) = \frac{1}{2}\sum_s \int d^3y G_{as}[\vec{x},\vec{y};\vec{\phi}]G_{sb}[\vec{x}',\vec{y};\vec{\phi}] \tag{43}$$

Consequently, $\langle \xi[\vec{x},t;\vec{\phi}]\rangle = 0$ and $\langle \xi[\vec{x},t;\vec{\phi}]\xi[\vec{x'},t';\vec{\phi}]\rangle = 2\mathsf{D}(x,x';[\phi])\delta(t-t')$.

The state of the system is given by a probability functional $P[\vec{\phi}]$, which evolves in time according to a functional Fokker-Planck equation. The rate of change of the probability function can be derived from the principle of probability conservation by noting that the functional divergence of net probability flux is equal to the rate of change of probability. Explicitly,

$$\frac{\partial P[\vec{\phi}]}{\partial t} = -\sum_a \int d^3x \frac{\delta}{\delta\phi_a(\vec{x})} J_a[\vec{x};\vec{\phi}] \tag{44}$$

where the flux field $J_a[\vec{x};\vec{\phi}]$ in turn can be split into two contributions (Wu and Wang, 2013a,b, 2014)

$$J_a[\vec{x};\vec{\phi}] = F_a[\vec{x};\vec{\phi}]P[\vec{\phi}] - \sum_b \int d^3x' \frac{\delta}{\delta\phi_b(\vec{x}')}\left(D_{ab}[\vec{x},\vec{x}';\vec{\phi}]P[\vec{\phi}]\right) \tag{45}$$

In analogy with the spatially homogenous case, the driving force can be expressed in terms of the functional gradient of a nonequilibrium potential field landscape and a

rotational curl flux field (Wu and Wang, 2013a,b, 2014)

$$\tilde{F}_a[\vec{x};\vec{\phi}] = -\sum_b \int d^3x' D_{ab}[\vec{x},\vec{x}';\vec{\phi}]\frac{\delta U[\vec{\phi}]}{\delta\phi_b(\vec{x}')} + \frac{J_a^{ss}[\vec{x};\vec{\phi}]}{P^{ss}[\vec{\phi}]}. \tag{46}$$

where $\tilde{F}_a[\vec{x};\vec{\phi}] = F_a[\vec{x};\vec{\phi}] - \sum_b \int d^3x' \frac{\delta}{\delta\phi_b(\vec{x}')} D_{ab}[\vec{x},\vec{x}';\vec{\phi}]$. The nonequilibrium potential landscape U is linked to the steady state probability, $U[\vec{\phi}] = -\ln P^{ss}[\vec{\phi}]$, whereas the steady state probability flux field satisfies divergent free condition

$$\sum_a \int d^3x \frac{\delta}{\delta\phi_a(\vec{x})} J_a^{ss}[\vec{x};\vec{\phi}] = 0. \tag{47}$$

The Lyapunov functional can be used to quantify the global stability of spatially-dependent nonequilibrium dynamical systems. The functional is determined by the intrinsic potential field in systems without fluctuations and by the free energy landscape for systems with finite fluctuations (Wu and Wang, 2013a,b, 2014). The free energy functional decreases monotonically for spatially-dependent stochastic systems because of the second law of thermodynamics. Therefore, nonequilibrium thermodynamics can be generalized from spatially homogeneous to heterogeneous systems (Wu and Wang, 2013a,b, 2014).

2. Generalized hydrodynamics

Entropy dissipation and entropy production can be expressed for spatially heterogeneous systems in a manner similar to that used for homogenous systems. The entropy production rate can be used to derive a phenomenological description of the system's dynamics by assuming the system is close to thermodynamic equilibrium (de Groot and Mazur, 1985). This condition states that each of the volume elements that the system comprisesis always in thermodynamic equilibrium. The equilibria may differ between different spatial elements such that the exchange of energy and matter between adjacent volume elements leads to quasistatic changes of their states. This approach is then limited to so-called hydrodynamic modes, which are characterized by a relaxation time τ that increases with decreasing wave number q as $\tau \propto q^{-2}$ and arise from conservation laws or broken continuous symmetries.

Because the system is in local thermodynamic equilibrium, the free energy $\mathcal{F}$ is defined by summing each volume element's free energy. For constant temperature T, one can then express the entropy production rate as

$$\dot{\mathcal{S}}_t = -\frac{1}{T}\dot{\mathcal{F}} = \int d^3x \sum_i J_i X_i \tag{48}$$

where the sum extends over all conjugated pairs of fluxes and forces. Expressions for the fluxes can be obtained by expanding them up to first order in the forces, similar to Eq. (24), where the now phenomenological coupling coefficients respect the Curie principle and the Onsager relations. For simple fluids, this approach leads to the Navier-Stokes equation, where the viscosities are the phenomenological coupling coefficients. This approach is therefore often called generalized hydrodynamics and has been applied successfully to cellular processes; see Sect. VI. For strongly nonequilibrium systems, the local equilibrium assumption breaks down. A more general approach such as landscape and flux field is required to accurately describe the underlying nonequilibrium processes.

3. A strong nonequilibrium spatial dynamical system: turbulence

As a specific example of a spatially heterogeneous system, consider the fluid dynamics of turbulent systems. Typically, the Reynolds number can inform if the inertial force dominates their viscous counterpart. For biological fluids, the Reynolds number is often low; however, they can still sometimes exhibit turbulent behavior, e.g. in bacterial suspensions (Dombrowski et al., 2004; Wensink et al., 2012). The nonequilibrium behavior of turbulence (Goldenfeld and Shih, 2017) can be characterized through energy cascade (Falkovich and Sreenivasan, 2006; Rose and Sulem, 1978). The notion of a cascade intuitively captures the energy flow from large to intermediate, then finally to small length scales where energy is dissipated (Richardson, 1922), quantified by Kolmogorov's scaling laws (Kolmogoroff, 1941a,b; Kolmogorov, 1962; Landau and Lifshits, 1987). A quantification of turbulence with an explicit detailed balance breaking description (Wu et al., 2018) can help reveal more insights into the nonequilibrium nature.

The potential landscape and flux field has been quantified through the stochastically forced Navier-Stokes equations that govern fully developed turbulence (Wu et al., 2018)

$$\partial_t \mathbf{u} = \mathbf{\Pi}^s(\nabla)\cdot(-\mathbf{u}\cdot\nabla\mathbf{u}) + \nu\Delta\mathbf{u} + \mathbf{f}^s \tag{49}$$

where $\mathbf{u}$ denotes the flow velocity field and $\mathbf{\Pi}^s(\nabla)\cdot(-\mathbf{u}\cdot\nabla\mathbf{u}) = -\mathbf{u}\cdot\nabla\mathbf{u} - \nabla p$ represents hydrostatic pressure and convection. They constitute the deterministic driving force together with the viscous force $\nu\Delta\mathbf{u}$. Finally, $\mathbf{f}^s$ denotes the stochastic stirring force.

The probability functional evolves according to

$$\partial_t P[\mathbf{u}] = -\int d^3x \frac{\delta}{\mathbf{u}(\vec{x})}\cdot\mathbf{J}[\vec{x};\mathbf{u}] \tag{50}$$

by probability conservation. At steady state, the flux field $\mathbf{J}^{ss}$ satisfies the divergence-free condition and is therefore a rotational curl flux. The flux field is deter-

mined by a reversible, pressure-convective force, an irreversible viscous force with diffusion in state space, as well as the stochastic stirring force as (Wu et al., 2018)

$$\mathbf{J}_{ss}(\mathbf{x})[\mathbf{u}] = \mathbf{J}^{ss}_{\rm rev}[\vec{x};\mathbf{u}] + \mathbf{J}^{ss}_{\rm irr}[\vec{x});\mathbf{u}] \tag{51}$$

The viscous force decomposition then becomes (Wu and Wang, 2013b, 2014; Wu et al., 2018)

$$\nu\Delta\mathbf{u} = -\int d\mathbf{x}'\, \mathsf{D}^{ss}(\mathbf{x}-\mathbf{x}')\cdot\frac{\delta}{\delta\mathbf{u}(\mathbf{x}')}\Phi[\mathbf{u}] + \frac{\mathbf{J}^{ss}_{\rm irr}[\vec{x});\mathbf{u}]}{P^{ss}[\vec{x};\mathbf{u}]} \tag{52}$$

where $\Phi[\mathbf{u}] = -\ln P^{ss}[\mathbf{u}]$ is the nonequilibrium potential landscape related to the steady-state probability (Wu et al., 2018). This landscape and flux field perspective of nonequilibrium dynamics applies to stochastic fluid systems with both low and high Reynolds numbers, such as biological fluids and turbulent systems, respectively.

The energy transfer $\mathcal{T}$ associated with the energy cascade is tightly related to the irreversible flux that breaks detailed balance by(Wu et al., 2018)

$$\mathcal{T}(\mathbf{k}) = -\mathcal{R}\left\{\int \mathbf{u}^*(\mathbf{k})\cdot\mathbf{J}^{ss}_{\rm irr}(\mathbf{k})[\mathbf{u}]\delta\mathbf{u}\right\} \tag{53}$$

where $\mathcal{R}$ denotes the real part of the function. This relation leads to the 4/5 scaling law for the third order structure function in turbulence (Frisch, 1995; Wu et al., 2018). It also leads to Komogorov's 5/3 scaling law for the second order structure function in turbulence under the hypothesis of self similarity (Wu et al., 2018). The driving force for stochastic fluid systems arises from the underlying potential landscape field gradient and the curl probability flux field for either physical/biological fluids or turbulence. A non-zero irreversible probability flux field indicates detailed balance breaking, which drives the energy cascade flow.

K. Nonequilibrium quantum landscape and flux

1. Nonequilibrium Quantum Dynamics

Nonequilibrium quantum phenomena are important in many branches of science, for example quantum transport (Bernevig and Zhang, 2006; Gelbart et al., 1972; Kuznetsov and Ulstrup, 1999; Laughlin, 1983; Lee et al., 2007; Majumder et al., 2005; Zhang et al., 2005). Electron and energy transport within and between molecules, e.g. in photosynthesis, has been explored intensively through both experiment (Avinun-Kalish et al., 2005; Ho, 2002; Ohtani et al., 1988; Park et al., 2000; Reed et al., 1997; Wu et al., 2004) and theory (Esposito and Galperin, 2009; Harbola et al., 2006; Tanimura, 2006). Unidirectional flow in nonequilibrium ultrafast electron transfer (Kao et al., 2012) was seen in recent experiments of oxidized photolyase photoreduction dynamics (Liu et al., 2013). Furthermore, quantum effects in transports provide a test ground for nonequilibrium thermodynamics, recently made possible in single molecule junctions (Ward et al., 2008). The coherence, representing pure quantum nature, contributes to the transport (Tanimura and Wolynes, 1992) in addition to the populations. This was seen for quantum coherent excitation (charge) transport in light harvesting complexes and photosynthetic reaction centers (Lee et al., 2007; Xu, 1992). Nonequilibrium dynamics is also important for the development of quantum devices (Nielsen and Chuang, 2000).

There are several theoretical approaches for quantum transport, including momentum balance and fluctuations in mesoscopic systems (Soree et al., 2002), the fluctuation-dissipation theorem (Baeriswyl, 2005; Kubo, 1957) and nonequilibrium Green's function method (Caroli et al., 1971; Combesco, 1971; Koentopp et al., 2008). However, these formalisms can only be applied successfully to systems near equilibrium. The quantum master equation (QME) provides a possible alternative for studying irreversible dynamics of quantum systems coupled to environments (Breuer, 2002a; Haake, 1973; Spohn, 1980) beyond the near equilibrium regime. This approach has been applied to decoherence dynamics in quantum optics (Carmichael, 2010; Scully and Zubairy, 1997a), chemical reactions, (Mukamel, 1999) and condensed matter systems (Weiss, 2012a).

In this section, we will illustrate an approach to nonequilibrium quantum dynamics in terms of population landscape, curl flux and coherence (Zhang and Wang, 2014) by exploring energy transfer(Gruebele and Wolynes, 2004; Leitner, 2010) and charge transport (Chen and Tao, 2009; Ohmine and Saito, 1999; Shishir et al., 2009; Zhu and Marcus, 2008) in biomolecules. Energy transport is often coupled to two heat environments, or bosonic baths, with different temperatures. For example, the light harvesting complex is coupled to both light, photonic baths and phononic baths induced by protein dynamics. Charge transport is often coupled to two chemical environments, or fermionic baths, with different chemical potentials. An example of this phenomenon is found in electron transfer between two metals.

Starting from the original Hamiltonian coupled with two environments, the corresponding quantum master equation can be derived. From there, the population landscape and curl flux can be uncovered to characterize nonequilibrium quantum systems. The curl flux provides a measure of detailed balance breaking and time-irreversibility, important in quantum transport. Nonequilibrium behavior from system-environment couplingcan significantly enhance steady state coherence (Li et al., 2015; Zhang and Wang, 2014), contrary to conventional wisdom that suggests the opposite is true(Breuer, 2002b; Manzano et al., 2012). The relationships among nonequilibriumness, curl flux, coherence, quantum transport and the energy/charge transfer efficiency are dis-

cussed in later sections.

2. Theory of nonequilibrium quantum dynamics in terms of flux, coherence and population landscape

In this section, a landscape and flux theory is developed (Wang et al., 2008, 2011) for the nonequilibrium quantum system (Zhang and Wang, 2014). The general Hamiltonian of a quantum system interacting with M environments can be written in the form

$$H_S = \sum_{n,m} H_{nm}|\psi_n\rangle\langle\psi_m| + \sum_{i=1}^{M}\sum_{\mathbf{k},\sigma}\hbar\omega_{\mathbf{k}\sigma}a_{\mathbf{k}\sigma}^{(i)\dagger}a_{\mathbf{k}\sigma}^{(i)}$$

$$H_{int} = \sum_{i,\langle n,m\rangle}\sum_{\mathbf{k},\sigma} g_{\mathbf{k}\sigma}^{nm(i)}\left(|\psi_n\rangle\langle\psi_m|a_{\mathbf{k}\sigma}^{(i)\dagger} + |\psi_m\rangle\langle\psi_n|a_{\mathbf{k}\sigma}^{(i)}\right) \tag{54}$$

where $\langle n,m\rangle$ denotes that only the pairs of states n,m with energies $E_n < E_m$ are considered. The first term of H_0 is the Hamiltonian of the system, the second term describes the environmental Hamiltonian, and the term H_{int} describes system-environmental coupling. Environments are often much larger in size than the system, so one can assume there are no reactions from the system back into the environment. Using this assumption, the system dynamics are uncovered by averaging over environments. This leads to themaster equation for reduced density matrix (Breuer, 2002a; Scully and Zubairy, 1997a; Zhang and Wang, 2014), given by

$$\frac{\partial\rho_S}{\partial t} = \frac{-1}{\hbar^2}\mathrm{Tr}_R\int_0^\infty ds\left[\tilde{H_{int}}(t),\left[\tilde{H}_{int}(t-s),\rho_S(t)\otimes\rho_R(0)\right]\right] + \mathcal{O}(g^2) \tag{55}$$

The density matrix can be expanded in terms of coupling strength between system and environments, explictly, $\rho(t) = \rho_S(t)\otimes\rho_R(0) + \rho_c(t)$. Under weak coupling, the quantum master equation can be truncated to second order, which gives the Redfield equation without secular approximation rather than the Lindblad equation. Written in Liouville space, this is$\dot{\rho_S} = \frac{i}{\hbar}[\rho_S, H_S] - \frac{1}{2\hbar^2}D(\rho_S)$ where H_S is the system Hamiltonian and $D(\rho_S)$ is the dissipation operator from system-bath coupling. The density matrix then forms the super vector $|\dot{\rho}_S\rangle = \hat{\mathcal{M}}|\rho_S\rangle$. By separating the ρ_c matrix on-diagonal population elements from the off-diagonal coherence elements, the matrix $\mathcal{M}$ is written as

$$\begin{pmatrix}\dot{\rho}_\mathrm{p}\\ \dot{\rho}_\mathrm{c}\end{pmatrix} = \begin{pmatrix}\mathcal{M}_\mathrm{p} & \mathcal{M}_\mathrm{pc}\\ \mathcal{M}_\mathrm{cp} & \mathcal{M}_\mathrm{c}\end{pmatrix}\begin{pmatrix}\rho_\mathrm{p}\\ \rho_\mathrm{c}\end{pmatrix} \tag{56}$$

where $\mathcal{M}_\mathrm{p}$ denotes the transition matrix in population space and $\mathcal{M}_\mathrm{c}$ is the transition matrix in coherence space (Zhang and Wang, 2014). The matrices $\mathcal{M}_\mathrm{pc}$ and $\mathcal{M}_\mathrm{cp}$ denote coupling transition matrices between population and coherence space.

At steady state, the coherence ρ_c can be substituted as a function of population ρ_p into the master equation (Zhang and Wang, 2014) to give a reduced population quantum master equation for ρ_p

$$\left(\mathcal{M}_\mathrm{p} - \mathcal{M}_\mathrm{pc}\mathcal{M}_\mathrm{c}^{-1}\mathcal{M}_\mathrm{cp}\right)\rho_\mathrm{p}^{ss} = 0 \tag{57}$$

The transfer matrix, which determines the temporal evolution of the density matrix, can now defined as $T_{mn} = \mathcal{A}^\mathrm{p}_{nn,mm}\rho^\mathrm{p}_{mm}$ for $m \neq n$ where $\mathcal{A}_\mathrm{p} \equiv \mathcal{M}_\mathrm{p} - \mathcal{M}_\mathrm{pc}\mathcal{M}_\mathrm{c}^{-1}\mathcal{M}_\mathrm{cp}$. For $m = n$, $T_{mn} = 0$. Because of its role in determining the dynamics of the density matrix, the transfer matrix is the driving force for stochastic probability evolution. The transfer matrix can be further decomposed into symmetric and anti-symmetric parts, given by $T_{mn} = \frac{T_{mn}+T_{nm}}{2} + \frac{T_{mn}-T_{nm}}{2}$ respectively. One can see that symmetric part of the transfer matrix $\mathcal{A}^{\mathrm{p},S}_{nn,mm} = \frac{T_{mn}+T_{nm}}{2}/\rho^\mathrm{p}_{mm}$ satisfies the detailed balance condition $(\frac{T_{mn}+T_{nm}}{2}/\rho^\mathrm{p}_{mm})\rho^\mathrm{p}_{mm} - (\frac{T_{nm}+T_{mn}}{2}/\rho^\mathrm{p}_{nn})\rho^\mathrm{p}_{nn} = 0$. Using similar methods, one can also check that the anti-symmetric part of the transfer matrix $\mathcal{A}^{\mathrm{p},A}_{nn,mm} = \frac{T_{mn}-T_{nm}}{2}/\rho^\mathrm{p}_{mm}$ does not preserve the detailed balance; $(\frac{T_{mn}-T_{nm}}{2}/\rho^\mathrm{p}_{mm})\rho^\mathrm{p}_{mm} - (\frac{T_{nm}-T_{mn}}{2}/\rho^\mathrm{p}_{nn})\rho^\mathrm{p}_{nn} \neq 0$, which leads to a non-zero steady state flux. Therefore, the population quantum dynamics are determined by two driving forces. The first part is a symmetric force $\mathcal{A}^{\mathrm{p},S}_{nn,mm} = \frac{T_{mn}+T_{nm}}{2}/\rho^\mathrm{p}_{mm}$ that is determined by steady-state population landscape and preserves detailed balance. The second part is the anti-symmetric part of the driving force $\mathcal{A}^{\mathrm{p},A}_{nn,mm} = \frac{T_{mn}-T_{nm}}{2}/\rho^\mathrm{p}_{mm}$, which breaks detailed balance (Zhang and Wang, 2014). Quantum flux can be further decomposed into a sum of fluxes through various loops in state space (Zhang and Wang, 2014, 2015a). The quantum flux is thus a rotational curl. The relationships among quantum coherence, transport, thermodynamics, fluctuation-dissipation relations and even underlying geometry/topology will be explored in later sections (Mehboudi et al., 2016; Zhang and Wang, 2014, 2015a,b, 2016).

Below we describe how the concepts developed in Sect. II have been applied to specific biological systems out of thermodynamic equilibrium on various length and time scales.

III. BIOMOLECULAR SYSTEMS AND EXPERIMENTAL QUANTIFICATION OF FLUX

As the fundamental building blocks of living organisms, biomolecules interact with each other to form complex molecular structures and dynamics. Because many biomolecular processes consume energy and exchange matter, they are considered far from equilibrium. This

holds notably for elementary biochemical reactions such as non-Michaelis-Menten kinetics (English et al., 2006; Min et al., 2006b); molecular dynamics in space and time such as Min-protein oscillations for cell-division site selection (Raskin and de Boer, 1999a); the organization of cytoskeletal structures like the assembly of actin filaments and microtubules (Fujiwara et al., 2007; Kuhn and Pollard, 2005; Mitchison and Kirschner, 1984; Stewman and Ma, 2018); and complicated molecular machines such as the bacterial flagellar rotation motor (Silverman and Simon, 1974). We will use rhodamine oxidation, cyanobacterial circadian rhythm, and energy transport in the light harvesting complex as three examples to illustrate nonequilibrium behavior occurring in molecular systems.

A. Non-Michaelis-Menten enzyme kinetics

In living cells, almost all biochemical reactions are catalyzed by enzymes that accelerate the conversion from substrates to products. Typically, kinetic rate is assumed to obey Michaelis-Mentin kinetics, the substrate and substrate-enzyme complex are in equilibrium (English et al., 2006; Michaelis and Menten, 1913; Xie, 2013). However, when energy enters or exits the system, the enzyme kinetics can deviate from Michaelis-Menten behavior (Cao, 2011; Min et al., 2006a; Qian and Elson, 2002) because of a rotational curl flux that breaks detailed balance (Liu and Wang, 2018). The landscape and fluxes are determined theoretically as the driving forces for nonequilibrium dynamics. Experimentally, the nonequilibrium landscape can be acquired by measuring the steady state distribution of the observables (Fang et al., 2018; Jiang et al., 2017). Experimental quantification of flux is more challenging but may be realized by measuring the deviation from the Michaelis-Menten kinetics (Liu and Wang, 2018).

The deviation from Michaelis-Menten kinetics can be illustrated experimentally by the catalysis of dihydrorhodamine 123 oxidation into fluorescent rhodamine 123 by the enzyme horseradish peroxidase in presence of hydrogen peroxide (H_2O_2). It is possible to study this reaction experimentally at the single molecule level because both the substrate and enzyme do not fluoresce, whereas the product does (Edman et al., 1999; Edman and Rigler, 2000; Hassler et al., 2007). Horseradish peroxidase has two different conformations, both of which can bind the substrate. The master equation corresponding to the kinetic scheme, Fig. 3(a), is given by (Liu and Wang, 2018)

$$\dot{P} = \begin{pmatrix} -sk_1 - \beta & \alpha & k_1 + k_3 \\ \beta & -sk_2 - \alpha & k_{-2} + k_4 \\ k_1 s & k_2 s & -k_{-1} - k_{-2} - k_3 - k_4 \end{pmatrix} P \tag{58}$$

where P is the vector (P_1, P_2, P_{ES}) of the probabilities P_1, P_2, and P_{ES} for the enzyme to be in conformational state 1, 2, or binding the substrate respectively.

The steady state probability flux is given by $J = \beta P_1^{ss} - \alpha P_2^{ss}$, where P_i^{ss} is the steady-state probability for being in state i. The flux is zero and detailed balance holds if

$$\frac{\alpha}{\beta} = \frac{k_{-1}k_2 + k_2 k_3}{k_{-2}k_1 + k_1 k_4}. \tag{59}$$

in which case Michaelis-Menten kinetics emerges and

$$\frac{1}{v} = C_0 + \frac{C_1}{[S]}, \tag{60}$$

where v is the reaction rate and $[S]$ the substrate concentration. C_0 and C_1 are constants that depend on the molecular rates. The inverse of the Michaelis-Menten rate is a linear function of the inverse of the substrate concentration. If detailed balance is broken, the steady-state probability flux is nonzero and the enzyme reaction rate is

$$\frac{1}{v} = C_0 + \frac{C_1}{[S]} + \frac{C_2}{[S] + \lambda} \tag{61}$$

which has an additional dependence on the substrate concentration containing the constants λ and C_2. In this case, the inverse reaction rate is no longer a linear function of the inverse substrate concentration and thus deviates from Mechalias-Menten kinetics. This behavior is observed experimentally for rhodamine oxidation by the horseradish peroxidase, shown in Fig. 3(b). Note that the extra term $\frac{C_2}{[S]+\lambda}$ results from the presence of a flux loop, but not directly from having more than one conformational state of the enzyme. The deviation from Michaelis-Menten kinetics is thus a consequence of breaking detailed balance, which in this case originates from heat absorption by the reaction (Liu and Wang, 2018). In more complex systems, each additional flux loop i contributes an additional term $\frac{C_i}{[S]+\lambda_i}$.

Exploiting the correlation function of the experimental fluorescence signals, the kinetic rate parameters are obtained. Doing so quantifies the enzymatic rate and the probability flux as a function of the substrate concentration (Liu and Wang, 2018) shown in Fig. 3 (b,c). Clearly, the experimentally-observed inverse enzyme rate versus inverse substrate deviates significantly from the conventional Michaelis-Menten rate, which predicts a straight line. The nonzero fluxes are quantified for different substrate concentrations(Liu and Wang, 2018).

As discussed, a non-Michaelis-Menten rate can be used to quantify the degree of detailed balance breaking through the corresponding rotational curl flux. The flux breaking detailed balance can lead to non-Michaelis-Menten enzyme kinetics, which is now quantified experimentally as a major driving force for nonequilibrium dynamics (Liu and Wang, 2018) and landscape shape (Fang

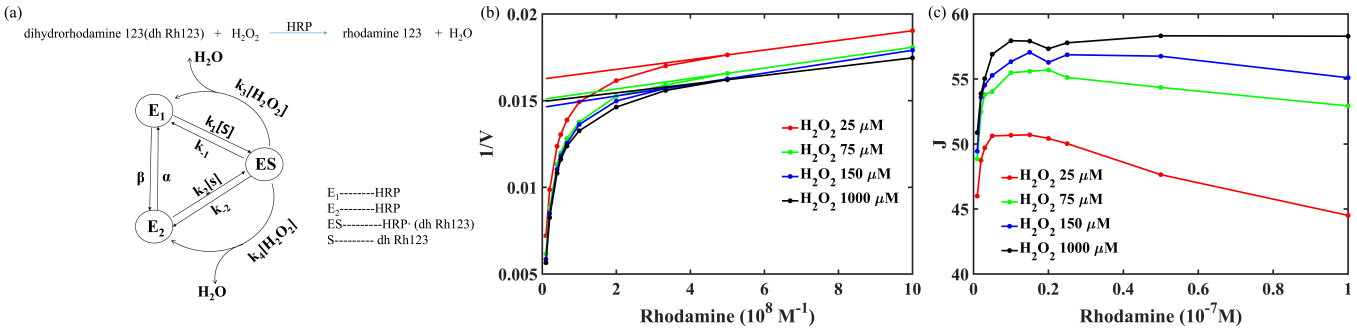

FIG. 3 Schematic of an enzyme reaction, non Michales-Menten kinetics and quantification of flux. (a): The simplest kinetic scheme with two unbound enzyme states. E_1 and E_2 denote the conformational states of enzymes, ES denotes the intermediate state of the enzyme reaction and P denotes product. α and β denote the conformation conversion rate. (b):Non-Michaelis Menten (curved lines) versus Michaelis Menten enzyme kinetics (straight lines) with respect to rhodamine 123 concentrations at different substrate concentrations. (c): Flux values with respect to rhodamine 123 concentrations at different substrate concentrations. (from Ref. (Liu and Wang, 2018)).

et al., 2018; Jiang et al., 2017). It is important to note that the breaking down of the detailed balance originates from energy imbalance of the enzyme reaction because of heat absorption(Liu and Wang, 2018).

B. Bacterial circadian rhythm

Circadian rhythms are biological processes that display sustainable oscillation of about 24 hours and allow organisms to anticipate predictable environmental changes that occur daily. Typically, these processes are generated through negative feedback regulation of so-called clock genes at the level of transcription or translation (Gonze et al., 2002; King et al., 1997; Novk and Tyson, 2008; Paijmans et al., 2016, 2017; van Zon et al., 2007; Zwicker et al., 2010). Acircadian rhythm of the cyanobacterium *Synechococcus elongatus* (Ishiura et al., 1998; Wang et al., 2009) can emerge from the relatively simple interaction of the proteins KaiA, KaiB, and KaiC. Remarkably, after addition of ATP, a mixture of these proteins *in vitro* generates circadian oscillations with only a weak dependence on temperature (Nakajima et al., 2005; Rust et al., 2007; Tomita et al., 2005). Of the three proteins, KaiC is a hexameric enzyme that can be phosphorylated at two of its amino acids: serine 431 (S431) and threonine 432 (T432). The enzyme can be in four different states: fully unphosphorylated (U-KaiC); partially phosphorylated either at S431 (S-KaiC) or at T432 (T-KaiC); or fully phosphorylated at both S431 and T432 (ST-KaiC). Furthermore, KaiA promotes KaiC phosphorylation, whereas KaiB antagonizes the activity of KaiA, Fig. 4(a).

The phosphorylation state of KaiC changes cyclically; KaiA promotes the transition from U-KaiC to T-KaiC and then into ST-KaiC. Afterwards, KaiC transforms into S-KaiC and finally into U-KaiC. The state ST-KaiC is effectively long-lived because KaiA promotes changes from S-KaiC back to ST-KaiC. Only when S-KaiC has reached a threshold value does the rate of transition from ST-KaiC to S-KaiC increase rapidly, because S-KaiC inhibits KaiA through KaiB. After S-KaiC has turned into U-KaiC, KaiA is reactivated and a new cycle begins, Fig. 4(b). Note, however, that the specific activation of KaiB by S-KaiC and the role of KaiA in rephosphorylating S-KaiC and thus generating ST-KaiC remain to be confirmed.

The nonequilibrium landscape of the KaiABC system has the form of a Mexican hat; the nonequilibrium flux drives the system along the hat's valley, explaining the stability of the oscillations. The entropy flow associated with the nonequilibrium flux and force, which is ultimately caused by ATP hydrolysis involved in the phosphorylation kinetics, provides the thermodynamic cost for maintaining robust and coherent circadian oscillation.

C. Nonequilibrium quantum transports in biomolecules

Representative examples of quantum mechanical biological processes include photosynthetic energy absorption, olfaction, bird magnetoreception, and electron/proton transports in enzymes (Brookes, 2017). As these processes involve the conversion of energy into forms usable for chemical transformations, they are out of equilibrium by nature.

To illustrate the nonequilibrium quantum dynamical nature of these processes, we explore the landscape and flux in two-site and two-level model systems (Zhang and Wang, 2014) coupled with two temperature or two chemical potential environments where analytical solutions can be obtained. Two-site and two-level systems have been widely investigated in condensed matter physics, chemistry, quantum optics and information (Benjacob and Gefen, 1985; Bennett, 1973; Deutsch, 1985; Landauer, 1961; Leggett et al., 1987; Nielsen and Chuang, 2000;

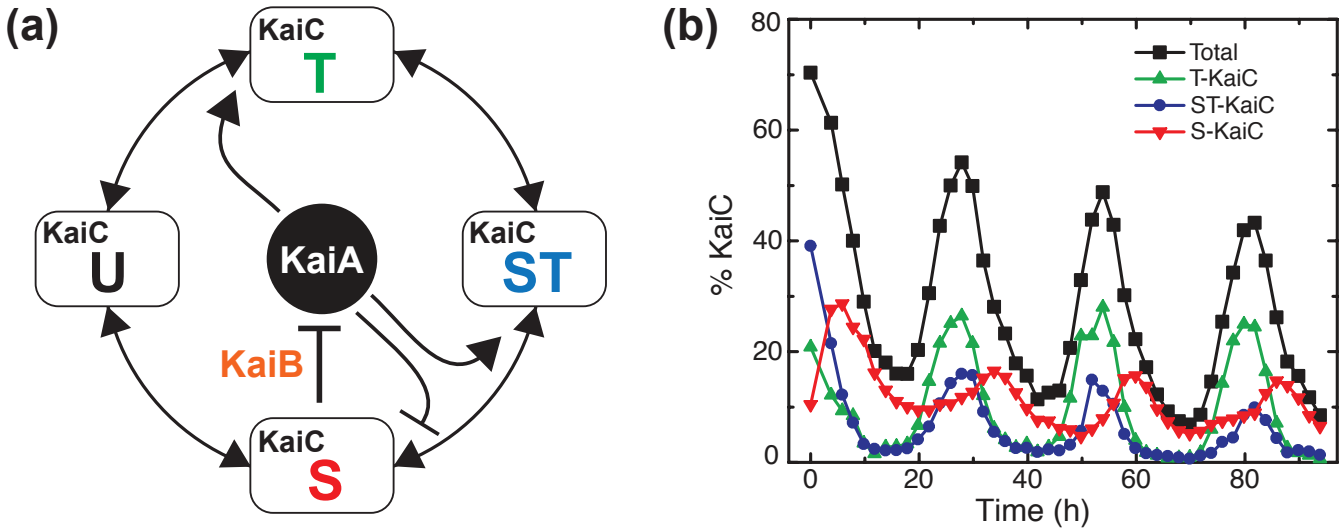

FIG. 4 The KaiABC circadian system of the cyanobacterium *Synechococcus elongatus*. (a) Reaction network. Two-headed arrows indicate transitions between phosphorylation states of KaiC, arrows emanating from KaiA indicate promotion and inhibition of transitions, the arrow from S-KaiC to KaiA, suppression of KaiA activity by KaiB in presence of S-KaiC. (b) Concentrations of phosphorylated KaiC as a function of time. From (Rust et al., 2007).

Onuchic and Wolynes, 1988; Palma et al., 1996; Preskill, 1998; Scully and Zubairy, 1997b; Unruh, 1995; Weiss, 2012b) to explore quantum dissipations and coherence. The system dynamics are often assumed to be coupled with a single environment. The steady state often becomes an equilibrium state with detailed balance and significantly reduced or zero coherence. There are examples of systems coupled to multiple environments, such as energy and charge transfer in photosynthesis (Garab, 1999; Lee et al., 2007) and nano-quantum transport (Ferry and Goodnick, 1997). For these systems, the final steady state is often not an equilibrium state and quantum coherence is not necessarily zero at steady state (Li et al., 2015; Zhang and Wang, 2014, 2015a,b, 2016). How the distance of a system from equilibrium influences quantum coherence and transport is a major challenge for photosynthesis in particular(Garab, 1999; Lee et al., 2007).

1. An analytical model for nonequilibrium quantum energy/charge transfers in biomolecules

To address these issues, let us consider a two-site system coupled with two environments. Each environment is in equilibrium with a different temperature or chemical potential environment and either obeys Bose or Fermi statistics. The two-site system connected by tunneling can be used to describe quantum transport, while the temperature or chemical potential difference measures the system's distance from equilibrium as they set up a nonequilibrium thermal or chemical battery or pump. The transition matrix asymmetry, probability flux, coherence, and quantum transport efficiency can be quantified by this same measure.The origin of the nonzero flux can then be identified as the temperature or chemical potential difference.

The two sites describe the transfer, while each level describes the ground state and the excitation shown in Fig. 5 (a) where the same ground state is shared between two sites.After being excited from ground state, the molecular energy transfer is often from donor to acceptor sites. For simplicity, one can assume the difference in excitation energies of the two sites are small in the near-resonance regime, $\varepsilon_2 - \varepsilon_1 \ll \min(\varepsilon_1, \varepsilon_2)$.

The energy transport in biomolecules can be described by the system interacting with two thermal environments in different temperatures. The free and interaction parts of the Hamiltonian are

$$H_S = E_g|\Omega\rangle\langle\Omega| + \varepsilon_1\eta_1^\dagger\eta_1 + \varepsilon_2\eta_2^\dagger\eta_2 + \Delta(\eta_1^\dagger\eta_2 + \eta_2^\dagger\eta_1)$$
$$H_R = \sum_{\mathbf{k},p}\hbar\omega_{\mathbf{k}p}a_{\mathbf{k}p}^\dagger a_{\mathbf{k}p} + \sum_{\mathbf{q},s}\hbar\omega_{\mathbf{q}s}b_{\mathbf{q}s}^\dagger b_{\mathbf{q}s} \tag{62}$$

$$H_{int} = \sum_{\mathbf{k},p}\lambda_{\mathbf{k}p}\left(\eta_2^\dagger a_{\mathbf{k}p} + \eta_2 a_{\mathbf{k}p}^\dagger\right) + \sum_{\mathbf{q},s}\lambda_{\mathbf{q}s}\left(\eta_1^\dagger b_{\mathbf{q}s} + \eta_1 b_{\mathbf{q}s}^\dagger\right) \tag{63}$$

where $|\Omega\rangle$ represents the ground state, while η and $\eta^\dagger$ represent the exciton annihilation and creation operators occupying the specific excited site (two sites) for the system. Excitons are bosons that obey an anti-commuting relationship within the site when constrained to only two energy levels and a commuting relationship between sites (Abramavicius et al., 2009). Both envi-

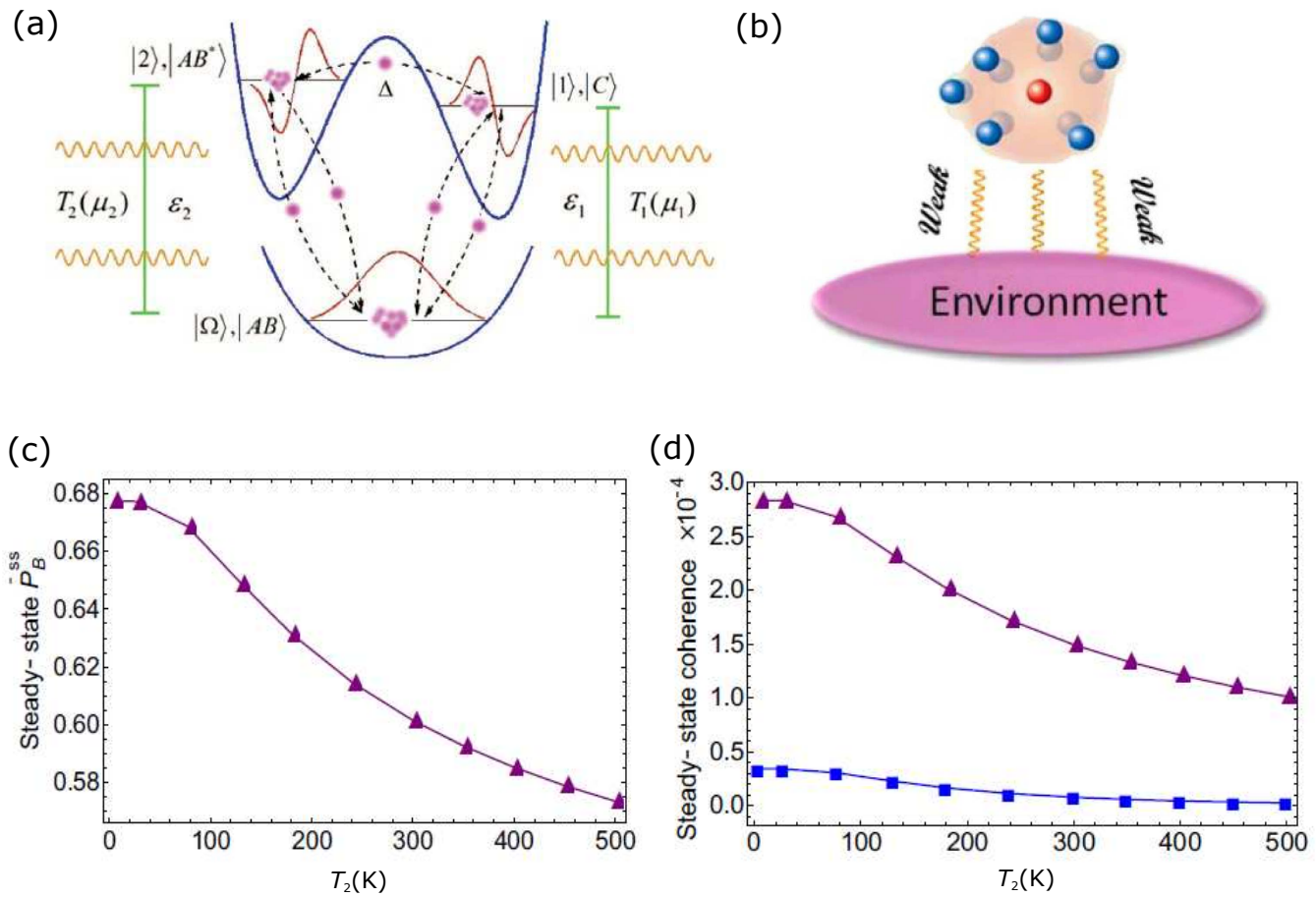

FIG. 5 Model for nonequilibrium transport, polarons and quantum transport efficiency. (a) Two-site, two-level quantum transport coupled with the two environmental baths (b). Polarons formed from strong interactions of excitons and vibrons lead to weak interactions with the environments and long time coherence. (c) Quantum transport efficiency represented by the steady-state population on pigment B (energy transfer is from pigment A to pigment B) with respect to the temperature of low-frequency fluctuations (low temperature here corresponding to high temperature difference between radiation bath and protein bath); (d) Steady-state quantum coherence varies as a function of the temperature of low frequency fluctuations. In (d) the purple and the blue lines denote the electronic (localized) coherence and excitonic (delocalized) coherence, respectively. (from Ref. (Zhang and Wang, 2014) and Ref. (Zhang and Wang, 2016)

ronmental annihilation/creation operators, a and $a^\dagger$ respectively, and reservoir annihilation/creation operators, b and $b^\dagger$, satisfy the Bose-Einstein commutation relations. That is, the environmental operators a and $a^\dagger$ follow $[a_{\mathbf{k}p}, a^\dagger_{\mathbf{k}'p'}] = \delta_{\mathbf{k}\mathbf{k}'}\delta_{pp'}$, $[a_{\mathbf{k}p}, a_{\mathbf{k}'p'}] = 0$ and the reservoir operators b and $b^\dagger$ follow $[b_{\mathbf{k}p}, b^\dagger_{\mathbf{k}'p'}] = \delta_{\mathbf{k}\mathbf{k}'}\delta_{pp'}$, $[b_{\mathbf{k}p}, b_{\mathbf{k}'p'}] = 0$. The operators a and b represent two environmental baths in equilibrium at different temperatures, obeying Bose statistics. Through coupling with the system, environments with different temperatures push the system away from equilibrium. The variable Δ represents electronic coupling, or tunnelling strength, between the two sites. Once the Hamiltonian is specified and the rotating wave approximation is used, the procedures outlined in the previous section can be followed to trace out the environments and derive the reduced system master equation. That is, the Redfield equation without secular approximation under Markovian approximation (Zhang and Wang, 2014) is derived. The analytical expressions for the elements in $\mathcal{M}$ are given in reference (Zhang and Wang, 2014). For a system coupled to a Fermionic environment, one can follow a similar procedure and obtain another reduced master equation (Zhang and Wang, 2014).

a. Curl quantum flux versus nonequilibriumness and tunnelling at steady state Following the procedure outlined in the previous section, one can decompose the driving force for the population evolution quantified by the kinetic transfer T-matrix into the following form (Zhang

and Wang, 2014, 2015a)

$$T=\begin{pmatrix}0 & \mathcal{A}_{gg}^{11}\rho_{gg} & \mathcal{A}_{22}^{gg}\rho_{22}\\ \mathcal{A}_{gg}^{11}\rho_{gg} & 0 & \mathcal{A}_{11}^{22}\rho_{11}\\ \mathcal{A}_{22}^{gg}\rho_{22} & \mathcal{A}_{11}^{22}\rho_{11} & 0\end{pmatrix}+\begin{pmatrix}0 & 0 & \mathcal{J}_q\\ \mathcal{J}_q & 0 & 0\\ 0 & \mathcal{J}_q & 0\end{pmatrix} \quad (64)$$

where the flux is $\mathcal{J}_q=\mathcal{A}_{22}^{11}\rho_{22}-\mathcal{A}_{11}^{22}\rho_{11}$. In Eq.(64) the first part of the transfer matrix describes the equilibrium under detailed balance and the second part represents the circular flow called the "curl nonequilibrium quantum flux," which is crucial for quantum transport. The analytical expressions for quantum flux can be derived for energy transport in bosonic and fermionic environments (Zhang and Wang, 2014)

$$\mathcal{J}_q^b=\frac{2\Gamma}{\hbar^2}\frac{v^b\frac{\Delta^2}{\hbar^2\omega^2}}{1+4u^b\frac{\Delta^2}{\hbar^2\omega^2}},\quad \mathcal{J}_q^f=\frac{2\Gamma}{\hbar^2}\frac{v^f\frac{\Delta^2}{\hbar^2\omega^2}}{1+4u^f\frac{\Delta^2}{\hbar^2\omega^2}} \quad (65)$$

where the forms of functions of u and v are given as

$$\begin{aligned}
v^b&=\frac{\left(n_\varepsilon^{T_2}-n_\varepsilon^{T_1}\right)\left(\bar{n}_\varepsilon+2\right)}{\left(1+2\bar{n}_\varepsilon+3n_\varepsilon^{T_1}n_\varepsilon^{T_2}\right)\left[1+\frac{\Gamma^2}{\hbar^4\omega^2}\left(\bar{n}_\varepsilon+2\right)^2\right]}\\
u^b&=\frac{\left(\bar{n}_\varepsilon+2\right)\left(3\bar{n}_\varepsilon+2\right)}{4\left(1+2\bar{n}_\varepsilon+3n_\varepsilon^{T_1}n_\varepsilon^{T_2}\right)\left[1+\frac{\Gamma^2}{\hbar^4\omega^2}\left(\bar{n}_\varepsilon+2\right)^2\right]}\\
v^f&=\frac{\left(n_\varepsilon^{\mu_2}-n_\varepsilon^{\mu_1}\right)\left(2-\bar{n}_\varepsilon\right)}{\left[1+\frac{\Gamma^2}{\hbar^4\omega^2}\left(2-\bar{n}_\varepsilon\right)^2\right]\left(1-n_\varepsilon^{\mu_1}n_\varepsilon^{\mu_2}\right)}\\
u^f&=\frac{\left(1-\frac{\bar{n}_\varepsilon^2}{4}\right)}{\left[1+\frac{\Gamma^2}{\hbar^4\omega^2}\left(2-\bar{n}_\varepsilon\right)^2\right]\left(1-n_\varepsilon^{\mu_1}n_\varepsilon^{\mu_2}\right)}
\end{aligned} \quad (66)$$

where $\bar{n}_\varepsilon\equiv n_\varepsilon^{T_1}+n_\varepsilon^{T_2}$ or $n_\varepsilon^{\mu_1}+n_\varepsilon^{\mu_2}$ and the f and b superscripts represent fermionic and bosonic versions of the functions respectively. The variable $n_\varepsilon^T=\frac{1}{e^{\frac{\varepsilon}{kT}}-1}$ is the particle occupation for bosons with energy ε at temperature T, while $n_\varepsilon^\mu=\frac{1}{e^{\frac{\varepsilon-\mu}{kT}}-1}$ is the particle occupation for fermions with energy ε at chemical potential μ and temperature T.

The function v as the occupation difference provides a measure for the effective voltage and detailed balance breaking induced from environments. Therefore, the effective potential v is directly related to the temperature difference of the bosonic baths or the chemical potential difference of the fermionic baths. The function u is a modulation factor for the flux and transport efficiency. As seen when the temperature difference or chemical potential difference is zero for the two baths, the effective voltage is zero, the flux is zero and the detailed balance is preserved. Therefore, v quantifies the degree of nonequilibriumness away from the equilibrium. The definition of others are given in (Zhang and Wang, 2014). One sees that the nonequilibrium quantum flux is governed by two ingredients: the nonequilibriumness and tunnelling for driving transport.

b. Enhancement of steady state coherence and entanglement from nonequilibriumness From the reduced quantum master equation, one can quantify the steady state quantum flux and the coherence to uncover their relationship (Zhang and Wang, 2014): $\mathcal{J}_q^{b(f)}=\frac{2\Delta}{\hbar}\times|\mathrm{Im}\rho_{12}|$. From this, one can conclude that at fixed tunneling strength, the increase in nonequilibrium flux will lead to a linear increase in steady state coherence. One can also find

$$|\mathrm{Im}\rho_{12}|=\frac{\Gamma v}{\hbar^2\omega}\frac{\frac{\Delta}{\hbar\omega}}{1+4u\frac{\Delta^2}{\hbar^2\omega^2}} \quad (67)$$

Steady state quantum coherence is promoted by the nonequilibrium effective voltage from the difference in two temperatures or chemical potentials of the environments at fixed tunneling, in contrast to the system coupled to a single environment, often with decoherence at equilibrium state. These two environments can create nonequilibriumness for maintaining non-zero quantum coherence, suggesting a possible application to quantum information devices for keeping coherence through nonequilibrium driving. (Zhang and Wang, 2014). On the other hand, to describe quantum entanglement, a quantum state must be described for the entire system. In other words, the quantum state of each system component such as a particle or quibit cannot be described independently from the rest of the system.Entanglement can be quantified by concurrence for low dimensional systems and negativity for high dimensional systems (K., 1998; Zyczkowski et al., 1998). It has recently been shown that steady state entanglement can be enhanced by nonequilibriumness, characterized by a temperature difference or chemical potential difference between environments (Eisler and Zimboras, 2005; Lambert et al., 2007; Quiroga et al., 2007; Sinaysky et al., 2008; Wang et al., 2018; Wu and Segal, 2011). It is worth mentioning that the off-diagonal elements of the steady state density matrix in the localized basis is zero when nonequilibrium voltage, and therefore flux, is zero. This is even true when we change to the eigenstate delocalized basis, though not necessarily general for other systems because the coherence is basis dependent. In either case, the steady state coherence and entanglement can be enhanced by pushing the system further from equilibrium. For the example of spin chains, nonequilibriumness also enhances dynamical coherence, entanglement, and fidelity (Zhang et al., 2017). One way of understanding this is by considering the global nature of the nonequilibrium flux spanning the state space, leading to enhancement of the quantum global nature characterized by coherence.

c. Quantum energy transfer efficiency at steady state Energy transfer efficiency can be introduced in terms of the steady state quantum flux (Zhang and Wang, 2014) so

that $\eta = \mathcal{J}_q/(\mathcal{J}_q + \mathcal{A}_{22}^{gg}\rho_{22})$. Then,

$$\eta^b = \frac{\left(n_\varepsilon^{T_2} - n_\varepsilon^{T_1}\right)\frac{\Delta^2}{\hbar^2\omega^2}}{n_\varepsilon^{T_2}\left[B\left(T_1,T_2,\omega\right) + \left(\bar{n}_\varepsilon + 2\right)\frac{\Delta^2}{\hbar^2\omega^2}\right]}$$
$$\eta^f = \frac{\left(n_\varepsilon^{\mu_2} - n_\varepsilon^{\mu_1}\right)\frac{\Delta^2}{\hbar^2\omega^2}}{n_\varepsilon^{\mu_2}\left[F\left(\mu_1,\mu_2,T,\omega\right) + \left(2 - \bar{n}_\varepsilon\right)\frac{\Delta^2}{\hbar^2\omega^2}\right]} \quad (68)$$

where the definition of two functions B and F are given in reference (Zhang and Wang, 2014). At fixed tunneling, the environments characterized by temperature or chemical potential difference enhance the transfer efficiency. Tunneling also increases the efficiency. The transfer efficiency is significantly higher for fermionic environments due to Pauli exclusion principle. (Zhang and Wang, 2014)

d. Dissipation and quantum thermodynamics at steady state

Heat dissipation through heat current and entropy production rate (EPR) measures the thermodynamic cost of transport. From the first and second laws of thermodynamics with energy conservation and the positivity of total entropy production in the nonequilibrium process, one sees $\dot{Q}_1 - \dot{Q}_2 = \dot{E}$ and $\dot{S_{env}} + \dot{S} = \dot{S_{tot}}$. $\dot{Q}_1 = Tr[H_S D^1(\rho_s)]$ and $\dot{Q}_2 = Tr[H_S D^2(\rho_s)]$ are the energy flowing into the system from high-temperature and low-temperature environments, respectively, and D^1 and D^2 are the dissipation operators from system-environment (1 and 2) coupling.(Werlang et al., 2014; Zhang and Wang, 2015a). $\dot{S}$ and $\dot{S_{tot}}$ are the rate of system entropy and total entropy production, respectively. Increasing nonequilibrium voltage enhances heat current $\dot{Q}$ and thermodynamic cost via entropy production $\dot{S}_{tot} = -\frac{\dot{Q}_1}{T_1} + \frac{\dot{Q}_2}{T_2}$, (Zhang and Wang, 2014, 2015a), closely related to the presence of quantum curl flux for driving nonequilibrium quantum dynamics.

2. Long time quantum coherence and efficient energy transport of the light-harvesting complex

The light-harvesting complex is a protein complex that increases the number of absorbed photons by the photosystem of photosynthetic organisms through transferring energy and electric charges efficiently to the photosynthetic reaction center. Experiments suggest that this process involves long-time quantum coherence at ambient temperatures (Garab, 1999; Lee et al., 2007). Great efforts have been taken towards understanding the mechanism underlying efficient energy transfer by the light-harvesting complex (Chen et al., 2013; Chin et al., 2013; Dorfman et al., 2013; Jang, 2011; Novelli et al., 2015).

In energy transfer, electronic excitons are coupled with molecular vibrational phonon environments. The two-site model mentioned earlier can be generalized to the N-site excitonic system (with $H_{sys_{ext}}$) connected by tunneling coupled (with H_{int}) to the phonon (with $H_{env_{phonon}}$) and the environment at room temperature and radiation environment at a higher temperature (with $H_{env_{rad}}$) by the energy function $H = H_{sys_{ext}} + H_{env_{rad}} + H_{env_{phonon}} + H_{int}$ (Zhang and Wang, 2016). Previous investigations often assumed that the phonon environments fluctuate much faster than the excitation system where the effect of phonons can be averaged. However, recent studies show that some discrete intramolecular vibrations have a lifetime similar to that of excitons (Christensson et al., 2012; Kolli et al., 2011; Tiwari et al., 2013; Womick and Moran, 2011). Therefore, phonon dynamics can have a crucial effect on energy transport when the energy quanta of vibrational modes are in resonance with energy splitting of excitons (Chin et al., 2013; O'Reilly and Olaya-Castro, 2014; Plenio et al., 2013; Romero et al., 2014). The persistence of quantum coherence originating from exciton-phonon coupling has been observed in experiments (Novelli et al., 2015).

The effects of quasi-resonant coupling between excitons and phonons for the lifetime of quantum coherence has been studied in an effective analytical theory (Zhang and Wang, 2016). There, a general scenario was investigated in which bare electrons/excitons are surrounded by discrete and continuous vibrational phonon modes and radiation environments. That is, $H_{env_{phonon}} = H_{env_{phonon_{discrete}}} + H_{env_{phonon_{continuous}}}$.The near resonant coupling between the electron/exciton system and discrete phonon modes can lead to strong interactions and the formation of polarons. In this case, the discrete vibrational modes originally from the phonon environments no longer weakly interact with the exciton system. Instead, due to strong interactions with the excitons they become part of the system in the form of composite as polarons, while the remaining phonon modes effectively become the new environments, along with the radiation baths.

In more details this leads to the effective Hamiltonian $\tilde{H_{eff}} = H_S + H_{ph} + H_{env_{rad}} + H_{int}$ (Zhang and Wang, 2016). H_S involves the renormalized exciton on-site energy, phonon mediated exciton-exciton interactions, the electronic coupling renormalized by the discrete exciton-vibrational interactions. H_{ph} denotes the energy of the remaining phonon environments. The discrete phonon modes strongly interact with excitons and form polarons characterized in the last term in H_S. H_{int} describes the coupling of the new composite polarons to the remaining phonon modes.

Because of the off resonances between the residual vibrational modes and the energy splitting of excitons, the resulting polarons are only weakly coupled to the remaining phonon environments (Chen et al., 2013; Chin et al., 2013; Dorfman et al., 2013; Grover and Silbey, 1970; Jang, 2011; O'Reilly and Olaya-Castro, 2014; Plenio et al., 2013; Romero et al., 2014; Zhang and Wang, 2016). The weak coupling of polarons to the remaining phonon environment leads to less dissipation and can

thus sustain quantum coherence significantly longer than the bare excitons alone, shown in Fig. 5(b). However, coherence alone can not guarantee efficient energy transfer. For this, detailed balance must be broken from the coupling of the light-harvesting complex to the nonequilibrium environments; for example, a coupling of high-temperature photons and low temperature vibrational modes to the protein can funnel the path and subsequently facilitate the coherent and unidirectional energy flow of excitations to the photosynthetic reaction center, Fig. 5 (c) (d) (Zhang and Wang, 2016). While the long time survival of dynamical coherence is dominated by the suppression of exciton-environment interaction, the nonequilibriumness is crucial for efficient energy transfer (Fig. 5 (c)) and the steady state coherence (Fig. 5 (d)) (Harbola et al., 2006; Zhang and Wang, 2014, 2015c, 2016).

IV. GENE REGULATORY CIRCUIT MOTIFS AND EXPERIMENTAL QUANTIFICATION OF LANDSCAPES

Genes encode for proteins, which provide the fundamental infrastructure for a functional cell. A certain class of proteins called transcription factors feed back on the expression of genes by binding to specific sites on the DNA called promoters, thus altering the rate of transcription. Specifically, 'activators' increase the rate, whereas 'repressors' inhibit expression. Together, genes and transcription factors form complex regulatory networks that have profound functional roles, for example, in decision making, differentiation and development. In addition to naturally existing networks, synthetic counterparts are now routinely implanted into living cells.

A. Naturally existing circuit motifs: lambda phage and bacteria competence

We use bacterial phage infection and natural competence as representative examples to highlight nonequilibrium behaviors of endogenous gene networks.

1. Landscape quantification of cell fates and their decision making of lambda phage

Lamda phage is a bacterial virus that infects the bacterium *Escherichia coli* (Balázsi and Collins, 2011; Ptashne, 2004b). The infection process involves three steps, including phage attachment to the bacterial cell wall, injection of its DNA into the host, and execution of its transcriptional circuitry, which then determines the next step the system will undertake. Specifically, the phage can either integrate its own DNA into the host chromosome in a process referred to as the lysogenic phase. Alternatively, the phage triggers the lytic cycle of self-replication and assembly, eventually causing lysis of the host.

The decision of the lambda phage to enter the lysogenic or lytic cycle is enabled through an underlying switch controlled by the two genes *cI* and *cro*. The two genes encode the transcriptional repressor proteins CI and Cro (Fig. 6a) (Ptashne, 2004b). In lysogeny, *cI* is expressed, while in lysis, *cro* is expressed.

Together, mutual repression of the two genes through transcriptional factor binding at a shared promoter constitutes the core of this two-state switch, although there are additional processes involved in viral decision making (Oppenheim et al., 2005; Ptashne, 2004b).

The nonequilibrium landscape provides a profound physical understanding of the lambda phage switch. The landscape can be inferred from the steady-state protein distribution, which can be obtained by simultaneous fluorescent labeling of several gene products and tracing the expression of individual genes over time (Elowitz et al., 2002; Yu et al., 2006). Note that due to the distinct maturation times of different fluorescent labels, care has to be taken to interpret these data. A co-localization method was suggested to resolve the issue (Fang et al., 2018; Pogliano et al., 2001), which is based on using the same fluorescent labels for different genes, but in different cellular locations.From the real time traces of the two gene expression levels, one can obtain joint histograms and therefore quantify the landscape directly from these experiments. The possible cell fates can then identified with the attractors of the landscape and the cell-fate decision-making process can be quantified by investigating the transitions between the corresponding basins of attraction (Balazsi et al., 2011; Fang et al., 2018; Li and Wang, 2013, 2015; Wang et al., 2010b, 2011; Xu et al., 2014b).

For the lambda phage switch, the underlying nonequilibrium landscape of CI and Cro shows four distinct states of (CI, Cro) with (high, low), (low, high), (high, high) and (low, low) expression levels (Fang et al., 2018), shown in Fig. 7a. The lysogenic and lytic cycles are associated with the (high, low) and the (low, high) states, respectively. In a system when the effective binding and unbinding rates of the transcription factors to the genes are large compared to their synthesis and degradation rates, in the so called adiabatic limit, one expects either high levels of CI with low levels of Cro or *vice versa*. The existence of two additional states is thus surprising (Little and Michalowski, 2010; Ptashne, 2004a). In a system where the effective binding and unbinding rates of the transcription factors to the genes are slower than or comparable to their synthesis and degradation rates, the system is in the non-adiabatic limit and thusall four states of (high, low), (low, high), (high, high) and (low, low) are expected from the effective weaker gene regulations(Chen and Wang, 2016; Feng et al., 2011; Feng and Wang, 2012; Hornos et al., 2005; Li and Wang, 2014b;

Schultz et al., 2007b; Zhang et al., 2013).

The landscape obtained from the joint histogram of the real time trace of CI and Cro contains additional information that can be extracted by considering the basins of attraction of the four states. Each basin has a different depth and width, and the barriers between each basin also differ from each other, which implies distinct transition rates between the various states, Fig. 7b. The residence times of individual states and switching times between states can be obtained from the experimental real-time traces of the CI and Cro expression levels by means of a hidden Markov model (Schliep et al., 2003). Perhaps less obviously, one can also infer the processes underlying switching. For example, switching from the (low, high) to the (high, low) state occurs preferentially via the (high, high) state rather than directly (Fang et al., 2018; Schultz et al., 2007b).

The new method of co-localization enables experimental monitoring the real time traces of the CI and Cro genes simultaneously. This leads to quantification of cell fate decision-making processes in terms of the underlying nonequilibrium landscape and nontrivial cell fate states as well as associated switches in response to environmental and genetic influences on gene regulation.

2. Bacterial competence

The transition of *Bacillus subtilis* from a vegetative state in which it reproduces asexually to a competent state in which it can take up DNA from the extracellular milieu is another example of a bacterium switching between two states (Grossman, 1995; Schultz et al., 2007a). When facing nutrient limitation, *B. subtilis* cells often develop into spores, whereas a small fraction of the population is competent to use exogenous DNA as food source or as genetic material for an enhanced mutation rate and evolvability. In this case, however, making a decision between different fates does not rely on a genetic switch, but rather on an excitable network. The underlying competence regulatory circuit is centered around ComK, a master regulator that activates the expression of a set of competence genes (Fig. 6b) (Süel et al., 2006). ComK activates its own production, whereas its degradation is subject to the multi-component molecular complex MecA. At the same time, ComK degradation is suppressed by ComS, a peptide that competes with ComK for the MecA complex. Additionally, there is an indirect negative feedback between ComK and ComS.

Together, ComK, ComS, and the MecA complex form an entangled regulatory network that involves both negative and positive feedback. That network can generate excitable dynamics involving pulses of ComK production and hence bacterial competence (Süel et al., 2006, 2007). Starting from a stochastic increase, the ComK level is amplified by autoregulation and then quickly increases to a maximal ComK expression, which leads to the transition to competence. At the same time, a high level of ComK causes the suppression of ComS production, which, in turn, causes rapid ComK degradation by the MecA complex and eventually termination of the ComK pulse. Because of molecular noise in the system, ComK excitation occurs continuously. A theoretical model was suggested to account for the noise controlled nonequilibrium transitions into and out of competence, with non-adiabaticity of comparable time scale of binding/unbinding relative to the synthesis/degradation. Taking non-adiabaticity into account allows the model to better align withexperiments (Grossman, 1995; Schultz et al., 2007a), which suggests again that non-adiabatic fluctuations can be crucial for biological functions.

B. Synthetic regulatory circuit motifs: genetic switch and oscillation, self regulator

With the advent of synthetic biology, a vast array of engineered gene networks have been successfully created since the year 2000. Examples include switches, oscillators, communication modules, patterning devices and others which are often out of equilibrium (Cameron et al., 2014).

1. Genetic switches

The toggle switch constructed by Collins and colleagues (Gardner et al., 2000) is a simplified version of the lambda phage switch discussed above. It consists of two genes that encode transcriptional repressors and two corresponding (or 'cognate') promoters. The genes and promoters are arranged to allow the repressor encoded from one gene to inhibit the expression of the other and *vice versa*, thus creating a circuit of mutual inhibition (Fig. 8a).

The mutual suppression topology of the network can, in principle, generate bistability, a dynamic property that enables the existence of two stable states of a system. Indeed, the circuit remains stable in both a state of high expression of one gene and low expression of the other and a state with the inverse expression profile, Fig. 8a. At the population level, the cells exhibit a bimodal distribution characteristic of a bistable system.

Two coupled negative feedback loops are topologically equivalent to a single positive feedback loop (Qi et al., 2013). Thus, the bistability demonstrated by the toggle switch should be possible in a network involving a single, self-activating gene. This idea was tested by creating an autoregulatory circuit using the right operator site of lambda phage and the *cI* gene (Fig. 8b) (Isaacs et al., 2003).

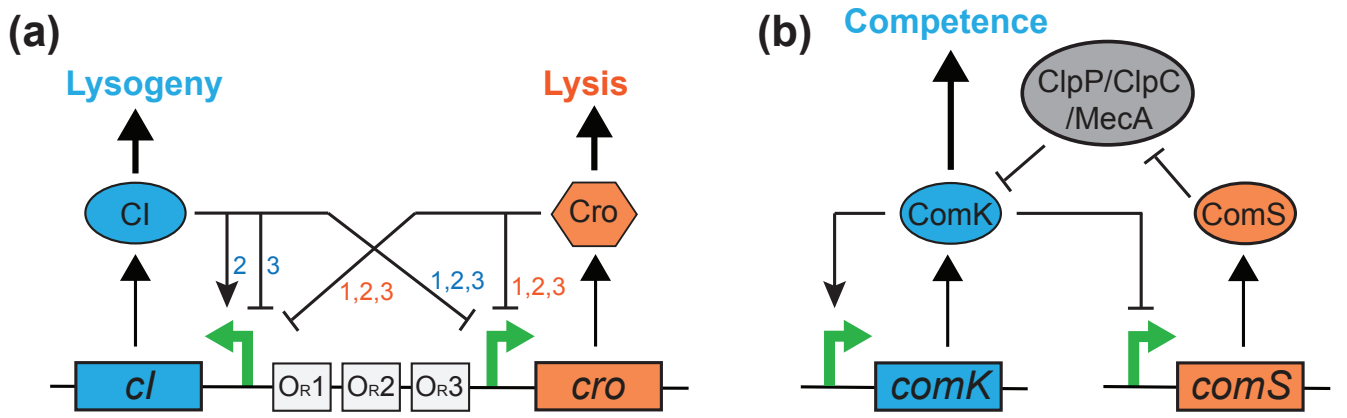

FIG. 6 Examples of natural gene regulatory networks. (a) The genetic switch between the lytic and the lysogenic life cycles of the bacterial phage λ (Ptashne, 2004b). CI is expressed in the lysogenic cycle and Cro is expressed in the lytic cycle. (b) The gene network underlying competence in *Bacillus subtilis* (Süel et al., 2006). ComK is a master regulator of competence; ComS inhibits ComK degradation by the ClpP-ClpC-MecA complex.

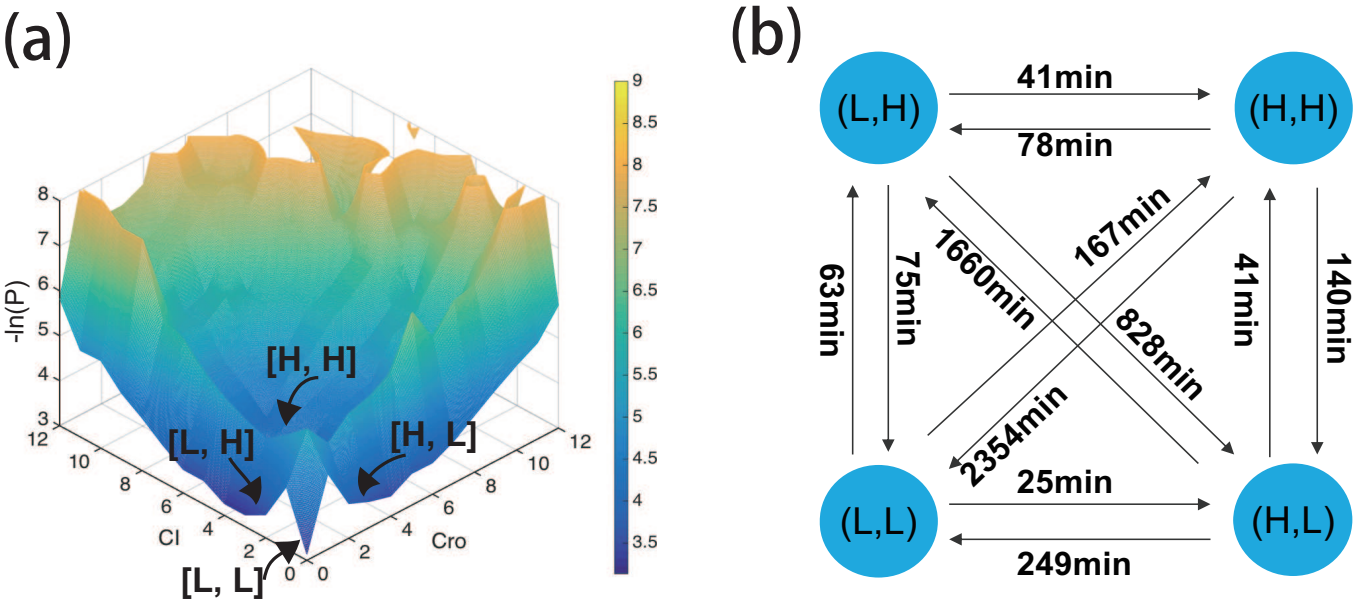

FIG. 7 Nonequilibrium landscape and switching times of Lambda Phage: (a) 2D histogram as the landscape of CI and Cro production per 5 min. (b) Switching times between states of (Cro, CI)as (L,H),(L,L),(H,L),(H,H).(from Ref. (Fang et al., 2018)).

2. Self repressor and experimental quantification of landscape

In extant gene regulatory networks, self-repression is much more common than self-activation (Alon, 2007). This motif can accelerate responses and increase the robustness of steady state expression level. In the adiabatic case, when binding and unbinding of the repressor are fast compared to its synthesis and degradation (Ackers et al., 1982), the dynamic effect of regulatory binding to and unbinding from the promoter averages out and a landscape with a single basin of attraction emerges. In contrast, if binding and unbinding are of the same order or slower than synthesis and degradation, the gene has some chance of being expressed despite the presence of repressor proteins. In this case,states of high expression, in addition to the repressed low expression state, can appear (Feng et al., 2011; Hornos et al., 2005). For a bimodal distribution of the expression levels, one obtains a nonequilibrium landscape with two basins of attraction (Jiang et al., 2017).

Experimentally, a self-repressing gene circuit based on the P_{tet} promoter and its repressor TetR was de-

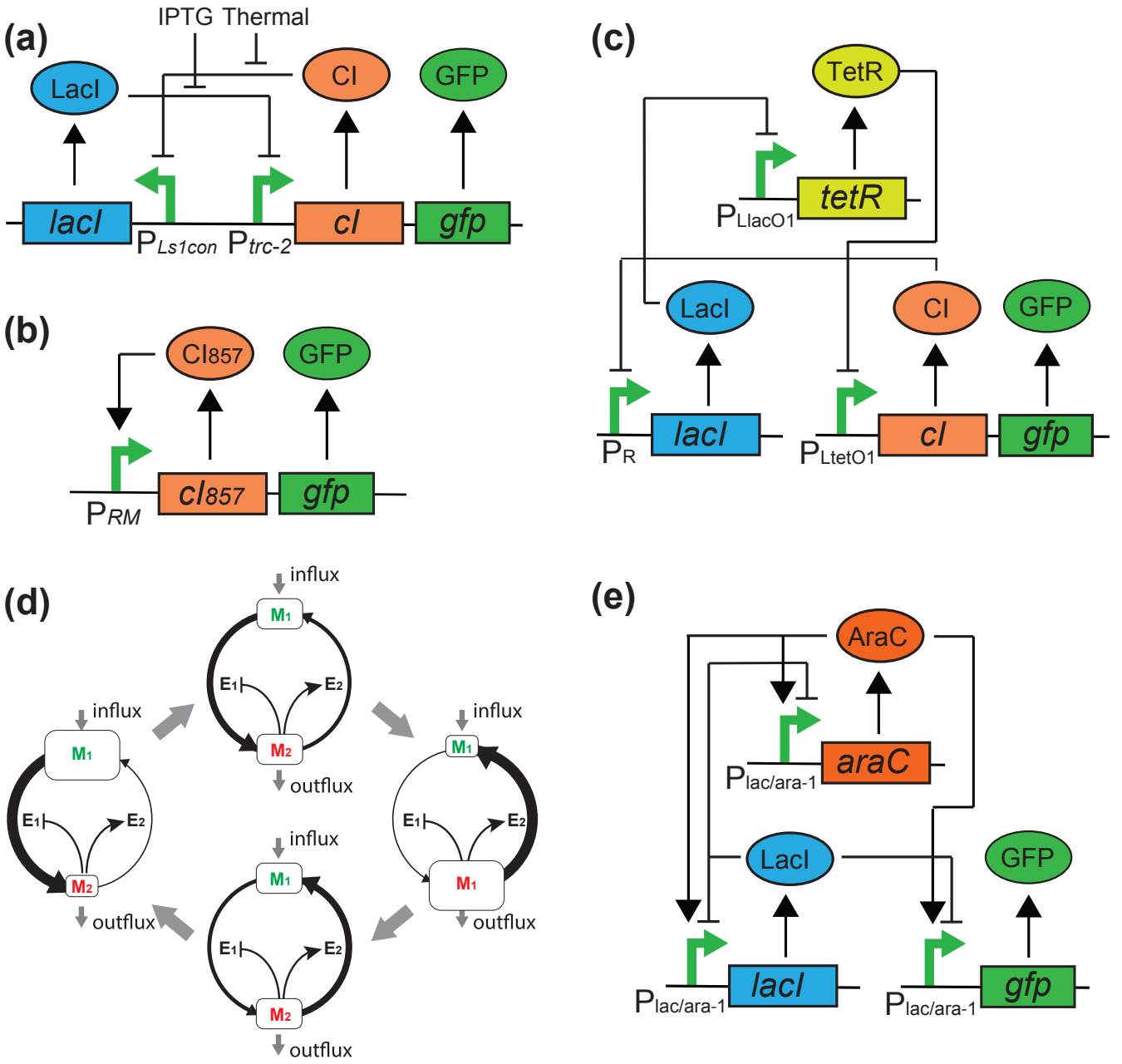

FIG. 8 Examples of synthetic nonequilibrium gene networks. (a) Genetic toggle switch (Gardner et al., 2000). (b) Auto-activation gene switch (Isaacs et al., 2003). (c) Repressive oscillator (Elowitz and Leibler, 2000). (d) A metabolic oscillator (Fung et al., 2005). (e) A fast and robust gene oscillator (Stricker et al., 2008).

signed and implemented in *E. coli* (Nevozhay et al., 2009; Ramos et al., 2005). Repressor binding can be controlled by a so-called inducer, a molecule that binds to the repressor to reduce its binding affinity. As a result, the distributions of TetR expression change with the inducer concentration, Fig. 9. With increasing inducer concentrations, the mean repressor concentration increases as binding of the inducer effectively reduces the affinity of the repressor for the promoter and the system eventually becomes nonadiabatic. For inducer concentrations above a critical level, the experimental expression distribution becomes bimodal. The landscape can thus be quantified as described above. The residence times in each state and associated switching rates can be obtained through real time trace analysis using a hidden Markov chain model (Jiang et al., 2017).

The two typical TetR concentrations in the bimodal case correspond to different cell fates. Through the real-time traces of TetR concentrations, one can quantify the landscape of cell fates and the associated decision making

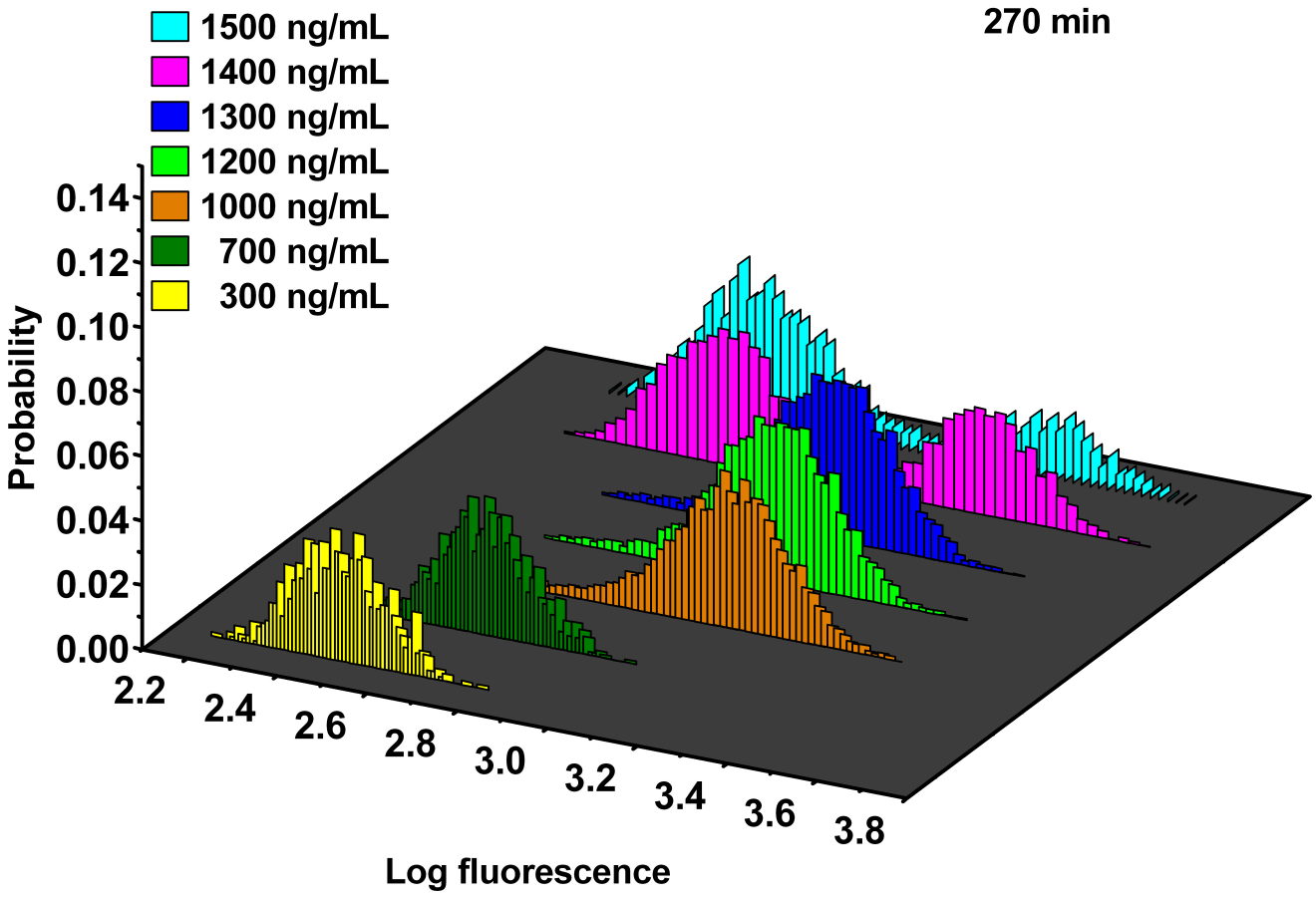

FIG. 9 Experimental expression distributions of the self-repressing gene circuit (MG::PR-8T) at different aTc concentrations observed under a microscope. (from Ref. (Jiang et al., 2017)). The negative logarithm of the distribution quantifies the landscape

(switching) speed between the fates (Jiang et al., 2017) related to the life time of each state.

3. Genetic oscillators

Adding one more repressor to the toggle switch discussed above, such that cyclic chain of repressors R_i represses R_{i+1}, alters the behavior significantly. Explicitly, when R_1 represses R_2, R_2 represses R_3, and R_3 represses R_1, a network called the repressilator is formed that can generate spontaneous oscillations (Elowitz and Leibler, 2000) (Fig. 8c). Quantitative analysis of the system suggests that in addition to sustained limit-cycle oscillation shown in the above experiment, the circuit exhibits different dynamic modes, including damped oscillations and bistability depending on parameter values. Indeed, the latter two types of dynamics were observed in another synthetic circuit implemented in *E. coli* (Atkinson et al., 2003). Oscillations can be generated not only by synthetic gene networks but also by metabolic networks. In a study by Fung *et al* (Fung et al., 2005), an oscillatory circuit called the metabolator was created by integrating cellular metabolism with transcriptional regulation (Fig. 8d).

The above examples demonstrated that oscillation can be generated using rationally designed circuits. However, they all are subject to a common challenge - each lacks circuit performance robustness. This difficulty was addressed by Stricker *et al* by creating a persistent genetic oscillator (Stricker et al., 2008) (Fig. 8e) that involves an activator gene *araC* and a repressor gene *lacI* that are co-regulated by a hybrid promoter $P_{lac/ara-1}$. The resulting intertwined positive and negative feedback loops confer the circuit robust oscillations (Feng et al., 2012). In experiment, the circuit was found to oscillate over a wide range of experimental conditions (Stricker et al., 2008). Thus, it will be interesting to explore the relationship between the circuit structure and the landscape/flux topography underlying robust oscillations.

V. GENE REGULATORY NETWORK: CELL CYCLE

The cell cycle encompasses key processes of life, from growth and DNA replication to division (Morgan, 2007). Many diseases involve cell cycle dysfunction; for example, cancer cells grow faster and divide more frequently than healthy cells (Weinberg, 2007). The eukaryotic cell cycle consists of two coordinated phases of growth, interphase and division (Morgan, 2007). The Interphase is distinguished further into a first gap phase, G_1, during which the cell accumulates mass; a synthesis phase, S, during which the DNA is replicated; and a second gap phase, G_2, during which the cell continues to grow. During the subsequent division or mitosis phase, M, the cell typically divides into two daughter cells. Progression through the cell cycle is tightly controlled by genetic networks (Chen et al., 2004; Li and Wang, 2014a; Sveiczer et al., 2004; Wang et al., 2010a). From a physics perspective, genetic control of the cell cycle is naturally considered as a limit cycle.This is indeed the case for the cell cycle of embryonic frog cells (Ferrell Jr. et al., 2011). For yeast and mammalian cells, several scenarios have been proposed, including treating the cell cycle as a discrete attractor (Li et al., 2004a), using bifurcations (Chen et al., 2004; Sveiczer et al., 2004), and using the limit cycle approach (Grard and Goldbeter, 2009; Li and Wang, 2014a; Lv et al., 2015; Wang et al., 2010a).

A. Embryonic cell cycle in frogs

As mentioned in Sec. III.B, limit cycle oscillations typically rely on a negative feedback loop. For the cell cycle in embryonic cells of the African clawed frog *Xenopus laevis*, the core negative feedback involves two genes. One of them encodes for a cyclin, while the other codes for the cyclin-dependent kinase Cdk1. Although the complete network is rather involved, the essence of the network can be captured by a two-component model (Tsai et al., 2014; Yang and Ferrell, 2013), which can be cast into two ordinary differential equations for the cyclin concentration Cyc and the Cdk1 concentration $Cdk1$, given by

$$\frac{d}{dt}Cyc = k_{\rm s} - k_{\rm d}Cyc \tag{69}$$

$$\frac{d}{dt}Cdk1 = k_{\rm s} + k_{\rm cdc}(Cyc - Cdk1) - (k_{\rm Wee1} + k_{\rm d})\,Cdk1. \tag{70}$$

The first equation describes the synthesis and degradation of cyclin with respective rates $k_{\rm s}$ and $k_{\rm d}$. Whereas $k_{\rm s}$ is constant, $k_{\rm d}$ increases with increasing Cdk1 concentration. The dependence is captured by a Hill function

$$k_{\rm d} = a_{\rm d} + b_{\rm d}\frac{Cdk1^n}{K^n + Cdk1^n}, \tag{71}$$

where K is the value at which the Cdk1-dependent part has reached half of its maximal value. The Hill exponent n has a high value, which makes the dependence on Cdk1 ultrasensitive. Equation (70) describes activation and inactivation of Cdk1. The rates $k_{\rm cdc}$ and $k_{\rm Wee1}$ depend on $Cdk1$ in a sigmoidal fashion described by a Hill function with proper values of K and n. These dependencies effectively account for the influence of other components in the cell cycle network.

The ultrasensitive dependence of the rates on Cdk1 leads to a time delay in the effect of Cdk1 on degradation. Cyclin first accumulates, accompanied by a moderate increase of Cdk1. After Cdk1 has passed a threshold, its activation is dramatically increased, which leads to a dramatic decrease in the amount of cyclin and simultaneously a dramatic deactivation of Cdk1, upon which cyclin accumulates again.

As explained in Sec. II.A.2, one can characterize the dynamics of Eqs. (69) and (70) in terms of a nonequilibrium potential landscape and a rotational curl flux (Zhang and Wang, 2018), Fig. 10. The landscape presents two attractor basin valleys and two saddle points with a narrow, stretched bottom basin valley. The G0/G1 phase and S/G2 phase are quantified on each side of the basin valley and the top basin valley quantifies the M phase. The state s_1 corresponds to a transition from M to G0/G1 when a cell matures and division occurs. The s_2 transition state corresponds to the transition from S/G2 to M, which can guarantee that DNA replication is achieved before reaching the next phase M. These transition phases are associated with so-called "check points" that assure the cell is ready to enter the next phase of the cycle. The system is periodically driven by rotational curl flux from one basin of attraction to the other via s_1 and s_2. While the landscape guarantees stability of the cell cycle path, the rotational curl flux guarantees the stable flow. This gives a global, physical picture of the cell cycle seen in several species (Li and Wang, 2014a; Luo et al., 2017; Wang et al., 2010a; Zhang and Wang, 2018).

Note that the speed at which the cycle is traversed depends on both the rotational curl flux and the transition states; this speed, and thus the cell cycle itself, is greatly accelerated for cancerous cells. The energy pump is the origin of the flux and energy dissipation in terms of the nutrition supply. To slow the cell cycle speed down for treatment, one can thus either decrease the flux by limiting the supply of nutrients or increase the barrier of check points by adjusting the associated key regulators.

B. Origins of single cell life through replication by energy pump

The cell cycle speed correlates quantitatively with energy dissipation (Li and Wang, 2014a; Wang et al., 2008; Zhang and Wang, 2018) which, as mentioned earlier, is directly related to the degree that detailed balance is

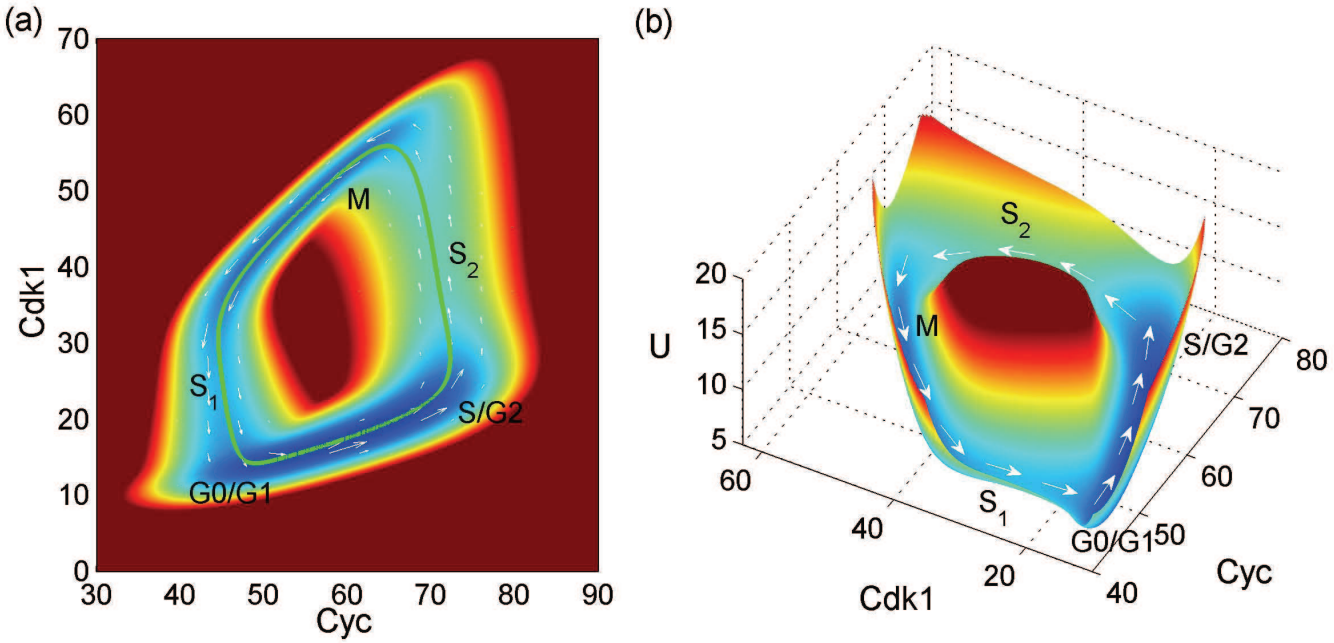

FIG. 10 Nonequilibrium landscape U and flux (arrows) for the cell cycle dynamics (69) and (70) in 2D (a) and 3D (b). The different phases of the cell cycle are indicated. From (Zhang and Wang, 2018).

broken. A faster progression through the cell cycle requires more energy consumption, plus there is an energy threshold to overcome in forming a stable cell cycle. Replication is a signature feature of living systems. As seen here, replication cannot proceed without an energy pump. Therefore, a necessary condition for life to begin is that an energy pump into the system must exist.The nonequilibriumness in thermodynamics and associated dynamics in terms of flux are thus required and can be quantified for the origin of single cell life (Englander, 2013; Li and Wang, 2014a; Wang et al., 2008; Zhang and Wang, 2018). Life may begin from cycles. The complexity of life may be built form multiplicative cycles and their associations.

C. Cell cycle in fission yeast

The gene regulatory network controlling the fission yeast cell cycle is complex and involves hundreds of genes (Sveiczer et al., 2004). Even a simplified network based on experimental studies still involves 10 key genes (Davidich and Bornholdt, 2008), Fig. 11(a). This network can be further simplified by reducing the states of individual genes to two: on or off. Boolean networks are particularly well-suited to explore the global dynamics and wiring topology of networks (Han and Wang, 2007, 2008; Kauffman, 1969; Li et al., 2004b). The corresponding boolean network for yeast cell cycle determination is a discrete, dynamic system with 2^{10} states.

In the presence of fluctuations, one can follow the master equation for the stochastic evolutionary dynamics of the fission yeast cell cycle. One can map out the landscape through the steady state solution of the corresponding master equation (8), where the transition rates T_{ij} are eventually determined by the original gene regulatory network. The resulting landscape has the form of a Mexican hat and the cell cycle path corresponds to the valley of the hat, Fig. 11(c). The cell cycle path is stable when states on the path have much lower potentials than those outside the path relative to the spectrum's standard deviation. This gap between potential minimum and average of other states not on the cell cycle, relative to variance, leads to a funneled potential landscape towards the cell cycle path and guarantees the stability, since states on oscillation path have much higher weights than other states. However, this analysis cannot guarantee directional flow for oscillations, Fig. 11 (c).

The steady state nonequilibrium probability flux provides a driving force in addition to the landscape gradient for nonequilibrium networks. Flux can be obtained from the steady state solution of the master equation based on the underlying gene regulatory networks (Han and Wang, 2007, 2008; Luo et al., 2017). As mentioned previously, the flux originates from the energy pump through nutrition supply. The nonequilibrium flux can be further decomposed into flux loops (Luo et al., 2017); doing so forms a nonequilibrium flux landscape. Fig. 11 (b) When there is a distinct separation between the nonequilibrium flux from the "native" biological cycle, Fig. 11, (b) and the rest relative to variance, the cell cycle becomes the dominant loop compared to the other possible loops, as

in Fig. 11 (d). Therefore, a funneled nonequilibrium flux landscape provides a physical mechanism to guarantee stable cell cycle flow (Luo et al., 2017).

By performing a global sensitivity analysis on the topography of the potential landscape and the flux loop landscape upon changes of genes and their mutual regulations, the identities of key genes and regulatory motifs for the network are revealed. This provides a possible way to control the cell cycle speed in the prevention or treatment of cancer.

It is worthwhile to note that the described gene network regulating cell cycle of *Xenopus* consists of two genes, though the described fission yeast network is much more complex and contains many more genes.This difference in the literature can be attributed to the fact that yeast has been studied as a model organism for decades, compared to *Xenopus*. Remarkably, similar cell cycle mechanisms are found in both organisms.

VI. CELLULAR STRUCTURE AND DYNAMICS

In this section, we turn to processes of intracellular organization. After discussing nonequilibrium aggregation and phase-separation phenomena, we focus on the cytoskeleton, the paradigmatic active gel that determines cell mechanical properties and drives vital cellular processes. Finally, we briefly address nonequilibrium aspects of cell signalling. Although landscape and flux theory has not been applied to cellular structure and dynamics due to technical challenges, other approaches such as those based on local thermal equilibrium, hydrodynamics, and active particle dynamics (Marchetti et al., 2013a; Wang and Wolynes, 2011) have been successfully applied to this exciting research area, which we briefly review.

A. Nonequilibrium phase separation

In animal and plant cells, important functional subunits are segregated into compartments surrounded by lipid bilayers. A plethora of proteins attach to and are embedded in these fluid membranes and can arrange into functional assemblies. In addition, there are important functional three-dimensional cellular subunits that lack a delimiting membrane. These structures can result from phase separation, with continuous exchange of matter and energy determining their size distributions and dynamics.

a. Lipid rafts There are two main equilibrium states of multicomponent lipid bilayers; well mixed or one in which the different kinds of lipids phase segregate into macroscopic domains of an extension that scales with the system size. For membranes of living cells, however, there is ample evidence for lipid microdomains of either varied composition or a different liquid phase compared to the environment. These microdomains are often called "rafts". Rafts have a comparatively small size of 10-200 nm and a lifetime of several milliseconds (Pike, 2006). At equilibrium, domains of this size should only exist in the presence of long-distance interactions (Seul and Andelman, 1995). A possible origin of such long-range interactions relevant for cells is a coupling between membrane curvature and lipid composition (Baumgart et al., 2003). Indeed, mixtures of lipids with different intrinsic curvatures have been observed to segregate into small budding domains (Baumgart et al., 2003). In mixtures of cholesterol and lipids with high and low melting temperatures, long-lived microdomains form, though these domains are probably caused by kinetic arrest in the coarsening process and are absent in the equilibrium state (Veatch and Keller, 2003).

Lipid nanodomains can robustly form via nonequilibrium processes, for example, in the presence presence of lipid exchange between the cytosol and the membrane (Fan et al., 2008; Foret, 2005; Gheber and Edidin, 1999; Turner et al., 2005) or of chemical reactions (Glotzer et al., 1995; Huberman, 1976). Let ϕ be the volume fraction of a lipid in a binary mixture with constant total density n_0. Then (Foret, 2005; Glotzer et al., 1995; Huberman, 1976)

$$\partial_t \phi = \mu \nabla^2 \frac{\delta F}{\delta \phi} - \frac{1}{\tau}\left(\phi - \bar{\phi}\right). \tag{72}$$

Here, μ is an effective mobility and F the corresponding free energy

$$F[\phi] = n_0 k_B T \int d^2\mathbf{r} \left[\frac{\xi_0^2}{2}\left(\nabla\phi\right)^2 + f\left(\phi\right)\right]. \tag{73}$$

For

$$f\left(\phi\right) = \phi \ln \phi + \left(1-\phi\right)\ln\left(1-\phi\right) + \chi\phi\left(1-\phi\right) \tag{74}$$

the first term in Eq. (72) is the familiar Cahn-Hilliard current. The parameter χ determines the strength of lipid-lipid interactions and demixing occurs for $\chi > 2$. The second term describes relaxation to the stationary density $\bar{\phi}$ with a characteristic time τ that is determined by the rates of lipid integration into the membrane and dissolution into the cytosol. For biologically relevant parameters, raft-like domains of sizes between 20 nm and 200 nm are formed for exchange times τ between 10^{-4} s and 1 s. Importantly, the mobility of cytosolic lipids is many orders of magnitude larger than for lipids in membranes, such that the spatial distribution of cytosolic lipids is essentially homogenous. In this way, dissociation leads to efficient mixing, which prevents the formation of macroscopic domains.

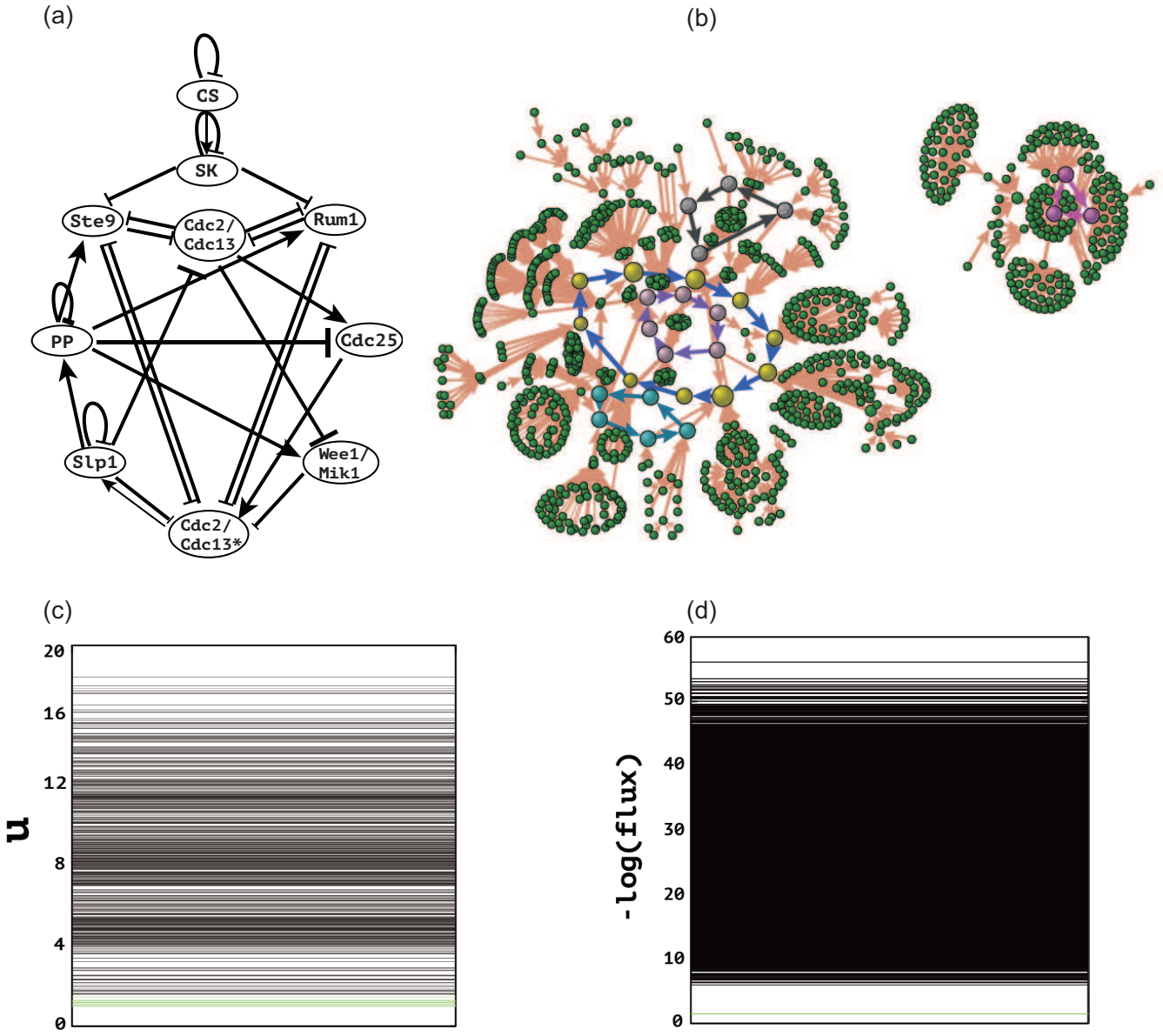

FIG. 11 (a) Simplified gene regulatory network of the fission yeast cell cycle. Arrows indicate activation, repressive interactions are indicated by −|. (b) Potential and flux landscapes. Each state is represented by a dot of a size representing their steady state probability, together forming the potential landscape. The flux landscape is represented by the different flux loops. The blue flux loop is the dominant one representing the biological oscillation path. (c) Potential landscape spectrum. The value of the potential landscape of each state is represented by a horizontal line. (d) Flux spectrum for all flux loops. The flux along each loop is represented by a horizontal line. In (c) and (d) the green lines correspond to the states and the flux loop of the "native" biological oscillation cycle path. From (Luo et al., 2017).

b. Clusters of membrane-associated proteins Through the preferential localization of proteins to specific lipids, the existence of lipid rafts implies the existence of protein clusters, for example protein coats during early phases of endocytosis (Faini et al., 2013), receptors (Maddock and Shapiro, 1993; Uhles et al., 2003), SNARE proteins (Low et al., 2006), and proteins involved in signaling (Bonny et al., 2016; Douglass and Vale, 2005; Fairn et al., 2011; Goswami et al., 2008; Tian et al., 2007). Mechanisms similar to those evoked to explain the formation of lipid rafts have been considered in this context (Destainville, 2008; Sieber et al., 2007), Fig. 12(a,b).

Some of these clusters form at specific positions. For example, receptor clusters in the rod-shaped bacterium *Escherichia coli* form at the cell ends (Maddock and Shapiro, 1993). Similarly, Spo0J/Soj in the likewise rod-shaped bacterium *Bacillus subtillus* localizes to the cell ends, although these proteins bind to

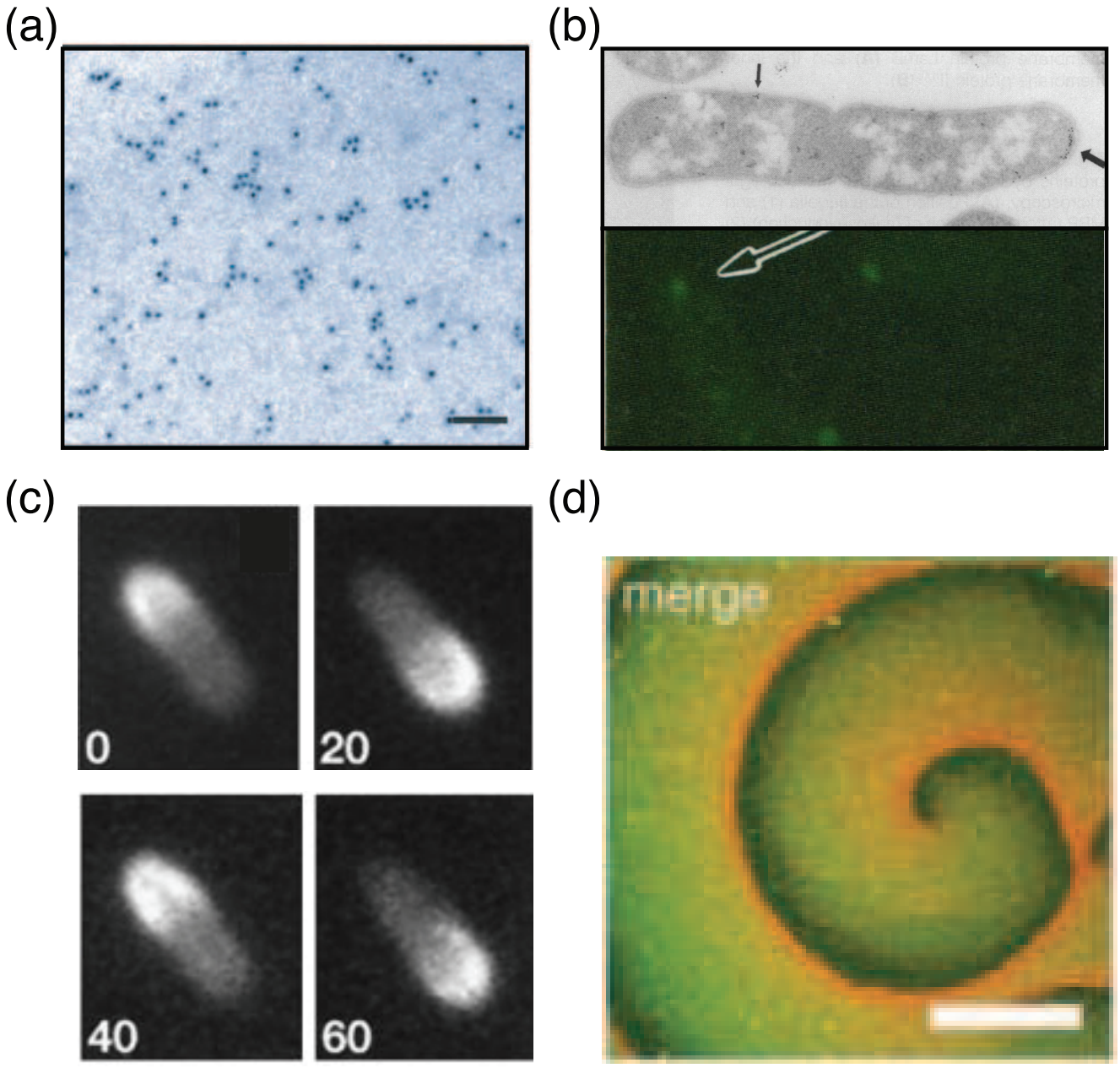

FIG. 12 Examples of protein clusters on cell membranes. (a) Electron microscopy image illustrating K-ras nanoclusters. Scale bar 50 nm. From (Prior et al., 2003). (b) Electron micrograph (top) and fluorescence image (bottom) of *E. coli* illustrating clustering of chemoreceptor Tsr. From (Maddock and Shapiro, 1993). (c) Min-protein oscillations in *E. coli*. Numbers indicate time in seconds. From (Raskin and de Boer, 1999b). (d) Spiral of MinD (green) and MinE (red) on a supported lipid bilayer. Scale bar 50 μm. From (Loose et al., 2008).

DNA and not to membrane (Marston and Errington, 1999; Quisel et al., 1999). Cell polarity in budding yeast *Saccharomyces cerevisiae* is established by localization of Cdc42 (Fairn et al., 2011). Cues like membrane-curvature or -composition and specific DNA sequences might be involved in positioning these aggregates. However, in the presence of cooperative effects during attachment, proteins can self-organize in clusters at specific locations by a Turing-like mechanism (Turing, 1952). A simple example is when membrane binding is facilitated by molecules that are already bound there, while detachment is spontaneous. The processes can be cap-

tured by the following toy model (Wettmann et al., 2014), where the distributions of cytosolic and membrane-bound molecules, c and m, along an interval of length L evolve according to

$$\partial_t c = \partial_x^2 c - \left(1 + m^2\right) c + km \tag{75}$$

$$\partial_t m = D\partial_x^2 m + \left(1 + m^2\right) c - km \tag{76}$$

with k being the detachment rate. For sufficiently small values of the ratio D of membrane-bound and cytosolic diffusion, the homogenous state can become unstable, leading to a maximum of m at one end of the interval. In a rod-shaped bacterium, this instability corresponds to an accumulation of proteins at one cell end. An analysis of the corresponding stochastic dynamics that accounts for the randomness inherent in molecular reactions shows that the lifetime of such clusters increases with molecule number and thus cell size (Wettmann et al., 2014). Similar observations had been made in detailed descriptions of the Spo0J/Soj proteins (Doubrovinski and Howard, 2005).

c. Surface waves The total number of particles $\int dx\,(c + m)$ is conserved by the above dynamics, which presents an interesting twist to the original Turing mechanism. Generally, one can expect the spontaneous emergence of traveling waves in such systems (Kessler and Levine, 2016). This phenomenon is exemplified by the proteins MinD and MinE in the rod-shaped bacterium *Escherichia coli* (Loose et al., 2011b). MinD and MinE direct the protein MinC, which inhibits assembly of the cell division machinery, to the vicinity of the cell poles, thus localizing division in the cell center. However, the Min proteins are not statically distributed at the two cell ends, but rather shuttle periodically between them with a period of about a minute (Raskin and de Boer, 1999b), Fig. 12(c).

MinD is an ATPase that clusters on the membrane after binding MinC by a mechanism that is still poorly understood (Hu et al., 2002). At the membrane, it recruits MinE which catalyzes ATP hydrolysis and drives MinD off the membrane. In presence of suitable cooperative effects during the formation of MinD clusters on the membrane, the oscillatory behavior observed *in vivo* can emerge spontaneously (Huang et al., 2003). Although MinD binding to the membrane was experimentally found to be cooperative, the molecular details are unknown. Currently, in most theoretical descriptions of the Min-protein dynamics, a process similar to the cooperative binding present in Eqs. (75)-(76) is assumed (Bonny et al., 2013; Huang et al., 2003), but alternative mechanisms have been proposed, where MinD forms complexes only after binding to the membrane (Kruse, 2002; Petrášek and Schwille, 2015; Walsh et al., 2015).

Physical studies of the mechanism generating the oscillatory patterns *in vivo* notably involved observing the Min-protein dynamics in different geometries. Varying the cell length revealed transitions from a bistable regime in short bacteria to standing and then to traveling waves (Bonny et al., 2013). The wave dynamics could be reconstituted in an open geometry *in vitro* on supported lipid bilayers (Loose et al., 2008), Fig. 12(d). This allowed for further molecular characterization of the Min-protein dynamics (Loose et al., 2011a; Schweizer et al., 2012). The *in vitro* approach has been extended to study waves in confined geometries (Caspi and Dekker, 2016; Zieske and Schwille, 2013). The patterns found in living cells could be reproduced in this situation, further supporting a common mechanism underlying the patterns in bacteria and in reconstituted systems.

B. Adhesion domains

Cells adhere to other cells, a substrate, or the extracellular matrix via transmembrane proteins like integrins and cadherins (Schwarz and Safran, 2013). These form initially submicrometer sized circular domains, which then mature into larger complexes of up to 10 μm that also involve cytoplasmic proteins, notably components of the cytoskeleton. Through cytoskeletal coupling, adhesion domains are subject to mechanical forces that are necessary for maturation (Balaban et al., 2001). The molecular mechanism involved in force sensing could notably depend on a force-dependent lifetime of individual adhesion bonds. In addition, there is a feedback from the adhesion domains to the organization of the actin cytoskeleton (Drees et al., 2005). Currently, there is no general theory of force-dependent formation of adhesion domains.

a. Membrane-less organelles In addition to membrane domains, cells contain three-dimensional membrane-less functional units. Originally suggested for so-called P granules in the developing nematode *Caenorhabditis elegans*. Such functional units can be described as liquid droplets that form through nucleation (Brangwynne et al., 2009). P granules are asymmetrically distributed in *C. elegans* embryos at the one-cell stage. After the first cell division, the daughter cell, rich in P granules, will eventually form a line of germ cells, whereas the other daughter cell will give rise to a somatic cell line. This asymmetric distribution is induced by a gradient in the distribution of the protein Mex-5 that promotes P-granule disassembly and thus effectively increases the concentration at which P-granule components saturate. The asymmetric state is out of equilbrium as droplets continuously form in regions of low Mex-5 concentrations and dissolve in regions of high Mex-5 concentrations (Lee

et al., 2013). Diffusion then leads to a permanent net droplet flux between the two regions and an oppositely directed flux of P-granule components.

P granules are liquid-like droplets with a viscosity of 1 Pa·s, that is, 3 orders of magnitude higher than the viscosity of water. These droplets have a surface tension on the order of 1 μN/m, that is, 5 orders of magnitude smaller than the air-water surface tension. These values of viscosity and surface tension allow rapid droplet formation. Other compartments have been found to similarly form liquid-like droplets (Brangwynne, 2011). Prominent examples are centrosomes (Zwicker et al., 2014) that serve as microtubule organizing centers and metaphase spindles that arrange the chromosomes during division, which can be described as liquid crystalline droplets (Reber et al., 2013). In the nucleolus, a large subcompartment of the nucleus in which ribosomes are created, subdomain structure has been ascribed to droplets of immiscible liquid-like phases (Feric et al., 2016).

Above the saturation threshold, P granules continue to grow and fuse, which leads to Oswald ripening (Brangwynne et al., 2009). In contrast, the two centrosomes present in cell division do not fuse, which indeed would be detrimental to the segregation of the chromosomes. The mechanism suppressing Oswald ripening in that case is similar to that proposed for limiting the size of lipid rafts: Constituents of the droplet continuously change between two different states with different physical properties such that in one state, the protein prefers the condensed phase, whereas the other form is soluble in the cytoplasm. In the case of centrosomes, this could be the case for spindle defect protein-5 that assumes different conformations depending on its phosphorylation state (Zwicker et al., 2014). Several such "active droplets" can stably co-exist, in which case they assume equal sizes (Zwicker et al., 2014). This is important as centrosome size seems to directly control spindle lengthin *C. elegans* (Greenan et al., 2010).

C. The cytoskeleton — an active material

The cytoskeleton is a network of filamentous protein assemblies that interact with a plethora of proteins, regulating filament length, cross-linking filaments and generating active stresses. This structure is involved in vital processes like cell division and migration and also determines cellular mechanical properties. From a physical point of view, the cytoskeleton is an active material, as its constituents are kept out of thermodynamic equilibrium by the hydrolysis of nucleoside triphosphates (NTP). We will present first generic physical properties of cytoskeletal systems and then turn to two biological applications that are of current interest, cell migration and the actin cortex.

1. Filaments

Cytoskeletal filaments fall into two classes, actin and tubulin, which, respectively, form actin filaments and microtubules. These structures can bind nucleotides and assume different states with different binding affinities depending on the nucleotide bound. In addition, actin filaments and microtubules are structurally polar assemblies. The structural polarity is expressed in different exchange kinetics at the two ends, which are commonly referred to the plus- and minus-ends, respectively, with exchange being more rapid at the plus-end (Fujiwara et al., 2007; Kuhn and Pollard, 2005). In contrast, proteins like vimentin or keratin form intermediate filaments that seem to play a structural role and are assembled in a one-state, non-polar fashion.

a. Filament length dynamics and treadmilling Coupling to NTP-hydrolysis, in combination with structural polarity, leads to assembly kinetics of actin filaments and microtubules that are alien to other commonly studied polymers. In particular, during assembly there can be an overshoot in the average filament length (Brooks and Carlsson, 2008) or even oscillations in length (Carlier et al., 1987). Most spectacularly, polarity can also lead to treadmilling, when filaments show net growth at the plus- and net shortening at the minus-end (Margolis and Wilson, 1978; Wegner, 1976). Observations of filament treadmilling have been reported *in vivo* (Rzadzinska et al., 2004; Waterman-Storer and Salmon, 1997) and *in vitro* (Carlier et al., 1997; Panda et al., 1999). Treadmilling relies on the establishment of an NTP-gradient along the assembling filament (Erlenkämper and Kruse, 2013); specifically, filament subunits with NTP bound have a higher affinity to bind to other subunits than NDP-bound subunits. In cells, hydrolysis of NTP bound to a filament subunit is essentially irreversible, such that the fraction of NDP-bound subunits increases towards the minus-end. In this way, assembly occurs preferentially at the plus end in the form of NTP-subunit attachment, whereas detachment occurs preferentially at the minus-end, where NDP-subunits leave the filament. This gradient also implies an effective length dependence of the depolymerization rate, which can lead to a finite typical filament length (Erlenkämper and Kruse, 2013; Mohapatra et al., 2016). Other mechanisms of length-dependent assembly and disassembly rates exist that involve proteins influencing the growth or shrinkage of cytoskeletal filaments (Mohapatra et al., 2016).

b. Nucleation promoting factors Filament assembly is directly utilized by cells for migration and to form protrusions. The polymerization of filaments anchored in a network or to a substrate can generate forces onto an object

either directly (Dogterom, 1997; Footer et al., 2007) or by generating stresses in non-flat networks (Prost, 2002). To see how stresses can arise from polymerization, note first that filaments do not appear spontaneously for the conditions present in cells. Instead, the emergence of filaments requires factors that promote the formation of filament nuclei, which can then grow either spontaneously or with the help of elongation factors. Important factors promoting the nucleation of actin filaments are complexes of actin related proteins 2 and 3 (Arp2/3) and members of the formin family. These are typically active only in the vicinity of a membrane. As a consequence, actin gels grow by adding material at the interface with a surface which leads to mechanical stresses if the surface is curved. These stresses are exploited, for example, by the bacterium *Listeria monocytogenes* for propulsion in the cytoplasm of a host cell (Prost, 2002).

The mechanisms underlying nucleation by the Arp2/3 complex and formins are different. The Arp2/3 complex branches new filaments from existing filaments. This process is used in particular to extend the leading edge of cells crawling on a substrate as it provides new free plus ends that can grow, whereas elongation of older plus ends is dampened by capping proteins. The interplay of Arp2/3 and capping proteins can lead to a variety of force-velocity curves for the advancing leading edge (Carlsson, 2003; Schreiber and Stewart, 2010; Weichsel and Schwarz, 2010).

Animal cells typically assemble a thin actin sheet below their plasma membrane. Filaments in this actin cortex nucleated by the Arp2/3 complex and formins form two subpopulations that can be distinguished through their different turnover rates (Fritzsche et al., 2013). Furthermore, formin nucleated filaments are typically 10 times longer than Arp2/3-nucleated filaments (Fritzsche et al., 2016), which in turn affects the gel's mechanical properties (Bai et al., 2011; Fritzsche et al., 2016). The mechanical properties of actin gels in presence of filament turnover are only beginning to be explored (Hiraiwa and Salbreux, 2016).

2. Motors

a. Single molecular motors Cytoskeletal motor proteins assure directed long-range transport in cells and generate mechanical stresses in the cytoskeletal network. Members of the myosin super family interact with actin filaments, whereas kinesins and dyneins interact with microtubules. These interacting proteins are ATPases that have various conformational states depending on the nucleotide bound. Thermodynamics shows that for motor proteins to move directionally, isotropy and detailed balance must be broken (Jülicher et al., 1997). Molecular motors are characterized by their force-velocity relation and their persistence. In many cases, the force-velocity relation is well approximated by

$$v = v_0 \left(1 - \frac{f}{f_s}\right) \tag{77}$$

where v_0 is the motor velocity in absence of a load, f_s the stall force at which the motor stops advancing, and f the magnitude of the force opposing motor movement. Although forces larger than the stall force should lead to backward motion of the motor, in practice, this is rarely observed; instead, the motor readily detaches.

The persistence is given by the average length a motor walks along the filament before detachment, equal to the ratio of the stepping to the detachment rates multiplied by the size of a single step. The detachment rate depends on the applied force and Kramers rate theory suggests

$$k_{\text{off}}(f) = k_{\text{off},0} \exp\left\{-\frac{|f|a}{k_B T}\right\} \tag{78}$$

where $k_B T$ is thermal energy and a a molecular length scale. However, myosin motors show catch-bond behavior, such that the detachment rate initially decreases with increasing applied force (Guo and Guilford, 2006).

b. Many motors on a single filament Collective transport phenomena are commonly studied using models in which the filament is represented by a one-dimensional lattice with N sites and motors by particles that occupy the sites. In this representation, bound particles hop at specific rates to neighboring sites. Often steric interactions between the motors are accounted for by an exclusion principle such that each lattice site can be occupied by one particle at most. If particles enter the lattice at one end and leave it at the opposite end and if hops occur only into one direction, one obtains the totally asymmetric exclusion process (TASEP) (Derrida et al., 1993; Schütz and Domany, 1993). Depending on the rates of particle entry and exit at the boundaries, the process displays a low density, a high density, and a maximal current phase (Krug, 1991), Fig. 13(a). Adding attachment and detachment of particles in the bulk (Langmuir kinetics), stable walls between high and low density domains can be formed (Parmeggiani et al., 2003), Fig. 13(b). If diffusing particles that cannot hop off the lattice at the ends are added, the two species can segregate (Johann et al., 2014; Pinkoviezky and Gov, 2017), Fig. 13(c). Similar segregation phenomena have been observed in mixtures of active and passive swimmers (McCandlish et al., 2012) and might also be relevant for the segregation of transcribed and not transcribed DNA in the cell nucleus (Grosberg and Joanny, 2015).

c. Length regulation involving molecular motors Some molecular motors are capable of removing subunits at

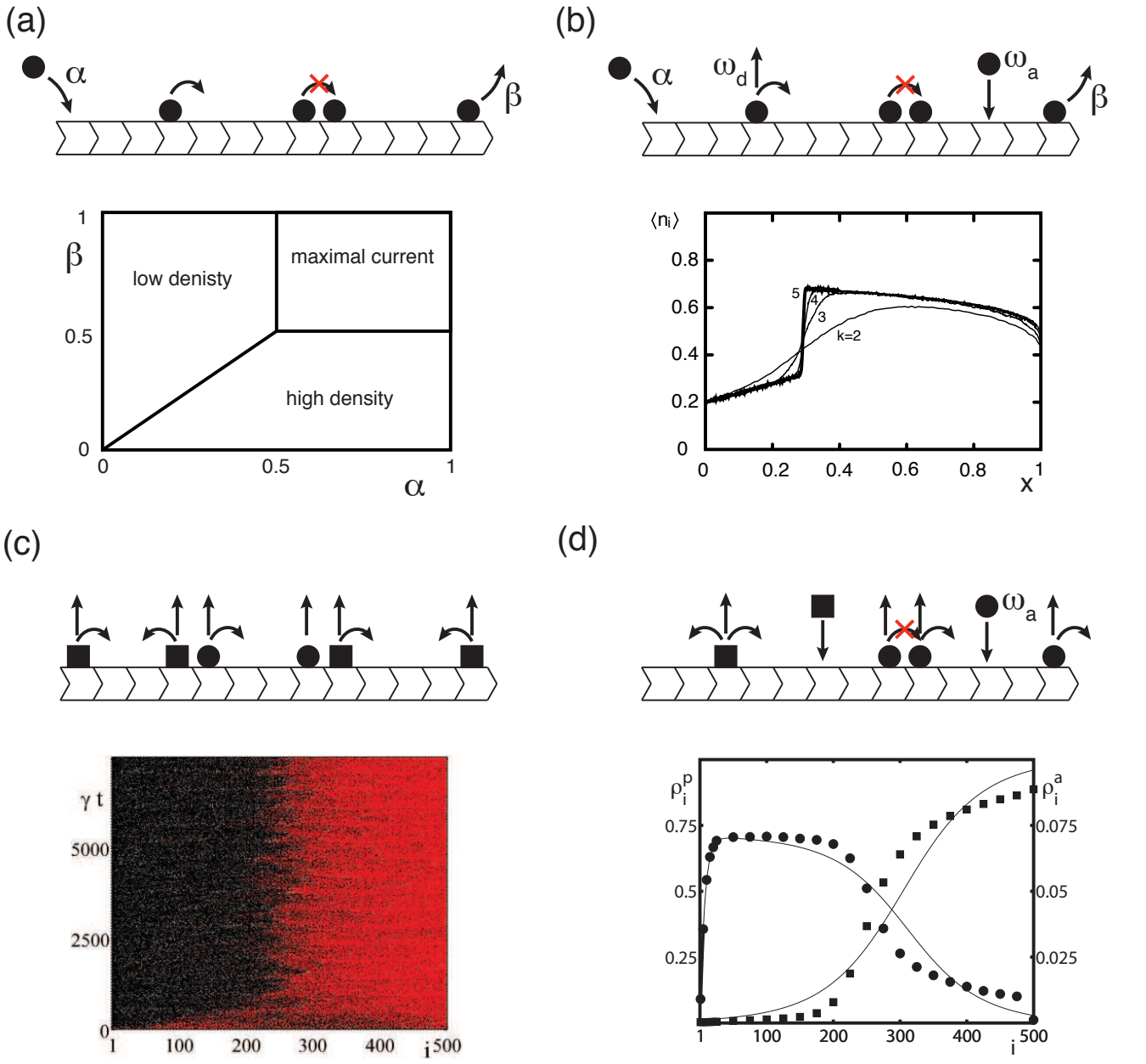

FIG. 13 Collective behavior of motors on a single filament. (a) Totally asymmetric exclusion process. Top: illustration of processes. Bottom: phase diagram. (b) Totally assymmetric exclusion process with Langmuir kinetics. Top: illustration of processes. In addition to (a), empty sites anywhere along the lattice are occupied at rate ω_a and particles can detach at rate ω_D anywhere from the lattice. Bottom: steady state density profiles revealing a domain boundary between low and high denisty phases. From (Parmeggiani et al., 2003). (c) Exclusion process of two particles species. Top: illustration of processes. The dynamics of circular particles as in (b), but without additional entry rate α and exit rate β at the ends. In addition, square particles hop at the same rate to free neighboring sites, but cannot hop off at the lattice ends. For clarity, processes have been distributed on two lattices. Bottom: Left: Space-time plot of the densities of square (red) and circle (white) particles. Right: Steady state density profiles of square and circle particles. Form (Johann et al., 2014).

filament ends (Desai et al., 1999; Hunter et al., 2003; Varga et al., 2006). For example, Kinesin 8 attaches anywhere along a microtubule and then moves towards its plus end. In this way, a concentration gradient of motors along the microtubule is established that leads to an effective length-dependent depolymerization rate at the plus end (Reese et al., 2011; Varga et al., 2006, 2009), which can be exploited to regulate the length of microtubules (Johann et al., 2012; Melbinger et al., 2012; Stewman and Ma, 2018). For actin cables, a similar mechanism was proposed that, in contrast, depended on a length-dependent assembly rate induced by molecular motors (Mohapatra et al., 2015). In this way, molecular motors provide specific realizations of a general strategy to regulate the length of cytoskeletal filaments (Mohapatra et al., 2016).

Molecular motors are also involved in axonal length sensing and regulation (Rishal et al., 2012). However, the mechanism does not rely on gradients. Instead, it has been proposed that motors moving towards the axon tip transport a promoter of axon extension that at the same time elicits the transport, in the opposite direction, of a factor that inhibits further transport of the extension promoter. This process can be captured by a system of coupled delayed differential equations for the concentration u_E of the extension promoter at the axon tip and u_I of the inhibitor (Karamched and Bressloff, 2015):

$$\frac{d}{dt}u_E(t) = I_0 - \gamma_E u_E(t) - W_I f(u_I(t-\tau)) \tag{79}$$

$$\frac{d}{dt}u_I(t) = -\gamma_I u_I(t) + W_E f(u_E(t-\tau)), \tag{80}$$

where f is a sigmoidal function and τ is the time motors of velocity v need to traverse the axon of length L, $\tau = L/v$. This system can generate an oscillation in u_E with a length-dependent period. This oscillating concentration of u_E can be transformed into a signal with a period- and thus length-dependent mean concentration allowing a nerve cell to sense and regulate its axon's length via a threshold mechanism (Bressloff and Karamched, 2015).

d. Bidirectional motion For directional transport in cells, vesicles are typically bound to several motors. In this case, the motors are mechanically coupled to each other because pulling of one motor exerts a force on the other motors and thereby changes their velocities as well as their persistences. If a vesicle is bound to motors of opposite directionality, bidirectional transport can occur (Grill et al., 2005; Mueller et al., 2008). Indeed, in a situation where a vesicle is stalled due to motors of acting antagonistically, a fluctuation that causes one motor to detach leaves the other motors of the same directionality carrying a higher load. This increases their detachment rates and thus starts an avalanche of detachment events of motors of one species. The vesicle will thus move into one direction until again another stalled situation occurs. At the end of the stall period, the vesicle can move in either direction. Whether this "tug-of-war" mechanism underlies cellular bidirectional transport is still debated (Klein et al., 2014).

Bidirectional transport can also be observed for a single motor type and in the absence of load-dependent detachment rates (Badoual et al., 2002; Jülicher and Prost, 1995). Experimentally, such bidirectional motion has been observed in gliding assays, where filaments move on a substrate covered with motors (Riveline et al., 1998), for non-directional motors (Endow and Higuchi, 2000), and for non-polar bundles of actin filaments moving on a carpet of myosin motors (Gilboa et al., 2009). The rate of switching between the two directions of motion was calculated along the lines presented in Sect. II.D (Guérin, T et al., 2011).

e. Spontaneous motor oscillations In addition to the chemical and genetic oscillators discussed above, cells can also present mechanical oscillations that are not the result of an underlying chemical pulse generator. Many cells possess filamentous protrusions called cilia or flagella that periodically change their shape or produce traveling waves. These include spermatozoa and algae that have one or two flagella, in addition to *Paramecia* that are covered by a dense carpet of cilia (Bray, 2001). The periodic deformations of cilia propel these cells in fluid environments. Strikingly, the main constituents of the appendages, microtubules and associated molecular motors, have been found in reconstitution experiments to spontaneously produce very similar patterns (Sanchez et al., 2011).

Jülicher and Prost found early that ensembles of molecular motors coupled to an elastic element can spontaneously develop oscillations (Jülicher and Prost, 1997). They studied the case in which motors are rigidly bound to a common backbone and switch between two internal states. An alternative possibility is that the motors detach from the filament in a force-dependent manner (Grill et al., 2005). The oscillatory regimes are distinct, as was shown in a model for "soft" motors that comprises both cases (Guerin et al., 2010). Spontaneous motor oscillations have been found in muscle sarcomeres (Günther and Kruse, 2007; Sato et al., 2013; Yasuda et al., 1996) and could be essential for the beating of eukaryotic flagella (Camalet and Jülicher, 2000).

3. Filament networks

a. Reconstituted filament networks Contraction of muscle sarcomeres relies on a crystal arrangement of the actin filaments that interdigitate with myosin filaments. Upon activation of the motors, the actin filaments are

drawn inwards, which results in contraction. Disordered cytoskeletal networks can also generate net contractile stresses (Szent-Györgyi, 1951). The dynamics of this process has been studied in reconstituted systems of filaments and motors (Backouche et al., 2006; Bendix et al., 2008; Foster et al., 2015; Linsmeier et al., 2016; Schuppler et al., 2016; Smith et al., 2007). In a disordered network, contraction starts at the boundaries of a gel slab and then propagates into the gel's interior.

Reconstituted networks have also been shown to self-organize into asters and vortices (Nedelec et al., 1997) and spindle-like assemblies (Surrey et al., 2001). Minimal networks of two microtubules, molecular motors, and passive crosslinkers showed that such molecules provide a minimal module for generating stable overlaps between antiparallel filaments as observed in spindle midzones (Bieling et al., 2010; Lansky et al., 2015). Mircotubule-organizing centers have been found to position themselves in microfluidic chambers either through polymerization-depolymerization (Faivre-Moskalenko and Dogterom, 2002; Holy et al., 1997) or through molecular motors at the chamber walls pulling on the filaments (Laan et al., 2012).

A somewhat different approach is followed in gliding assays, where filaments at high density move on substrates covered with motors (Butt et al., 2010; Schaller et al., 2010) and which are more akin to self-propelled particles.

For investigating motor-filament systems, different theoretical approaches have been developed. Stochastic simulations aim to account for the various constituents individually (Dasanayake and Carlsson, 2013; Nedelec and Foethke, 2007). Kinetic descriptions take a mean-field approach and describe the system state in terms of densities of the various components (Kruse and Jülicher, 2000, 2003; Liverpool and Marchetti, 2003). Finally, phenomenological descriptions mostly neglect molecular properties and focus on symmetries and conservation laws (Kruse et al., 2004, 2005).

b. Kinetic descriptions of filament networks In the kinetic approach and in the limit of a purely viscous system, filaments are typically assumed to be rigid rods. The state of the filament network can be captured by the density c of filament plus-ends. This density depends on the position $\mathbf{r}$ of the plus-end, the orientation $\hat{\mathbf{u}}$ of the filament with $\hat{\mathbf{u}}$ pointing form the plus- to the minus end and $\hat{\mathbf{u}}^2 = 1$, and the filament length ℓ. For motors, it is often appropriate to distinguish between the densities m_b of motors bound to filaments and m_u of unbound motors. The time evolution of the density is then given by a continuity equation

$$\partial_t c + \nabla \cdot \mathbf{j}_{\text{trans}} + \hat{\mathbf{u}} \times \nabla_{\hat{\mathbf{u}}} \cdot \mathbf{j}_{\text{rot}} + \partial_\ell j_\ell = S \tag{81}$$

$$\partial_t m_b + \nabla \cdot \mathbf{j}_{\text{mot}} = R \tag{82}$$

$$\partial_t m_u - D\Delta m_u = -R \tag{83}$$

where $\mathbf{j}_{\text{trans}}$ is a translational current caused by the activity of molecular motors and filament assembly at the plus end, $\mathbf{j}_{\text{rot}}$ a rotational current that accounts for changes in filament orientation, and j_ℓ a current describing the net effect of filament assembly on the filament length. The source term S accounts for filament degradation, whereas filament nucleation is captured by a boundary condition on j_ℓ at $\ell = 0$. The current j_{mot} describes the flux of bound motors, D is the diffusion constant of unbound motors, and the source term R describes the binding and unbinding dynamics.

It can be useful to distinguish between different filament populations, for example, to account for microtubules with shrinking and growing plus ends or for kinetic differences between filaments with capping proteins bound or not(Stewman and Ma, 2018). In the simplest case, filaments form a bundle and have a fixed length. If the bundle is aligned with the x-axis, Eq. (81) can be written as

$$\partial_t c(x, \pm\mathbf{e}_x) = -\partial_x j^{\pm} \tag{84}$$

In the viscous limit, attention is typically restricted to motor-mediated interactions between filament pairs. In the case of a bundle, the current takes the form (Kruse and Jülicher, 2003)

$$j^{\pm}(x) = \int_{-\ell}^{\ell} d\xi \left[v^{\pm\pm}(\xi) c^{\pm}(x+\xi) + v^{\pm\mp}(\xi) c^{\mp}(x+\xi) \right] c^{\pm}(x) \tag{85}$$

where the motor-induced sliding velocities obey $v^{\pm\pm}(\xi) = -v^{\pm\pm}(-\xi)$ and $v^{+-}(\xi) = -v^{-+}(-\xi)$ to respect momentum conservation. In this case, the motor density is assumed to be homogenous. A similar form of the interaction kernel can be obtained from analogies with collision terms used for granular materials (Aranson and Tsimring, 2005). Kinetic approaches have also been used to describe (viso)elastic motor-filament systems (Günther and Kruse, 2007; Lenz et al., 2012a; Peter et al., 2008)

The kinetic approach has been used to study motor-induced contraction of filament bundles (Kruse and Jülicher, 2000) and the stability of isotropic filament solutions (Liverpool and Marchetti, 2003). Instabilities rely in both cases on interactions between filaments with orientations $\hat{\mathbf{u}}_1$ and $\hat{\mathbf{u}}_2$ such that

$$\hat{\mathbf{u}}_1 \cdot \hat{\mathbf{u}}_2 > 0. \tag{86}$$

On a molecular level, such interactions rely on end effects, for example, on motors getting stuck at a filament end (Nedelec et al., 1997) and also lead to the generation of net mechanical stresses in isotropic networks.

c. Mechanisms of stress generation In the kinematic framework, mechanical stresses can be calculated by analyzing the momentum flux (Kruse and Jülicher, 2003). In a homogenous filament bundle, antiparallel filaments do not generate a net contractile stress as there are as many contraction as extension events, Fig. 14(a). In skeletal muscle, this problem is solved by the sarcomeric arrangement of the actin filaments, Fig. 14(b). If motors stall at the filament ends, then interactions between parallel filaments generate a net stress, Fig. 14(c). Another mechanism depends on nonlinear filament elasticity: as filaments buckle more easily than they are stretched, contraction is favoured over extension, generating a net contractile stress (Lenz et al., 2012b), Fig. 14(d), and filament buckling has indeed been observed in reconstituted actomyosin bundles (Thoresen et al., 2011). Other mechanisms can be envisioned (Lenz, 2014): myosin motors are not point-like, but form themselves into minifilaments. If they prefer to be aligned with the filaments they will generate net contractile stresses, as has been found in stochastic simulations (Dasanayake et al., 2011; Dasanayake and Carlsson, 2013). In similar simulations, it was found that motors can also generate net extensile stresses, because motors are more likely to link two filaments that have a finite overlap and are so persistent as to stay bound until they fully extend a filament pair (Gao et al., 2015). Finally, filament treadmilling can contribute to the generation of filament overlaps that favour contraction (Oelz et al., 2015), Fig. 14(e), even in absence of active crosslinkers (Zumdieck et al., 2007).

The above mechanisms rely essentially on accounting for local differences in motor distributions. In addition, the local organization of the filament network has a significant impact on contractility (Ennomani et al., 2016). In bundles, filaments could form bipolar structures, Fig. 14(f), for example, through motors linking filament plus ends, which would lead to contraction as was proposed for contractile rings (Wollrab et al., 2016). In higher dimensions these structures correspond to asters.

4. Hydrodynamics of motor-filament networks

a. Hydrodynamics of active polar gels Many interesting features of motor-filament networks can be discussed without referring to a specific molecular mechanism of stress generation by using the formalism of generalized hydrodynamics outlined in Sec. II.J.2 (de Groot and Mazur, 1985). Within this approach, the cytoskeleton is one instance of an active polar gel (Kruse et al., 2004, 2005). In this context, "active" refers to the coupling of mechanical stresses to a chemical reaction (ATP hydrolysis), although the class of active matter is somewhat broader (Marchetti et al., 2013b). Active polar gels are defined on one hand by conserved quantities: the gel components, momentum, and angular momentum. One typically assumes the system to be at constant temperature such that energy is not conserved. On the other hand, polar filaments can locally align to generate macroscopic polar order, such that polarity provides an order parameter of a broken continuous symmetry.

The fluxes appearing in the conservation laws could be obtained from microscopic descriptions, as in the kinetic theories presented above. In the framework of nonequilibrium thermodynamics, however, one uses phenomenological expressions. To this end, one first identifies the pairs of conjugated generalized (thermodynamic) currents and generalized (thermodynamic) forces. An expression for the currents is then obtained by expanding them in terms of the forces up to linear order.

In the simplest version, an active gel can be described as an effective one-component fluid that is coupled to the hydrolysis of ATP. If the densities n_T, n_D, and n_P of ATP and its hydrolysis products ADP and P_i, respectively, are spatially homogenous, then the conservation laws are (Kruse et al., 2004, 2005)

$$\partial_t \rho + \partial_\alpha \rho v_\alpha = 0 \tag{87}$$

$$\partial_t g_\alpha + \partial_\beta \sigma^{\rm tot}_{\alpha\beta} = f^{\rm ext}_\alpha \tag{88}$$

$$\dot{n}_{\rm T} = -\dot{n}_{\rm D} = -\dot{n}_{\rm P} = r \tag{89}$$

where $\mathbf{g} = \rho \mathbf{v}$ denotes the momentum density and $\sigma^{\rm tot}$ is the corresponding momentum flux density, equal to the mechanical stress tensor. Externally applied forces $\mathbf{f}^{\rm ext}$ provide possible momentum sources. Angular momentum has not been listed explicitly, which is appropriate in the absence of torques not resultant from external forces. In addition, there is a dynamic equation for the evolution of the polarization field $\mathbf{p}$. The part of the free energy associated with distortions in the polar field, F_d, is commonly taken to be

$$F_d = \frac{1}{2}\int d^3\mathbf{r} \Big\{ K_1 \left(\nabla \cdot \mathbf{p}\right)^2 + K_2 \left[\mathbf{p} \cdot (\nabla \times \mathbf{p})\right]^2 + \tag{90}$$

$$K_3 \left[\mathbf{p} \times (\nabla \times \mathbf{p})\right]^2 \Big\} \tag{91}$$

where K_1, K_2, and K_3 are the Frank elastic constants for splay, twist, and bend, respectively.

The conjugated pairs of forces and fluxes are then $v_{\alpha\beta} \leftrightarrow \sigma^d_{\alpha\beta}$, $p_\alpha \leftrightarrow h_\alpha$, and $r \leftrightarrow \Delta\mu$, where $v_{\alpha\beta} = \left(\partial_\alpha v_\beta + \partial_\beta v_\alpha\right)/2$ are the components of the rate of strain tensor. Furthermore, σ^d is the deviatoric stress, $\mathbf{h} = -\delta F_d/\delta \mathbf{p}$ the molecular field conjugate to the polarization, and $\Delta\mu$ the difference between the chemical potentials of ATP and its hydrolysis products.

The total stress has two parts, a hydrostatic part σ^e, called the Erickson stress, and a deviatoric part. The first part is the generalization of the hydrostatic pressure to the case of a polar fluid (Ericksen, 1962), and the second, deviatoric part such that$\sigma^{\rm tot}_{\alpha\beta} = \sigma^d_{\alpha\beta} - \frac{1}{2}\left(p_\alpha h_\beta - p_\beta h_\alpha\right) + \sigma^e_{\alpha\beta}$, where σ^d is the symmetric part

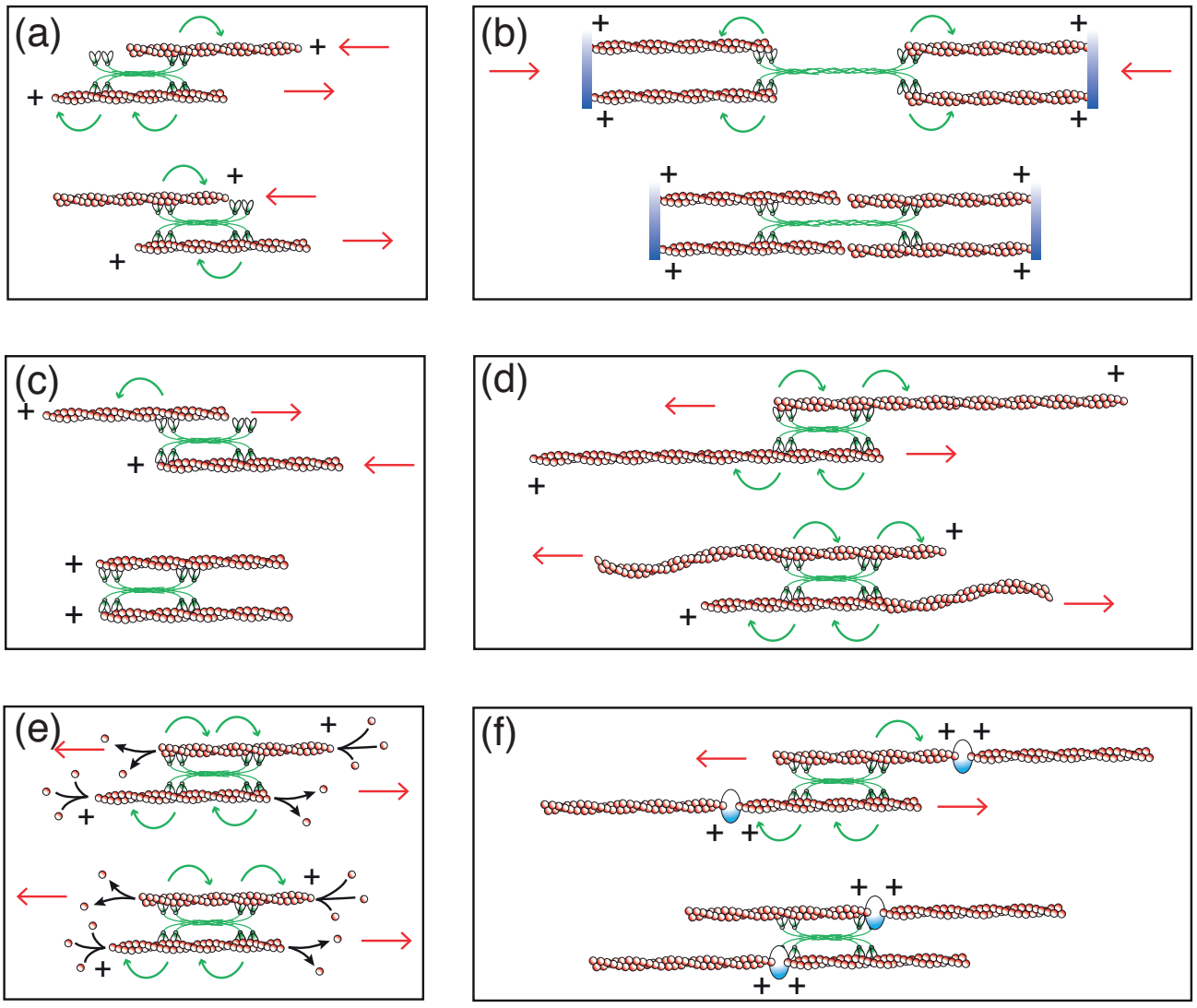

FIG. 14 Possible mechanism of net stress generation for rigid filament pairs. (a) Antiparallel filaments first contract then expand implying no net stress. (b) Arrangements of actin filaments and motors in a muscle sarcomere leading to contractions only. (c) If motors stall at the filament ends, net stresses are generated in parallel filament pairs. (d) The buckling of filaments can break the symmetry between contraction and extension of antiparallel filaments. (e) Filament treadmilling leads to to extended times of contractile overlaps. If these times exceed the time a motor is bound, net stresses are generated. (f) Biopolar structures generate a structure that is reminiscent of the filament arrangement in a sarcomere.

of the deviatoric stress and $-\frac{1}{2}(p_\alpha h_\beta - p_\beta h_\alpha)$ its antisymmetric part. The constitutive equation for the symmetric part of the deviatory stress can be divided in three components as

$$\sigma^d_{\alpha\beta} = \sigma^{\rm visc} + \sigma^{\rm dist} + \sigma^{\rm act} \tag{92}$$

where the viscous stress $\sigma^{\rm visc}$ is that of a Stokesian fluid with $\sigma^{\rm visc}_{\alpha\beta} = 2\eta v_{\alpha\beta}$ and $\sigma^{\rm dist}$ is the stress resulting from distortions in the polar field,

$$\sigma^{\rm dist}_{\alpha\beta} = \frac{\nu}{2}(p_\alpha h_\beta + p_\beta h_\alpha) + \bar\nu_1 p_\gamma p_\gamma \delta_{\alpha\beta} \tag{93}$$

The expression for $\sigma^{\rm dist}$ is the same as for a nematic liquid crystal, but with the polarization replaced by the director field. Finally, the stress component $\sigma^{\rm act}$ resulting from activity is

$$-\sigma^{\rm act}_{\alpha\beta} = p_\alpha p_\beta \zeta \Delta\mu + \bar\zeta \Delta\mu \delta_{\alpha\beta} + p_\gamma p_\gamma \tilde\zeta \Delta\mu \delta_{\alpha\beta}. \tag{94}$$

The equation for the evolution of the polarization vector is

$$\frac{D}{Dt} p_\alpha = \frac{1}{\gamma} h_\alpha + \lambda_1 p_\alpha \Delta\mu - \nu_1 p_\beta v_{\alpha\beta} - \bar\nu_1 v_{\beta\beta}, \tag{95}$$

which contains the active term $\lambda_1 p_\alpha \Delta\mu$. Here, the coefficients ν_1 and $\bar\nu_1$ are imposed by the Onsager reci-

procity relations. This hydrodynamic approach to active gels has been generalized to elastic (Banerjee and Marchetti, 2011) and to multicomponent viscoelastic active polar gels (Callan-Jones and Jülicher, 2011; Günther and Kruse, 2007; Joanny et al., 2007).

b. Spontaneous flows One of the most spectacular properties of polar active gels is their ability to spontaneously generate flows. Beyond a critical activity, a stationary state with homogenous polar order will be unstable against small perturbations (Voituriez et al., 2007). In this case, gradients in the polar order parameter will develop, which in turn lead to a spontaneous flow. In a Taylor-Couette geometry where the active gel is confined in the interstitial space between two coaxial cylinders, this flow can set the two cylinders into relative rotational motion (Fürthauer et al., 2012). The resulting torque-rotational velocity relation can display regions with multiple unstable branches and the coexistence of states with rotations in the opposite direction. For higher activities, secondary instabilities have been reported that lead to the emergence of topological point defects and possibly chaotic behavior (Neef and Kruse, 2014), Fig. 15(b), which has been observed in extensile active nematics (Sanchez et al., 2012), Fig. 15(c). These phenomena are reminiscent of the dynamics of bacterial suspensions confined in circular domains (Lushi et al., 2014; Wioland et al., 2013). Gradients in the polar order parameter also generate flows around spiral defects (Kruse et al., 2004), Fig. 15(a).

c. Topological defects Topological defects in the polarization field readily develop in reconstituted filament-motor systems (Keber et al., 2014; Sanchez et al., 2012). Beyond a certain activity threshold, asters and vortices that are stable defects in equilibrium give way to spirals and spontaneously start to rotate (Kruse et al., 2004, 2005). Defects of topological charge $\pm 1/2$ in active nematics form spontaneously, Fig. 15(d). Furthermore, these defects can annihilate (Sanchez et al., 2012) and can show oscillatory behavior when confined to a spherical surface (Keber et al., 2014). The dynamics of topological defects in active nematics has been studied numerically (Giomi et al., 2013; Thampi et al., 2013) and analytically (Pismen, 2013).

d. Spontaneous actin waves In a number of diverse adhering cells, the actin cytoskeleton has been found to spontaneously represent waves. Actin polymerization waves, first observed in *Dictyostelium discoideum* (Vicker, 2000), have now been seen in various cell types (Gerisch et al., 2004; Weiner et al., 2007) and are often linked to cell motility (Allard and Mogilner, 2013). Circular dorsal ruffles, which are protrusions on the upper side of an adhering cell and for which no function is currently known, result from polymerization waves (Bernitt et al., 2015). The basic underlying mechanism seems to be a negative feedback between actin filaments and the activity of a nucleation promoting factor (Carlsson, 2010; Doubrovinski and Kruse, 2008; Weiner et al., 2007), which leads to a dynamic that is reminiscent of excitable systems (Bernitt and Döbereiner, 2017; Ryan et al., 2012; Whitelam et al., 2009).

There are also spontaneous actin waves that depend in an essential way on stresses generated by molecular motors (Barnhart et al., 2011; Doebereiner et al., 2006; Giannone et al., 2004). A generic mechanism for such waves that results from the coupling of a regulator to an active gel has been studied in (Bois et al., 2011; Kumar et al., 2014). Similarly, they are generic properties of active elastic materials with stress-dependent motor regulation (Günther and Kruse, 2007; Radszuweit et al., 2013) or in the presence of turnover (Dierkes et al., 2014). In combination with filament treadmilling, motors can also generate waves in actomyosin bundles (Oelz and Mogilner, 2016; Torres et al., 2010; Wollrab et al., 2016) as were observed in cytokinetic rings in fission yeast (Wollrab et al., 2016). Lateral waves, observed during the spreading of fibroblasts (Doebereiner et al., 2006; Giannone et al., 2004), have been proposed to result from cytoskeleton-membrane interactions (Gholami et al., 2012; Shlomovitz and Gov, 2007; Zimmermann et al., 2010).

e. Cell migration Simply put, the motion of cells crawling on solid substrates comprises extension of a flat, veil-like protrusion called lamella, its anchoring to the substrate, release of surface attachments in the cell's rear, and forward locomotion of the cell body containing the nucleus. Physical analysis has focused on specific aspects of this integrated process. Notably, the extension of lamellae by actin polymerization was described in terms of a "Brownian ratchet" (Mogilner and Oster, 1996) or through blebbing, a process that leads to the detachment of the cell membrane from the actin network and its bulging out due cytosolic pressure (Charras and Paluch, 2008). On this basis, the force-velocity relation of cell-crawling has been analyzed (Carlsson, 2003; Schreiber and Stewart, 2010; Weichsel and Schwarz, 2010). In the frame of the substrate, actin flows from the leading edge towards the cell body in a process called retrograde flow. Hydrodynamic analysis of this phenomenon suggests that it results form contractile activity of myosin motors (Kruse et al., 2006). The combined effect of polymerization and contraction on the force-velocity relation was studied in (Recho and Truskinovsky, 2013).

On the other hand, the experimental observation of crawling cell fragments (Euteneuer and Schliwa, 1984;

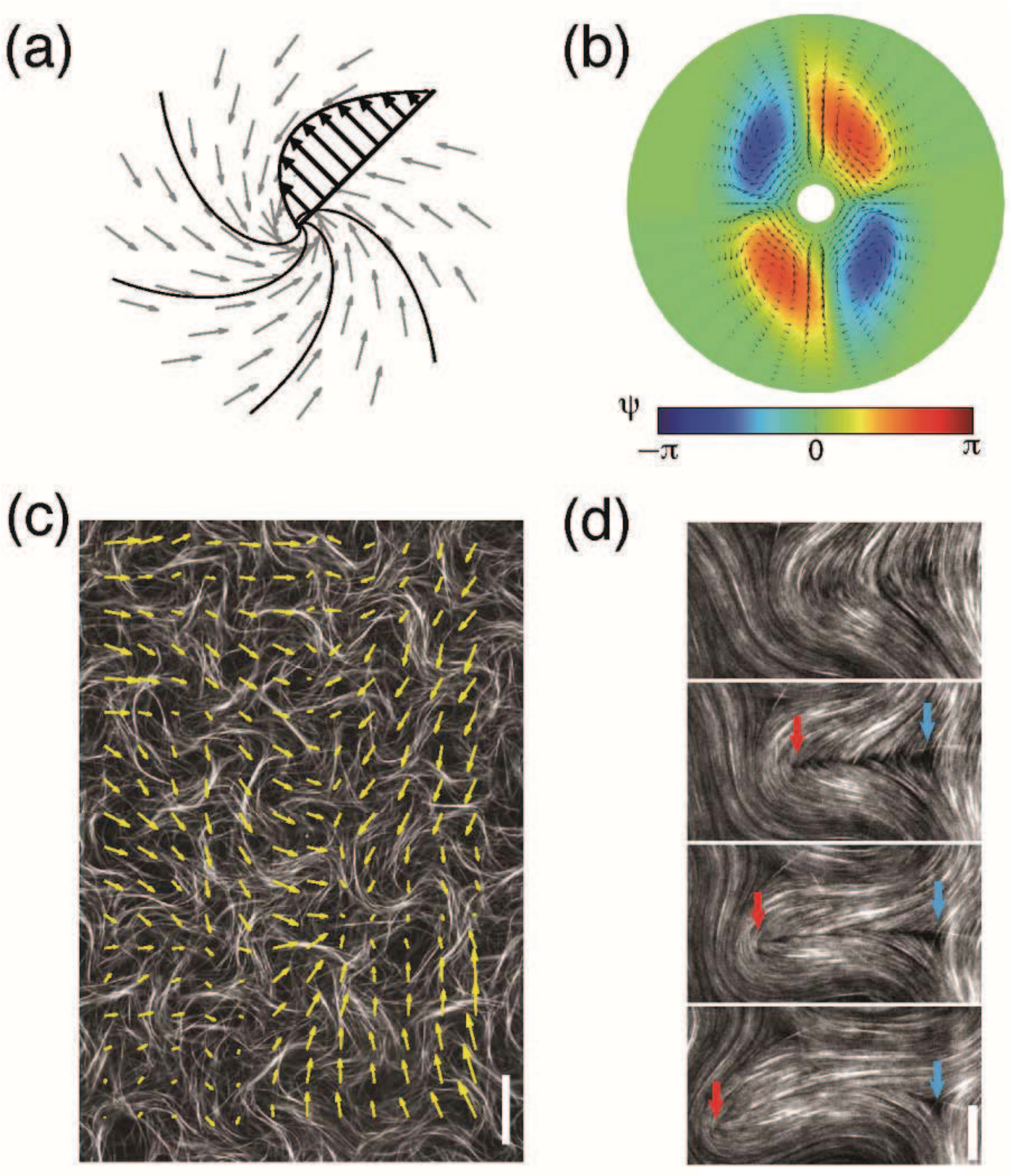

FIG. 15 Spontaneous flows in active polar gels. (a) Illustration of the spontaneous circular flow around a spiral point defect. From (Kruse et al., 2004). (b) Flows around vortices in a ring. Arrows indicate the flow, colours the orientation angle ψ of the polarization field with respect to the radial direction. From (Neef and Kruse, 2014). (c) Spontaneous flow field (arrows) in a reconstituted system of microtubules and motor complexes. Scale bar: 80 μm. (d) Generation and separation of two topological point defects of charges $\pm 1/2$ in the system (c). Scale bar: 20 μm. (c) and (d) from (Sanchez et al., 2012).

Malawista and Van Blaricom, 1987) suggested that the actin cytoskeleton can autonomously generate cell migration. As a consequence, droplets of active gels were analyzed. In this context, one has to deal with a dynamic boundary. Studies with sharp boundaries therefore focused on cytoskeletal dynamics in regions of fixed shape (Whitfield et al., 2014) or on the stability of circular shapes (Callan-Jones et al., 2008), although full crawling was also considered (Doubrovinski and Kruse, 2011). Alternatively, phase-field models have been used (Shao et al., 2010; Ziebert et al., 2012).

A phase field is an auxiliary field that equals one in the cell interior and zero outside. The dynamics of the phase field ψ is given by (Shao et al., 2010; Ziebert et al., 2012)

$$\partial_t \psi = D_\psi \Delta \psi + \frac{\delta F}{\delta \psi} + \text{coupling terms} \qquad (96)$$

Notably, the diffusion terms set the surface tension associated with the phase-field boundary. The free energy F is commonly taken to be quartic in the phase field such that the derivative $\delta F/\delta\psi = \kappa\psi\,(1-\psi)\,(\psi-\delta)$ is cubic in ψ. Here, δ can be dynamically adjusted to maintain a constant cell volume $\delta = \frac{1}{2} + \epsilon\left(d^3\mathbf{r}\psi\,(\mathbf{r}) - V_0\right)$, where v_0 is the target volume size (Ziebert et al., 2012). The coupling terms describe the interaction of the phase field with the actin cytoskeleton. This interaction is commonly described by $-\beta\mathbf{p}\cdot\nabla\psi$, which confines the interaction to the "cell" boundary.

The phase-field approach has been used to study spontaneous cell polarization (Shao et al., 2010; Ziebert et al., 2012), the effects of adhesion (Shao et al., 2012; Ziebert and Aranson, 2013), the migration of cells on micropatterns (Camley et al., 2013), and the effects of substrate stiffness on migration (Löber et al., 2014; Ziebert and Aranson, 2013). In these studies, the contractile stresses generated by the actin network play an essential role. Spontaneous polymerization waves can also orchestrate the cytoskeleton to generate cell crawling (Doubrovinski and Kruse, 2011; Weiner et al., 2007). These waves can generate erratic motion through a deterministic mechanism (Dreher et al., 2014).

As an alternative to adhesion-based motility, cells can also move by "flowing and squeezing" (Laemmermann et al., 2008). In this case, the cell does not establish adhesion sites with a substrate; rather, the necessary environmental coupling can be obtained from pushing on the environment (Hawkins et al., 2009). Furthermore, spontaneous actin flows either in the bulk (Recho et al., 2013; Tjhung et al., 2012; Whitfield et al., 2014) or below the cell membrane (Hawkins et al., 2011) can generate migration. Similarly, asymmetric contraction of the cytoskeletal network can push the cytosol to extend the leading edge (Callan-Jones and Voituriez, 2013), which is a behavior similar to blebbing.

f. Cortex instabilities In animal cells, the actin cytoskeleton forms a thin layer below the cell membrane known as the actin cortex. This mesh determines cellular shape and mechanical properties (Chalut and Paluch, 2016). The actin cortex hosts vital structures like contractile rings that, for example, cleave the cell during division, play an important part in endocytosis, and contribute to the formation of cellular protrusions. Its physical properties have been probed via atomic force microscopy (Matzke et al., 2001; Pesen and Hoh, 2005) and laser ablation (Saha et al., 2016). The cortex thickness has been measured at about 200nm (Clark et al., 2013), which is much smaller than the length of many cortical actin filaments (Fritzsche et al., 2016). By making an analogy with pre-wetting, it was suggested that myosin motors are cclultimately at the origin of the well-defined actin cortex (Joanny et al., 2013).

Gradients and anisotropies in tension generate flows of cortical actin (Mayer et al., 2010). These flows can lead to formation of contractile rings (Salbreux et al., 2009; Turlier et al., 2014) as well as an alignment of the filaments in the ring (Reymann et al., 2016). Asymmetries in cortical tension make the contractile ring position unstable and can lead to ring oscillations (Sedzinski et al., 2011). Oscillations have also been observed for actomyosin rings (Paluch et al., 2005) and of cellular shapes (Salbreux et al., 2007) in nondividing cells. A framework for analyzing cortex-driven shape changes has been formulated for active, elastic, thin shells (Berthoumieux et al., 2014). In general, however, motion of actomyosin rings depend on ring contractility in addition to cortical flows (Behrndt et al., 2012). Furthermore, cortical flows help to establish cell polarity by transporting certain proteins from one cell end to the other (Goehring et al., 2011). Remarkably, the actomyosin cortex in *Caenorhabditis elegans* embryos generates chiral torques, which generates counterrotating cortical flows that are used to establish the left-right symmetry of the developing organism (Naganathan et al., 2014). Finally, let us note that the contractility of thin active gel layers, be it the actin cortex or a cell monolayer, can generate instabilities that lead to three dimensional shape changes (Hannezo et al., 2011; Ideses et al., 2018; Shyer et al., 2017).

VII. NEURAL NETWORKS AND BRAIN FUNCTION

Understanding brain function is a grand goal for biology. The brain consists of a tightly connected network of billions of nerve cells called neurons (Dayan and Abbott, 2001). From a physical point of view, a nerve cell or an individual neuron is an electrically excitable unit. For a strong enough excitation above a threshold, the cell sends out an electrochemical pulse referred to as an action potential. This signal travels along the axon, which is a lin-

ear extension of the nerve cell. The transport of an action potential along an axon is quantitatively described by the Hodgkin-Huxley model (Hodgkin and Huxley, 1952), the essence of which is captured by the FitzHugh-Nagumo model (FitzHugh, 1961; Nagumo et al., 1962). At the end of the axon, the action potential can be transmitted to other nerve cells that receive the signal in extensions called dendrites. The coupling between an axon and dendrites occurs through synapses that chemically excite or de-excite the postsynaptic nerve cell by releasing biomolecules called neurotransmitters.

The activity of the brain is represented by the electrical activity of the whole neural network rather than that of individual neurons. The brain function closely associated with the activity is then determined by the underlying neural networks (Abbott, 2008; Hopfield, 1982). Therefore, one needs to explore the underlying neural network dynamics for specific functions. The physical and quantitative understanding of global brain functions such as learning and memory, decision making, and attention, as well as associated nonequilibrium neural network dynamics, are still challenging at present (Dayan and Abbott, 2001). We will quantify the nonequilibrium landscape and flux and associated nonequilibrium thermodynamics to explore these brain functions. For reviews of other aspects of dynamics of neural networks, see (Amit, 1989; Dayan and Abbott, 2001).

A. Learning and memory

To theoretically study cerebral processes, certain neural networks have been introduced where in neuron dynamics can be simplified. The state of neuron i is given by the continuous variable u_i representing its electrical potential and connects to another neuron j with strength T_{ij}. The state of neuron i changes due to the input from other neurons, a leak of ions that will bring an unstimulated neuron back to its resting potential $u_i = 0$ and a possible external input current I_i, such that

$$C_i \frac{du_i}{dt} = \sum_{j \neq i} T_{ij} f_j(u_j) - \frac{1}{R_i} + I_i, \tag{97}$$

where C_i and R_i, respectively, denote the capacity and resistance of neuron i and where f_j is a monotonically increasing sigmoidal function such that neuron i receives input from neuron j only if the "activity" of the latter is above a certain threshold. An important subclass of such networks are Hopfield networks, for which the weights are symmetric, $T_{ij} = T_{ji}$ (Hopfield, 1982).

The attractors of such a network are often interpreted as patterns stored within it.Given a certain distribution of input currents I_i, the network should settle into an attractor that associates this input with a previously learned pattern, where "learning" refers to adjusting the connection strengths T_{ij} such that certain inputs yield distinct activation patterns of the network. There are several different learning algorithms, that is, dynamics for the T_{ij} that yield the desired network properties. In the case of a symmetric network with $T_{ij} = T_{ji}$, the underlying dynamics are determined by the gradient of a potential energy (Hopfield, 1982) defined as

$$E = -\frac{1}{2} \sum_{i,j} T_{ij} f_i(u_i) f_j(u_j) + \sum_i \frac{1}{R_i} \int_0^{u_i} \xi f_i'(\xi) d\xi + \sum_i I_i f_i(u_i) \tag{98}$$

with $dE/dt \leq 0$. Consequently, E is a Lyapunov function of the system and will always settle in one of the steady state attractors (Hopfield, 1982). Symmetric connections imply an underlying neural network with behavior determined by purely potential energy. Memory is stored in the neural connection patterns forming the basins of attractions on the landscape. Learning can then be understood as the way of retrieving information from the initial queue near specific memory basins.

In the realistic neural networks of the brain, neural connections are not symmetric, that is $T_{ij} \neq T_{ji}$ so the energy E, Eq. (98), is no longer a Lyapunov function. Still, Equation (97) describes the neural network dynamics, which now also depends on the nonequilibrium potential landscape related to the steady state probability distribution and steady state rotational curl probability flux breaking the detailed balance. The rotational curl flux of neural networks emerges when neural connections are asymmetric (Yan et al., 2013). As a consequence, continuous line attractors can emerge (Yan et al., 2013). These attractors could provide a physical origin of associations between memories by flux.

B. Cycling of sleep phases

Movement between neural network states can be shown in an example connecting different phases during sleep, where periods of rapid eye movement (REM) alternate with non-REM periods (Mccarley and Massaquoi, 1986). The two phases are regulated by the interaction of two neural populations. The main contribution for the underlying circuit of REM sleep is an activation-repression loop inferred from experimental studies (Mccarley and Massaquoi, 1986). The dynamics follow the equation of motion $\frac{dx}{dt} = aA(x)xS_1(x) - bB(x)xy$ and $\frac{dy}{dt} = -cy + dxyS_2(y)$ where x and y represent the activities of REM-on and REM-off neural populations, respectively. The constants a, b, c, d and the sigmoidal functions A, B, S_1, and S_2, respectively, specify the interaction strengths between the populations (Yan et al., 2013). From a stochastic version of the equation of motion for x and y, one can obtain the Mexican hat-shaped landscape as a continuous close line attractor from the

steady state solution of the corresponding Fokker-Planck equation. The rotational curl flux driving the REM sleep flow can be directly derived from the force decomposition as in Sect. II.A.2. In addition, limit cycle stability can be assessed in terms of the landscape topography, that is, the height of the Mexican hat potential's center, and the frequency of the REM/non-REM cycle as a function of the release of the neurotransmitters acetylcholine and norepinephrine (Yan et al., 2013). It is shown that the nonequilibrium rotational curl flux from asymmetrical neural connections is crucial for generating the REM sleep rhythm, while for symmetrical neural connections, limit cycle oscillations cannot appear (Yan et al., 2013).

C. Brain decision making

One key aspect of cognition is decision making. Studies in monkeys have linked the process of decision making to the neural activity of a specific area of the cerebral cortex (Huk and Shadlen, 2005; Roitman and Shadlen, 2002; Shadlen and Newsome, 1996, 2001). In these experiments, trained monkeys were presented for a few seconds with a pattern of randomly arranged dots that moved coherently in one direction against a background of randomly appearing and disappearing stationary dots. Some time after the patterns were switched off, the monkeys were asked to make a decision about the average direction of motion of the dots.

a. The physics of decision making The neural network underlying decision making in this motion discrimination task consists of two populations of nerve cells competing with each other for selecting the leftward or rightward direction (Roitman and Shadlen, 2002; Shadlen and Newsome, 2001; Wong et al., 2007; Wong and Wang, 2006). The two populations self-activate and at the same time mutually inhibit each other. The sensory input current $I_{\text{motion},i}$ into population $i = 1, 2$ depends on the fraction of coherently moving dots or 'coherence' c as $I_{\text{motion},i} = \hat{I}(1 \pm c)$, where $\hat{I}$ is the input in absence of coherent motion and the plus and minus signs are respectively used when the motion is in the preferred direction of the population or opposite to it. The total input currents are then given by

$$I_{\text{tot},1} = J_{11}S_1 - J_{12}S_2 + I_0 + I_{\text{motion},1} \tag{99}$$

$$I_{\text{tot},2} = -J_{21}S_1 + J_{22}S_2 + I_0 + I_{\text{motion},2}. \tag{100}$$

Here, I_0 is the average background synaptic input, J_{ij} the synaptic coupling constants, and S_i the average gating variables. Their value is determined dynamically through

$$\dot{S}_i = -\frac{1}{\tau_S}S_i + \gamma(1 - S_i)r_i \tag{101}$$

with characteristic times τ_S and γ, and where r_i is the firing rate of the neural population i. The firing rateis essentially zero below a threshold value and then increases almost linearly as a function of the total input current (Roitman and Shadlen, 2002; Shadlen and Newsome, 2001; Wong et al., 2007; Wong and Wang, 2006).

Stochastic dynamics in the nonequilibrium landscape unveil the physical mechanism behind decision making (Yan et al., 2016), Fig. 16a. In the absence of a stimulus, $\hat{I} = 0$, there are three stable attractors corresponding to the undecided state and the two decided states. In the decided states, the populations has a high activity, otherwise all activities are low. With increasing stimulus, the stability of the undecided state decreases until it eventually becomes unstable, such that only the two decided states remain and the animal has to make a decision, Fig. 16b. For non-coherent patterns, $c = 0$, the decision is random, whereas for $c \neq 0$ it is biased towards the correct decision because the basin of attraction of the correct decided state grows while the that of the incorrect decided state shrinks. Furthermore, as the stimulus is reduced, the barriers around the decided states still remain for some time, which endows the systems with some memory for the decision made. Once an incorrect decision is made, it takes a much longer time to go over the barrier to reach the incorrect basin. This explains why there is a longer decision time for incorrect decisions than for correct ones. These findings are in agreement with the results from monkey experiments (Mazurek et al., 2003; Roitman and Shadlen, 2002; Shadlen and Newsome, 2001; Wong et al., 2007; Wong and Wang, 2006).

b. Speed, accuracy and dissipation tradeoff in decision making The process of decision making can be optimized for several quantities, notably, accuracy, speed, and dissipation. One can quantify the decision time by the corresponding mean first passage time from an undecided state to a decided state. One can also quantify the performance or accuracy of the neural network through a path integral method (Wang et al., 2010c) by defining the accuracy of the decision-making task as the ratio in probabilities between the optimal correct path and the error path. The dissipation in terms of entropy production is directly related to the rotational curl flux. As stated previously, this measures the system's distance from equilibrium and can therefore be quantified for decision-making (Yan et al., 2016).

Let us now focus on the speed-accuracy-dissipation tradeoff mechanism by varying input threshold. If speed is the main focus of decision-making, there is an optimal decision speed with almost minimum dissipation cost and reasonable accuracy. However, higher accuracy requires longer decision time, and thus a slower decision speed. If accuracy is the major concern of the decision-

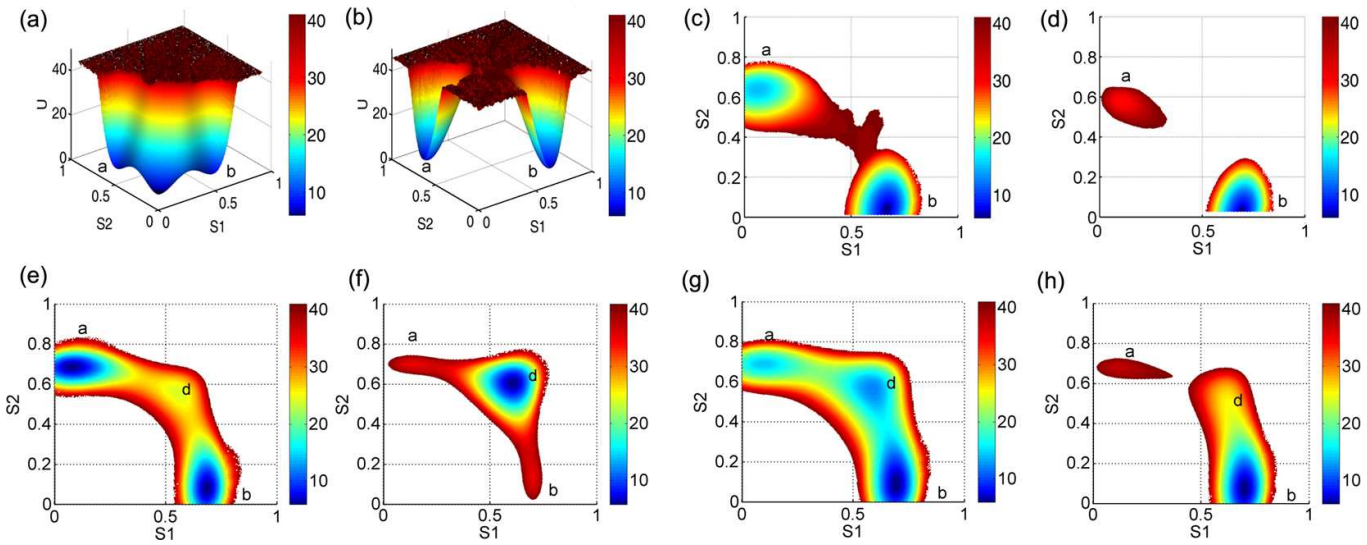

FIG. 16 Nonequilibrium potential landscapes for brain decision making and mind changes (a)(b) Potential landscapes at the zero coherence level for different stimulus inputs for decision making, $\mu_0 = 0$ and 30 Hz, respectively. c denotes undecided state, and a and b denote decided states. (c)(d) Potential landscapes at the non-zero coherence level, where $\mu == 30$ Hz and the coherence $c = 0.2$ and 0.65, respectively. (e)(f) Potential landscapes with different large inputs for mind changes. at zero coherence level. The strength of stimulus $\mu_0 = 50$ and 65 Hz respectively. (g)(h) The potential landscapes with different large inputs for mind changes. at different coherence levels. ($\mu_0 = 55$) when coherence $c' = 0.02$ and 0.12, respectively. In all subgraphs, parameters $a = 269.5, b = 108$, and $D = 3.6 \times 10^{-7}$) (from Ref. (Yan et al., 2016)).

making, both the dissipation cost and decision time are higher than optimum at the best accuracy, but there is a suboptimal accuracy with optimal speed and dissipation cost. When dissipation cost is the main concern for decision-making, the decision accuracy may not be the best nor will the speed be the greatest with the smallest dissipation cost. One sees that reasonable accuracy performance can be reached with minimum dissipation cost and fast decision time, though (Yan et al., 2016).

c. Mechanisms of mind changes Changes of mind occur often in making decisions. In this scenario, the initial choice can be altered. Decisions can be changed in two cases. For an incoherent stimulus $c = 0$, the system will settle in one of the two decided states as the strength of the stimulus is increased Fig. 16(e). Upon a further increase of the stimulus, a new attractor appears with high activity in both populations and the system will eventually settle in this state, Fig. 16(f). As the stimulus is again reduced, the high activity state disappears and the system will eventually settle in one of the decided states. However, this state will not necessarily match the original one; the decision can be changed. The emergence of a new attractor with increasing input strength has been observed experimentally (Resulaj et al., 2009). Studies suggested that the changes of mind might be due to the unprocessed information before the first decision (Resulaj et al., 2009).

For coherent inputs with $c > 0$, the correct choice state is more attractive and changes from an initial correct choice are unlikely to occur. However, when the network makes a wrong decision at the beginning, changes can occur relatively easily. This is because although there is a second chance (new center basin state) to make a decision due to large stimulus input, a network is still more likely to be attracted to the stronger basin of attraction for the correct choice, as shown in Fig. 16(g,h). This observation is supported by experimental data showing that the probability of changes to the wrong choice from the correct one decreases monotonically with increasing coherence (Albantakis et al., 2012; Albantakis and Deco, 2011; Resulaj et al., 2009). Therefore, the process of changes of mind can be described in three steps: making the initial decision, attraction to the new basin state, and at last making a different decision. As seen above, a change of mind can be understood through landscape topography.

VIII. THE GENETIC BASIS OF ORGANISMAL PROGRESSION

Two major processes transform the appearance and capabilities of organisms during their lifetime: development and ageing. Development is often accompanied by morphogenesis, and D'Arcy Thompson's seminal book On Growth and Form (Thompson, 1941) emphasized the need for physics in understanding morphogenesis early on. We refer the reader to recent reviews on the physics

of morphogenesis for a description of the current state of this field (Lecuit and Lenne, 2007; Mirabet et al., 2011; Sun and Jiang, 2011). We instead will focus on genetic aspects of development and ageing that so far receive less attention among physicists and present examples of how nonequilibrium landscapes can help to deepen our understanding of these processes.

A. Stem cell differentiation

Stem cells are undifferentiated cells capable of giving rise to specialized cells. Although a fertilized egg has the potential to develop into all the cell types of a body, differentiation typically occurs in a sequence of several steps, such that cells emerging at various stages of this process become more and more specialized. In 1957, Waddington suggested a pictorial way to visualize the developmental process in terms of a ball rolling down an increasingly fragmenting valley (Waddington, 1957). Though intuitive, this picture lacks a physical foundation and had noquantification. The Waddington landscape has received recent attention among physicists and other scientists for global quantification of development and reprogramming (Ashwin and Sasai, 2015; Chickarmane and Peterson, 2008; Feng and Wang, 2012; Huang et al., 2009; Jiang et al., 2008; Li and Wang, 2013, 2014b, 2015; Sasai et al., 2013; Wang et al., 2010b, 2011; Xu et al., 2014b).

Biologists have long thought that differentiation was irrevocable. This view was shattered after the identification of the core genetic network underlying differentiation. A typical core motif for these networks involves two self activating genes mutually repressing each other (Ashwin and Sasai, 2015; Chickarmane and Peterson, 2008; Feng and Wang, 2012; Huang et al., 2009; Jiang et al., 2008; Li and Wang, 2013, 2014b, 2015; Sasai et al., 2013; Wang et al., 2010b, 2011; Xu et al., 2014b). Some examples include the PU.1-GATA1 gene pair, which directs the differentiation of a common myeloid progenitor (CMP) into either myeloid cell or erythroid cell in blood cell formation; Oct4 and Cdx2 gene pair for the inner cell mass/trophectoderm lineage decision; and Nanog and Gata6 gene pair for segregation of primitive endoderm and epiblast within the inner cell mass, Fig. 17a. Another example involves the mutual regulations of the transcription factors Oct-4 and NANOG (Chambers et al., 2007; Kalmar et al., 2009; Takahashi and Yamanaka, 2006a). Both activate themselves; NANOG also activates Oct-4, whereas Oct-4 activates NANOG at low and suppresses it at high levels. This network topology generates a bimodal distribution of NANOG expression (Kalmar et al., 2009). Although the possibility of noise-induced transitions between the two principle states cannot be excluded, the existence of two subpopulations is rather thought to result from excitable dynamics of the regulatory network (Kalmar et al., 2009). Remarkably, controlled upregulation of NANOG leads to the reversal of a differentiated cell into a pluripotent stem cell (e.g. embryonic stem cells are pluripotent) (Takahashi and Yamanaka, 2006a), thus revoking the previous paradigm that differentiated cells cannot return to the pluripotent state. Waddington's picture is unsuitable for describing this process; instead, nonequilibrium landscapes and fluxes provide an appropriate framework for in-depth analysis.

The dynamics of gene regulatory networks can be captured by

$$\frac{dX_i}{dt} = -K_i X_i + \sum_j \frac{a_{ij} X_j^n}{S^n + X_j^n} + \sum_j \frac{b_{ij} S^n}{S^n + X_j^n}. \quad (102)$$

where X_i denotes the expression level of gene i, K_i represents the rate of degradation, and the next two terms are for activation and repression respectively. The activation strength of gene j on gene i is given by a_{ij}, whereas b_{ij} quantifies the repression strength. If the expression of i is independent of j, $a_{ij} = b_{ij} = 0$. The parameter S represents the "activation threshold" and n quantifies the cooperativity of regulation (Li and Wang, 2013).

The dynamics underlying differentiation were studied by analyzing Eq. (102) for a gene regulatory network motif of two self-activating and mutually repressing genes (Ashwin and Sasai, 2015; Chickarmane and Peterson, 2008; Feng and Wang, 2012; Huang et al., 2009; Jiang et al., 2008; Li and Wang, 2013, 2014b, 2015; Sasai et al., 2013; Wang et al., 2010b, 2011; Xu et al., 2014b). As discussed previously, this gene motif appears often in stem cell differentiation and reprogramming (Xu et al., 2014a). The cell starts from the stem cell state basin and eventually transforms to differentiated state basins during the developmental process. Here, the developmental direction is dictated by the change of the effective self regulations, which was unspecified in the original Waddington picture (Waddington, 1957; Wang et al., 2011). The differentiation process can be viewed as the evolution of the landscapes along development. (Wang et al., 2011).

The effects of development and of external interventions for dedifferentiation or reprogramming were captured by changing the interaction strengths a_{ij} and b_{ij}. In this way bifurcations were generated that correspond to the dedifferentiation process. The analysis showed that the differentiation and reprogramming pathways are typically irreversible, which is in contrast to Waddington's picture, Fig. 17. A detailed understanding of these pathways can guide the design of reprogramming pathways.

To this end, a more complete gene regulatory network underlying a human stem-cell differentiation has been explored that has resulted in optimal reprogramming paths that are consistent with experiments (Li and Wang, 2013). Furthermore, two attractors corresponding to two different cell types can coexist, and the rate

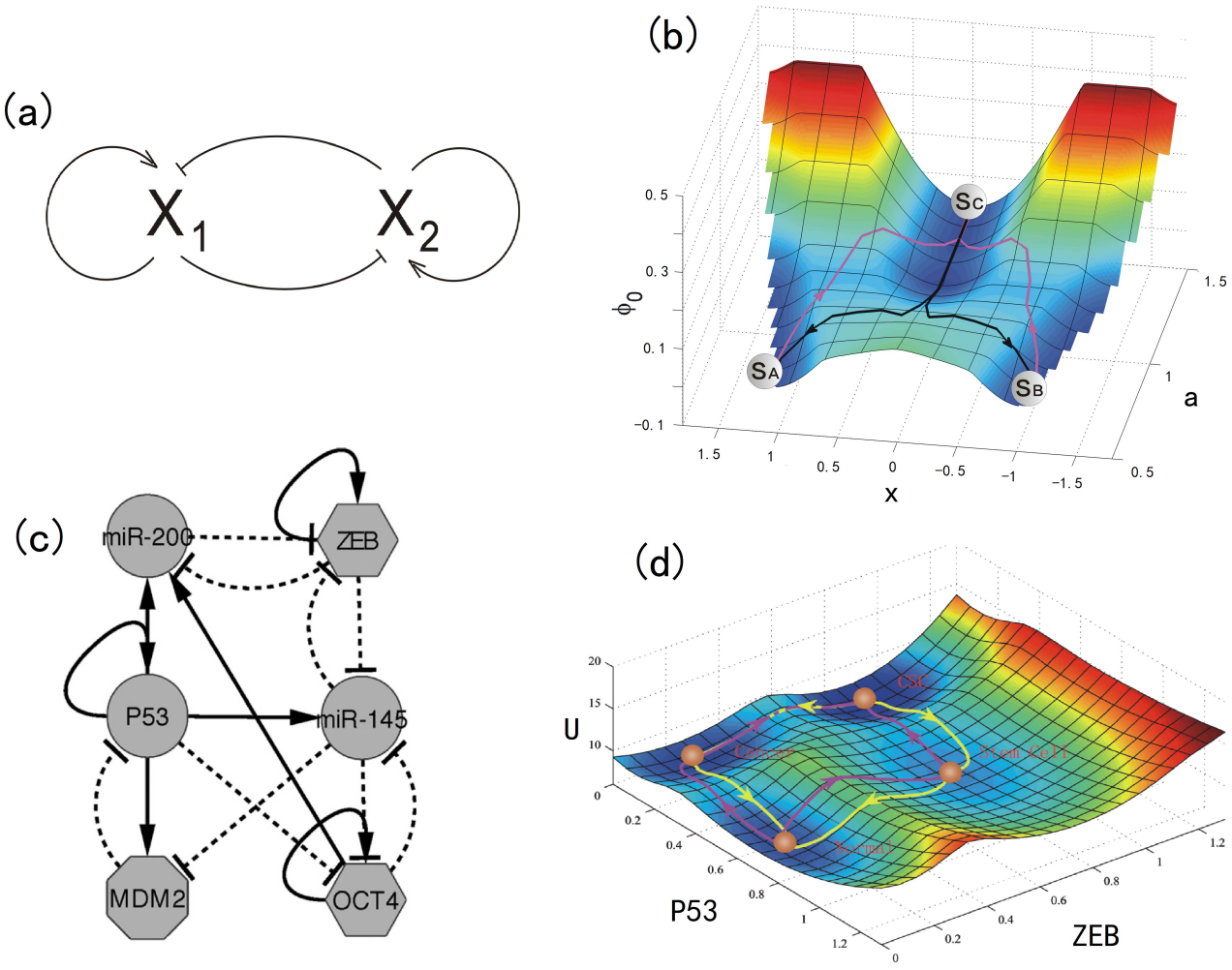

FIG. 17 Stem cell differentiation and cancer-development. (a) The wiring diagram of core gene regulatory motif of differentiation and development. (b) The quantified Waddington developmental landscape and dominant transition paths for differentiation, reprogramming and trans-differentiation paths. S_c denotes stem cell state while S_a and S_b denote differentiated cell states. (c) The wiring diagram of the core gene regulatory motif of cancer and development. (d) The landscape and the dominant transition paths between different cell states for cancer and development. (from Ref. (Li and Wang, 2015; Xu et al., 2014a)).

of noise or input-induced switches between them can be quantified (Xu et al., 2014a). The paths between two differentiated states may, but need not, pass through a stem-cell like state (Wang et al., 2011; Xu et al., 2014b), making the direct trans-differentiation possible. This is quite important because reprogramming often encounters a cancer state (Takahashi and Yamanaka, 2006a). These findings are particularly relevant in the context of the heterogeneity of stem-cell differentiation due to environmental and epigenetic influences (Ashwin and Sasai, 2015; Feng and Wang, 2012; Li and Wang, 2014b; Sasai et al., 2013).

B. Ageing

Ageing has been thought of as an inevitable process of continuous decay of physiological functions that eventually leads to death, but experiments on model organisms show that ageing can be significantly delayed by suitable genetic manipulations and in appropriate environments (Gems and L., 2013; Kenyon, 2010; Kirkwood, 2005). This suggests that the ageing process is regulated and programmed. Therefore, finding out the underlying genetic regulations and environmental influences is vital, though currently challenging. One can study ageing using *C elegans* as a model organism.

Based on experimental studies of pathways with an im-

pact on ageing a network of 11 genes and miRNAs involving DAF-2, DAF-16, SKN-1, AAK-2, AAKG-4 genes, TORC1, RSKS-1, PHA-4, HIF-1, miR-71 and miR-228 was established (Zhao and Wang, 2016), Fig. 18a. Its dynamics are given by Eq. (102) with appropriate connection strengths a_{ij} and b_{ij}. The nonequilibrium landscape displays two attractors. In the "ageing" state, expressions of genes with lifespan-limiting effects predominate, whereas in the "rejuvenating" state, genes that enhance the lifespan prevail, Fig. 18b. Since the ageing state is more stable than the rejuvenating state, most worms are expected to age "normally"; only a small fraction have an extended lifespan. The network, though, can switch between ageing and rejuvenation following genetic or environmental interventions. On a molecular level, further analysis suggested that self-degradation of lifespan-limiting and longevity-promoting genes leads to an increased stability of the ageing and rejuvenation states, respectively. This finding is consistent with experiments (Apfeld et al., 2004; Kenyon et al., 1993; Kimura et al., 1997; Lee et al., 2003; Samuelson et al., 2007) that also suggest why the ageing state becomes more probable with increasing lifetime. DAF-16 negatively regulates the target of rapamycin complex 1 (TORC1), which plays an important function in monitoring the metabolic state of a cell and in regulating protein synthesis. This negative regulation by DAF-16 has a dramatic effect on the lifespan of *C. elegans* (Kenyon et al., 1993; Wolff and Dillin, 2006), possiblybecause of damage accumulation. Along with a weakening of this connection, the dominant state can switch from rejuvenation to ageing. When increasing this negative regulation strength, the process reverts. Moreover, ageing and rejuvenation switching paths can be quantified, although they do not overlap much due to the presence of nonequilibrium rotational curl flux. This indicates, at least in principle, there is a possibility for reverting the ageing process through interventions (such as increasing the DAF-16 negative regulation to TORC1) (Zhao and Wang, 2016). The first hint of such success is from the stem cell reprogramming discussed earlier where the differentiated cells can be turned back to iPS progenitor cells (Takahashi and Yamanaka, 2006b; Wang et al., 2011).

Further analysis of the ageing and rejuvenation attractors suggests that self-degradation of lifespan-limiting and longevity-promoting genes leads to an increased stability of the ageing and rejuvenation states, respectively, which is consistent with experiments (Apfeld et al., 2004; Kenyon et al., 1993; Kimura et al., 1997; Lee et al., 2003; Samuelson et al., 2007).

Whereas the 'rejuvenation' state in *C. elegans* rather slows down or arrests ageing instead of reverting it, there are a few organisms that can revert to earlier developmental stages. Notably, the jellyfish *Turritopsis dohrnii* has normal ageing process which proceeds from young to old, though they can also change from the sexually mature medusa stage, in which they live as individuals, back to the sexually immature and colonial polyp stage (Bavestrello et al., 1992; Piraino et al., 1996). This process can be repeated as the old to young and young to old oscillation continues. By performing this oscillation, a jellyfish can live forever unless an accident, a predator, or a disease interrupts these cycles. The regulatory network in Fig. 18a is capable of producing sustained limit-cycle oscillations, where it switches periodically between ageing and rejuvenating phases (Zhao and Wang, 2016). Stability of the limit cycle path is guaranteed by the Mexican hat-shaped landscape, while the nonequilibrium rotational curl flux guarantees the stability of the oscillation flow and therefore the possibility of immortality through the forever oscillations. If these oscillation dynamics can emerge in more complex biological systems such as animals or human, this will provide new perspectives to understand and control the aging process for ourselves.

IX. CANCER

Cancer is a leading cause of death in human populations worldwide. In spite of decades of effort to understand the mechanisms leading to cancer, many open questions remain (Weinberg, 2007). Through these decades of work, several hallmarks of cancer have been identified (Hanahan and Weinberg, 2000, 2011) and are the aim of anti-cancer strategies. The processes of tumor growth, vasculation, and spreading during metastasis depend strongly on physical properties. It is thus of no surprise that physicists are heavily involved in understanding cancer (Ramis-Conde et al., 2009; Welter et al., 2009; Wirtz et al., 2011). Physical cancer treatments are still routinely employed. Beyond this obvious connection between cancer and physics, nonequilibrium concepts can be used to unravel the genetic and epigenetic conditions for the development of tumors and to explore new strategies for curing the disease (Welter and Rieger, 2013). Although cancer is still mostly viewed as a disease caused by mutations, there is growing evidence from a physical perspective that the focus on genetics is too restrictive and that environmental aspects have to be taken into account (Ao et al., 2008; Bar-Yam et al., 2009; Basan et al., 2009; Chen and Wang, 2016; Creixell et al., 2012; Gatenby and Vincent, 2003; Huang et al., 2009; Kauffman, 1971; Li and Wang, 2014a,b, 2015; Lu et al., 2013, 2014b; Tian et al., 2013; Wang et al., 2007; Yu and Wang, 2016). Cancer can more usefully be thought of as a disease state of the whole gene network. Environmental changes can lead to changes or imbalances in regulation of genes in the network, some of which favor the cancer state. This suggests that cancer treatment needs to target a collection of key genes and regulations. Several questions related to this strategy remain unanswered.

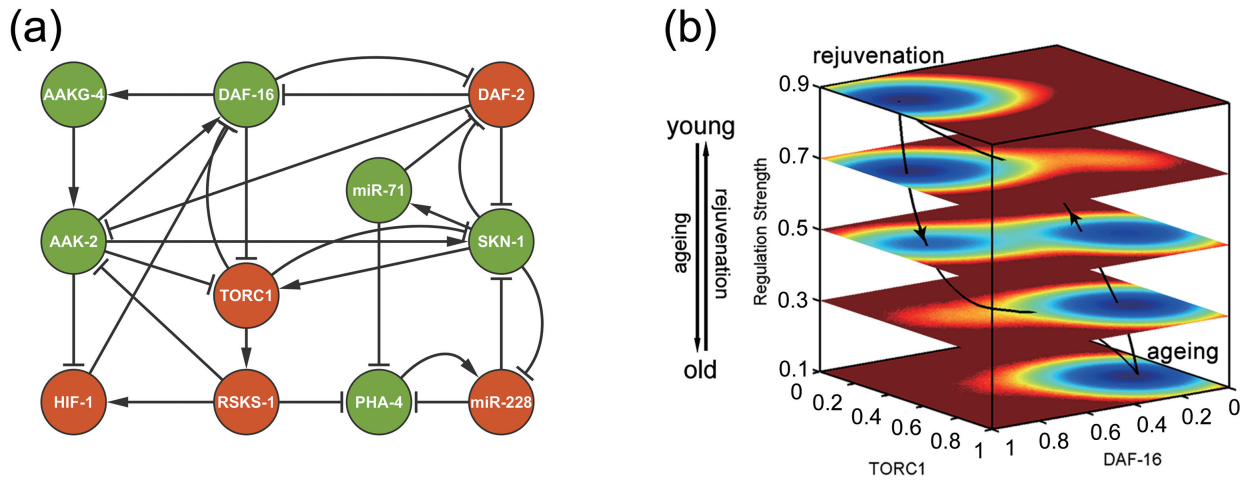

FIG. 18 Gene network and nonequilibrium landscape of ageing and rejuvenation. (a) The wiring diagram of the core gene regulatory network of ageing of *C. elegans*. (b) Dynamical landscape of *C. elegans* aging process. The horizontal coordinates denote the gene expression levels of DAF-16 and TORC1, the vertical coordinate denotes the regulation strength at which DAF-16 inhibits TORC1 Rejuvenation and aging attractors are labeled as Rejuvenation and Ageing, and black lines denote the optimal paths between the rejuvenation and aging attractors upon changes in regulation strengths. (from Ref. (Zhao and Wang, 2016)).

How do we quantify the cancer state? Can cells or tissues revert from a cancerous to a healthy state? How can we identify key genes and regulators? In this section, it is not our aim to give a comprehensive review of the physics of cancer. Rather we highlight how nonequilibrium concepts, notably, nonequilibrium landscapes and rotational curl fluxes as well as the homeostatic pressure, have advanced our understanding of this devastating disease.

A. Quantifying the landscape of cancer

To illustrate the application of nonequilibrium landscapes to cancer, consider breast cancer for which a core gene regulatory network consisting of 15 genes was constructed (Yu and Wang, 2016). This core network consists of oncogenes BRCA1, MDM2, RAS, HER2; tumor suppressor genes TP53, P21, RB; kinases CHEK1, CHEK2, AKT1, CDK2, RAF, for cell cycle regulation; the transcription factor E2F1; and ATM and ATR, important for early signal transduction through cell-cycle checkpoints. The wiring diagram of the network is described in (Yu and Wang, 2016), shown in Fig. 19 (a).

The dynamics of the gene regulatory network are captured by a type of equation similar to Eq. (102).

The landscape projected on the expression levels of the oncogene *BRCA1* and the transcription factor E2F1, which is a marker for breast cancer, exhibits three attractors, Fig. 19b, corresponding to the normal, the cancer, and a premalignant state. The respective gene expression levels associated with the attractors are consistent with experimental findings (Lu et al., 2013; Tian et al., 2013; Yu and Wang, 2016). In comparison to the premalignant state, the attractors of the normal and the cancer state are much more stable, indicating the importance of detecting the disease in early stages; whereas appropriate treatment might be able to revert cells from the premalignant to the normal state, the transition to the cancer state is practically irreversible. The dominant pathways of switching can be identified and used to quantify the process of how the normal state changes to the cancer state and vice versa.

Beyond these general statements, landscape analysis can provide more specific information. For example, changes in the expression of the central tumor suppressor gene *TP53* change the depths of and the barriers between attractors. Notably, an increased repression of *TP53* facilitates the transition first to the premalignant and then to the cancer state, which eventually has the dominant basin of attraction (Yu and Wang, 2016). Global sensitivity analysis based on the barrier heights allows one to identify key genes and regulations for breast cancer formation and dysfunction. Four key regulations (HER2⊣TP53, TP53→ATM, ATM→MDM2, CDK2⊣BRCA1) and six key genes (HER2, TP53, ATM, MDM2, BRCA1 and CDK2) are identified. These regu-

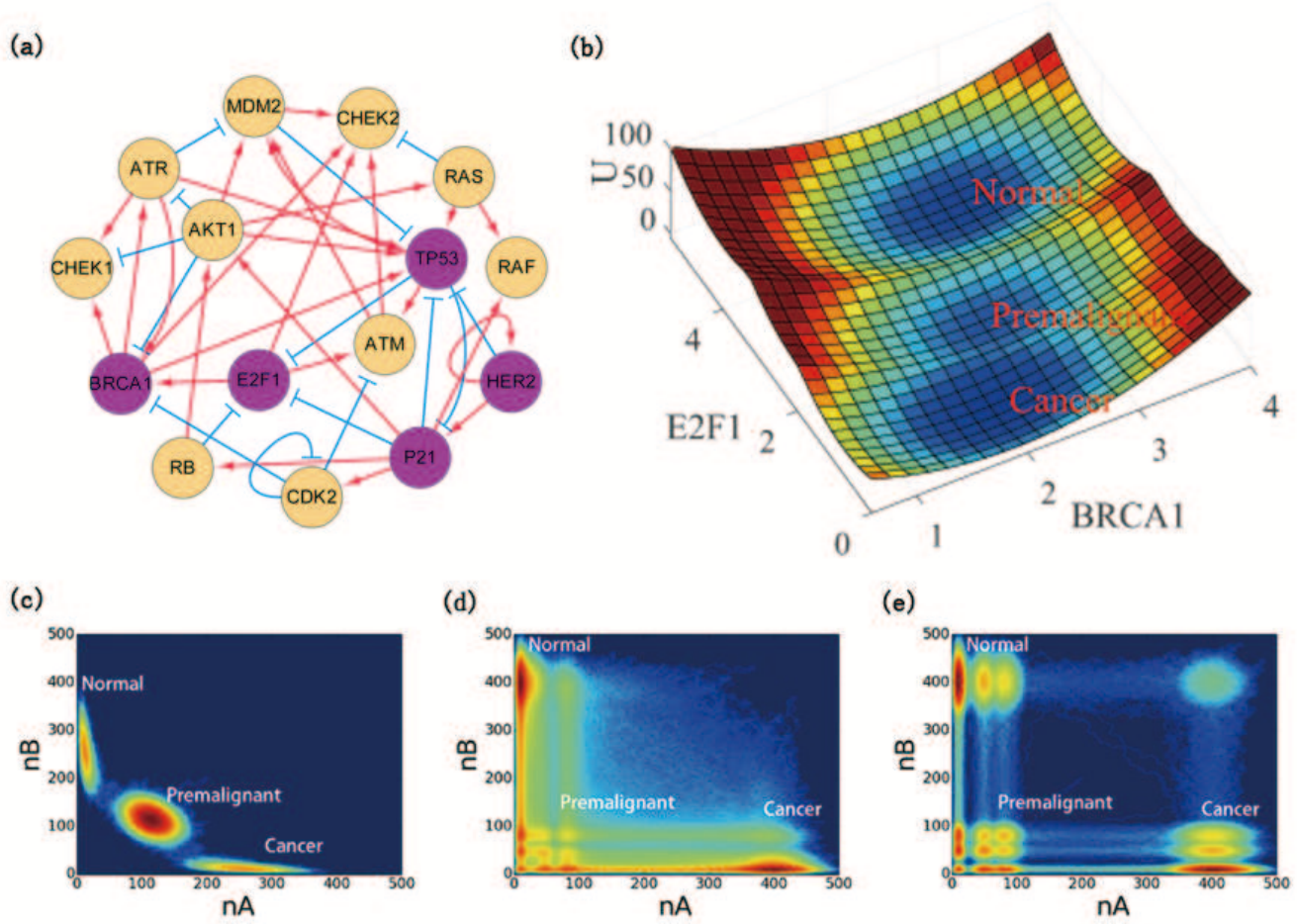

FIG. 19 Gene network and nonequilibrium landscapes of cancer (a): Underlying gene regulatory network for breast cancer. $->$ represents activation regulations while $-|$ represents repression regulations. (b) The tristable landscape of the breast cancer gene regulatory network. (c)(d)(e): Landscapes from fast to slow epigenetic regulations. (from Ref. (Chen and Wang, 2016; Yu and Wang, 2016)).

latory links could serve as the targets for network-based drug discovery.

B. Cancer and Development

A hallmark of cancer is the abnormal growth of cells (Hanahan and Weinberg, 2000, 2011). Development at the cellular level often refers to the differentiation process from primary stem cells (Waddington, 1957; Wang et al., 2011). A hint of the possible connection between cancer and differentiation lies in the fact that cancer often regrows after the radiation and chemo treatments (Marotta and Polyak, 2009). The possibility of the existence of the seeds for cancer in the form of cancer stem cells has been explored recently (Lobo et al., 2007). To understand the underlying mechanism of the cancer stem cell and the relationship between cancer and development, one needs to explore the underlying regulatory interactions among genes.

There are intimate connections between gene regulatory networks for healthy tissue growth and tumor development. For example, the tumor suppressor TP53 and its suppressor MDM2, as well as ZEB and OCT4, play a role in differentiation. ZEB is known to be a major player in the epithelial-to-mesenchymal transition, often linked to cancer metastasis and formation of CSCs. The miRNA regulates both cancer and development and therefore mediates the interactions between cancer and developmental genes. The core gene regulatory motif for cancer and development is illustrated in (Li and Wang, 2015) Fig. 17(c).

The dynamics of this core regulatory motif can be described by Eq. (102). An analysis of the corresponding nonequlibrium landscape reveals four attractors corresponding to the stem-cell, cancer stem-cell, healthy

differentiated, and differentiated cancer states (Li and Wang, 2015), Fig. 17(d). Normal differentiated state emerges with high TP53 and low ZEB expressions, while the differentiated cancer state emerges with low TP53 and low ZEB expressions. The stem cell state emerges with high TP53 and high ZEB expressions, while the cancer stem cell state emerges with low TP53 and high ZEB expression. Based on the landscape topography, the stem cell is most likely to transit into the normal differentiated state from which it can move to the cancer cell state. However, the stem cell can also change into a cancer stem cell, which then provides another route into the cancer state. From the landscape analysis it was also found that, consistent with experiment (Li and Wang, 2015; Lobo et al., 2007; Marotta and Polyak, 2009), the cancer cell state re-emerges after eliminating all cancer cells. Furthermore, it helped to identify in this network motif the key elements responsible for generating new cancer seeds. These findings can help suggest potential strategies for regulating cancer stem cells as a novel and robust anti-cancer therapy.

C. Cancer heterogeneity

Cancers are often heterogeneous. This is a critical issue for radiation and chemotherapy, because a radiation dose or single drug might not be able to kill all cancer related cells in a heterogeneous population (Marusyk et al., 2012). Heterogeneity might be due to genetic differences between the cells that result from mutations accumulating during cancer progression. Alternatively, and maybe more importantly, intra-cellular heterogeneity might be primarily caused by epigenetic modifications (Shackleton et al., 2009). These are chemical modifications such as methylation, applied to DNA and to accessory proteins like histones. These modifications do not change genome sequence but affect, for example, DNA organization and transcription. Notably, they can lead to regulatory delays. As a consequence, a larger variety of states can emerge (Chen and Wang, 2016)

The idea of heterogeneity was illustrated by a core gene motif of cancer with mutual repressions and self activations. The genes produce proteins and proteins regulate genes and determine whether the genes are turned on or switched off. When the speed of genetic regulation by proteins is fastcompared to their production/degradation rate, then the proteins and genes are inseparable and can be treated with the same identity. Alternatively, when the genetic regulation speed is slow compared with the protein production/degradation rate, proteins and genes must be treated distinctly. It was found (Chen and Wang, 2016) in Fig. 19 (c)(d)(e) that when regulatory binding/unbinding is fast compared to synthesis/degradation, that is, in the adiabatic limit, three states quantified by the basins of attractions emerge: the normal state, the cancer state, and an intermediate premalignant state. When regulatory binding/unbinding is comparable to or even slower than the synthesis/degrdation corresponding to the epigenetic case, that is, the nonadiabatic limit, heterogeniety emerges with extra time scales involving histone remodification and DNA methylation. Both premalignant and cancer state basins are surrounded by a significant number of shallower and less stable state basins (Chen and Wang, 2016). The interactions among genes are made effectively weaker by epigenetics, illustrated in this context by longer regulation time compared with protein synthesis/degradation. This weakening can lead to fewer constraints and more freedom for each gene, which in turn can lead to the emergence of more metastable states in the regulatory landscape. By targeting epigenetics and environments, an understanding and control over cancer heterogeniety may be possible.

D. Homeostatic pressure

Primary tumors are rarely lethal, but cells can leave a tumor and invade other parts of the organism. When these cells leave the tumor and subsequently metastasize they produce secondary tumors that can be much more dangerous. Cancer cells that cause secondary tumors are mainly transported by the blood stream. However, the distribution of metastases is not fully determined by the blood flow pattern, as the receiving tissue must in some sense be compatible with the metastatic cell. This phenomenon has been captured by the seed-and-soil hypothesis (Weinberg, 2007).

This hypothesis can be conceptualized by homeostatic pressure, which is a tissue-inherent quantity that describes the pressure exerted by an expanding tissue of proliferating, growing, and dying cells (Basan et al., 2009). A planar interface between two tissues of different homeostatic pressures will move into the direction of the tissue with the lower homeostatic pressure. For a spherical clump of cells, interfacial stresses are also considered.

If cell growth is independent of the size of the tissue, then cell spheroids will expand in a surrounding tissue only if they exceed a certain size (Basan et al., 2009). Taking into account the stochastic nature of cell growth, division, and death, the homeostatic pressure provides a quantitative conceptualization of the seed-and-soil hypothesis. To be useful for therapy, biochemical or immunological means of affecting the homeostatic pressure need to be uncovered.

E. Cancer and immunity

Tumor cells express antigens and are thus prone to be eliminated by the immune system (Hanahan and Wein-

berg, 2011). This avenue is exploited by cancer immunotherapy, which has achieved spectacular results for specific types of cancer. (Sabado and Bhardwaj, 2015) However, cancer can manipulate the immune system. This leads to two hallmarks of cancer immunity, avoiding immune destruction and tumor promotion inflammation (Hanahan and Weinberg, 2011). A profound understanding of the relation between cancer and the immune system remains elusive.

Theoretical studies of the complex interaction between cancer and the immune system that take spatial aspects into account are commonly based on active particles (Bellomo and Delitala, 2008). Such descriptions can be fairly comprehensive, but the large number of details that are accounted for make a thoroughanalysis rather difficult and often prohibit an understanding of the fundamental principles. In contrast, non-spatial ordinary differential equation models that describe tumor-host interactions are generally simple enough to be comprehensively analyzed (Eftimie et al., 2011; Pappalardo et al., 2014; Wilkie and Hahnfeldt, 2013).

Cancer and immune cells can communicate and influence each other either through direct contact or via cytokines, which are a small signaling molecules secreted by cells, notably during an immune response. The dynamics of the respective cell and cytokine concentrations can be formulated in equations similar to Eq. (102) (Li and Wang, 2017), with several essential modifications. The degradation rate of a cell type depends on the concentration of other cell types and of cytokines. While the net regulation of cells by others take the additive form, the net regulation of cytokine concentrations by others take the multiplicative form. Similarly to gene regulation networks, the proliferation of cells and the secretion of cytokines can be either enhanced or diminished by the presence of other cell types and cytokines. The concentration dependencies of the various rates is given in terms of Hill functions and the coupling coefficients encode for the network structure.

The nonequilibrium landscape for a network consisting of one cancer cell type, 12 immune cell types, and 13 types of cytokines has three attractors corresponding to a healthy state and states of, respectively, low and high tumor cell concentration (Li and Wang, 2017). In the healthy state, both cancer and immunity cell concentrations are low. Both low and high cancer states, the innate immune response leads to an increased presence of natural killer cells, a type of white blood cells with the task to destroy infected cells. On the other hand, in both low and high cancer states, the adaptive immune response leads to an increase of in the concentration of a kind of white blood cells, namely $CD8^+$ cells. However, their concentration is higher for the state with lower concentration of tumor cells, and lower for the state with higher tumor cell concentration. (Li and Wang, 2017; Lu et al., 2014a). This finding suggests that the adaptive immune system is suppressed by cancer cells.

The interaction between cancer and the immune system depends on the state of progression as the interactions between different cells or cells and cytokines are modified in the environment of a developing tumor. The various effects of the immune system in different stages of developing tumors is known as cancer immunoediting (Dunn et al., 2002). Correspondingly, the nonequilibirum landscape attractors of the immune system-cancer network change with changing interaction strengths and several stages can be distinguished (Li and Wang, 2017), Fig. 20b. In stage 1, only the healthy state attractor exists. It is controlled by the immune system and nascent tumors are repressed, corresponding to the elimination phase of cancer immunoediting. In stage 2 a low cancer expression state begins to emerge, and in stages 3 and 4 low and high cancer expression states emerge in addition to the normal state. These three stages correspond to the equilibrium phase of cancer immunoediting, which is the phase persisting the longest. In stages 5 and 6 only the low and high cancer expression states remain, corresponding to the escape phase of cancer immunoediting, when the cancer has escaped the organism's immune response. Important immunotherapy targets are predicted from the landscape approach through global sensitivity analysis, including three types of immune cells (mature dendritic, natural killer, and CD8+ T-cells) and two types of cytokines (IL-10 and IL-12) (Li and Wang, 2017). The oscillation behavior of immune-cancer network dynamics was also expected in some cases. (Li and Wang, 2017)

X. POPULATION DYNAMICS AND ECOLOGY

Living organisms are highly social by nature and often coordinate with each other to generate collective behaviors in space and time. Studying the dynamics of population and ecology provided some early examples of nonequilibrium dynamics. In the following, we will highlight some recent developments on microbial population and ecology.

A. Populations of microorganisms

Population dynamics is typically studied through field research; however, it often requires significant effort and suffers from a lack of control over environmental conditions. By contrast, microbial populations are much more amenable to manipulation and quantification while still possessingintricate dynamics. Thus, synthetic microbial populations have been recently exploited as model systems to study population dynamics (Brenner et al., 2008; Chuang et al., 2009; De Roy et al., 2014; Gore et al., 2009; Großkopf and Soyer, 2014; Kong et al., 2018; Lu

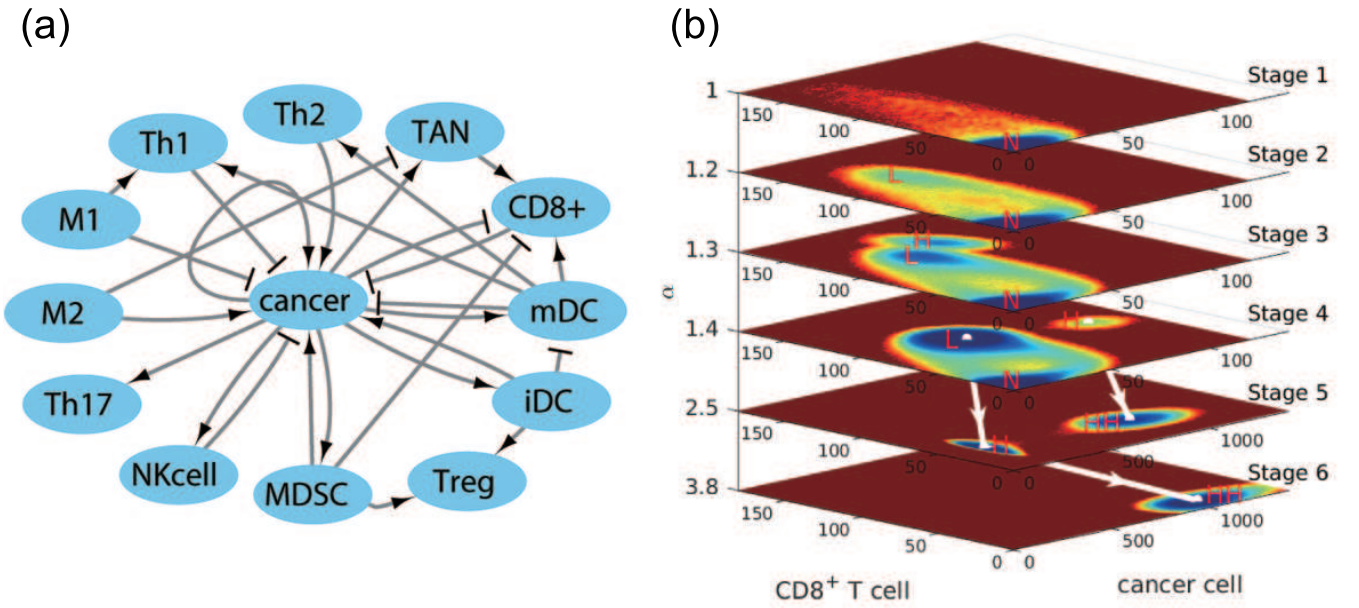

FIG. 20 Gene network and nonequilibrium landscape of cancer-immune system (a) A core cancer-immune cell-cell interaction network. (b)Cancer-Immune landscapes at various stages of tumor development (from Ref. (Li and Wang, 2017)).

et al., 2007; Ozgen et al., 2018; Shou et al., 2007; Xavier, 2011). Microorganisms can establish coordination and create collective behaviors among populations by secreting and detecting chemicals. One common way to generate population behaviors is using quorum sensing, a mechanism that enables cells to sense the density of their peers and respond accordingly (Kong et al., 2014; Miller and Bassler, 2001).

A gene network based on quorum sensing was designed and implemented in *E. coli* to generate synchronous population oscillations (Danino et al., 2010). In this network (Fig. 21a), expression of the genes $luxI$ and $aiiA$ is controlled by the P_{lux} promoter. The enzyme LuxI synthesizes the quorum sensing molecule N-Acyl homoserine lactone (AHL), which activates the P_{lux} promoter after binding to LuxR and, hence, promotes its own expression. In contrast, AiiA degrades AHL, which provides a negative feedback on LuxI production. In each cell, such a topology leads to the oscillation of P_{lux} promoter activity. Because AHL can diffuse from cells to their neighbors,it couples individual cells and generates synchronous oscillation of thousands of cells in a square region with area 10^4 μm^2 (Danino et al., 2010). The distance over which the population synchronizes depends on the diffusion constant of the quorum sensing molecule. Using a similar approach in which H_2O_2 was used as a signaling mechanism to overcome the slow diffusion obstacle for long-range coupling, synchronized oscillations were observed for several millions of bacteria across a distance of 5 mm Fig. 21b) (Prindle et al., 2012).The same oscillation mechanism that involves activation and repression can also be realized through multiple strains (Chen et al., 2015b) (Fig. 21c).

In addition to synthetic populations, natural organisms exhibit remarkable collective behaviors that are far from equilibrium. The formation of multicellular life forms from unicellular microorganisms is a representative class of such processes (Claessen et al., 2014; Lyons and Kolter, 2015). Multicellularity can arise from simple cellular aggregation as a consequence of incomplete separation after cell division. Another way collective behavior arises is through dynamic aggregation of previously individual cells, which involves cellular communication and differentiation, partitioning of tasks, and spatial organization. Well-studied examples of the latter route are fruiting body formation of myxobacteria and of the slime mold *Dictyostelium disoideum* (Muñoz-Dorado et al., 2016; Zusman et al., 2007). In nutrient-limited conditions, cells communicate through multiple modes of interactions and self-organize into complex, three-dimensional structures. Within the fruiting bodies, a subset of the cells differentiate into non-reproductive cells, while the remaining cells become reproductive spores.

B. Ecology

Populations are typically not isolated; instead, they often compete and cooperate with populations of other species in nature. This is a topic of ecology (Levin, 1981; Levin and Segel, 1985; Murray, 1998; Touboul et al., 2018a; Vandermeer and Goldberg, 2003). Predator-prey systems have been of particular interest in this field since

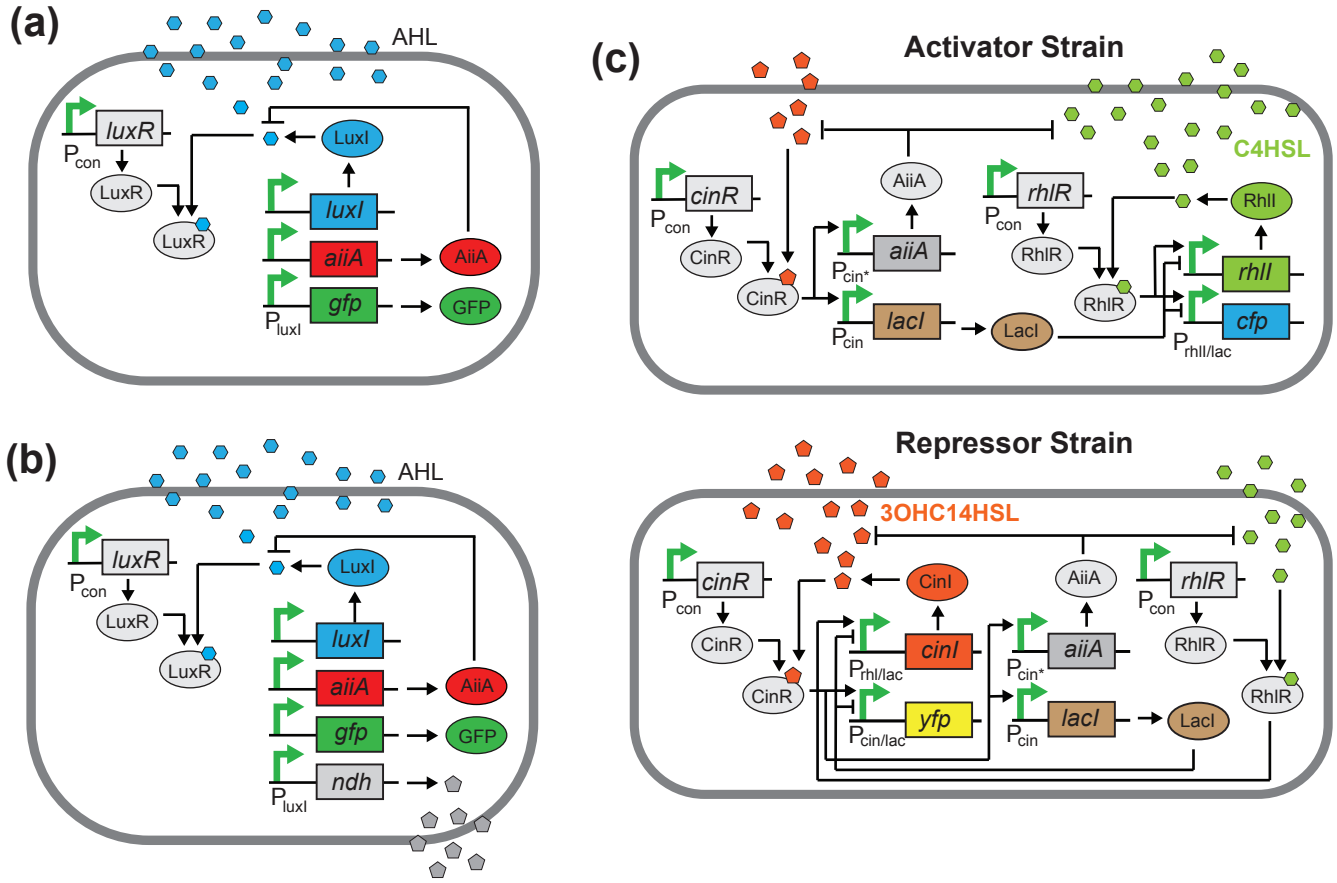

FIG. 21 Microbial oscillations at the population and multi-strain levels. (a) A gene circuit that enables synchronized oscillation of individual bacterial colonies (Danino et al., 2010). (b) A gene circuit that synchronizes the oscillation of thousands of bacterial colonies (Prindle et al., 2012) (c) A gene circuit that allows stable oscillations of two bacterial strains (Chen et al., 2015b).

the work of Lotka and Volterra (Lotka, 1925; Volterra, 1927). Their model showed that the systems can generate various dynamics including sustained oscillations. Observed in animal populations in nature (Murray, 1998), such dynamics have been recently observed in populations of engineered bacteria that utilize quorum sensing machineries (Fig. 22a) (Balagaddé et al., 2008). Experiments in microchemostats confirmed distinct types of population dynamics, namely coexistence, extinction and oscillation. The underlying landscape for global description of the dynamics has also been quantified (Li et al., 2011b; Xu et al., 2014a).

Beyond well-mixed cultures, microbial populations have also been used to study spatial ecology. An example is provided by a system of three *E. coli* strains that populate a petri dish (Kerr et al., 2002). The ecosystem consists of a strain producing the toxin colicin (C), a strain sensitive to colicin (S), and a strain resistant to it (R) (Fig. 22b). In this setting, strain C kills strain S by releasing colicin, strain S in turn outgrows strain R because it does not synthesize resistance proteins, and strain R has a higher fitness than strain C as it does not produce toxins. Together, these strains form a fitness advantage loop, resembling an ecological version of the rock-paper-scissors game. The corresponding experiments showed that a single species rapidly dominates in the well-mixed case while, on plates, the ecosystem exhibited coexistence (Kerr et al., 2002).

C. Landscape and flux analysis of ecosystems

One of the central questions of ecology concerns the coexistence of species. Under which conditions is this possible? How many species can coexist in a given environment? This translates into the question of whether or not an ecosystem is stable. The analysis of stability against small perturbations is standard, and in some cases Lyapunov functions have been found (Goh, 1976, 1977; Harrison, 1979; Hastings, 1978; Holling, 1965; Hsu, 1978; Levin, 1979, 1987; Levin and Segel, 1976; Lotka, 1925; Murdoch and Oaten, 1975; Touboul et al., 2018b; Volterra, 1931). Both well mixed and spatial deterministic and stochastic ecological dynamics have been inten-

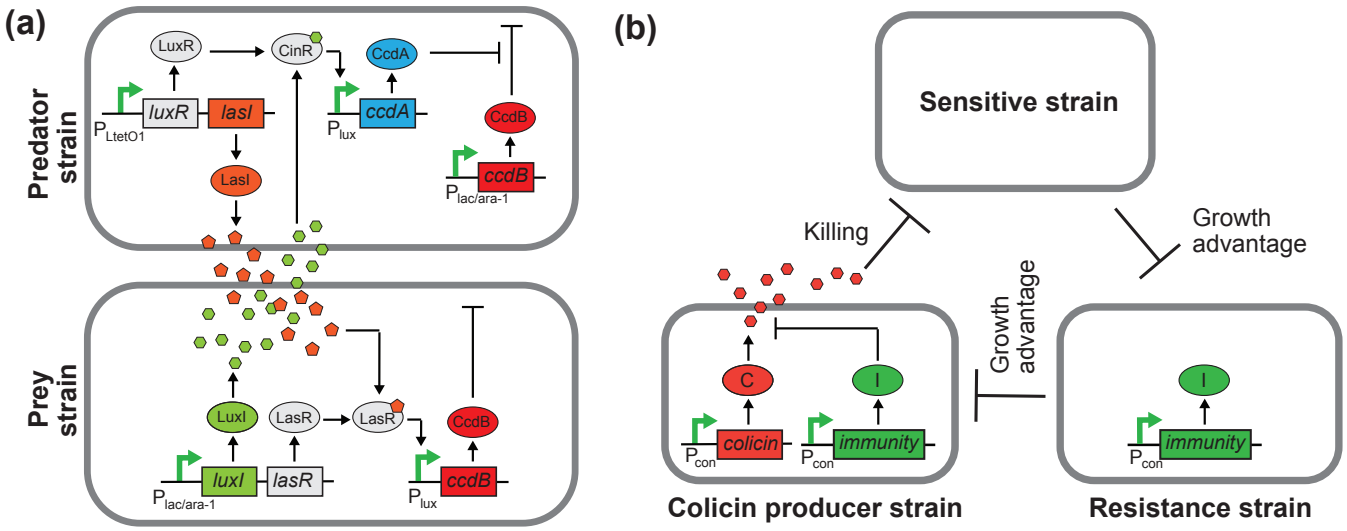

FIG. 22 Microbial ecosystems. (a) A synthetic predator-prey system (Balagaddé et al., 2008). (b) A three-strain ecosystem resembling a rock-paper-scissor game (Kerr et al., 2002).

sively investigated (Bassler et al., 2019; Biancalani et al., 2015; Black and McKane, 2012; Butler and Goldenfeld, 2009; Levin, 1979, 1987; Levin and Segel, 1976; Reichenbach and Frey, 2008; Reichenbach et al., 2007; Shih et al., 2016; Touboul et al., 2018b). A general way to assess the global stability of states, however, is in demand. The theory of nonequilibrium landscapes and fluxes is useful in this context (Han and Wang, 2007; Lapidus et al., 2008; Wang et al., 2006a, 2008; Xu et al., 2013, 2014a; Zhang et al., 2012). Intrinsic nonequilibrium landscapes provide Lyapunov functions for quantifying global stability of the ecosystems (Xu et al., 2014a); we illustrate with few examples. In the following, C_1 and C_2 denote the sizes of two populations.

a. Predator and prey Consider the following model for a population of predators C_1 and of prey C_2 (Murray, 1998) (Fig. 23(a))

$$\frac{dC_1}{dt} = C_1(1-C_1) - \frac{aC_1C_2}{C_1+d} \tag{103}$$

$$\frac{dC_2}{dt} = bC_2(1-\frac{C_2}{C_1}). \tag{104}$$

In the absence of predators, the prey population evolves according to the logistic growth model. The rate at which predators feed on the prey is quantified by the parameter a, and d denotes the prey population size at which prey are consumed by the predators at their maximum rate. The population of the predators also grow according to the logistic growth model. The ratio of the birth rates of both populations is b and the capacity of the system for prey is C_1. When the number of predators increases, more prey will be eaten. The shortage of food will lead to a population reduction for the predators. The prey population will then increase, which subsequently promotes an increase of the predator population. This is the origin of the limit cycle found in predator-prey dynamics. The nonequilibrium landscape has the shape of a Mexican hat, Fig. 23(d), revealing an oscillatory state that is globally stable, while the rotational curl flux enables the stability of the oscillation flow (Xu et al., 2014a).

b. Cooperation and competition Cooperation and competition between two species can be described by (Bazykin, 1985) (Fig. 23(b)(c)):

$$\begin{aligned} \frac{dC_1}{dt} &= C_1(C_1-L_1)(1-C_1) + a_1C_1C_2 \\ \frac{1}{\alpha}\frac{dC_2}{dt} &= C_2(C_2-L_2)(1-C_2) + a_2C_1C_2 \end{aligned} \tag{105}$$

The factors $(C_i - L_i)$, $i = 1, 2$, modifying the logistic growth model assure that the population size does not drop below L_i when the other species is absent.The terms proportional to C_1C_2 describe the interaction between the two species, which is cooperative if $a_1, a_2 > 0$ and competitive if $a_1, a_2 < 0$. The parameter α quantifies differences in the growth rates of two species. Four different steady states are possible: extinction ($C_1 = C_2 = 0$), mutual exclusion (either $C_1 = 0$ or $C_2 = 0$), or coexistence (C_1 and C_2 are nonzero). Through the corresponding basins of attraction, the potential landscapes determine which of these states is stable for a given set of parameters, Fig. 23(e) (Xu et al., 2014a).

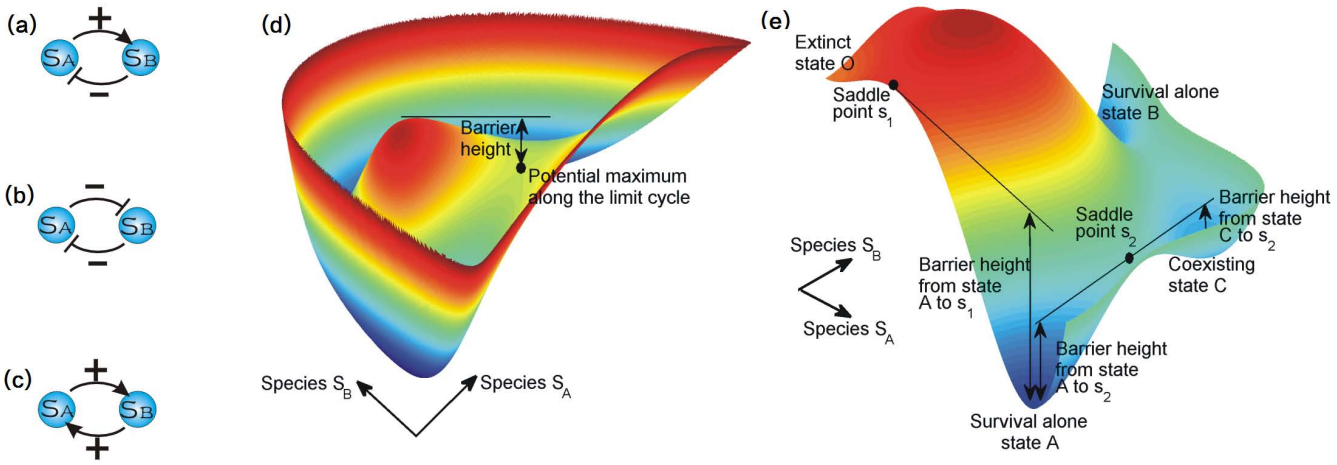

FIG. 23 The schematic diagram for the ecological models and associated landscapes. (a)Predation model. (b)Competition model. (c)Mutualism model. (d) Limit cycle attractor landscape for predation model. (e) Multiple attractors for competition and cooperation models (from Ref. (Xu et al., 2014a)).

XI. EVOLUTION

Evolution is the essence of biology. After Darwin laid out the principles of evolution by variation and natural selection (Darwin, 1873), a significant fraction of subsequent research has focused on quantifying evolutionary processes. Concerned with the process of adaptation, Sewall Wright introduced the concept of an adaptive landscape for evolution (Ewens, 2004; Fisher, 1930; Rice, 2004; Svirezhev and Passekov, 1990; Wright, 1941). Adaptation, or "shifting-balance" in Wright's terms, then refers to reaching summits in this landscape by random genetic drift from mutations and selection pressure. Through these sources of adaptation, evolutionary dynamics will follow a gradient until an optimum is reached. The parallels to energy minimization in physics are obvious. The virtues and shortcomings of the adaptive landscape metaphor are still debated (Pigliucci, 2008; Rice, 2004).

The central results of quantitative genetics is "Fisher's fundamental theorem", which states that the rate of evolution, quantified by the rate of change of average fitness, is equal to the statistical variance of the population's fitness. Still, some critical issues remain. How general is Wright and Fisher's evolution theory? Can it explain how evolution can continue indefinitely?

A key assumption in Wright and Fisher's theory is that selection force is independent of the relative proportion that a gene variant, an "allele", appears in a population at a specific site or "locus" on the chromosome. In other words, the assumption is that the selection driving force is independent of the interactions among gene species, referred to as the allele frequency independent selection, or linkage equilibrium (LE) (Neher and Shraiman, 2011). However, in general, trait selection can have allele frequency dependence. This is apparent in coevolution, where two or more species mutually affect their evolution. In these situations, Wright and Fisher's theory breaks down. Furthermore, LE cannot explain open-ended evolution that is clearly observed in bacterial colonies that have been evolving under constant physical and chemical conditions for tens of thousands of generations (Elena and Lenski, 2003). The theory also fails to describe molecular evolution experiments, wherein a molecular species constitutes the building blocks for a new species, which in turn can form another molecular species and so on (Worst et al., 2016).

The key to resolve above issues lies in the fact that the adaptive landscape is not the only driving force for the general evolutionary dynamics as Wright and Fisher theory stated. In the following section we discuss how a generalization of the adaptive landscape to include nonequilibrium fluxes as an additional driving force for general evolutionary dynamics overcomes the restrictions of Wright and Fisher's assumptions. (Xu and Wang, 2017b; Zhang et al., 2012).

A. Single-locus multi-allele evolution

Consider a single gene at a fixed position or locus on a chromosome of a diploid organism such that each chromosome is present in two (non-identical) copies. For each locus there are several different DNA sequences present in a population. The dynamics of the fractions x_i of allele A_i, $i = 1, \ldots, n$ in the population is determined by its fitness w_i. In an individual, the genotype A_iA_j has the fitness w_{ij}, which depends on both alleles such that $w_i = \sum_{j=1}^{n} w_{ij}x_j$. The population's mean fitness is then $\bar{w} \equiv \sum_{i,j=1}^{n} w_{ij}x_ix_j$. The probability P of having the relative allele frequencies $\{x_i\}_{i=1,\ldots,n}$ evolves according

to

$$\partial_t P = -\nabla \cdot \left[\left(\mathbf{F}^S + \mathbf{F}^M \right) P - D \nabla \cdot (\mathsf{G} P) \right], \quad (106)$$

where

$$F_i^S = \frac{x_i \left(x_i - \bar{w} \right)}{\bar{w}} \quad (107)$$

describes the effects of natural selection and

$$F_i^M = \sum\nolimits_{j=1}^{n} x_j m_{ji} - x_i \sum\nolimits_{j=1}^{n} m_{ij} \quad (108)$$

captures the effects of mutations with m_{ij} being the rate of mutation from allele A_j to A_i. The diffusion term accounts for genetic drift resultant from stochasticity of the reproduction process (Kimura et al., 1997; Rice, 2004; Svirezhev and Passekov, 1990). Here, $G_{ij} = x_i(\delta_{ij} - x_j)$ and $D = 1/(4N_e)$ with N_e being the effective population size.

In the limit of small fluctuations, which occurs for a large population size, $D \ll 1$ or $N_e \gg 1$, the landscape satisfies to lowest order

$$(\mathbf{F}^S + \mathbf{F}^M) \cdot \nabla \phi_0 + \nabla \phi_0 \cdot \mathsf{G} \cdot \nabla \phi_0 = 0 \quad (109)$$

where ϕ_0 is the leading order term in an expansion of U in terms of D. This equation is the Hamilton-Jacobi equation (6) and ϕ_0 thus a Lyapunov function for the dynamic system Eqs. (106)-(108).

In a case where the fitness of each genotype is independent of the allele frequencies and in absence of mutations, the steady state flux vanishes, $\mathbf{J}_{ss} = 0$, and the intrinsic landscape ϕ_0 is

$$\phi_0 = -\frac{1}{2} \ln \bar{w} \quad (110)$$

(Zhang et al., 2012). Furthermore, one can show that $d\bar{w}/dt = \mathbf{F} \cdot \nabla \bar{w} = -2\bar{w}\mathbf{F} \cdot \nabla \phi_0 = 2\bar{w} \nabla \phi_0 \cdot \mathsf{G} \cdot \nabla \phi_0 \geq 0$ (Zhang et al., 2012). Consequently, the mean fitness is a Lyapunov function of the dynamics and hence puts Wright's metaphor on solid ground.

In the general case, where the fitness can depend on the allele frequencies, one finds $\mathbf{F}^S + \mathbf{F}^M = -D\nabla \cdot (\mathsf{G} U) + \mathbf{J}_{ss}/P_{ss}$, where $U = -\ln P_{ss}$ is the nonequilibrium landscape (Zhang et al., 2012) while $G_{ij} = C_i(\delta_{ij} - C_j)$ is from the sampling feature of the genetic drift and D gives the scale of the fluctuations. The driving force of evolution can thus be decomposed into the gradient of the landscape associated with the steady state probability and the steady state probability flux, which is typically different from zero due to interactions between individuals and hence allele-frequency dependent selection. Note that for $J_{ss} \neq 0$, the nonequilibrium landscape is no longer directly related to the fitness landscape. This decouples the link between the fitness and evolutionary probability. Consequently, states with lower mean fitness may have a higher probability.

We now turn to Fisher's fundamental theorem of natural selection (Fisher, 1930). Consider the adaptive rate for evolutionary dynamics under selection and random mating:

$$\begin{aligned} d\phi_0/dt &= -\nabla \phi_0 \cdot \mathbf{D} \cdot \nabla \phi_0 \\ &= -\mathbf{F} \cdot \mathbf{D}^{-1} \cdot \mathbf{F} + \mathbf{V} \cdot \mathbf{D}^{-1} \cdot \mathbf{V}. \end{aligned} \quad (111)$$

where $\mathbf{V}$ is the steady state probability flux velocity defined as $\mathbf{V} = \mathbf{J}_{ss}/P_{ss}$. The diffusion matrix $\mathbf{D}$ describes the sampling nature of the random mating. In fact, $d\phi_0(\mathbf{G})/dt$ is related to the genetic variance: $V_A(w^{(i)})/(\bar{w}^{(i)})^2 = 2\ \mathbf{F}^{(i)} \cdot (\mathbf{G}^{-1})^{(i)} \cdot \mathbf{F}^{(i)}$, where $V_A(w^{(i)}) = 2\sum_{k=1}^{n_i} C_k^{(i)} (w_k^{(i)} - \bar{w}^{(i)})^2$ is the genetic variance (Zhang et al., 2012). One can see

$$\frac{d\phi_0(\mathbf{G})}{dt} = -\frac{1}{2} \frac{V_A(w)}{\bar{w}^2} + \mathbf{V}(\mathbf{G}) \cdot \mathbf{G}^{-1} \cdot \mathbf{V}(\mathbf{G}) \quad (112)$$

Under frequency-independent selection, the intrinsic flux velocity is zero $\mathbf{V}(\mathbf{D}) = 0$. In this case, detailed balance is preserved (equilibrium) and the intrinsic potential $\phi_0 = -(1/2)\ln\bar{w}$. This reduces to Fisher's fundamental theorem of natural selection, that adaptation rate is monotonic and only depends on genetic variance, $d\bar{w}/dt = V_A(w)/\bar{w}$. As seen previously, Eq.(112) works for the general evolution beyond equilibrium case, with nonzero flux breaking the detailed balance. Thus, Eq.(112) generalizes the Fisher's fundamental theorem of natural selection. The adaptive rate for general evolution depends on both the genetic variance proposed by Fisher and the intrinsic flux velocity $\mathbf{V}$ resulting from the complex biotic interactions which breaks the detailed balance, missing in the Fisher's theorem. (Zhang et al., 2012).

The new landscape and flux theory for evolution provides a natural explanation of coevolution with direct implications for the Red Queen hypothesis of nonstop evolution, even when reaching the optimum of an adaptive landscape (such as limit cycle). (Van Valen, 1973a; Zhang et al., 2012) When reaching the evolutionary optima once attracted to the oscillation path, evolution still proceeds due to the rotational curl flux driving force originated from the biotic interactions. This gives the origin of non-zero genetic variance $\frac{1}{2}\frac{V_A(w)}{\bar{w}^2} = \mathbf{V}(\mathbf{G}) \cdot \mathbf{G}^{-1} \cdot \mathbf{V}(\mathbf{G})$ even at the evolution optima $\frac{d\phi_0(\mathbf{G})}{dt} = 0$. Therefore, natural selection can influence certain species to change their allele frequencies and thus lead to genetic variance even if the overall population reaches its optima (Zhang et al., 2012).

Another generalized form of Fisher's theorem was proposed by Price (Price, 1972a, 1970, 1972b) considering various effects including mutations on the adaptation rate dynamics beyond genetic variance. Replicator mutator dynamics have also been suggested to study evolutionary dynamics, including mutations (Allen and Rosenbloom, 2012; Bladon et al., 2010; Nowak, 2004).

B. Multi-locus multi-allele evolution

The interactions among genes are critical in understanding evolution. Loci representing the locations of genes are not independent. In particular, recombination provides an additional way of changing alleles on a chromosome, and the fitness of an allele might depend on the genetic background, a phenomenon called epistasis. These interactions can lead to linkage disequilibrium. They need to be considered in addition to the well known selection, mutation, migration and random mating for multi-locus multi-allele evolution.

Some models of multi-locus evolution were suggested with certain limitations (Ewens, 2004; Rice, 2004; Svirezhev and Passekov, 1990). For example, the adaptive landscape is not quantified in the most general evolution scenarios (Ewens, 2004; Neher and Shraiman, 2011; Rice, 2004; Svirezhev and Passekov, 1990); only time dependent adaptation was considered (Mustonen and Lassig, 2009, 2010). Certain adaptive landscape approaches have not been directly applied to multi-locus evolution. (Ao, 2006) In fact, Wright, Fisher and quasi-linkage equilibrium (QLE) theories can only be applied to special evolutionary scenarios.

For multi-locus multi-allele evolution, allele frequencies alone do not have enough information for quantifying genotype frequencies. Gamete frequencies can be used instead at different loci in multi-locus-multi-allele evolution (Ewens, 2004; Rice, 2004; Svirezhev and Passekov, 1990), where "gamete" refers to the set of alleles at the L loci under consideration, such that gamete $\mathbf{i} \equiv (i_1, i_2, \ldots, i_L)$ has allele $A_{i_j}^j$ at locus j. One can derive the driving forces of the evolution.

The gamete frequency $x_{\mathbf{i}}$ evolves according to

$$\frac{dC_{\mathbf{i}}}{dt} = \mathbf{F}_{\mathbf{i}}^S + \mathbf{F}_{\mathbf{i}}^M + \mathbf{F}_{\mathbf{i}}^R. \tag{113}$$

Here, the first two terms describe the effects of natural selection and of mutations similar to the single-locus case. The effect of recombination is captured by the last term, which reads

$$\mathbf{F}_{\mathbf{i}}^R = -{\sum_Q}' r_Q D_{\mathbf{i},Q}, \tag{114}$$

where the sum extends over all subsets of loci other than the empty set or the full set of all L loci. Furthermore, r_Q is the rate of recombination for set Q and $D_{\mathbf{i},Q} = C_{\mathbf{i}} - C_{\mathbf{i}_Q} C_{\mathbf{i}_{\overline{Q}}}$ the linkage disequilibrium coefficient for locus group Q. Here, $C_{\mathbf{i}_Q}$ denotes the total frequency of all gametes that are identical to $\mathbf{i}$ at the loci in Q and $C_{\mathbf{i}_{\overline{Q}}}$ that of all gametes that are identical to $\mathbf{i}$ at all loci not in Q. (Ewens, 2004; Rice, 2004; Svirezhev and Passekov, 1990)

The evolution of gamete frequency under selection was given as —cclin (Ewens, 2004; Rice, 2004; Svirezhev and Passekov, 1990): $F_{\mathbf{i}}^S = C_{\mathbf{i}}(w_{\mathbf{i}} - \overline{w})$ where $w_{\mathbf{i}}$ denotes the marginal fitness of the gamete $\mathbf{i}$ and the $\overline{w}$ denotes the total fitness of all gametes in the L loci system. Evolution of gamete frequencies under mutation was also studied (Neher and Shraiman, 2011). One can take all these driving forces together to study the evolution of gamete frequencies.

The genetic variance of gamete fitness under selection and recombination can be shown as (Ewens, 2004; Rice, 2004; Svirezhev and Passekov, 1990):

$$\frac{d\overline{w}}{\partial t} = V_A + V_R \tag{115}$$

$V_A = 2\sum_{\mathbf{i}} C_{\mathbf{i}}(w_{\mathbf{i}} - \overline{w})^2$ represents the total gametic variance from natural selection and $V_R = -2\sum_{\mathbf{i}} \sum_{Q,Q\neq\emptyset,L} w_{\mathbf{i}} r_Q D_{\mathbf{i},Q}$ represents the epistatic gametic variance from the linkage disequilibrium of the loci (Ewens, 2004; Neher and Shraiman, 2011; Rice, 2004; Svirezhev and Passekov, 1990). One can see that the mean fitness increases as recombination decreases. The generalized form of Fisher's fundamental theorem presented here considers the additional contribution from linkage disequilibrium due to recombination (Ewens, 2004; Neher and Shraiman, 2011; Rice, 2004; Svirezhev and Passekov, 1990; Xu and Wang, 2017b).

C. Evolution adaptive landscape and flux under different evolution scenarios

The nonequilibrium landscape and flux theory can be applied to the general case of multi-locus multi-allele evolution after a suitable generalization of Eq. (106), which also includes recombination force $\mathbf{F}_{\mathbf{i}}^R$ and others such as epistasis. We discuss the results in various evolutionary scenarios listed below.

a. Absence of recombination ($r_Q = 0$) and mutations ($m = 0$) Under non-epistatic selection and genetic drift from random mating in the population of a multi-locus-multi-allele system, the Hardy-Weinberg principle and linkage equilibrium is achieved (Ewens, 2004; Rice, 2004; Svirezhev and Passekov, 1990; Xu and Wang, 2017b): all gamete frequencies are the products of the frequencies of the constituting alleles. This reduces effectively to one locus multi-allele evolutionary dynamics (Zhang et al., 2012). For allele frequency independent selection, the Wright and Fisher theory works. For allele frequency dependent selection, the Wright and Fisher theory breaks down. The evolutionary dynamics are no longer determined by the adaptive landscape alone, but also by the curl flux due to the biotic interactions. The Red Queen hypothesis can be explained by the presence of curl flux driving the evolution and giving the genetic variations at optimal adaptation (Zhang et al., 2012).

b. Presence of recombination ($r_Q > 0$), absence of epistasis ($\epsilon_{ij} = 0$) and mutations ($m = 0$) When the fitness matrix is additive without epistasis, Wright's fitness landscape concept and the generalized Fisher's fundamental theorem can still be applied (Ewens, 2004; Neher and Shraiman, 2011; Rice, 2004; Svirezhev and Passekov, 1990). The mean fitness never decreases because the additive form of fitness leads to $V_R = 0$. However, this does not necessarily mean that the rotational curl flux vanishes. In fact, the curl of the recombination force from gamete frequency evolution $\nabla \times (\mathbf{G}^{-1} \cdot \mathbf{F}_R)$ can be non-zero. Therefore, for recombination $r_Q > 0$ and epistatic selection $\epsilon_{ij} = 0$, evolutionary adaptive dynamics are determined by the gradient potential or the mean fitness, as well as the non-zero flux (Xu and Wang, 2017b).

c. Presence of recombination ($r_Q > 0$) and epistatic selection ($\epsilon_{ij} \neq 0$), absence of mutations ($m = 0$) When both recombination and non-zero epistasis effects (non-additive fitness matrix) are present for evolution, the dynamics becomes intrinsically nonequilibrium (Akin, 1982; Hastings, 1981). Even under gamete/allele frequency independent selection, with recombination $r_Q > 0$ and epistasis $\epsilon_{ij} \neq 0$, the dynamics are determined by the gradient of the evolution landscape and non-zero flux, which breaks detailed balance (Xu and Wang, 2017b). Recombination and epistasis can contribute to the breakdown of the detailed balance which leads to the breakdown of the Wright and Fisher theory for evolution.

d. Presence of mutations ($m \neq 0$) In multi-locus-multi-allele evolution, mutations are often frequency-dependent. Therefore, the mutation can also lead to nonequilibrium behavior, giving another source for breaking detailed balance (Xu and Wang, 2017b).

e. Quasi-linkage equilibrium ($r_Q \gg 0$, $m = 0$, $\epsilon_{ij} = 0$) If selection is weak such that adaption is much smaller than recombination, the linkage disequilibrium exponentially decreases due to recombination. A state called quasi-linkage equilibrium (QLE) emerges (Rice, 2004). QLE is a good approximation for multi-locus evolution at high recombination rates and in the absence of epistasis. When the system relaxes to QLE (Neher and Shraiman, 2011; Rice, 2004), a generalized Fisher's law holds approximately. The dynamics can then be simplified as depending on allele frequency rather than gamete frequency (Nagylaki, 1993; Nagylaki et al., 1999). The landscape and flux theory works beyond these restrictions of weak selections and the QLE (Xu and Wang, 2017b). It is important to note that in general, mean fitness and optimal probability of the state do not coincide. As a result, adaptive fitness should be quantified by the potential landscape rather than mean fitness, since the landscape directly reflects the probability of the state. Furthermore, evolutionary dynamics are determined by both the landscape gradient and rotational curl flux breaking the detailed balance originated from the recombination, mutation, epistasis, or gamete/allele frequency dependent selection (Xu and Wang, 2017b).

f. Red Queen Hypothesis Fisher's and Wright's analysis imply that evolution will eventually come to a halt when the maximum fitness is reached. This does not need to be the case as can be illustrated by the coevolution of a predator and a prey species (Dieckmann et al., 1995; Vermeij, 1994). Assume that the predator captures prey by running faster and by being able to spot them against the background. Improving the speed and the ability to spot the prey increases the predator's fitness. As a result, the prey species will evolve its speed and camouflage to survive. Inversely, if the prey improves these traits, the predator will evolve in response to run faster and to spot the prey better. Such a competition causes an 'arms race' between the two species, which can lead to sustained oscillations of the species' genotype frequencies.

This evolutionary process represents a case of the Red Queen hypothesis (Van Valen, 1973a), which explains the persistence of sexual reproduction and recombination. Namely, it provides an accelerated evolution rate of a species and hence allows it to outcompete its predators and parasites. In fact, the hypothesis has been experimentally supported by a number of coevolution examples such as plant-pathogen systems (Clay and Kover, 1996) and parasite-fish ecosystems (Lively et al., 1990).

While the Red Queen hypothesis challenges Wright and Fisher's adaptive landscape theory of evolution(Fisher, 1930; Wright, 1941), the associated coevolution scenario fits naturally into the picture of nonequilibrium landscape and flux theory. It allows for evolution to continue even if the physical environment is invariant or the landscape reaches the optimum (Xu and Wang, 2017b; Zhang et al., 2012). The origin of such continuing evolution was suggested to be the rotational curl flux breaking the detailed balance as a result of gamete/allele frequency dependent selection, mutation, recombination, or epistasis (Xu and Wang, 2017b; Zhang et al., 2012). Another possible cause of open-ended evolution was suggested by molecular evolution experiments (Worst et al., 2016), which can be interpreted as that the evolution of a species suddenly opens the possibility of evolving new traits and thus occupation of a new ecological niche. The time dependent landscape was also suggested for explaining Red Queen hypothesis for part of the system, such as predator or prey(Van Valen, 1973b; Zliobaite et al., 2017). For the whole predator-prey system, the evolutionary landscape can still be time independent.

D. Evolutionary game theory

Evolutionary game theory provides a framework for exploring the origin of a large variety of human and animal behaviors (Maynard and Price, 1973; Nowak, 2004; Sandholm, 2009). Originally, game theory focused on the study of cooperative and competitive strategies adopted from rational decision-makers. Evolution game theory was born by applying game theory to evolutionary biology and population dynamics for exploring the strategic interactions among large populations of agents (Hofbauer, 2011; Sandholm, 2009). Using game theory can assist in understanding a variety of human and animal behaviors (Maynard and Price, 1973; Nowak, 2004; Sandholm, 2009). In evolutionary biology, one important question is how cooperators can survive when they can be taken advantage of by "cheaters." Experimental efforts in yeast (Gore et al., 2009) showed that cooperators can survive even in the presence of cheaters, and their interactions are through a feedback loop. The evolutionary consequences of the cooperative inactivation of antibiotics by bacteria has recently been explored experimentally (Artemova1 et al., 2015; Yurtsev et al., 2013). In a game designed to model cooperative trade-offs, each player receives a particular payoff depending on the actions chosen by their peers. Repeated games wherein players have several subsequent encounters can reach steady states or limit cycles (Cason and Friedman, 2003; Hofbauer, 2011; Sandholm, 2009). For example, in the classic Prisoner's Dilemma, two players can choose either to cooperate or not. They both receive a reward R as payoff if they cooperate, and a punishment P if both do not cooperate. However, in the case where just one player chooses to cooperate, she receives a temptation payoff T while the other player gets a "sucker" payoff S. The various payoffs satisfy $T > R > P > S$ to reflect the intuitive notions associated with the game.

In repeated games, where players have several subsequent encounters, different strategies can be defined. In the example of the Prisoner's Dilemma, one could choose either to always cooperate or not. A player can also play 'tit-for-tat', where the player cooperates on the first encounter, then choose to cooperate or defect on any other encounter based on the action of the other player in the previous encounter. This strategy requires a memory and thus has some cost. The payoff matrix conveniently summarizes the results of encounters of players with various strategies. Let C_i denote the fraction of players with strategy i and A_{ij} the payoff for a player employing strategy i upon an encounter with a player using strategy j. Then AC gives the average payoff for each strategy. In the example

$$\mathsf{A} = \begin{pmatrix} P & P & T \\ P-c & R-c & R-c \\ S & R & R \end{pmatrix}. \tag{116}$$

Stationary distributions of strategies for noncooperative games like the Prisoner's Dilemma, in which nobody can gain by changing only her strategy are called Nash equilibria (Nowak, 2004). Characterizing such "optimal" solutions is an important task of game theory. The local stability of Nash equilibria has been studied and for very simple models Lyapunov functions have been found to characterize global stability (Sandholm, 2009). In general, though, it remains at present a challenging task.

Evolutionary games are repeated games where the average payoffs determine the fitness of a strategy. Explicitly, the time evolution of the fractions C_i follows the rule that population C_i grows if their average payoff is above the mean and shrinks in the opposite case. Mutations are implemented through rates of switching from one to an alternative strategy. The dynamics can be written as

$$\frac{dC_i}{dt} = \sum_j C_i f_i(C) Q_{ij} - C_i \bar{f}. \tag{117}$$

where $f_i = \sum_j A_{ij} C_j$ is the average payoff (or fitness) of population i and $\bar{f} = \mathbf{C} \cdot \mathsf{AC}$ the mean population payoff (or fitness) (Allen and Rosenbloom, 2012; Bladon et al., 2010; Nowak, 2004). For a uniform mutation rate μ, $Q_{ii} = 1 - 2\mu$ and $Q_{ij} = \mu$ if $i \neq j$.

For the Prisoner's Dilemma and starting with a random initial distribution of strategies, at first the defectors will typically win. Then, however, a small population of tit-for-tat players will invade the game and replace the defectors. In certain regions of parameter space, subsequently, cooperators will take over, which in turn will be replaced by defectors and so on. This cycle has been interpreted to mimic oscillations between war and peace in animal or even human species (Nowak, 2004).

The nonequilibrium landscape for the above game reveals that, for a small cost c of the tit-for-tat strategy, the cooperator strategy is the most stable one and has the largest basin of attraction (Xu and Wang, 2017a), Fig. 24. As the cost c increases, the basin of the noncooperator state increases and a mixed strategy state appears. In this case, the payoff for defectors increases, the defector state gains stability and, eventually, becomes the most stable state. Similarly, increasing the reward R or the punishment P favors the cooperative state. A Lyapunov function can be found quantifying the global stability of the system dynamics (Xu and Wang, 2017a). In this way, cooperative behavior can emerge in populations of selfish individuals. Similarly, competing traits can coevolve in species.

XII. NONEQUILIBRIUM ECONOMY

Although typically not considered to be a biological field, economics reflects biological activities at human

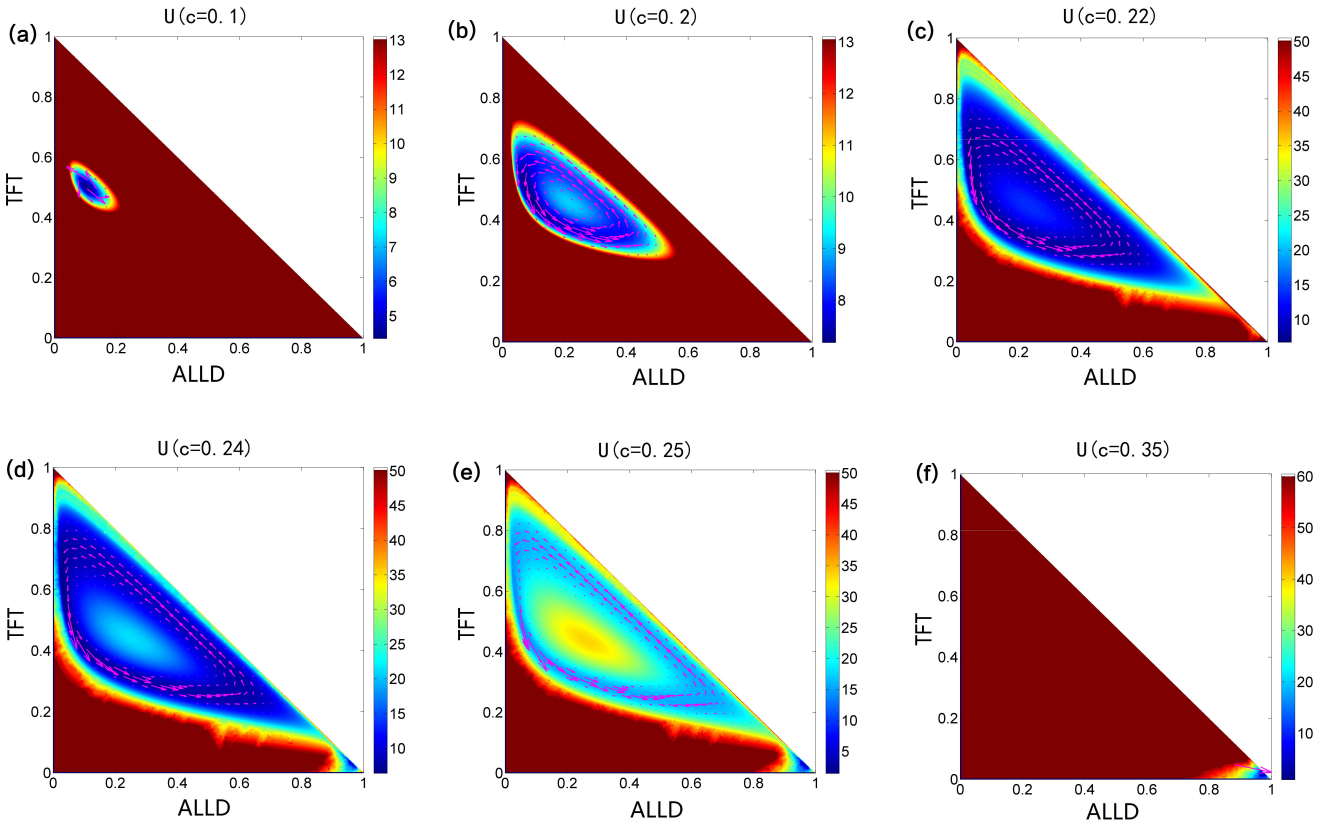

FIG. 24 The nonequilibrium landscapes for game theory of repeated prisoner's dilemma for different cost c. (a) Monostable peace state where Tit-for-tat strategy dominates at small cost $c = 0.1$. (b)(c)(d)(e) Limit cycle oscillations between peace state with tit-for-tat strategy and war state with all-defect strategy at $c = 0.2$, $c = 0.22$, $c = 0.24$ and $c = 0.25$. (f). As cost increases and monostable war state with all-defect strategy at large cost ($c = 0.35$) emerges. (from Ref. (Xu and Wang, 2017a)).

scales. An important aspect of economics is the balance between supply and demand (Marshall, 1890; Walras, 1874). Traditionally, the focus has been on economic equilibrium, when supply and demand are balanced, but this approach cannot explain economic cycles of growth and stagnation or decline, let alone economic crises (Fisher, 1933; Goodwin, 1967; Keen, 1994, 2001; Keynes, 1936; Marx, 1887; Minsky, 1977; Schumpeter, 1934). Thus, nonequilibrium economic theory is necessary. Furthermore, the driving forces of economy need to be identified and quantified (Zhang and Wang, 2017).

In conventional economics, supply and demand are often assumed to be monotonic with respect to price under a complete competition market or close to equilibrium condition economy (Marshall, 1890). As a result, only one equilibrium emerges. The economic dynamics are then described by the shift of this equilibrium point. However, nonequilibrium economic behavior such as inflation, under-employment, and overproduction are present (Keen, 1994, 2001; Keynes, 1936). This will often lead to non-monotonic relationship of demand and supply with respect to the price (Beckmann and Ryder, 1969; Marshall, 1890; Mascolell, 1986). As a result, multiple stable states and even limit cycles can emerge. The competition and monopoly/oligopoly model provides a good example to illustrate this (Zhang and Wang, 2017).

Experience tells us that the price of a good increases if the demand exceeds the available supply and that the production of a good increases with the price of the good, but decreases with the available supply (Beckmann and Ryder, 1969; Marshall, 1890; Mascolell, 1986). This leads to the following dynamic system for the price P and the quantity Q of a good

$$\frac{dP}{dt} = F(P) - Q \tag{118}$$

$$\frac{dQ}{dt} = P - C(Q). \tag{119}$$

Here, $F(P)$ describes the demand of the good as a function of its current price and $C(Q)$ is the marginal cost of producing the good, that is, the cost of producing one additional unit. For convenience, P and Q can take on any real value. Positive values are obtained after an appropriate shift of the origin.

Specific choices of the demand and cost functions are $F = (-1 + a)P + c$ and $C(Q) = (d + bQ^2)Q$, where $a < 1$ and $b \geq 0$ (Zhang and Wang, 2017). The demand is monotonically decreasing with increasing price, but the cost function presents a nonlinear dependence on the quantity of the good, which can be non-monotonic. Typically, the cost for producing another unit decreases with the amount units produced. The case that production cost increases with the supply is encountered, for example, when income effect becomes significant (storage costs are often encountered in industries and agricultural productions). Due to the nonlinearity of the cost function, two stable steady states can appear if $a < 0$. One of them corresponds to the case when customers buy the commodity at a low price due to a rich supply of products. The other corresponds to a monopoly/oligopoly, where customers will still purchase it even at a higher price. When $0 < a < 1$, limit cycles can emerge with coherent oscillations between competition and monopoly. As the demand slope changes, the market can switch from monopoly to competition or vice versa. The resulting underlying bistable landscape topography through barrier height between monopoly and competition basins can be used to quantify the stability and switching of these states. For limit cycle dynamics, the resulting Mexican hat shaped landscapes guarantees the stability of the oscillation path, while the rotational curl flux drives the oscillation flow between the monopoly and competition (Zhang and Wang, 2017).

The stability of these states can be determined by the nonequilibrium landscape (Zhang and Wang, 2017), as shown in Fig. 25. It changes as the demand curve is shifted. When the demand curve shifts to the right over certain value, the basin of attraction of the competition state becomes deeper and more prominent relative to the monopoly state. Eventually, only a competition state survives, as shown in Fig. 25 (a). The model then returns to the conventional supply and demand model where only one equilibrium state typically appears. When demand increases, more sellers join the production for goods, more competitors form a more competitive environment leading to bistability shown in Fig. 25 (b). When demand decreases, more sellers leave the commodity market. This leads to a less competitive environment with monopoly/oligopoly shown in Fig. 25 (c).

The driving force of nonequilibrium economy is determined by both landscape and curl flux (Zhang and Wang, 2017). While the landscape topography provides the quantifications and stability of economic states, the flux representing the nonequilibriumness can help to shape the dynamics. Furthermore, the flux leads to certain unstable states, but helps to maintain the stable flow among states. The global sensitivity analysis based on landscape and flux can be used to identify elements key to economic stability. (Zhang and Wang, 2017). Furthermore, due to the presence of flux, new states can emerge in the nonequilibrium economy beyond the single equilibrium state assumed in the conventional equilibrium economic theory. For example, a monopoly/oligopoly state or limit cycle can emerge from the competition state, or vice versa. This discussion is quite general and can be applied to other nonequilibrium economical studies.

XIII. OUTLOOK

As we have seen, the landscape and flux theory as well as generalized hydrodynamics provide frameworks for studying large classes of systems that are out of thermodynamic equilibrium. Notably, these concepts provide insight into the physical foundations of biological processes, ranging from efficient electron transport in biomolecules to cellular dynamics and tissue development. Beyond these scales, they apply to the dynamics of populations and whole ecosystems, including the behavior of human societies as well as biological evolution. Although not limited to such cases, the landscape and flux theory is particularly suited for describing systems with a finite number of degrees of freedom, whereas generalized hydrodynamics provides a particularly powerful approach to collective phenomena in spatially extended systems. Our review can only give a glimpse of successful applications to biological processes and we expect many more fundamental insights into the phenomenon of life.

In particular, further physical analysis should shed light on the question of what separates living systems from other physical (or chemical) systems out of thermodynamic equilibrium. Beyond physical aspects, living beings and their assemblies are often associated with qualities such as function, information processing, or consciousness. How can currently extant as well as future physical concepts be linked to these functions? For example, how do organizational principles of nonequilibrium systems constrain and guide the evolution of functions that provide ever better fits of a species to its environment? How does the unfolding of genetic information during the development of organisms depend on general laws governing dynamics out of thermodynamic equilibrium? There is an already fruitful connection between the theory of information and that of statistical physics. It seems safe to speculate that the links between these two fields will further tighten and lead to new insights into the efficiency, speed and energy cost of information processing. We expect that the study of cell signal transduction, neural networks in the brain, and organisms will play a leading role in this endeavor (Bialek, 2012; Levchenko and Nemenman, 2014; Press et al., 2013; Yan et al., 2016; Zeng and Wang, 2017) that has only just begun.

Molecular biology, which owes a large deal to physics, provides us with a rather detailed picture of the molecular inventory. This inventory contains a daunting set

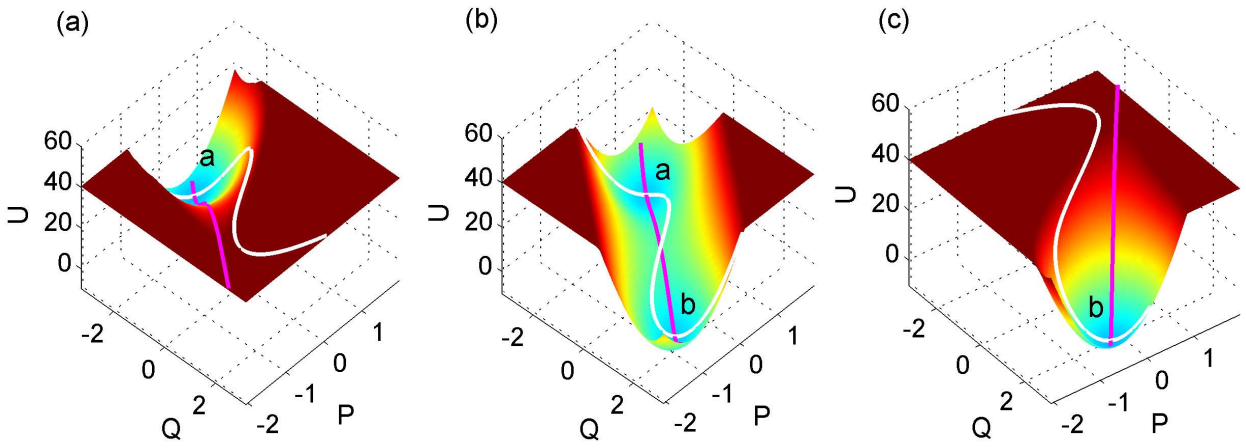

FIG. 25 Nonequilibrium landscapes and shifted demand curves (purple lines) in a bistable economic model for the quantity Q and the price P of a commodity, from (Zhang and Wang, 2017). (a) The left shifted (decreased) demand curve and monopoly state dominant landscape. (b) The middle located demand curve and monopoly/competition bi-stable state coexisting landscape. (c) The right shifted (increased) demand curve and competition state dominant landscape. From (Zhang and Wang, 2017).

of a large variety of highly complex molecular machines, some of which have been characterized individually in awesome detail. On the other hand, although there is already much known about biological processes on larger scales, much of it remains to be described. Recent years have seen striking progress in experimental techniques, which allow us now to follow the embryonic development of organisms or the dynamics of bird flocks in great detail, and further advances can be expected. The situation is thus somewhat opposite to that in the 19th century, when the molecular properties of materials were essentially unknown, whereas their macroscopic properties could be measured. In spite of this difference, the question of how to bridge the gap between the microscopic dynamics and the macroscopic thermodynamics/function across spatial and temporal scales attracts researchers of biological systems now as much as condensed matter physicists were to these problems in the 20th century. Some progress has been made in understanding the macromolecular organization such as genome folding, transcription and translation machines, and molecular motors (Tokuda et al., 2012; Zhang and Wolynes, 2015). Also, efficient methods for large-scale simulations of cellular networks and the whole cell at various temporal and spatial scales are being developed (Roberts et al., 2011). Time will tell whether computer simulations will be the golden path towards an understanding of the relation between the microscopic and the macroscopic behavior of a biological system. In any case, new ideas and concepts are probably needed to reach this goal.

On the other hand, new experimental methods and techniques need to be developed to investigate the mechanism and function of biological objects. For example, to study the dynamics of cells and cellular networks, *in vivo* measurements of the kinetic rates are crucial and necessary. Experimental explorations are not only important to quantify the deviation from equilibrium and the role of nonequilibriumness for the function of a biological system. They are also crucial for probing and verifying fundamental laws of nonequilibrium physics such as landscape and flux, as well as thermodynamic cost and dissipation in the context of single molecule enzyme dynamics, single molecular motors, the regulation dynamics of gene motifs, cell cycle, and spatial organization of the cells, and of brain function. Furthermore, low throughput and high throughput data from experiments can help us to pin down the underlying mechanisms and nonequilibrium physics for the subject of interests, for example, single cell data for understanding function and diseases and connectome from understanding the brain function. From these studies, new biological functional phases or new forms of active matter as a result of the nonequilibriumness and environmental changes can be uncovered. This may provide opportunities to design functions even beyond living world.

Nonequilibrium physics will be important for biological applications such as enzyme dynamics, metabolism, gene regulations, structure, function and dynamics of cells, physiology, cancer, differentiation and development, immune, ageing and other human diseases, evolution/ecology, sociology, human networks, economics, even perhaps psychology and politics, to name but a few.

With the ever increasing possibilities to manipulate and interrogate biological systems, a vast playground lies at our feet. It has the potential to produce gargantuan amounts of data that will dwarf the already enormous sets currently produced every day. Without a conceptual framework guiding experiments, the sheer quantity

of the data risks to severely obstruct our advances in understanding Life. The physics of nonequilibrium systems will play a crucial role in this quest, aiding design of future experiments and providing a guide for data analysis. The concepts presented in this review are just a beginning.

ACKNOWLEDGEMENT

The authors wish to thank our mentors as well as past and current collaborators for sharing their insights and enthusiasm in our exploration of the nonequilibrium behavior of biological systems. They are too numerous to be listed here. XF was supported in part by National Natural Science Foundation of China (NSFC-91430217) and MOST, China. (2016YFA0203200 and 2013YQ170585). TL was supported in part by National Science Foundation (1227034, 1553649), Office of Naval Research (N000141622525) and Department of Energy (DE-SC0018420, DE-SC0019185). KK was supported in part by Deutsche Forschungsgemeinschaft through SFB 1027. JW was supported in part by National Science Foundation (USA: NSF-76066, NSF-1808474) and National Institutes of Health (NIH-1R01GM124177-01A1). JW would like to thank Dr. Li Xu for help on editing.

REFERENCES

Abbott, L., 2008. Theoretical neuroscience rising. Neuron 60 (3), 489–495.

Abramavicius, D., Palmieri, B., Voronine, D., F., S., Mukamel, S., 2009. Coherent multidimensional optical spectroscopy of excitons in molecular aggregates; quasiparticle versus supermolecule perspectives. Chem. Rev. 109 (6), 2350–2408.

Ackers, G., Johnson, A., Shea, M., 1982. Quantitative model for gene-regulation by lambda-phage repressor. Proc. Natl. Acad. Sci. U.S.A. 79 (4), 1129–1133.

Akin, E., 1982. Cycling in simple genetic systems. J Math Biol 13 (3), 305–324.

Albantakis, L., Branzi, F., Costa, A., Deco, G., 2012. A multiple-choice task with changes of mind. PloS one 7 (8), e43131.

Albantakis, L., Deco, G., 2011. Changes of mind in an attractor network of decision-making. PLoS Comput. Biol. 7 (6), e1002086.

Allard, J. F., Mogilner, A., Feb. 2013. Traveling waves in actin dynamics and cell motility. Curr Opin Cell Biol 25 (1), 107–115.

Allen, B., Rosenbloom, D., 2012. Mutation rate evolution in replicator dynamics. B Math Biol 74 (11), 2650–2675.

Alon, U., 2007. An introduction to systems biology: design principles of biological circuits. Boca Raton: Chapman & Hall/CRC.

Amit, D. J., 1989. Modeling brain function : the world of attractor neural networks. Cambridge University Press.

Anderson, P., 1972. More is different - broken symmetry and nature of hierarchical structure of science. Science 177 (4047), 393–396.

Ao, P., 2004. Potential in stochastic differential equations: novel construction. J Phys a-Math Gen 37 (3), L25–L30.

Ao, P., 2006. Three laws in darwinian evolutionary theory. Phys. Life Rev. 2 (2), 117–156.

Ao, P., 2008. Emerging of stochastic dynamical equalities and steady state thermodynamics from darwinian dynamics. Commun. Theor. Phys. 49 (5), 1073–1090.

Ao, P., Galas, D., Hood, L., Zhu, X., 2008. Cancer as robust intrinsic state of endogenous molecular-cellular network shaped by evolution. Med Hypotheses 70 (3), 678–684.

Apfeld, J., O'Connor, G., McDonagh, T., DiStefano, P., Curtis, R., 2004. The amp-activated protein kinase aak-2 links energy levels and insulin-like signals to lifespan in c-elegans. Gene Dev 18 (24), 3004–3009.

Aranson, I. S., Tsimring, L. S., May 2005. Pattern formation of microtubules and motors: Inelastic interaction of polar rods. Phys Rev E Stat Nonlin Soft Matter Phys 71 (5).

Artemova1, T., Gerardin, Y., Dudley, C., Vega, N., Gore, J., 2015. Isolated cell behavior drives the evolution of antibiotic resistance. Mol. Sys. Biol. 11, 882.

Ashwin, S., Sasai, M., 2015. Effects of collective histone state dynamics on epigenetic landscape and kinetics of cell reprogramming. Sci. Rep. 5, 16746.

Assaf, M., Roberts, E., Luthey-Schulten, Z., 2011. Determining the stability of genetic switches: Explicitly accounting for mrna noise. Phys. Rev. Lett. 106 (24), 248102.

Atkinson, M., Savageau, M., Myers, J., Ninfa, A. J., 2003. Development of genetic circuitry exhibiting toggle switch or oscillatory behavior in escherichia coli. Cell 113 (5), 597–607.

Aurell, E., Sneppen, K., 2002. Epigenetics as a first exit problem. Phys. Rev. Lett. 88 (4), 048101.

Avinun-Kalish, M., Heiblum, M., Zarchin, O., Mahalu, D., Umansky, V., 2005. Crossover from 'mesoscopic' to 'universal' phase for electron transmission in quantum dots. Nature 436 (7050), 529–533.

Backouche, F., Haviv, L., Groswasser, D., Bernheim-Groswasser, A., Dec. 2006. Active gels: dynamics of patterning and self-organization. Physical Biology 3 (4), 264–273.

Badoual, M., Jülicher, F., Prost, J., May 2002. Bidirectional cooperative motion of molecular motors. Proc Natl Acad Sci USA 99 (10), 6696–6701.

Baeriswyl, D.and Degiorgi, L., 2005. Strongly Interaction in Low Dimensions. Springer, Berlin.

Bai, M., Missel, A., Levine, A., Klug, W., May 2011. On the role of the filament length distribution in the mechanics of semiflexible networks. Acta Biomaterialia 7 (5), 2109–2118.

Balaban, N. Q., Schwarz, U. S., Riveline, D., Goichberg, P., Tzur, G., Sabanay, I., Mahalu, D., Safran, S., Bershadsky, A., Addadi, L., Geiger, B., May 2001. Force and focal adhesion assembly: a close relationship studied using elastic micropatterned substrates. Nat Cell Biol 3 (5), 466–472.

Balagaddé, F., Song, H., Ozaki, J., Collins, C. H., Barnet, M., Arnold, F., Quake, S., You, L., 2008. A synthetic escherichia coli predator–prey ecosystem. Molecular systems biology 4 (1), 187.

Balázsi, Gá.and van Oudenaarden, A., Collins, J., 2011. Cellular decision making and biological noise: from microbes to mammals. Cell 144 (6), 910–925.

Balazsi, G., van Oudenaarden, A., Collins, J., 2011. Cellular decision making and biological noise: From microbes to mammals. Cell 144 (6), 910–925.

Banerjee, S., Marchetti, M. C., Jan. 2011. Instabilities and oscillations in isotropic active gels. Soft Matter 7 (2), 463–473.

Bar-Yam, Y., Harmon, D., de Bivort, B., 2009. Systems biology attractors and democratic dynamics. Science 323 (5917), 1016–1017.

Barato, A., Hartich, D., Seifert, U., 2013. Information-theoretic versus thermodynamic entropy production in autonomous sensory networks. Phys Rev E 87 (4), 042104.

Barato, A., Seifert, U., 2014. Stochastic thermodynamics with information reservoirs. Phys Rev E 90 (4), 042150.

Barnhart, E. L., Lee, K., Keren, K., Mogilner, A., Theriot, J., May 2011. An Adhesion-Dependent Switch between Mechanisms That Determine Motile Cell Shape. Plos Biol 9 (5).

Basan, M., Risler, T., Joanny, J., Garau, X. S., 2009. Homeostatic competition drives tumor growth and metastasis nucleation . HFSP J. 3 (4), 265–272.

Bassler, K., Frey, E., Zia, R., 2019. Coevolution of nodes and links: Diversity-driven coexistence in cyclic competition of three species. Phys. Rev. E. 99 (2), 022309.

Baumgart, T., Hess, S. T., Webb, W. W., 2003. Imaging coexisting fluid domains in biomembrane models coupling curvature and line tension. Nature 425 (6960), 821–824.

Bavestrello, G., Sommer, C., Sar, M., 1992. Bi-directional conversion in turritopsis nutricula (hydrozoa). Scientia Marina 56 (2-3), 137–140.

Bazykin, A., 1985. Mathematical Biophysics of Interacting Populations(in Russian). Nauka, Moscow.

Becker, N., Mugler, A., ten Wolde, P. R., 2015. Optimal prediction by cellular signaling networks. Phys.Rev.Lett. 115 (25), 258103.

Beckmann, M., Ryder, H., 1969. Simultaneous price and quantity adjustment in a single market. Econometrica 37 (3), 470–484.

Behrndt, M., Salbreux, G., Campinho, P., Hauschild, R., Oswald, F., Roensch, J., Grill, S., Heisenberg, C., 2012. Forces Driving Epithelial Spreading in Zebrafish Gastrulation. Science 338 (6104), 257–260.

Bellomo, N., Delitala, M., 2008. From the mathematical kinetic, and stochastic game theory to modelling mutations, onset, progression and immune competition of cancer cells. Phys. Life Rev. 5, 183–206.

Bendix, P. M., Koenderink, G. H., Cuvelier, D., Dogic, Z., Koeleman, B. N., Brieher, W. M., Field, C. M., Mahadevan, L., Weitz, D. A., 2008. A quantitative analysis of contractility in active cytoskeletal protein networks. Biophys J 94 (8), 3126–3136.

Benjacob, E., Gefen, Y., 1985. New quantum oscillations in current driven small junctions. Phys Lett A 108 (5-6), 289–292.

Bennett, C., 1973. Logical reversibility of computation. Ibm J Res Dev 17 (6), 525–532.

Bernevig, B., Zhang, S., 2006. Quantum spin hall effect. Phys. Rev. Lett. 96 (10), 106802.

Bernitt, E., Döbereiner, H., Jan. 2017. Spatiotemporal Patterns of Noise-Driven Confined Actin Waves in Living Cells. Phys. Rev. Lett. 118 (4), 048102–5.

Bernitt, E., Koh, C., Gov, N., Döbereiner, H., 2015. Dynamics of actin waves on patterned substrates: a quantitative analysis of circular dorsal ruffles. PLoS ONE 10 (1), e0115857.

Berthoumieux, H., Maitre, J. L., Heisenberg, C. P., Paluch, E. K., Juelicher, F., Salbreux, G., 2014. Active elastic thin shell theory for cellular deformations. New J Phys 16.

Bialek, W., 2012. Biophysics:Searching for Principles. Princeton University Press.

Biancalani, T., DeVille, L., Goldenfeld, N., 2015. Nigel goldenfeld. framework for analyzing ecological trait-based models in multidimensional niche spaces. Phys. Rev. E. 91, 052107.

Bieling, P., Telley, I., Surrey, T., Aug. 2010. A Minimal Midzone Protein Module Controls Formation and Length of Antiparallel Microtubule Overlaps. Cell 142 (3), 420–432.

Black, A. J., McKane, A. J., 2012. Stochastic formulation of ecological models and their applications. Trends in Ecology and Evolution 27 (6), 337–345.

Bladon, A., Galla, T., McKane, A., 2010. Evolutionary dynamics, intrinsic noise, and cycles of cooperation. Phys Rev E 81 (6), 066122.

Bois, J., Jülicher, F., Grill, S., Jan. 2011. Pattern Formation in Active Fluids. Phys. Rev. Lett. 106 (2), 028103.

Bonny, M., Fischer, F. E., Loose, M., Schwille, P., Kruse, K., 2013. Membrane Binding of MinE Allows for a Comprehensive Description of Min-Protein Pattern Formation. PLoS Comput Biol 9 (12), e1003347.

Bonny, M., Hui, X., Schweizer, J., Kaestner, L., Zeug, A., Kruse, K., Lipp, P., Nov. 2016. C2-domain mediated nanocluster formation increases calcium signaling efficiency. Sci. Rep. 6, 36028.

Brangwynne, C., Mar. 2011. Soft active aggregates: mechanics, dynamics and self-assembly of liquid-like intracellular protein bodies. Soft Matter 7 (7), 3052–3059.

Brangwynne, C., Eckmann, C., Courson, D. S., Rybarska, A., Hoege, C., Gharakhani, J., Juelicher, F., Hyman, A. A., 2009. Germline P Granules Are Liquid Droplets That Localize by Controlled Dissolution/Condensation. Science 324 (5935), 1729–1732.

Bray, D., 2001. Cell movements. Garland Pub.

Brenner, K., You, L., Arnold, F., 2008. Engineering microbial consortia: a new frontier in synthetic biology. Trends. Biotechnol. 26 (9), 483–489.

Bressloff, P. C., Karamched, B. R., 2015. A frequency-dependent decoding mechanism for axonal length sensing. Frontiers in Cellular Neuroscience 9, 281.

Breuer, H. P.and Petruccione, F., 2002a. The Theory of Open Quantum Systems. Oxford University Press, Oxford.

Breuer, H., 2002b. The Theory of Open Quantum Systems. Oxford University Press.

Brookes, J. C., 2017. Quantum effects in biology: golden rule in enzymes, olfaction, photosynthesis and magnetodetection. In: Proc. R. Soc. A. Vol. 473. The Royal Society, p. 20160822.

Brooks, F. J., Carlsson, A. E., Aug. 2008. Actin polymerization overshoots and ATP hydrolysis as assayed by pyrene fluorescence. Biophys J 95 (3), 1050–1062.

Butler, T., Goldenfeld, N., 2009. Robust ecological pattern formation induced by demographic noise. Phys. Rev. E. Rapid Communications 80 (030902), 1–4.

Butt, T., Mufti, T., Humayun, A., Rosenthal, P. B., Khan, S., Khan, S., Molloy, J. E., Feb. 2010. Myosin Motors Drive Long Range Alignment of Actin Filaments. Journal of Biological Chemistry 285 (7), 4964–4974.

Callan-Jones, A. C., Joanny, J. F., Prost, J., Jun. 2008. Viscous-fingering-like instability of cell fragments. Phys. Rev. Lett. 100 (25), 258106.

Callan-Jones, A. C., Jülicher, F., 2011. Hydrodynamics of active permeating gels - IOPscience. New J Phys.

Callan-Jones, A. C., Voituriez, R., 2013. Active gel model of amoeboid cell motility. New J Phys 15 (2), 025022.

Camalet, S., Jülicher, F., 2000. Generic aspects of axonemal beating. New J Phys 2, 241–2423.

Cameron, D. E., Bashor, C., Collins, J., 2014. A brief history of synthetic biology. Nature Reviews Microbiology 12 (5), 381–390.

Camley, B. A., Zhao, Y., Li, B., Levine, H., Rappel, W. J., 2013. Periodic migration in a physical model of cells on micropatterns. Phys. Rev. Lett. 111 (15), 158102.

Cao, J., 2011. Michaelis-menten equation and detailed balance in enzymatic networks. J. Phys. Chem. B 115 (18), 5493–5498.

Cao, Y., Lu, H., Liang, J., 2010. Probability landscape of heritable and robust epigenetic state of lysogeny in phage lambda. Proc. Natl. Acad. Sci. USA 107, 18445–18450.

Carlier, M. F., Laurent, V., Santolini, J., Melki, R., Didry, D., Xia, G. X., Hong, Y., Chua, N. H., Pantaloni, D., Mar. 1997. Actin depolymerizing factor (ADF/cofilin) enhances the rate of filament turnover: implication in actin-based motility. J Cell Biol 136 (6), 1307–1322.

Carlier, M. F., Melki, R., Pantaloni, D., Hill, T. L., Chen, Y., Aug. 1987. Synchronous oscillations in microtubule polymerization. Proc Natl Acad Sci USA 84 (15), 5257–5261.

Carlsson, A., Jun. 2010. Dendritic actin filament nucleation causes traveling waves and patches. Phys. Rev. Lett. 104 (22), 228102.

Carlsson, A. E., May 2003. Growth velocities of branched actin networks. Biophys J 84 (5), 2907–2918.

Carmichael, H. J., 2010. Statistical Methods in Quantum Optics : 1 Master Equations and Fokker-Planck Equations. Springer, Berlin.

Caroli, C., Combesco.R, Nozieres, P., Saintjam.D, 1971. Direct calculation of tunneling current. J Phys Part C Solid 4 (8), 916.

Cason, T. N., Friedman, D., 2003. Buyer search and price dispersion: a laboratory study. Journal of Economic Theory 112 (2), 232–260.

Caspi, Y., Dekker, C., 2016. Mapping out Min protein patterns in fully confined fluidic chambers. Elife 5, e19271.

Chalut, K., Paluch, E., Sep. 2016. The Actin Cortex: A Bridge between Cell Shape and Function. Developmental Cell 38 (6), 571–573.

Chambers, I., Silva, J., Colby, D., Nichols, J., Nijmeijer, B., Robertson, M., Vrana, J., Jones, K., Grotewold, L., Smith, A., 2007. Nanog safeguards pluripotency and mediates germline development. Nature 450 (7173), 1230–1234.

Charras, G., Paluch, E., Sep. 2008. Blebs lead the way: how to migrate without lamellipodia. Nat Rev Mol Cell Bio 9 (9), 730–736.

Chen, C., Wang, J., 2016. A physical mechanism of cancer heterogeneity. Sci. Rep. 6, 20679.

Chen, C., Zhang, K., Feng, H., Sasai, M., Wang, J., 2015a. Multiple coupled landscapes and non-adiabatic dynamics with applications to self-activating genes. Phys Chem Chem Phys 17 (43), 29036–29044.

Chen, F., Tao, N., 2009. Electron transport in single molecules: From benzene to graphene. Accounts Chem Res 42 (3), 429–438.

Chen, K., Calzone, L., Csikasz-Nagy, A., Cross, F., Novak, B., Tyson, J., 2004. Integrative analysis of cell cycle control in budding yeast. Mol Biol Cell 15 (8), 3841–3862.

Chen, X., Cao, J., Silbey, R., 2013. A novel construction of complex-valued gaussian processes with arbitrary spectral densities and its application to excitation energy transfer. J. Chem. Phys. 138 (22), 224104–224117.

Chen, Y., Kim, J., Hirning, A., Josić, K., Bennett, M. R., 2015b. Emergent genetic oscillations in a synthetic microbial consortium. Science 349 (6251), 986–989.

Chickarmane, V., Peterson, C., 2008. A computational model for understanding stem cell, trophectoderm and endoderm lineage determination. PloS one 3 (10), e3478.

Chin, A., Prior, J., Rosenbach, R., Caycedo-Soler, F., Huelga, S., Plenio, M., 2013. The role of non-equilibrium vibrational structures in electronic coherence and recoherence in pigment-protein complexes. Nat Phys 9 (2), 113–118.

Christensson, N., Kauffmann, H., Pullerits, T., Mancal, T., 2012. Origin of long-lived coherences in light-harvesting complexes. J. Phys. Chem. B 116 (25), 7449–7454.

Chuang, J. S., Rivoire, O., Leibler, S., 2009. Simpson's paradox in a synthetic microbial system. Science 323 (5911), 272–275.

Claessen, D., Rozen, D. E., Kuipers, O., Søgaard-Andersen, L., Van Wezel, G., 2014. Bacterial solutions to multicellularity: a tale of biofilms, filaments and fruiting bodies. Nature Reviews Microbiology 12 (2), 115–124.

Clark, A. G., Dierkes, K., Paluch, E. K., 2013. Monitoring Actin Cortex Thickness in Live Cells. Biophys J 105 (3), 570–580.

Clay, K., Kover, P., 1996. The red queen hypothesis and plant/pathogen interactions. Annual review of phytopathology 34 (1), 29–50.

Collin, D., Ritort, F., Jarzynski, C., Smith, S., Tinoco, I., Bustamante, C., 2005. Verification of the crooks fluctuation theorem and recovery of rna folding free energies. Nature 431, 231.

Combesco, R., 1971. A direct calculation of the tunnelling current. iii. effect of localized impurity states in the barrier. J. Phys. C 4, 2611.

Creixell, P., Schoof, E., Erler, J., Linding, R., 2012. Navigating cancer network attractors for tumor-specific therapy. Nat Biotechnol 30 (9), 842–848.

Crooks, G., 1998. Nonequilibrium measurements of free energy differences for microscopically reversible markovian systems. J Stat Phys 90 (5-6), 1481–1487.

Crooks, G., 1999. Entropy production fluctuation theorem and the nonequilibrium work relation for free energy differences. Phys Rev E 60 (3), 2721–2726.

Cugliandolo, L. F., Dean, D., Kurchan, J., 1997. Fluctuation-dissipation theorems and entropy production in relaxational systems. Phys. Rev. Lett. 79, 2168.

Danino, T., Mondragón-Palomino, O., Tsimring, L., Hasty, J., 2010. A synchronized quorum of genetic clocks. Nature 463 (7279), 326–330.

Darwin, C., 1873. The Origin of Species. London Pub.

Dasanayake, N., Michalski, P. J., Carlsson, A. E., Sep. 2011. General Mechanism of Actomyosin Contractility. Phys. Rev. Lett. 107 (11), 118101–4.

Dasanayake, N. L., Carlsson, A. E., Jun. 2013. Stress generation by myosin minifilaments in actin bundles. Physical Biology 10 (3), 036006.

Davidich, M., Bornholdt, S., 2008. Boolean network model predicts cell cycle sequence of fission yeast. PloS one 3 (2), e1672.

Dayan, P., Abbott, L. F., 2001. Theoretical Neuroscience. The MIT Press.

de Groot, S. R., Mazur, P., Jul. 1985. Non-Equilibrium Thermodynamics. Dover Publications Inc, New York.

De Roy, K., Marzorati, M., Van den Abbeele, P., Van de Wiele, T., Boon, N., 2014. Synthetic microbial ecosystems: an exciting tool to understand and apply microbial communities. Environ. Microbiol. 16 (6), 1472–1481.

Derrida, B., Evans, M. R., Hakim, V., Pasquier, V., Dec. 1993. Exact solution of a 1D asymmetric exclusion model using a matrix formulation. Journal of Physics A: Mathematical and General 26 (7), 1493–1517.

Desai, A., Verma, S., Mitchison, T. J., Walczak, C. E., 1999. Kin I kinesins are microtubule-destabilizing enzymes. Cell 96 (1), 69–78.

Destainville, N., Jan. 2008. Cluster phases of membrane proteins. Phys Rev E Stat Nonlin Soft Matter Phys 77 (1), 011905–5.

Deutsch, D., 1985. Quantum theory, the church-turing principle and the universal quantum computer 400 (1818): 97c117. Proc. Royal Soc. A. 400 (1818), 97–117.

Diana, G., Esposito, M., 2014. Mutual entropy-production in bipartite systems. J Stat Mech: Theor Exp, P04010.

Dieckmann, U., Marrow, P., Law, R., 1995. Evolutionary cycling in predator-prey interactions: population dynamics and the red queen. Journal of theoretical biology 176 (1), 91–102.

Dierkes, K., Sumi, A., Solon, J., Salbreux, G., 2014. Spontaneous Oscillations of Elastic Contractile Materials with Turnover. Phys. Rev. Lett. 113 (14), 148102.

Doebereiner, H., Dubin-Thaler, B., Hofman, J., Xenias, H., Sims, T., Giannone, G., Dustin, M. L., Wiggins, C. H., Sheetz, M., 2006. Lateral membrane waves constitute a universal dynamic pattern of motile cells. Phys. Rev. Lett. 97 (3), 038102.

Dogterom, M., 1997. Measurement of the Force-Velocity Relation for Growing Microtubules. Science 278 (5339), 856–860.

Dombrowski, C., Cisneros, L., Chatkaew, S., Goldstein, R. E., Kessler, J. O., 2004. Self-concentration and large-scale coherence in bacterial dynamics. Phys. Rev. Lett. 93 (9).

Dorfman, K., Voronine, D., Mukamel, S., Scully, M., 2013. Photosynthetic reaction center as a quantum heat engine. Proc. Natl. Acad. Sci. USA 110 (8), 2746–2751.

Doubrovinski, K., Howard, M., Jul. 2005. Stochastic model for Soj relocation dynamics in Bacillus subtilis. Proc Natl Acad Sci USA 102 (28), 9808–9813.

Doubrovinski, K., Kruse, K., 2008. Cytoskeletal waves in the absence of molecular motors. Epl-Europhys Lett 83 (1), 18003.

Doubrovinski, K., Kruse, K., Dec. 2011. Cell motility resulting from spontaneous polymerization waves. Phys. Rev. Lett. 107 (25), 258103.

Douglass, A., Vale, R., Jun. 2005. Single-Molecule Microscopy Reveals Plasma Membrane Microdomains Created by Protein-Protein Networks that Exclude or Trap Signaling Molecules in T Cells. Cell 121 (6), 937–950.

Drees, F., Pokutta, S., Yamada, S., Nelson, W. J., Weis, W. I., 2005. alpha-catenin is a molecular switch that binds E-cadherin-beta-catenin and regulates actin-filament assembly. Cell 123 (5), 903–915.

Dreher, A., Aranson, I. S., Kruse, K., 2014. Spiral actin-polymerization waves can generate amoeboidal cell crawling. New J Phys 16, 055007.

Dunn, G., Bruce, A., Ikeda, H., Old, L., Schreiber, R., 2002. Cancer immunoediting: from immunosurveillance to tumor escape. Nat Immunol 3 (11), 991–998.

Edman, L., FiSldes-Papp, Z., Wennmalm, S., Rigler, R., 1999. The fluctuating enzyme: a single molecule approach. Chemical Physics 247, 11–22.

Edman, L., Rigler, R., 2000. Memory landscapes of single-enzyme molecules. Proc. Natl. Acad. Sci. USA 97, 8266 C 8271.

Eftimie, R., Bramson, J., Earn, D., 2011. Interactions between the immune system and cancer: A brief review of non-spatial mathematical models. Bull Math Biol 73 (1), 2–32.

Eisler, V., Zimboras, Z., 2005. Entanglement in the xx spin chain with an energy current. Phys. Rev. A 71, 042318.

Elber, R., Meller, J., Olender, R., 1999. Stochastic path approach to compute atomically detailed trajectories: Application to the folding of c peptide. J. Phys. Chem. B 103 (6), 899–911.

Elena, S., Lenski, R., Jun. 2003. Microbial genetics: Evolution experiments with microorganisms: the dynamics and genetic bases of adaptation. Nat Rev Genet 4 (6), 457–469.

Elowitz, M., Leibler, S., 2000. A synthetic oscillatory network of transcriptional regulators. Nature 403 (6767), 335–338.

Elowitz, M., Levine, A., Siggia, E., Swain, P., 2002. Stochastic gene expression in a single cell. Science 297 (5584), 1183–1186.

Endow, S. A., Higuchi, H., 2000. A mutant of the motor protein kinesin that moves in both directions on microtubules. Nature 406 (6798), 913–916.

Englander, J., 2013. Statistical physics of self-replication. J. Chem. Phys. 139, 121923.

English, B. P., Min, W., Van Oijen, A. M., Lee, K. T., Luo, G., Sun, H., Cherayil, B., Kou, S., Xie, X. S., 2006. Ever-fluctuating single enzyme molecules: Michaelis-menten equation revisited. Nature chemical biology 2 (2), 87–94.

Ennomani, H., Letort, G., Guérin, C., Martiel, J., Cao, W., Nedelec, F., De la Cruz, E., Thery, M., Blanchoin, L., 2016. Architecture and Connectivity Govern Actin Network Contractility. Curr Biol 26 (5), 616–626.

Ericksen, J. L., 1962. Hydrostatic theory of liquid crystals. Arch. Rational Mech. Anal. 9 (1), 371–378.

Erlenkämper, C., Kruse, K., 2013. Treadmilling and length distributions of active polar filaments. The Journal of chemical physics 139 (16), 164907–12.

Esposito, M., Galperin, M., 2009. Transport in molecular states language: Generalized quantum master equation approach. Phys Rev B 79 (20).

Euteneuer, U., Schliwa, M., Jul. 1984. Persistent, directional motility of cells and cytoplasmic fragments in the absence of microtubules. Nature 310 (5972), 58–61.

Ewens, W., 2004. Mathematical Population Genetics 1. Theoretical Introduction. Springer.

Faccioli, P., Sega, M., Pederiva, F., Orland, H., 2006. Dominant pathways in protein folding. Phys. Rev. Lett. 97 (10), 108101.

Faini, M., Beck, R., Wieland, F. T., Briggs, J. A. G., Jun. 2013. Vesicle coats: structure, function, and general principles of assembly. Trends in cell biology 23 (6), 279–288.

Fairn, G., Hermansson, M., Somerharju, P., Grinstein, S., Oct. 2011. Phosphatidylserine is polarized and required for proper Cdc42 localization and for development of cell polarity. Nat Cell Biol 13 (12), 1424–1430.

Faivre-Moskalenko, C., Dogterom, M., 2002. Dynamics of microtubule asters in microfabricated chambers: The role of

catastrophes. Proc Natl Acad Sci USA 99 (26), 16788–16793.

Falkovich, G., Sreenivasan, K., 2006. Lessons from hydrodynamic turbulence. Phys Today 59 (4), 43–49.

Fan, J., Sammalkorpi, M., Haataja, M., Apr. 2008. Domain Formation in the Plasma Membrane: Roles of Nonequilibrium Lipid Transport and Membrane Proteins. Phys. Rev. Lett. 100 (17), 178102.

Fang, X., Liu, Q., Bohrer, C., Hensel, Z., Han, W., Wang, J., Xiao, J., 2018. Cell fate potentials and switching kinetics uncovered in a classic bistable genetic switch. Nature Communications 9, 2787.

Feng, H., Han, B., Wang, J., 2010. Dominant kinetic paths of complex systems: Gene networks. J Phys Chem Lett 1 (12), 1836–1840.

Feng, H., Han, B., Wang, J., 2011. Adiabatic and non-adiabatic non-equilibrium stochastic dynamics of single regulating genes. J. Phys. Chem. B 115 (5), 1254–1261.

Feng, H., Han, B., Wang, J., 2012. Landscape and global stability of nonadiabatic and adiabatic oscillations in a gene network. Biophys. J. 102 (5), 1001–1010.

Feng, H., Wang, J., 2011. Potential and flux decomposition for dynamical systems and non-equilibrium thermodynamics: Curvature, gauge field, and generalized fluctuation-dissipation theorem. J. Chem. Phys. 135 (23), 234511.

Feng, H., Wang, J., 2012. A new mechanism of stem cell differentiation through slow binding/unbinding of regulators to genes. Sci. Rep. 2, 550.

Feng, H., Zhang, K., Wang, J., 2014. Non-equilibrium transition state rate theory. Chem Sci 5 (10), 3761–3769.

Feric, M., Vaidya, N., Harmon, T., Mitrea, D., Zhu, L., Richardson, T., Kriwacki, R., Pappu, R., Brangwynne, C., 2016. Coexisting Liquid Phases Underlie Nucleolar Subcompartments. Cell 165 (7), 1686–1697.

Ferrell Jr., J. E., Tsai, T. Y.-C., Yang, Q., 2011. Modeling the Cell Cycle: Why Do Certain Circuits Oscillate? Cell 144, 874–885.

Ferry, D. K., Goodnick, S. M., 1997. Transport in Nanostructures. Cambrdige University Press.

Feynman, R. P., Hibbs, A. R., 1965. Quantum Mechanics and Path Integrals. McGraw-Hill, New York.

Fisher, I., 1933. The debt-deflation theory of great depressions. Econometrica 1 (4), 337–357.

Fisher, R., 1930. The genetical theory of natural selection. Oxford University Press, Oxford.

FitzHugh, R., 1961. Impulses and physiological states in theoretical models of nerve membrane. Biophysical J. 1, 445C466.

Footer, M., Kerssemakers, J. W. J., Theriot, J., Dogterom, M., Feb. 2007. Direct measurement of force generation by actin filament polymerization using an optical trap. Proc Natl Acad Sci USA 104 (7), 2181–2186.

Foret, L., Aug. 2005. A simple mechanism of raft formation in two-component fluid membranes. Europhys Lett 71 (3), 508–514.

Foster, P., Fürthauer, S., Shelley, M., Needleman, D., 2015. Active contraction of microtubule networks. Elife 4.

Frauenfelder, H., Wolynes, P., 1994. Biomolecules - where the physics of complexity and simplicity meet. Phys Today 47 (2), 58–64.

Freidlin, M., Wentzell, A., 1984. Random Perturbations of Dynamical Systems. Springer, New York/Berlin.

Frisch, U., 1995. Turbulence: The Legacy of A. N. Kolmogorov. New York: Cambridge University Press.

Fritzsche, M., Erlenkämper, C., Moeendarbary, E., Charras, G., Kruse, K., Apr. 2016. Actin kinetics shapes cortical network structure and mechanics. Sci Adv 2 (4), e1501337.

Fritzsche, M., Lewalle, A., Duke, T., Kruse, K., Charras, G., Mar. 2013. Analysis of turnover dynamics of the submembranous actin cortex. Molecular Biology of the Cell 24 (6), 757–767.

Fujiwara, I., Vavylonis, D., Pollard, T., May 2007. Polymerization kinetics of ADP- and ADP-Pi-actin determined by fluorescence microscopy. Proc Natl Acad Sci USA 104 (21), 8827–8832.

Fung, E., Wong, W. W., Suen, J., Bulter, T., Lee, S., Liao, J., 2005. A synthetic gene–metabolic oscillator. Nature 435 (7038), 118–122.

Fürthauer, S., Neef, M., Grill, S. W., Kruse, K., Jülicher, F., Feb. 2012. The Taylor–Couette motor: spontaneous flows of active polar fluids between two coaxial cylinders. New J Phys 14 (2), 023001.

Gao, T., Blackwell, R., Glaser, M. A., Betterton, M. D., Shelley, M. J., 2015. Multiscale Polar Theory of Microtubule and Motor-Protein Assemblies. Phys. Rev. Lett. 114 (4).

Garab, G., 1999. Photosynthesis: Mechanisms and Effects. Springer Science and Business Media, B.V.

Gardiner, C., 1983. Handbook of Stochastic Mechods. Springer, New York.

Gardner, T., Cantor, C., Collins, J., 2000. Construction of a genetic toggle switch in escherichia coli. Nature 403 (6767), 339–342.

Gaspard, P., 1998. Chaos, scattering and statistical mechanics. Cambridge University Press, Cambridge UK.

Gatenby, R., Vincent, T., 2003. An evolutionary model of carcinogenesis. Cancer Res 63 (19), 6212–6220.

Ge, H., 2014. Time reversibility and nonequilibrium thermodynamics of second-order stochastic processes. Phys Rev E 89 (2), 022127.

Ge, H., Qian, H., 2010. Physical origins of entropy production, free energy dissipation, and their mathematical representations. Phys Rev E 81 (5), 051133.

Gelbart, W., Rice, S., Freed, K., 1972. Random matrix theory and the master equation for finite systems. J. Chem. Phys. 57, 4699.

Gems, D., L., P., 2013. Genetics of longevity in model organisms: debates and paradigm shifts. Annu. Rev. Physiol. 75, 621C644.

Gerisch, G., Bretschneider, T., Muller-Taubenberger, A., Simmeth, E., Ecke, M., Diez, S., Anderson, K., 2004. Mobile actin clusters and traveling waves in cells recovering from actin depolymerization. Biophys J 87 (5), 3493–3503.

Getling, A. V., 1998. Rayleigh-Bnard Convection:Structures and Dynamics. World Scientific, Singapore.

Gheber, L. A., Edidin, M., Dec. 1999. A model for membrane patchiness: Lateral diffusion in the presence of barriers and vesicle traffic. Biophys J 77 (6), 3163–3175.

Gholami, A., Enculescu, M., Falcke, M., 2012. Membrane waves driven by forces from actin filaments. New J Phys 14, 115002.

Giannone, G., Dubin-Thaler, B. J., Dobereiner, H., Kieffer, N., Bresnick, A., Sheetz, M., 2004. Periodic lamellipodial contractions correlate with rearward actin waves. Cell 116 (3), 431–443.

Gilboa, B., Gillo, D., Farago, O., Bernheim-Groswasser, A., 2009. Bidirectional cooperative motion of myosin-II motors on actin tracks with randomly alternating polarities. Soft Matter 5 (11), 2223–2231.

Gillespie, D., 1976. A general method for numerically simulating the stochastic time evolution of coupled chemical reactions. J. Comput. Phys. 22 (4), 403–434.

Giomi, L., Bowick, M. J., Ma, X., Marchetti, M. C., 2013. Defect Annihilation and Proliferation in Active Nematics. Phys. Rev. Lett. 110 (22), 228101.

Glotzer, S. C., Di Marzio, E., Muthukumar, M., Jan. 1995. Reaction-controlled morphology of phase-separating mixtures. Phys. Rev. Lett. 74 (11), 2034–2037.

Goehring, N., Trong, P. K., Bois, J. S., Chowdhury, D., Nicola, E., Hyman, A., Grill, S., 2011. Polarization of PAR Proteins by Advective Triggering of a Pattern-Forming System. Science 334 (6059), 1137–1141.

Goh, B., 1976. Global stability in two species interactions. J. Math. Biol. 3, 313–318.

Goh, B., 1977. Global stability in many-species systems. Am Nat 111, 135–143.

Goldenfeld, N., Shih, H. Y., 2017. Turbulence as a problem in non-equilibrium statistical mechanics. J. Stat. Phys. 167, 575–594.

Gonze, D., Halloy, J., Goldbeter, A., 2002. Robustness of circadian rhythms with respect to molecular noise. Proceedings of the National Academy of Sciences of the United States of America 99 (2), 673–678.

Goodwin, R., 1967. A Growth Cycle in C.H. Feinstein, editor, Socialism, Capitalism and Economic Growth. Cambridge: Cambridge University Press.

Gore, J., Youk, H., van Oudenaarden, A., 2009. Snowdrift game dynamics and facultative cheating in yeast. Nature 459, 253.

Goswami, D., Gowrishankar, K., Bilgrami, S., Ghosh, S., Raghupathy, R., Chadda, R., Vishwakarma, R., Rao, M., Mayor, S., 2008. Nanoclusters of GPI-Anchored Proteins Are Formed by Cortical Actin-Driven Activity. Cell 135 (6), 1085–1097.

Graham, R., 1989. Macroscopic potentials, bifurcations and noise in *Noise in Nonlinear Dynamical Systems*. Cambridege Unviersity Press.

Greenan, G., Brangwynne, C., Jaensch, S., Gharakhani, J., Juelicher, F., Hyman, A. A., 2010. Centrosome Size Sets Mitotic Spindle Length in Caenorhabditis elegans Embryos. Curr Biol 20 (4), 353–358.

Grill, S. W., Kruse, K., Jülicher, F., 2005. Theory of mitotic spindle oscillations. Phys. Rev. Lett. 94 (10).

Grosberg, A. Y., Joanny, J. F., 2015. Nonequilibrium statistical mechanics of mixtures of particles in contact with different thermostats. Phys. Rev. E 92, 032118.

Großkopf, T., Soyer, O. S., 2014. Synthetic microbial communities. Curr. Opin. Microbiol. 18, 72–77.

Grossman, A., 1995. Genetic networks controlling the initiation of sporulation and the development of genetic competence in bacillus subtilis. Annual review of genetics 29 (1), 477–508.

Grover, M. K., Silbey, R., 1970. Excitoncphonon interactions in molecular crystals. Journal of Chemical Physics 52 (4), 2099–2108.

Gruebele, M., Wolynes, P., 2004. Vibrational energy flow and chemical reactions. Accounts Chem Res 37 (4), 261–267.

Guerin, T., Prost, J., Joanny, J., 2010. Dynamic Instabilities in Assemblies of Molecular Motors with Finite Stiffness. Phys. Rev. Lett. 104 (24), 248102.

Guérin, T, Prost, Jacques, Joanny, J F, 2011. Motion Reversal of Molecular Motor Assemblies due to Weak Noise. Phys. Rev. Lett. 106, 068101.

Günther, S., Kruse, K., 2007. Spontaneous waves in muscle fibres. New J Phys 9 (11), 417–417.

Guo, B., Guilford, W., 2006. Mechanics of actomyosin bonds in different nucleotide states are tuned to muscle contraction. Proc Natl Acad Sci USA 103 (26), 9844–9849.

Grard, C., Goldbeter, A., 2009. Temporal self-organization of the cyclin/cdk network driving the mammalian cell cycle. Proceedings of the National Academy of Sciences of the United States of America 106 (51), 21643–21648.

Haake, F., 1973. Statistical Treatment of Open Systems Springer Tracts in Modern Physics vol. 66. Springer, Berlin.

Haken, H., 1987. Advanced Synergetics : instability hierarchies of self-organizing systems and devices. Springer, Berlin.

Haken, H., 2000. Information and Self-Organization: A macroscopic approach to complex systems. Springer, Berlin.

Han, B., Wang, J., 2007. Quantifying robustness and dissipation cost of yeast cell cycle network: The funneled energy landscape perspectives. Biophy. J. 92 (11), 3755–3763.

Han, B., Wang, J., 2008. Least dissipation cost as a design principle for robustness and function of cellular networks. Phys Rev E 77 (3), 031922.

Hanahan, D., Weinberg, R., 2000. The hallmarks of cancer. Cell 100 (1), 57–70.

Hanahan, D., Weinberg, R., 2011. Hallmarks of cancer: The next generation. Cell 144 (5), 646–674.

Hannezo, E., Prost, J., Joanny, J. F., 2011. Instabilities of Monolayered Epithelia: Shape and Structure of Villi and Crypts. Phys. Rev. Lett. 107, 078104.

Harbola, U., Esposito, M., Mukamel, S., 2006. Quantum master equation for electron transport through quantum dots and single molecules. Phys Rev B 74 (23), 235309.

Harrison, G., 1979. Global stability of predator-prey interactions. J. Math. Biology 8, 159–171.

Hartich, D., Barato, A. C., Seifert, U., 2014. Stochastic thermodynamics of bipartite systems: transfer entropy inequalities and a maxwell's demon interpretation. J. of Stat. Mech. P02016 (2014), P02016.

Hassler, K., Rigler, P., Blom, H., Rigler, R., Widengren, J., Lasser, T., 2007. Dynamic disorder in horseradish peroxidase observed with total internal reflection fluorescence correlation spectroscopy. OPTICS EXPRESS 15, 5366–5375.

Hastings, A., 1978. Global stability of two species systems. J. Math. Biol. 5, 399–403.

Hastings, A., 1981. Disequilibrium, selection, and recombination: limits in two-locus, two-allele models. Genetics 98 (3), 659–668.

Hatano, T., Sasa, S., 2001. Steady-state thermodynamics of langevin systems. Phys. Rev. Lett. 86 (16), 3463–3466.

Hawkins, R., Piel, M., Faure-Andre, G., Lennon-Dumenil, A. M., Joanny, J. F., Prost, J., Voituriez, R., Feb. 2009. Pushing off the Walls: A Mechanism of Cell Motility in Confinement. Phys. Rev. Lett. 102 (5), 058103–4.

Hawkins, R., Poincloux, R., Benichou, O., Piel, M., Chavrier, P., Voituriez, R., Sep. 2011. Spontaneous Contractility-Mediated Cortical Flow Generates Cell Migration in Three-Dimensional Environments. Biophys J 101 (5), 1041–1045.

Hiraiwa, T., Salbreux, G., 2016. Role of Turnover in Active Stress Generation in a Filament Network. Phys. Rev. Lett. 116 (18).

Ho, W., 2002. Single-molecule chemistry. J. Chem. Phys. 117 (24), 11033–11061.

Hodgkin, A., Huxley, A., 1952. A quantitative description of membrane current and its application to conduction and excitation in nerve. J Physiol 117, 500C544.

Hofbauer, J., 2011. Deterministic evolutionary game dynamics. Proc Sym Ap 69, 61–79.

Holling, C., 1965. The functional response of predators to prey density and its role in mimicry and population regulation. Mem. Ent. Soc. Can. 45, 1–60.

Holy, T. E., Dogterom, M., Yurke, B., Leibler, S., 1997. Assembly and positioning of microtubule asters in microfabricated chambers. Proc Natl Acad Sci USA 94 (12), 6228–6231.

Hopfield, J., 1982. Neural networks and physical systems with emergent collective computational abilities. Proc. Natl. Acad. Sci. USA. 79 (8), 2554–2558.

Hopfield, J., 1994. Physics, computation, and why biology looks so different. J Theor Biol 171 (1), 53–60.

Hornos, J., Schultz, D., Innocentini, G., Wang, J., Walczak, A., Onuchic, J., Wolynes, P., 2005. Self-regulating gene: An exact solution. Phys Rev E 72 (5), 051907.

Horowitz, J., Esposito, M., 2014. Thermodynamics with continuous information flow. Phys Rev X 4 (3), 031015.

Hsu, S., 1978. On global stability of a predator prey system. Math. Biosci. 39, 1–10.

Hu, G., 1995. Stochastic Force and Nonlinear Systems. Shanghai Science Education, Shanghai.

Hu, Z., Gogol, E., Lutkenhaus, J., May 2002. Dynamic assembly of MinD on phospholipid vesicles regulated by ATP and MinE. Proc Natl Acad Sci USA 99 (10), 6761–6766.

Huang, K. C., Meir, Y., Wingreen, N. S., 2003. Dynamic structures in Escherichia coli: Spontaneous formation of MinE rings and MinD polar zones. Proc Natl Acad Sci USA 100 (22), 12724–12728.

Huang, S., Ernberg, I., Kauffman, S., 2009. Cancer attractors: A systems view of tumors from a gene network dynamics and developmental perspective. Semin Cell Dev Biol 20 (7), 869–876.

Huberman, B. A., Sep. 1976. Striations in chemical reactions. The Journal of chemical physics 65 (5), 2013–2019.

Huk, A., Shadlen, M., 2005. Neural activity in macaque parietal cortex reflects temporal integration of visual motion signals during perceptual decision making. J Neurosci 25 (45), 10420–10436.

Hunt, K., Ross, J., 1981. Path integral solutions of stochastic-equations for non-linear irreversible-processes - the uniqueness of the thermodynamic lagrangian. J. Chem. Phys. 75 (2), 976–984.

Hunter, A. W., Caplow, M., Coy, D. L., Hancock, W. O., Diez, S., Wordeman, L., Howard, J., Feb. 2003. The kinesin-related protein MCAK is a microtubule depolymerase that forms an ATP-hydrolyzing complex at microtubule ends. Mol Cell 11 (2), 445–457.

Ideses, Y., Erukhimovitch, V., Brand, R., Jourdain, D., Hernandez, J. S., Gabineti, U. R., Safran, S. A., Kruse, K., Bernheim-Groswasser, A., 2018. Spontaneous buckling of contractile poroelastic actomyosin sheets. Nat. Comms. 9, 2461.

Isaacs, F., Hasty, J., Cantor, C., Collins, J., 2003. Prediction and measurement of an autoregulatory genetic module. Proceedings of the National Academy of Sciences 100 (13), 7714–7719.

Ishiura, M., Kutsuna, S., Aoki, S., Iwasaki, H., Andersson, C., Tanabe, A., Golden, S., Johnson, C., Kondo, T., 1998. Expression of a gene cluster kaiabc as a circadian feedback process in cyanobacteria. Science 281 (5382), 1519–1523.

Jackson, E., 1989. Perspectives of Nonlinear Dynamics. Cambridge Unversity Press, Cambridge.

Jaeger, J., Surkova, S., Blagov, M., Janssens, H., Kosman, D., Kozlov, K., Manu, Myasnikova, E., Vanario-Alonso, C., Samsonova, M., Sharp, D., Reinitz, J., 2004. Dynamic control of positional information in the early drosophila embryo. Nature 430 (6997), 368–371.

Jang, S., 2011. Theory of multichromophoric coherent resonance energy transfer: A polaronic quantum master equation approach. J. Chem. Phys. 135 (3), 034105–034113.

Jiang, J., Chan, Y., Loh, Y., Cai, J., Tong, G., Lim, C., Robson, P., Zhong, S., Ng, H., 2008. A core klf circuitry regulates self-renewal of embryonic stem cells. Nat Cell Biol 10 (3), 353–360.

Jiang, D. Q.and Qian, M., 2003. Mathematical Theory of Nonequilibrium Steady States: On the Frontier of Probability and Dynamical Systems. Springer, New York.

Jiang, Z., Tian, L., Fang, X., Zhang, K., Liu, Q., Dong, Q., Wang, J., 2017. The emergence of the two cell fates and their associated switching for a negative auto-regulating gene. ArXiv 1707, 00854.

Joanny, J., Juelicher, F., Kruse, K., Prost, J., 2007. Hydrodynamic theory for multi-component active polar gels - IOPscience. New J Phys 9, 422.

Joanny, J. F., Kruse, K., Prost, J., Ramaswamy, S., May 2013. The actin cortex as an active wetting layer. Eur Phys J E 36 (5), 52.

Johann, D., Erlenkaemper, C., Kruse, K., 2012. Length Regulation of Active Biopolymers by Molecular Motors. Phys. Rev. Lett. 108 (25), 258103.

Johann, D., Goswami, D., Kruse, K., 2014. Segregation of diffusible and directionally moving particles on a polar filament. Phys Rev E 89 (4), 042713.

Jülicher, F., Ajdari, A., Prost, J., 1997. Modeling molecular motors. Rev Mod Phys 69 (4), 1269–1281.

Jülicher, F., Prost, J., Sep. 1995. Cooperative molecular motors. Phys. Rev. Lett. 75 (13), 2618–2621.

Jülicher, F., Prost, J., 1997. Spontaneous oscillations of collective molecular motors. Phys. Rev. Lett. 78 (23), 4510–4513.

K., W., 1998. Entanglement of formation of an arbitrary state of two qubits. Phys. Rev. Lett. 80, 2245.

Kalmar, T., Lim, C., Hayward, P., Muñoz-Descalzo, S., Nichols, J., Garcia-Ojalvo, J., Arias, A. M., 2009. Regulated fluctuations in nanog expression mediate cell fate decisions in embryonic stem cells. PLoS Biol 7 (7), e1000149.

Kao, Y., Guo, X., Yang, Y., Liu, Z., Hassanali, A., Song, Q., Wang, L., Zhong, D., 2012. Ultrafast dynamics of nonequilibrium electron transfer in photoinduced redox cycle: Solvent mediation and conformation flexibility. J. Phys. Chem. B 116 (30), 9130–9140.

Karamched, B., Bressloff, P., May 2015. Delayed Feedback Model of Axonal Length Sensing. Biophys J 108 (9), 2408–2419.

Kauffman, S., 1969. Homeostasis and differentiation in random genetic control networks. Nature 224 (5215), 177–178.

Kauffman, S., 1971. Differentiation of malignant to benign cells. J Theor Biol 31 (3), 429–451.

Keber, F. C., Loiseau, E., Sanchez, T., DeCamp, S. J., Giomi, L., Bowick, M. J., Marchetti, M., Dogic, Z., Bausch, A. R., 2014. Topology and dynamics of active nematic vesicles. Science (New York, N.Y.) 345 (6201), 1135–1139.

Keen, S., 1994. Finance and economic breakdown: Modeling minskys financial instability hypothesis. Journal of Post Keynesian Economics 17 (4), 607–635.

Keen, S., 2001. Debunking Economics: The Naked Emperor of the Social Sciences. Pluto Press Australia.

Kenyon, C., Chang, J., Gensch, E., Rudner, A., Tabtiang, R., 1993. A c-elegans mutant that lives twice as long as wild-type. Nature 366 (6454), 461–464.

Kenyon, C. J., 2010. The genetics of ageing. Nature 464, 504–512.

Kerr, B., Riley, M., Feldman, M., Bohannan, B., 2002. Local dispersal promotes biodiversity in a real-life game of rock–paper–scissors. Nature 418 (6894), 171–174.

Kessler, D., Levine, H., Dec. 2016. Nonlinear self-adapting wave patterns. New J Phys 18 (12).

Keynes, J., 1936. The General Theory of Employment,Interest and Money. London: Macmillan.

Kimura, K., Tissenbaum, H., Liu, Y., Ruvkun, G., 1997. daf-2, an insulin receptor-like gene that regulates longevity and diapause in caenorhabditis elegans. Science 277 (5328), 942–946.

King, D. P., Zhao, Y., Sangoram, A. M., Wilsbacher, L. D., Tanaka, M., Antoch, M. P., Steeves, T. D., Vitaterna, M. H., Kornhauser, J. M., Lowrey, P. L., 1997. Positional cloning of the mouse circadian clock gene. Cell 89 (4), 641–653.

Kirkwood, T., 2005. Understanding the odd science of aging. Cell 120 (4), 437–447.

Klein, S., Appert-Rolland, C., Santen, L., 2014. Environmental control of microtubule-based bidirectional cargo transport. EPL (Europhysics Letters) 107 (1), 18004–7.

Koentopp, M., Chang, C., Burke, K., Car, R., 2008. Density functional calculations of nanoscale conductance. J Phys-Condens Mat 20 (8), 083203.

Kolli, A., Nazir, A., Olaya-Castro, A., 2011. Electronic excitation dynamics in multichromophoric systems described via a polaron-representation master equation. J. Chem. Phys. 135 (15), 154112–154124.

Kolmogoroff, A., 1941a. Dissipation of energy in the locally isotropic turbulence. Cr Acad Sci Urss 32, 16–18.

Kolmogoroff, A., 1941b. The local structure of turbulence in incompressible viscous fluid for very large reynolds numbers. Cr Acad Sci Urss 30, 301–305.

Kolmogorov, A., 1962. A refinement of previous hypotheses concerning the local structure of turbulence in a viscous incompressible fluid at high reynolds number. J Fluid Mech 13 (1), 82–85.

Kong, W., Celik, V., Liao, C., Hua, Q., Lu, T., 2014. Programming the group behaviors of bacterial communities with synthetic cellular communication. Bioresources and Bioprocessing 1 (1), 24.

Kong, W., Meldgin, D. R., Collins, J. J., Lu, T., 2018. Designing microbial consortia with defined social interactions. Nat. Chem. Biol. 14 (8), 821.

Kramers, H., 1940. Brownian motion in a field of force and the diffusion model of chemical reactions. Physica 7, 284–304.

Krauth, W., 2006. Statistical Mechanics: Algorithms and Computations. Oxford Master Series in Physics. Oxford University Press, USA.

Krug, J., 1991. Boundary-Induced Phase-Transitions in Driven Diffusive Systems. Phys. Rev. Lett. 67 (14), 1882–1885.

Kruse, K., Feb. 2002. A dynamic model for determining the middle of Escherichia coli. Biophys J 82 (2), 618–627.

Kruse, K., Joanny, J., Jülicher, F., Prost, J., Sekimoto, K., Feb. 2004. Asters, vortices, and rotating spirals in active gels of polar filaments. Phys. Rev. Lett. 92 (7), 078101.

Kruse, K., Joanny, J. F., Jülicher, F., Prost, J., Jun. 2006. Contractility and retrograde flow in lamellipodium motion. Physical Biology 3 (2), 130–137.

Kruse, K., Joanny, J. F., Jülicher, F., Prost, J., Sekimoto, K., Jan. 2005. Generic theory of active polar gels: a paradigm for cytoskeletal dynamics. Eur Phys J E Soft Matter 16 (1), 5–16.

Kruse, K., Jülicher, F., Aug. 2000. Actively Contracting Bundles of Polar Filaments. Phys. Rev. Lett. 85 (8), 1778–1781.

Kruse, K., Jülicher, F., May 2003. Self-organization and mechanical properties of active filament bundles. Phys Rev E Stat Nonlin Soft Matter Phys 67 (5 Pt 1), 051913.

Kubo, R., 1957. Statistical-mechanical theory of irreversible processes. i. general theory and simple applications to magnetic and conduction problems. J. Phys. Soc. Jap. 12, 570.

Kubo, R., 1966. The fluctuation-dissipation theorem. Rep. Prog. Phys. 29, 255–284.

Kuhn, J., Pollard, T., 2005. Real-time measurements of actin filament polymerization by total internal reflection fluorescence microscopy. Biophys J 88 (2), 1387–1402.

Kumar, K. V., Bois, J. S., Juelicher, F., Grill, S. W., 2014. Pulsatory Patterns in Active Fluids. Phys. Rev. Lett. 112 (20).

Kuznetsov, A. M., Ulstrup, J., 1999. Electron transfer in chemistry and biology pp. An introduction to the theory. Wiley, Chichester, U.K.

Laan, L., Pavin, N., Husson, J., Romet-Lemonne, G., van Duijn, M., Lopez, M. P., Vale, R., Juelicher, F., Reck-Peterson, S., Dogterom, M., 2012. Cortical Dynein Controls Microtubule Dynamics to Generate Pulling Forces that Position Microtubule Asters. Cell 148 (3), 502–514.

Laemmermann, T., Bader, B. L., Monkley, S. J., Worbs, T., Wedlich-Soeldner, R., Hirsch, K., Keller, M., Foerster, R., Critchley, D., Faessler, R., Sixt, M., 2008. Rapid leukocyte migration by integrin-independent flowing and squeezing. Nature 453 (7191), 51.

Lambert, N., Aguardo, R., Brandes, T., 2007. Nonequilibrium entanglement and noise in coupled qubits. Phys. Rev. B. 75, 045340.

Lan, G., Sartori, P., Neumann, S., Sourjik, V., Tu, Y., 2012. The energy-speed-accuracy trade-off in sensory adaptation. Nature Physics 8, 422–428.

Landau, L. D., Lifshits, E. M., 1987. Fluid mechanics. Pergamon Press.

Landauer, R., 1961. Irreversibility and heat generation in the computing process. Ibm J Res Dev 5 (3), 183–191.

Lansky, Z., Braun, M., Luedecke, A., Schlierf, M., ten Wolde, P., Janson, M., Diez, S., 2015. Diffusible Crosslinkers Generate Directed Forces in Microtubule Networks. Cell 160 (6), 1159–1168.

Lapidus, S., Han, B., Wang, J., 2008. Intrinsic noise, dissipation cost, and robustness of cellular networks: The underlying energy landscape of mapk signal transduction. P Natl Acad Sci USA 105 (16), 6039–6044.

Laughlin, R., 1983. Anomalous quantum hall-effect - an incompressible quantum fluid with fractionally charged excitations. Phys. Rev. Lett. 50 (18), 1395–1398.

Laughlin, R. B., Pines, D., Schmalian, J., Stojkovic, B. P., Wolynes, P., 2000. The middle way. Proc. Natl. Acad. Sci. USA. 97 (1), 32–37.

Lecuit, T., Lenne, P.-F., 2007. Cell surface mechanics and the control of cell shape, tissue patterns and morphogenesis. Nat. Rev. Mol. Cell Bio. 8, 633–644.

Lee, C. F., Brangwynne, C. P., Gharakhani, J., Hyman, A. A., Juelicher, F., 2013. Spatial Organization of the Cell Cytoplasm by Position-Dependent Phase Separation. Phys. Rev. Lett. 111 (8), 088101.

Lee, H., Cheng, Y., Fleming, G., 2007. Coherence dynamics in photosynthesis: Protein protection of excitonic coherence. Science 316 (5830), 1462–1465.

Lee, S., Kennedy, S., Tolonen, A., Ruvkun, G., 2003. Daf-16 target genes that control c-elegans life-span and metabolism. Science 300 (5619), 644–647.

Leggett, A. J., Chakravarty, S., Dorsey, A. T., Fisher, M. P. A., Garg, A., Zwerger, W., 1987. Dynamics of the dissipative two-state system. Rev. of Mod. Phys. 59, 1–85.

Leitner, D., 2010. Quantum localization and protein-assisted vibrational energy flow in cofactors. New J Phys 12, 085004.

Lenz, M., 2014. Geometrical Origins of Contractility in Disordered Actomyosin Networks. Phys. Rev. X 4 (4), 041002–9.

Lenz, M., Gardel, M., Dinner, A., Mar. 2012a. Requirements for contractility in disordered cytoskeletal bundles. New J Phys 14 (3), 033037.

Lenz, M., Thoresen, T., Gardel, M. L., Dinner, A., Jun. 2012b. Contractile Units in Disordered Actomyosin Bundles Arise from F-Actin Buckling. Phys. Rev. Lett. 108 (23), 238107–5.

Levchenko, A., Nemenman, I., 2014. Cellular noise and information transmission. Curr Opin Biotech 28, 156–164.

Levin, S., 1979. Multiple equilibria in ecological models. In Proceedings of International Symposium on Mathematical Modelling of Man-Environment Interaction. Telavi, Georgia, USSR, September 1978. Computation Center of Academy of Sciences of USSR.

Levin, S., 1981. Populations in heterogeneous environments. BioScience 31 (9), 678.

Levin, S., 1987. Scale and predictability in ecological modeling. Modeling and Management of Resources Under Uncertainty. Proceedings, Honolulu 1985. Lecture Notes in Biomathematics 72. Springer-Verlag, Heidelberg.

Levin, S., Segel, L., 1976. Hypothesis for origin of planktonic patchiness. Nature 1976 (259), 659.

Levin, S., Segel, L., 1985. Pattern generation in space and aspect. SIAM Review 27 (1), 45–67.

Li, C., Wang, E., Wang, J., 2011a. Landscape, flux, correlation, resonance, coherence, stability, and key network wirings of stochastic circadian oscillation. Biophys. J. 101 (6), 1335–1344.

Li, C., Wang, E., Wang, J., 2011b. Potential landscape and probabilistic flux of a predator prey network. PLoS One 6 (3), e17888.

Li, C., Wang, J., 2013. Quantifying cell fate decisions for differentiation and reprogramming of a human stem cell network: Landscape and biological paths. PLoS Comput. Biol. 9 (8), e1003165.

Li, C., Wang, J., 2014a. Landscape and flux reveal a new global view and physical quantification of mammalian cell cycle. Proc. Natl. Acad. Sci. USA. 111 (39), 14130–14135.

Li, C., Wang, J., 2014b. Quantifying the underlying landscape and paths of cancer. J R Soc Interface 11 (100), 20140774.

Li, C., Wang, J., 2015. Quantifying the landscape for development and cancer from a core cancer stem cell circuit. Cancer Res 75 (13), 2607–2618.

Li, F., Long, T., Lu, Y., Ouyang, Q., Tang, C., 2004a. The yeast cell-cycle network is robustly designed. Proc. Natl. Acad. Sci. USA 101 (14), 4781–4786.

Li, F., Long, T., Lu, Y., Ouyang, Q., Tang, C., 2004b. The yeast cell-cycle network is robustly designed. Proc. Natl. Acad. Sci. USA 101 (14), 4781–4786.

Li, S., Cai, C., Sun, C., 2015. Steady quantum coherence in non-equilibrium environment. Ann Phys-New York 360, 19–32.

Li, W., Wang, J., 2017. Uncovering the underlying mechanism of cancer tumorigenesis and development under an immune microenvironment from global quantification of the landscape. J. R. Soc. Interface 14, 20170105.

Linsmeier, I., Banerjee, S., Oakes, P., Jung, W., Kim, T., Murrell, M., 2016. Disordered actomyosin networks are sufficient to produce cooperative and telescopic contractility. Nature Communications 7, 12615.

Liphardt, J., Dumont, S., Smith, S., Tinoco, I., Bustamante, C., 2002. Equilibrium information from nonequilibrium measurements in an experimental test of jarzynski's equality. Science 296 (5574), 1832–1835.

Little, J., Michalowski, C., 2010. Stability and instability in the lysogenic state of phage lambda. J Bacteriol 192 (22), 6064–6076.

Liu, Q., Wang, J., 2018. Quantifying the detailed balance breaking flux as the origin of the non mechalis-menton kinetics. ArXiv, 1808.04013.

Liu, Z., Zhang, M., Guo, X., Tan, C., Li, J., Wang, L., Sancar, A., Zhong, D., 2013. Dynamic determination of the functional state in photolyase and the implication for cryptochrome. Proc. Natl. Acad. Sci. USA 110 (32), 12972–12977.

Lively, C., Craddock, C., Vrijenhoek, R., 1990. Red queen hypothesis supported by parasitism in sexual and clonal fish. Nature 344 (6269), 864.

Liverpool, T., Marchetti, M. C., 2003. Instabilities of isotropic solutions of active polar filaments. Phys. Rev. Lett. 90 (13), 138102.

Löber, J., Ziebert, F., Aranson, I. S., 2014. Modeling crawling cell movement on soft engineered substrates . Soft Matter 10 (9), 1365–1373.

Lobo, N., Shimono, Y., Qian, D., Clarke, M., 2007. The biology of cancer stem cells. Annu Rev Cell Dev Bi 23, 675–699.

Loose, M., Fischer-Friedrich, E., Herold, C., Kruse, K., Schwille, P., Apr. 2011a. Min protein patterns emerge from rapid rebinding and membrane interaction of MinE. Nat. Struct. Mol. Biol. 18 (5), 577–583.

Loose, M., Fischer-Friedrich, E., Ries, J., Kruse, K., Schwille, P., May 2008. Spatial regulators for bacterial cell division self-organize into surface waves in vitro. Science 320 (5877), 789–792.

Loose, M., Kruse, K., Schwille, P., Jun. 2011b. Protein self-organization: lessons from the min system. Annu Rev Biophys 40, 315–336.

Lotka, A., 1925. Elements of Physical Biology. Williams and Wilkins, Baltimore.

Low, S. H., Vasanji, A., Nanduri, J., He, M., Sharma, N., Koo, M., Drazba, J., Weimbs, T., Feb. 2006. Syntaxins 3 and 4 are concentrated in separate clusters on the plasma membrane before the establishment of cell polarity. Molecular Biology of the Cell 17 (2), 977–989.

Lu, M., Huang, B., Hanash, S., Onuchic, J., Ben-Jacob, E., 2014a. Modeling putative therapeutic implications of exosome exchange between tumor and immune cells. Proc.

Natl. Acad. Sci. USA 111 (40), E4165–E4174.

Lu, M., Jolly, M., Levine, H., Onuchic, J., Ben-Jacob, E., 2013. Microrna-based regulation of epithelial-hybrid-mesenchymal fate determination. Proc. Natl. Acad. Sci. USA 110, 18144–18149.

Lu, M., Jolly, M. K., Onuchic, J., Benjacob, E., 2014b. Toward decoding the principles of cancer metastasis circuits. Cancer Research 74 (17), 4574–4587.

Lu, T., Shen, T., Bennett, M. R., Wolynes, P., Hasty, J., 2007. Phenotypic variability of growing cellular populations. Proceedings of the National Academy of Sciences 104 (48), 18982–18987.

Luo, X.and Xu, L., Han, B., Wang, J., 2017. Funneled potential and flux landscapes dictate the stabilities of both the states and the flow: Fission yeast cell cycle. PLoS Comput Biol 13, e1005710.

Lushi, E., Wioland, H., Goldstein, R. E., 2014. Fluid flows created by swimming bacteria drive self-organization in confined suspensions. Proc Natl Acad Sci USA 111 (27), 9733–9738.

Lv, C., Li, X., Li, F., Li, T., 2014. Constructing the energy landscape for genetic switching system driven by intrinsic noise. PloS one 9 (2), e88167.

Lv, C., Li, X., Li, F., Li, T., 2015. Energy landscape reveals that the budding yeast cell cycle is a robust and adaptive multi-stage process. PLoS Comp. Biol. 11, e1004156.

Lyons, N., Kolter, R., 2015. On the evolution of bacterial multicellularity. Current opinion in microbiology 24, 21–28.

Maddock, J. R., Shapiro, L., Mar. 1993. Polar location of the chemoreceptor complex in the Escherichia coli cell. Science 259 (5102), 1717–1723.

Maier, R., Stein, D., 1997. Limiting exit location distributions in the stochastic exit problem. Siam J Appl Math 57 (3), 752–790.

Majumder, M., Chopra, N., Andrews, R., Hinds, B., 2005. Nanoscale hydrodynamics - enhanced flow in carbon nanotubes. Nature 438 (7064), 44–44.

Malawista, S. E., Van Blaricom, G., Jan. 1987. Cytoplasts made from human blood polymorphonuclear leukocytes with or without heat: preservation of both motile function and respiratory burst oxidase activity. Proc Natl Acad Sci USA 84 (2), 454–458.

Manzano, D., Tiersch, M., Asadian, A., Briegel, H., 2012. Quantum transport efficiency and fourier's law. Phys Rev E 86 (6), 061118.

Marchetti, M., Joanny, J., Ramaswamy, S., Liverpool, T., Prost, J., Rao, M., Simha, R., 2013a. Hydrodynamics of soft active matter. Rev Mod Phys 85 (3), 1143.

Marchetti, M. C., Joanny, J. F., Ramaswamy, S., Liverpool, T., Prost, J., Rao, M., Simha, R., 2013b. Hydrodynamics of soft active matter. Rev Mod Phys 85 (3), 1143.

Marcus, R., 1964. Chemical + electrochemical electron-transfer theory. Annu Rev Phys Chem 15, 155–196.

Margolis, R., Wilson, L., Jan. 1978. Opposite end assembly and disassembly of microtubules at steady state in vitro. Cell 13 (1), 1–8.

Marotta, L., Polyak, K., 2009. Cancer stem cells: a model in the making. Curr Opin Genet Dev 19 (1), 44–50.

Marshall, A., 1890. Principles of Economics. MacMillan,London.

Marston, A. L., Errington, J., Nov. 1999. Dynamic movement of the ParA-like Soj protein of B. subtilis and its dual role in nucleoid organization and developmental regulation. Mol Cell 4 (5), 673–682.

Marusyk, A., Almendro, V., Polyak, K., 2012. Intra-tumour heterogeneity: a looking glass for cancer? Nat. Rev. Cancer 12 (5), 323–334.

Marx, K., 1887. Capital I: The Process of Production of Capital. Publisher: Progress Publishers, Moscow, USSR.

Mascolell, A., 1986. The price equilibrium existence problem in topological vector lattices. Econometrica 54 (5), 1039–1053.

Matzke, R., Jacobson, K., Radmacher, M., Jun. 2001. Direct, high-resolution measurement of furrow stiffening during division of adherent cells. Nat Cell Biol 3 (6), 607–610.

Mayer, M., Depken, M., Bois, J. S., Jülicher, F., Grill, S. W., Sep. 2010. Anisotropies in cortical tension reveal the physical basis of polarizing cortical flows. Nature 467 (7315), 617–621.

Maynard, S., Price, G. R., 1973. The logic of animal conflict. Nature 246 (5427), 15–18.

Mazurek, M., Roitman, J., Ditterich, J., Shadlen, M., 2003. A role for neural integrators in perceptual decision making. Cereb Cortex 13 (11), 1257–1269.

McCandlish, S. R., Baskaran, A., Hagan, M., 2012. Spontaneous segregation of self-propelled particles with different motilities . Soft Matter 8 (8), 2527–2534.

Mccarley, R. W., Massaquoi, S. G., 1986. A limit cycle mathematical model of the rem sleep oscillator system. American Journal of Physiology 251 (2), 1011–1029.

Mehboudi, M., Sanpera, A., Parrondo, J. M. R., 2016. Fluctuation-dissipation theorem for non-equilibrium quantum systems. Epl 115 (2), 20004.

Melbinger, A., Reese, L., Frey, E., 2012. Microtubule Length Regulation by Molecular Motors. Phys. Rev. Lett. 108 (25), 258104.

Michaelis, L., Menten, M., 1913. Die kinetik der invertinwirkung. Biochem Z. 49, 333–369.

Miller, M., Bassler, B., 2001. Quorum sensing in bacteria. Annual Reviews in Microbiology 55 (1), 165–199.

Min, W., Gopich, I., English, B., Kou, S., Xie, X., Szabo, A., 2006a. When does the michaelis-menten equation hold for fluctuating enzymes? J. Phys. Chem. B 110 (41), 20093–20097.

Min, W., Gopich, I., English, B., Kou, S., Xie, X. S., Szabo, A., 2006b. When does the michaelis- menten equation hold for fluctuating enzymes? The Journal of Physical Chemistry B 110 (41), 20093–20097.

Minsky, H. P., 1977. The financial instability hypothesis: An interpretation of keynes and an alternative to "standard" theory. Challenge 20 (1), 20–27.

Mirabet, V., Das, P., Boudaoud, A., Hamant, O., 2011. The Role of Mechanical Forces in Plant Morphogenesis. Annu. Rev. Plant Biol. 62, 365–385.

Mitchison, T., Kirschner, M., 1984. Dynamic instability of microtubule growth. nature 312 (5991), 237–242.

Mogilner, A., Oster, G., Dec. 1996. Cell motility driven by actin polymerization. Biophys J 71 (6), 3030–3045.

Mohapatra, L., Goode, B., Jelenkovic, P., Phillips, R., Kondev, J., Jul. 2016. Design Principles of Length Control of Cytoskeletal Structures. Annu Rev Biophys 45 (1), 85–116.

Mohapatra, L., Goode, B., Kondev, J., Jun. 2015. Antenna Mechanism of Length Control of Actin Cables. PLoS Comput Biol 11 (6).

Morgan, D. O., 2007. Cell Cycle: Principles and Controls. OUP/New Science Press.

Morgan, J., Wolynes, P., 1987. Adiabaticity of electron-transfer at an electrode. J Phys Chem-Us 91 (4), 874–883.

Mueller, M., Klumpp, S., Lipowsky, R., 2008. Tug-of-war as a cooperative mechanism for bidirectional cargo transport by molecular motors. Proc Natl Acad Sci USA 105 (12), 4609–4614.

Mukamel, S., 1999. Principles of Nonlinear Optical Spectroscopy. Oxford University Press, New York.

Muñoz-Dorado, J., Marcos-Torres, F. J., García-Bravo, E., Moraleda-Muñoz, A., Pérez, J., 2016. Myxobacteria: moving, killing, feeding, and surviving together. Frontiers in Microbiology 7.

Murdoch, W., Oaten, A., 1975. Predation and population stability. Advan. EcoL. ReS. 9, 1–131.

Murray, J., 1998. Mathematical Biology. Springer-Verlag Berlin Heidelberg, New York.

Mustonen, V., Lassig, M., 2009. From fitness landscapes to seascapes: non-equilibrium dynamics of selection and adaptation. Trends Genet 25 (3), 111–119.

Mustonen, V., Lassig, M., 2010. Fitness flux and ubiquity of adaptive evolution. Proc. Natl. Acad. Sci. USA 107 (9), 4248–4251.

Naganathan, S. R., Fürthauer, S., Nishikawa, M., Jülicher, F., Grill, S. W., 2014. Active torque generation by the actomyosin cell cortex drives left-right symmetry breaking. Elife 3, e04165.

Nagumo, J., Arimoto, S., , Yoshizawa, S., 1962. An active pulse transmission line simulating nerve axon. Proc. IRE. 50, 2061–2070.

Nagylaki, T., 1993. The evolution of multilocus systems under weak selection. Genetics 134 (2), 627–647.

Nagylaki, T., Brunovsky, P., Hofbauer, J., 1999. Convergence of multilocus systems under weak epistasis or weak selection. J. Math. Biol. 38 (2), 103.

Nakajima, M., Imai, K., Ito, H., Nishiwaki, T., Murayama, Y., Iwasaki, H., Oyama, T., Kondo, T., 2005. Reconstitution of circadian oscillation of cyanobacterial kaic phosphorylation in vitro. Science 308 (5720), 414–415.

Nedelec, F., Foethke, D., 2007. Collective Langevin dynamics of flexible cytoskeletal fibers. New J Phys 9 (11).

Nedelec, F. J., Surrey, T., Maggs, A. C., Leibler, S., 1997. Self-organization of microtubules and motors. Nature 389 (6648), 305–308.

Neef, M., Kruse, K., 2014. Generation of stationary and moving vortices in active polar fluids in the planar Taylor-Couette geometry. Phys Rev E Stat Nonlin Soft Matter Phys 90 (5).

Neher, R., Shraiman, B., 2011. Statistical genetics and evolution of quantitative traits. Rev Mod Phys 83 (4), 1283.

Nevozhay, D., Adams, R., Murphy, K., Josic, K., Balazsi, G., 2009. Negative autoregulation linearizes the dose-response and suppresses the heterogeneity of gene expression. Proc. Natl. Acad. Sci. USA 106 (13), 5123–5128.

Nicolas, G., Prigogine, I., 1989. Exploring Complexity: An Introduction. New York: Freeman and Co.

Nicolis, G., Prigogine, I., 1977. Self-organization in nonequilibrium systems : from dissipative structures to order through fluctuations. Wiley, New York.

Nielsen, M. A., Chuang, I. L., 2000. Quantum Computation and Quantum Information. Cambridge University Press, New York.

Novelli, F., Nazir, A., Richards, G., Roozbeh, A., Wilk, K., Curmi, P., Davis, J., 2015. Vibronic resonances facilitate excited-state coherence in light-harvesting proteins at room temperature. J Phys Chem Lett 6 (22), 4573–4580.

Novk, B., Tyson, J. J., 2008. Design principles of biochemical oscillators. Nat Rev Mol Cell Biol 9 (12), 981–991.

Nowak, M., 2004. Evolutionary Dynamics. Cambridge, MA: Harvard University Press.

Oelz, D., Mogilner, A., 2016. Actomyosin contraction, aggregation and traveling waves in a treadmilling actin array. Physica D 318, 70–83.

Oelz, D., Rubinstein, B., Mogilner, A., Nov. 2015. A Combination of Actin Treadmilling and Cross-Linking Drives Contraction of Random Actomyosin Arrays. Biophys J 109 (9), 1818–1829.

Ohmine, I., Saito, S., 1999. Water dynamics: Fluctuation, relaxation, and chemical reactions in hydrogen bond network rearrangement. Accounts Chem Res 32 (9), 741–749.

Ohtani, H., Wilson, R., Chiang, S., Mate, C., 1988. Scanning tunneling microscopy observations of benzene molecules on the rh(111)-(3x3)(c6h6+2co)surface. Phys. Rev. Lett. 60 (23), 2398–2401.

Olender, R., Elber, R., 1996. Calculation of classical trajectories with a very large time step: Formalism and numerical examples. J. Chem. Phys. 105 (20), 9299–9315.

Onsager, L., 1931. Reciprocal relations in irreversible processes. i. Physical Review 38 (37), 405–426.

Onsager, L., Machlup, S., 1953. Fluctuations and irreversible processes. Phys Rev 91 (6), 1505–1512.

Onuchic, J., Wolynes, P., 1988. Classical and quantum pictures of reaction dynamics in condensed matter - resonances, dephasing, and all that. J Phys Chem-Us 92 (23), 6495–6503.

Oppenheim, A., Kobiler, O., Stavans, J., Court, D., Adhya, S., 2005. Switches in bacteriophage lambda development. Annu. Rev. Genet. 39, 409–429.

O'Reilly, E., Olaya-Castro, A., 2014. Non-classicality of the molecular vibrations assisting exciton energy transfer at room temperature. Nat Commun 5, 3012–3021.

Ozgen, V. C., Kong, W., Blanchard, A. E., Liu, F., Lu, T., 2018. Spatial interference scale as a determinant of microbial range expansion. Sci. Adv. 4 (11), eaau0695.

Paijmans, J., Lubensky, D. K., Ten Wolde, P. R., 2016. A thermodynamically consistent model of the post-translational kai circadian clock. Plos Computational Biology 13 (3), e1005415.

Paijmans, J., Lubensky, D. K., Ten Wolde, P. R., 2017. Period robustness and entrainability of the kai system to changing nucleotide concentrations. Biophysical Journal 113 (1), 157–173.

Palma, G., Suominen, K., Ekert, A., 1996. Quantum computers and dissipation. P Roy Soc a-Math Phy 452 (1946), 567–584.

Paluch, E., Piel, M., Prost, J., Bornens, M., Sykes, C., Jul. 2005. Cortical Actomyosin Breakage Triggers Shape Oscillations in Cells and Cell Fragments. Biophys J 89 (1), 724–733.

Panda, D., Miller, H. P., Wilson, L., Oct. 1999. Rapid treadmilling of brain microtubules free of microtubule-associated proteins in vitro and its suppression by tau. Proc Natl Acad Sci USA 96 (22), 12459–12464.

Pappalardo, F., Pennisi, M., Ricupito, A., Topputo, F., Bellone, M., 2014. Induction of t-cell memory by a dendritic cell vaccine: a computational model. Bioinformatics 30 (13), 1884–1891.

Park, H., Park, J., Lim, A., Anderson, E., Alivisatos, A., McEuen, P., 2000. Nanomechanical oscillations in a single-

c-60 transistor. Nature 407 (6800), 57–60.
Parmeggiani, A., Franosch, T., Frey, E., 2003. Phase coexistence in driven one-dimensional transport. Phys. Rev. Lett. 90 (8).
Pesen, D., Hoh, J., Jan. 2005. Micromechanical Architecture of the Endothelial Cell Cortex. Biophys J 88 (1), 670–679.
Peskin, M. E., Schroeder, D. V., 1995. An Introduction to Quantum Field Theory. Addison-Wesley, Reading, MA.
Peter, R., Schaller, V., Ziebert, F., Zimmermann, W., 2008. Pattern formation in active cytoskeletal networks. New J Phys 10 (3).
Petrášek, Z., Schwille, P., Apr. 2015. Simple membrane-based model of the Min oscillator. New J Phys 17 (4), 1–14.
Pigliucci, M., 2008. Sewall Wright's adaptive landscapes: 1932 vs. 1988. Biol. Philos. 23, 591–603.
Pike, L., Jul. 2006. Rafts defined: a report on the Keystone Symposium on Lipid Rafts and Cell Function. Journal of Lipid Research 47 (7), 1597–1598.
Pinkoviezky, I., Gov, N., 2017. Exclusion and Hierarchy of Time Scales Lead to Spatial Segregation of Molecular Motors in Cellular Protrusions. Phys. Rev. Lett. 118 (1).
Piraino, S., Boero, F., Aeschbach, B., Schmid, V., 1996. Reversing the life cycle: Medusae transforming into polyps and cell transdifferentiation in turritopsis nutricula (cnidaria, hydrozoa). Biol Bull 190 (3), 302–312.
Pismen, L. M., 2013. Dynamics of defects in an active nematic layer. Phys Rev E 88 (5), 050502.
Plenio, M., Almeida, J., Huelga, S., 2013. Origin of long-lived oscillations in 2d-spectra of a quantum vibronic model: Electronic versus vibrational coherence. J. Chem. Phys. 139 (23), 235102–235111.
Pogliano, J., Ho, T., Zhong, Z., Helinski, D., 2001. Multicopy plasmids are clustered and localized in escherichia coli. Proc. Natl. Acad. Sci. USA 98 (8), 4486–4491.
Polettini, M., 2012. Nonequilibrium thermodynamics as a gauge theory. Europhysics Letters 97 (3), 30003.
Preskill, J., 1998. Quantum Information and Quantum Computation. Califoinia Institute of Technology Press.
Press, S., Ghosh, K., Lee, J., Dill, K., 2013. Principles of maximum entropy and maximum caliber in statitistical physics. Rev. Mod. Phys. 85 (3), 1115–1141.
Price, G., 1972a. Fisher's "fundamental theorem" made clear. Annals of Human Genetics 36 (2), 129–140.
Price, G. R., 1970. Selection and covariance. Nature 227 (5257), 520–521.
Price, G. R., 1972b. Extension of covariance selection mathematics. Annals of Human Genetics 35 (4), 485–490.
Prigogine, I., Stengers, I., 1984. Order Out of Chaos. New Sci. Lib. Shambhala Pub., Boulder, CO.
Prindle, A., Samayoa, P., Razinkov, I., Danino, T., Tsimring, L., Hasty, J., 2012. A sensing array of radically coupled genetic/biopixels/'. Nature 481 (7379), 39–44.
Prior, I., Muncke, C., Parton, R., Hancock, J., Jan. 2003. Direct visualization of Ras proteins in spatially distinct cell surface microdomains. J. Cell Biol. 160 (2), 165–170.
Prost, J., 2002. The Physics of Listeria Propulsion. In: Flyvbjerg, H., Jülicher, F., Ormos, P., David, F. (Eds.), Physics of Bio-molecules and Cells, Les Houches Session LXXV, 2-27 July 2001. Springer.
Prost, J., Joanny, J.-F., Parrondo, J. M. R., 2009. Generalized fluctuation-dissipation theorem for steady-state systems. Phys. Rev. Lett. 103, 090601.
Ptashne, M., 2004a. Genetic Switch: Phage Lambda. Cold Spring Harbor Laboratory Press.
Ptashne, M., 2004b. A genetic switch: phage lambda revisited. Vol. 3. Cold Spring Harbor Laboratory Press Cold Spring Harbor, NY:.
Qi, H., Blanchard, A., Lu, T., 2013. Engineered genetic information processing circuits. Wiley Interdisciplinary Reviews: Systems Biology and Medicine 5 (3), 273–287.
Qian, H., 2007. Phosphorylation energy hypothesis: Open chemical systems and their biological functions. Annu Rev Phys Chem 58, 113–142.
Qian, H., 2009. Entropy demystified the "thermo"-dynamics of stochastically fluctuating systems. Method. Enzymol. 467, 111.
Qian, H., 2014. The zeroth law of thermodynamics and volume-preserving conservative system in equilibrium with stochastic damping. Phys Lett A 378 (7-8), 609–616.
Qian, H., Ao, P., Tu, Y., Wang, J., 2016. A framework towards understanding mesoscopic phenomena: Emergent unpredictability, symmetry breaking and dynamics across scales. Chem Phys Lett 665, 153–161.
Qian, H., Elson, E., 2002. Single-molecule enzymology: stochastic michaeliscmenten kinetics. Biophys. Chem. 101-102, 565C576.
Qian, M., Hou, Z. T., 1979. Reversible Markov Process. Hunan Scientific Publisher, Changsha.
Quiroga, L., Rodriguez, F. J., Ramirez, M. E., Paris, R., 2007. Nonequilibrium thermal entanglement. Phys. Rev. A. 75, 032308.
Quisel, J. D., Lin, D. C., Grossman, A. D., Nov. 1999. Control of development by altered localization of a transcription factor in B. subtilis. Mol Cell 4 (5), 665–672.
Radszuweit, M., Alonso, S., Engel, H., Bär, M., Mar. 2013. Intracellular mechanochemical waves in an active poroelastic model. Phys. Rev. Lett. 110 (13), 138102.
Ramis-Conde, I., Chaplain, M. A. J., Anderson, A. R. A., Drasdo, D., 2009. Multi-scale modelling of cancer cell intravasation: the role of cadherins in metastasis. Phys. Biol. 6, 016008.
Ramos, J., Martinez-Bueno, M., Molina-Henares, A., Teran, W., Watanabe, K., Zhang, X., Gallegos, M., Brennan, R., Tobes, R., 2005. The tetr family of transcriptional repressors. Microbiol Mol Biol R 69 (2), 326–356.
Raskin, D., de Boer, P., 1999a. Rapid pole-to-pole oscillation of a protein required for directing division to the middle of escherichia coli. Proceedings of the National Academy of Sciences 96 (9), 4971–4976.
Raskin, D. M., de Boer, P. A. J., Apr. 1999b. Rapid pole-to-pole oscillation of a protein required for directing division to the middle of Escherichia coli. Proc Natl Acad Sci USA 96 (9), 4971–4976.
Reber, S. B., Baumgart, J., Widlund, P. O., Pozniakovsky, A., Howard, J., Hyman, A. A., Jülicher, F., 2013. XMAP215 activity sets spindle length by controlling the total mass of spindle microtubules. Nat Cell Biol 15 (9), 1116–1122.
Recho, P., Putelat, T., Truskinovsky, L., 2013. Contraction-Driven Cell Motility. Phys. Rev. Lett. 111 (10), 108102.
Recho, P., Truskinovsky, L., Feb. 2013. Asymmetry between pushing and pulling for crawling cells. Phys Rev E Stat Nonlin Soft Matter Phys 87 (2), 022720–19.
Reed, M., Zhou, C., Muller, C., Burgin, T., Tour, J., 1997. Conductance of a molecular junction. Science 278 (5336), 252–254.
Reese, L., Melbinger, A., Frey, E., Nov. 2011. Crowding of molecular motors determines microtubule depolymerization. Biophys J 101 (9), 2190–2200.

Reichenbach, T., Frey, E., 2008. Instability of spatial patterns and its ambiguous impact on species diversity. Phys. Rev. Lett. 101 (5), 058102.

Reichenbach, T., Mobilia, M., Frey, E., 2007. Noise and correlations in a spatial population model with cyclic competition. Phys. Rev. Lett. 99 (23), 238105.

Resulaj, A., Kiani, R., Wolpert, D., Shadlen, M., 2009. Changes of mind in decision-making. Nature 461 (7261), 263.

Reymann, A., Staniscia, F., Erzberger, A., Salbreux, G., Grill, S., 2016. Cortical flow aligns actin filaments to form a furrow. Elife 5.

Rice, S., 2004. Evolutionary theory : mathematical and conceptual foundations. Sinauer Associates, Massachusetts.

Richardson, L. F., 1922. Weather Prediction by Numerical Process. Cambridge: Cambridge University Press.

Rishal, I., Kam, N., Perry, R. B., Shinder, V., Fisher, E. C., Schiavo, G., Fainzilber, M., Jun. 2012. A motor-driven mechanism for cell-length sensing. Cell Rep 1 (6), 608–616.

Risken, H., 1989. The Fokker-Planck Equation: Methods of Solution and Applications. Berlin, Heidelberg: Springer-Verlag.

Riveline, D., Ott, A., Jülicher, F., Winkelmann, D. A., Cardoso, O., Lacapere, J. J., Magnusdottir, S., Viovy, J. L., Gorre-Talini, L., Prost, J., 1998. Acting on actin: the electric motility assay. European biophysics journal : EBJ 27 (4), 403–408.

Roberts, E., Magis, A., Ortiz, J., Baumeister, W., Luthey-Schulten, Z., 2011. Noise contributions in an inducible genetic switch: a whole-cell simulation study. Plos Comp. Biol. 7, e1002010.

Roitman, J., Shadlen, M., 2002. Response of neurons in the lateral intraparietal area during a combined visual discrimination reaction time task. J Neurosci 22 (21), 9475–9489.

Roma, D., O'Flanagan, R., Ruckenstein, A., Sengupta, A., Mukhopadhyay, R., 2005. Optimal path to epigenetic switching. Phys Rev E 71 (1), 011902.

Romero, E., Augulis, R., Novoderezhkin, V., Ferretti, M., Thieme, J., Zigmantas, D., van Grondelle, R., 2014. Quantum coherence in photosynthesis for efficient solar-energy conversion. Nat Phys 10 (9), 677–683.

Rose, H., Sulem, P., 1978. Fully developed turbulence and statistical-mechanics. J Phys-Paris 39 (5), 441–484.

Rust, M., Markson, J. S., Lane, W. S., Fisher, D., O'shea, E., 2007. Ordered phosphorylation governs oscillation of a three-protein circadian clock. Science 318 (5851), 809–812.

Ryan, G. L., Petroccia, H. M., Watanabe, N., Vavylonis, D., 2012. Excitable Actin Dynamics in Lamellipodial Protrusion and Retraction. Biophys J 102 (7), 1493–1502.

Rzadzinska, A. K., Schneider, M. E., Davies, C., Riordan, G., Kachar, B., Mar. 2004. An actin molecular treadmill and myosins maintain stereocilia functional architecture and self-renewal. J Cell Biol 164 (6), 887–897.

S., U., 2012. Stochastic thermodynamics, fluctuation theorems and molecular machines. Reports on progress in physics 75 (12), 126001.

Sabado, R., Bhardwaj, N., 2015. Cancer immunotherapy dendritic-cell vaccines on the move. Nature 519 (7543), 300–301.

Sagawa, T., 2013. Thermodynamics of Information Processing in Small Systems. Springer Pub. Japan.

Saha, A., Nishikawa, M., Behrndt, M., Heisenberg, C., Jülicher, F., Grill, S., Mar. 2016. Determining Physical Properties of the Cell Cortex. Biophys J 110 (6), 1421–1429.

Salbreux, G., Joanny, J. F., Prost, J., Pullarkat, P., Dec. 2007. Shape oscillations of non-adhering fibroblast cells. Physical Biology 4 (4), 268–284.

Salbreux, G., Prost, J., Joanny, J. F., Jul. 2009. Hydrodynamics of cellular cortical flows and the formation of contractile rings. Phys. Rev. Lett. 103 (5), 058102.

Samuelson, A., Carr, C., Ruvkun, G., 2007. Gene activities that mediate increased life span of c. elegans insulin-like signaling mutants. Gene Dev 21 (22), 2976–2994.

Sanchez, T., Chen, D. N., DeCamp, S., Heymann, M., Dogic, Z., 2012. Spontaneous motion in hierarchically assembled active matter. Nature 491 (7424), 431–434.

Sanchez, T., Welch, D., Nicastro, D., Dogic, Z., Jul. 2011. Cilia-like beating of active microtubule bundles. Science (New York, N.Y.) 333 (6041), 456–459.

Sandholm, W., 2009. Evolutionary Game Theory in Encyclopedia of Complexity and System Science. New York: Springer.

Sasai, M., Kawabata, Y., Makishi, K., Itoh, K., Terada, T., 2013. Time scales in epigenetic dynamics and phenotypic heterogeneity of embryonic stem cells. Plos. Comp. Biol. 9, e1003380.

Sasai, M., Wolynes, P. G., 2003. Stochastic gene expression as a many-body problem. P Natl Acad Sci USA 100 (5), 2374–9.

Sato, K., Kuramoto, Y., Ohtaki, M., Shimamoto, Y., Ishiwata, S., 2013. Locally and globally coupled oscillators in muscle. Phys. Rev. Lett. 111 (10), 108104.

Schaller, V., Weber, C., Semmrich, C., Frey, E., Bausch, A., 2010. Polar patterns of driven filaments. Nature 467 (7311), 73–77.

Schliep, A., Schonhuth, A., Steinhoff, C., 2003. Using hidden markov models to analyze gene expression time course data. Bioinformatics 19, i255–i263.

Schnakenberg, J., 1976. Network theory of microscopic and macroscopic behavior of master equation systems. Rev. Mod. Phys. 48 (4), 571–585.

Schreiber, C., Stewart, M.and Duke, T., 2010. Simulation of cell motility that reproduces the force-velocity relationship. Proc Natl Acad Sci USA 107 (20), 9141–9146.

Schrodinger, E., 1944. What is Life. Cambridge University Press, Cambridge.

Schuler, S., Speck, T., Tietz, C., Wrachtrup, J., Seifert, U., 2005. Experimental test of the fluctuation theorem for a driven two-level system with time-dependent rates. Phys. Rev. Lett. 94, 180602.

Schultz, D., Jacob, E. B., Onuchic, J., Wolynes, P., 2007a. Molecular level stochastic model for competence cycles in bacillus subtilis. Proceedings of the National Academy of Sciences 104 (45), 17582–17587.

Schultz, D., Onuchic, J., Wolynes, P., 2007b. Understanding stochastic simulations of the smallest genetic networks. J. Chem. Phys. 126 (24), 245102.

Schumpeter, J. A., 1934. The Theory of Economic Development: An inquiry into profits, capital,credit, interest and the business cycle. Cambridge,MA: Harvard University Press.

Schuppler, M., Keber, F., Kröger, M., Bausch, A., Oct. 2016. Boundaries steer the contraction of active gels. Nature Communications 7, 13120.

Schuss, Z., 2010. Theory and Applications of Stochastic Processes. Sprnger-Verlag, New York.

Schütz, G., Domany, E., Jul. 1993. Phase-Transitions in an Exactly Soluble One-Dimensional Exclusion Process. J Stat Phys 72 (1-2), 277–296.

Schwarz, U. S., Safran, S. A., 2013. Physics of adherent cells. Rev Mod Phys 85 (3), 1327–1381.

Schweizer, J., Loose, M., Bonny, M., Kruse, K., Mönch, I., Schwille, P., Sep. 2012. Geometry sensing by self-organized protein patterns. Proc. Natl. Acad. Sci. USA 109 (38), 15283–15288.

Scully, M. O., Zubairy, M. S., 1997a. Quantum Optics. Cambridge University Press, Cambridge.

Scully, M. O., Zubairy, M. S., 1997b. Quantum Optics. Cambridge University Press.

Sedzinski, J., Biro, M., Oswald, A., Tinevez, J., Salbreux, G., Paluch, E., Aug. 2011. Polar actomyosin contractility destabilizes the position of the cytokinetic furrow. Nature 476 (7361), 462–466.

Seifert, U., 2005. Entropy production along a stochastic trajectory and an integral fluctuation theorem. Phys. Rev. Lett. 95 (4), 040602.

Seifert, U., 2008. Stochastic thermodynamics: principles and perspectives. Eur Phys J B 64 (3-4), 423–431.

Seifert, U., Speck, T., 2010. Fluctuation-dissipation theorem in nonequilibrium steady states. Euro. Phys. Lett. 89, 10007.

Seul, M., Andelman, D., 1995. Domain Shapes and Patterns - the Phenomenology of Modulated Phases. Science 267 (5197), 476–483.

Shackleton, M., Quintana, E., Fearon, E., Morrison, S., 2009. Heterogeneity in cancer: Cancer stem cells versus clonal evolution. Cell 138 (5), 822–829.

Shadlen, M., Newsome, W., 1996. Motion perception: Seeing and deciding. Proc. Natl. Acad. Sci. USA 93 (2), 628–633.

Shadlen, M., Newsome, W., 2001. Neural basis of a perceptual decision in the parietal cortex (area lip) of the rhesus monkey. J Neurophysiol 86 (4), 1916–1936.

Shao, D., Levine, H., Rappel, W., May 2012. Coupling actin flow, adhesion, and morphology in a computational cell motility model. Proc. Natl. Acad. Sci. USA 109 (18), 6851–6856.

Shao, D., Rappel, W., Levine, H., Sep. 2010. Computational model for cell morphodynamics. Phys. Rev. Lett. 105 (10), 108104.

Shih, H., Hsieh, T., Goldenfeld, N., 2016. Ecological collapse and the emergence of travelling waves at the onset of shear turbulence. Nature Physics 12, 246–248.

Shishir, R., Chen, F., Xia, J., Tao, N., Ferry, D., 2009. Theory and measurements of room temperature transport in graphene using sio2 backgate and electrochemical gate. J Vac Sci Technol B 27 (4), 2003–2007.

Shlomovitz, R., Gov, N. S., 2007. Membrane waves driven by actin and myosin. Phys. Rev. Lett. 98 (16), 168103.

Shou, W., Ram, S., Vilar, J., 2007. Synthetic cooperation in engineered yeast populations. Proc. Natl. Acad. Sci.USA 104 (6), 1877–1882.

Shyer, A. E., Rodrigues, A. R., Schroeder, G. G., Kassianidou, E., Kumar, S., Harland, R. M., 2017. Emergent cellular self-organization and mechanosensation initiate follicle pattern in the avian skin. Science 356, 811–815.

Sieber, J. J., Willig, K. I., Kutzner, C., Gerding-Reimers, C., Harke, B., Donnert, G., Rammner, B., Eggeling, C., Hell, S. W., Grubmuller, H., Lang, T., Aug. 2007. Anatomy and Dynamics of a Supramolecular Membrane Protein Cluster. Science (New York, N.Y.) 317 (5841), 1072–1076.

Silverman, M., Simon, M., 1974. Flagellar rotation and the mechanism of bacterial motility. Nature 249, 73–74.

Sinaysky, I., Petruccione, F., Burgarth, D., 2008. Dynamics of nonequilibrium thermal entanglement. Phys. Rev. A. 78, 062301.

Sloane, N. J. A., Wyner, A. D., 1993. Claude Elwood Shannon Collected Papers. Wiley-intersci, A John WILEY and SONS, INC., Publication.

Smith, D., Ziebert, F., Humphrey, D., Duggan, C., Steinbeck, M., Zimmermann, W., Kaes, J., 2007. Molecular motor-induced instabilities and cross linkers determine biopolymer organization. Biophys J 93 (12), 4445–4452.

Soree, B., Magnus, W., Schoenmaker, W., 2002. Energy and momentum balance equations: An approach to quantum transport in closed circuits. Phys Rev B 66 (3).

Spohn, H., 1980. Kinetic-equations from hamiltonian-dynamics - markovian limits. Rev Mod Phys 52 (3), 569–615.

Stewman, S., Ma, A., 2018. A structural mechano-chemical model for dynamic instability of microtubule. Biorxiv, 291682.

Stricker, J., Cookson, S., Bennett, M.R .and Mather, W., Tsimring, L., Hasty, J., 2008. A fast, robust and tunable synthetic gene oscillator. Nature 456 (7221), 516–519.

Süel, G. M., Garcia-Ojalvo, J., Liberman, L. M., Elowitz, M., 2006. An excitable gene regulatory circuit induces transient cellular differentiation. Nature 440 (7083), 545–550.

Süel, G. M., Kulkarni, R. P., Dworkin, J., Garcia-Ojalvo, J., Elowitz, M. B., 2007. Tunability and noise dependence in differentiation dynamics. Science 315 (5819), 1716–1719.

Sun, S. X., Jiang, H., 2011. Physics of Bacterial Morphogenesis. Microbiol. Mol. Biol. Rev. 75, 543–565.

Surrey, T., Nedelec, F., Leibler, S., Karsenti, E., 2001. Physical properties determining self-organization of motors and microtubules. Science 292 (5519), 1167–1171.

Sveiczer, A. L., Tyson, J. J., Novak, B., 2004. Modelling the fission yeast cell cycle. Brief Funct Genomic Proteomic 2 (4), 298–307.

Svirezhev, Y., Passekov, V., 1990. Fundamentals of mathematical evolutionary genetics. Kluwer Academic Publishers, Massachusetts.

Swain, P., Elowitz, M., Siggia, E., 2002. Intrinsic and extrinsic contributions to stochasticity in gene expression. Proc. Natl. Acad. Sci. USA 99 (20), 12795–12800.

Szent-Györgyi, A., 1951. Chemistry of muscular contraction, 2nd Edition. Academic Press, New York.

Takahashi, K., Yamanaka, S., 2006a. Induction of pluripotent stem cells from mouse embryonic and adult fibroblast cultures by defined factors. cell 126 (4), 663–676.

Takahashi, K., Yamanaka, S., 2006b. Induction of pluripotent stem cells from mouse embryonic and adult fibroblast cultures by defined factors. Cell 126 (4), 663–676.

Tanimura, Y., 2006. Stochastic liouville, langevin, fokker-planck, and master equation approaches to quantum dissipative systems. Journal of the Physical Society of Japan 75 (8), 082001.

Tanimura, Y., Wolynes, P., 1992. The interplay of tunneling, resonance, and dissipation in quantum barrier crossing - a numerical study. J. Chem. Phys. 96 (11), 8485–8496.

Thampi, S. P., Golestanian, R., Yeomans, J. M., 2013. Velocity Correlations in an Active Nematic. Phys. Rev. Lett. 111 (11), 118101.

Thompson, W., 1941. On Growth and Form: The Complete Revised Edition. Dover Publications Inc., New York.

Thoresen, T., Lenz, M., Gardel, M. L., Jun. 2011. Reconstitution of Contractile Actomyosin Bundles. Biophys J 100 (11), 2698–2705.

Tian, T., Harding, A., Inder, K., Plowman, S., Parton, R. G., Hancock, J. F., Aug. 2007. Plasma membrane nanoswitches generate high-fidelity Ras signal transduction. Nat Cell Biol 9 (8), 905–U60.

Tian, X., Zhang, H., Xing, J., 2013. Coupled reversible and irreversible bistable switches underlying tgfb-induced epithelial to mesenchymal transition. Biophys. J. 105, 1079–1089.

Tiwari, V., Peters, W., Jonas, D., 2013. Electronic resonance with anticorrelated pigment vibrations drives photosynthetic energy transfer outside the adiabatic framework. Proc. Natl. Acad. Sci. USA 110 (4), 1203–1208.

Tjhung, E., Marenduzzo, D., Cates, M. E., Jul. 2012. Spontaneous symmetry breaking in active droplets provides a generic route to motility. Proc. Natl. Acad. Sci. USA 109 (31), 12381–12386.

Tokuda, N., Terada, T., Sasai, M., 2012. Dynamical modeling of three-dimensional genome organization in interphase budding yeast. Biophys J. 102, 296.

Tomita, J., Nakajima, M., Kondo, T., Iwasaki, H., 2005. No transcription-translation feedback in circadian rhythm of kaic phosphorylation. Science 307 (5707), 251–254.

Torres, P. G., Doubrovinski, K., Kruse, K., 2010. Filament turnover stabilizes contractile cytoskeletal structures. Epl-Europhys Lett 91 (6), –.

Touboul, J., Staver, A. C., Levin, S., 2018a. On the complex dynamics of savanna landscapes. Proceedings of the National Academy of Sciences 115 (7), E1336–E1345.

Touboul, J. D., Staver, A. C., Levin, S. A., 2018b. On the complex dynamics of savanna landscapes. Proc. Natl. Acad. Sci.USA 115 (7), E1336–E1345.

Tsai, T., Theriot, J., Ferrell, J., 2014. Changes in oscillatory dynamics in the cell cycle of early xenopus laevis embryos. PLoS biology 12 (2), e1001788.

Turing, A. M., Aug. 1952. The Chemical Basis of Morphogenesis. Philos T Roy Soc B 237 (641), 37–72.

Turlier, H., Audoly, B., Prost, J., Joanny, J. F., 2014. Furrow Constriction in Animal Cell Cytokinesis. Biophys J 106 (1), 114–123.

Turner, M., Sens, P., Socci, N. D., Oct. 2005. Nonequilibrium Raftlike Membrane Domains under Continuous Recycling. Phys. Rev. Lett. 95 (16), 168301–4.

Uhles, S., Moede, T., Leibiger, B., Berggren, P., Leibiger, I., Dec. 2003. Isoform-specific insulin receptor signaling involves different plasma membrane domains. J. Cell Biol. 163 (6), 1327–1337.

Unruh, W., 1995. Maintaining coherence in quantum computers. Phys Rev A 51 (2), 992–997.

Van, D., Esposito, M., 2010. Three faces of the second law. ii. fokker-planck formulation. Phys. Rev. E 82 (1), 011144.

Van Kampen, N., 2007. Stochastic Processes in Physics and Chemistry. Elsevier, Amsterdam.

Van Valen, L., 1973a. A new evolutionary law. Evol. Theory 1, 1–30.

Van Valen, L., 1973b. A new evolutionary law. Evolutionary Theory 1 (1), 1–30.

van Zon, J. S., Lubensky, D. K., Altena, P. R., ten Wolde, P. R., 2007. An allosteric model of circadian kaic phosphorylation. Proceedings of the National Academy of Sciences of the United States of America 104 (18), 7420–7425.

Vandermeer, J., Goldberg, D., 2003. Population ecology: First principles. Princeton University Press, Woodstock, Oxfordshire.

Varga, V., Helenius, J., Tanaka, K., Hyman, A. A., Tanaka, T. U., Howard, J., 2006. Yeast kinesin-8 depolymerizes microtubules in a length-dependent manner. Nat Cell Biol 8 (9), 957–962.

Varga, V., Leduc, C., Bormuth, V., Diez, S., Howard, J., 2009. Kinesin-8 Motors Act Cooperatively to Mediate Length-Dependent Microtubule Depolymerization. Cell 138 (6), 1174–1183.

Veatch, S. L., Keller, S. L., 2003. Separation of liquid phases in giant vesicles of ternary mixtures of phospholipids and cholesterol. Biophys J 85 (5), 3074–3083.

Vermeij, G., 1994. The evolutionary interaction among species: selection, escalation, and coevolution. Annual Review of Ecology and Systematics 25 (1), 219–236.

Vicker, M., 2000. Reaction-diffusion waves of actin filament polymerization/depolymerization in Dictyostelium pseudopodium extension and cell locomotion. Biophys Chem 84 (2), 87–98.

Voituriez, R., Joanny, J. F., Prost, J., Jan. 2007. Spontaneous flow transition in active polar gels. EPL (Europhysics Letters) 70 (3), 404–410.

Volterra, V., 1927. Variazioni e fluttuazioni del numero d'individui in specie animali conviventi. C. Ferrari.

Volterra, V., 1931. Lecons sur la Theorie Mathematique de la Lutte pour la Vie. Gauthier- Villars, Paris.

Waddington, C. H., 1957. The Strategy of the Genes. London Pub.

Walczak, A., Onuchic, J., Wolynes, P., 2005. Absolute rate theories of epigenetic stability. Proc. Natl. Acad. Sci. USA 102 (52), 18926–18931.

Walras, L., 1874. Elements of Economic Politique Pure, 1st Edition, Lausanne:F. Rouge; English translation, William Jaffe, 1954, Elements of Pure Economics. London: Allen and Unwin.

Walsh, J., Angstmann, C., Duggin, I., Curmi, P., May 2015. Molecular Interactions of the Min Protein System Reproduce Spatiotemporal Patterning in Growing and Dividing Escherichia coli Cells. PLoS ONE 10 (5), e0128148.

Wang, E., Lenferink, A., Connor-McCourt, M., 2007. Cancer systems biology: exploring cancer-associated genes on cellular networks. Cell Mol Life Sci 64 (14), 1752–1762.

Wang, J., 2015. Landscape and flux theory of non-equilibrium dynamical systems with application to biology. Adv Phys 64 (1), 1–137.

Wang, J., Huang, B., Xia, X., Sun, Z., 2006a. Funneled landscape leads to robustness of cell networks: Yeast cell cycle. PLoS Comput. Biol. 2 (11), 1385–1394.

Wang, J., Li, C., Wang, E., 2010a. Potential and flux landscapes quantify the stability and robustness of budding yeast cell cycle network. Proc. Natl. Acad. Sci. USA. 107 (18), 8195–8200.

Wang, J., Xu, L., Wang, E., 2008. Potential landscape and flux framework of nonequilibrium networks: Robustness, dissipation, and coherence of biochemical oscillations. P Natl Acad Sci USA 105 (34), 12271–12276.

Wang, J., Xu, L., Wang, E., 2009. Robustness and coherence of a three-protein circadian oscillator: landscape and flux perspectives. Biophysical journal 97 (11), 3038–3046.

Wang, J., Xu, L., Wang, E., Huang, S., 2010b. The potential landscape of genetic circuits imposes the arrow of time in stem cell differentiation. Biophys. J. 99 (1), 29–39.

Wang, J., Zhang, K., Lu, H., Wang, E., 2005. Quantifying kinetic paths of protein folding. Biophys. J. 89 (3), 1612–1620.

Wang, J., Zhang, K., Lu, H., Wang, E., 2006b. Dominant kinetic paths on biomolecular binding-folding energy landscape. Phys. Rev. Lett. 96 (16), 168101.

Wang, J., Zhang, K., Lu, H., Wang, E., 2006c. Quantifying the kinetic paths of flexible biomolecular recognition. Biophys. J. 91 (3), 866–872.

Wang, J., Zhang, K., Wang, E., 2010c. Kinetic paths, time scale, and underlying landscapes: A path integral framework to study global natures of nonequilibrium systems and networks. J. Chem. Phys. 133 (12), 125103.

Wang, J., Zhang, K., Xu, L., Wang, E., 2011. Quantifying the waddington landscape and biological paths for development and differentiation. Proc. Natl. Acad. Sci. USA. 108 (20), 8257–8262.

Wang, S., Wolynes, P. G., 2011. On the spontaneous collective motion of active matter. Proceedings of the National Academy of Sciences of the United States of America 108 (37), 15184–15189.

Wang, Z., Wu, W., Wang, J., 2018. Steady-state entanglement and coherence of the coupled qubit system in equilibrium and nonequilibrium environments. arXiv:, 1812.04799.

Ward, D., Halas, N., Ciszek, J., Tour, J., Wu, Y., Nordlander, P., Natelson, D., 2008. Simultaneous measurements of electronic conduction and raman response in molecular junctions. Nano Lett 8 (3), 919–924.

Waterman-Storer, C. M., Salmon, E. D., Jun. 1997. Microtubule dynamics: treadmilling comes around again. Curr Biol 7 (6), R369–72.

Wegner, A., 1976. Head to Tail Polymerization of Actin. J Mol Biol 108 (1), 139–150.

Weichsel, J., Schwarz, U. S., Apr. 2010. Two competing orientation patterns explain experimentally observed anomalies in growing actin networks. Proc. Natl. Acad. Sci. USA 107 (14), 6304–6309.

Weinberg, R., 2007. The Biology of Cancer. Garland Science.

Weiner, O., Marganski, W. A., Wu, L. F., Altschuler, S., Kirschner, M., Sep. 2007. An actin-based wave generator organizes cell motility. Plos Biol 5 (9), e221.

Weiss, U., 2012a. Quantum Dissipative Systems. World Scientific, Singapore.

Weiss, U., 2012b. Quantum Dissipative Systems. World Scientific Publishing Company.

Welter, M., Bartha, K., Rieger, H., 2009. Vascular remodelling of an arterio-venous blood vessel network during solid tumour growth. J. Theor. Biol. 259, 405–422.

Welter, M., Rieger, H., 2013. Interstitial Fluid Flow and Drug Delivery in Vascularized Tumors: A Computational Model. PLoS ONE 8, e70395.

Wensink, H., Dunkel, J., Heidenreich, S., Drescher, K., Goldstein, R., Löwen, H., Yeomans, J., Sep. 2012. Meso-scale turbulence in living fluids. Proc. Natl. Acad. Sci. USA 109 (36), 14308–14313.

Werlang, T., Marchiori, M., Cornelio, M., Valente, D., 2014. Optimal rectification in the ultrastrong coupling regime. Phys. Rev. E. 89, 062109.

Wettmann, L., Bonny, M., Kruse, K., 2014. Effects of molecular noise on bistable protein distributions in rod-shaped bacteria. Interface Focus 4 (6), 20140039–20140039.

Whitelam, S., Bretschneider, T., Burroughs, N. J., May 2009. Transformation from Spots to Waves in a Model of Actin Pattern Formation. Phys. Rev. Lett. 102 (19), 198103.

Whitfield, C. A., Marenduzzo, D., Voituriez, R., Hawkins, R. J., 2014. Active polar fluid flow in finite droplets. Eur Phys J E 37 (2), 8.

Wiener, N., 1964. Generalized Harmonic Analysis and Tauberian Theorems. M.I.T. Press,Boston.

Wilkie, K., Hahnfeldt, P., 2013. Mathematical models of immune-induced cancer dormancy and the emergence of immune evasion. Interface Focus 3 (4), 20130010.

Wioland, H., Woodhouse, F. G., Dunkel, J., Kessler, J. O., Goldstein, R. E., 2013. Confinement Stabilizes a Bacterial Suspension into a Spiral Vortex. Phys. Rev. Lett. 110 (26), 268102.

Wirtz, D., Konstantopoulos, K., Searson, P. C., 2011. The physics of cancer: the role of physical interactions and mechanical forces in metastasis. Nature Rev. Cancer 11, 512–522.

Wolff, S., Dillin, A., 2006. The trifecta of aging in caenorhabditis elegans. Exp Gerontol 41 (10), 894–903.

Wollrab, V., Thiagarajan, R., Wald, A., Kruse, K., Riveline, D., 2016. Still and rotating myosin clusters determine cytokinetic ring constriction. Nature Communications 7, 11860.

Wolynes, P., 1996. Symmetry and the energy landscapes of biomolecules. Proc. Natl. Acad. Sci. USA 93 (25), 14249–14255.

Womick, J., Moran, A., 2011. Vibronic enhancement of exciton sizes and energy transport in photosynthetic complexes. J. Phys. Chem. B 115 (6), 1347–1356.

Wong, K., Huk, A., Shadlen, M., Wang, X., 2007. Neural circuit dynamics underlying accumulation of time-varying evidence during perceptual decision making. Front Comput Neurosc 1.

Wong, K., Wang, X., 2006. A recurrent network mechanism of time integration in perceptual decisions. J Neurosci 26 (4), 1314–1328.

Worst, E., Zimmer, P., Wollrab, E., Kruse, K., Ott, A., 2016. Unbounded growth patterns of reproducing, competing polymers-similarities to biological evolution. New J Phys 18 (10).

Wright, S., 1941. Statistical genetics and evolution. Bull. Amer. Math. Soc. 48 (4), 223–246.

Wu, L. A., Segal, D., 2011. Quantum effects in thermal conduction: Nonequilibrium quantum discord and entanglement. Phys. Rev. A. 84, 012319.

Wu, S., Nazin, G., Chen, X., Qiu, X., Ho, W., 2004. Control of relative tunneling rates in single molecule bipolar electron transport. Phys. Rev. Lett. 93 (23), 236802.

Wu, W., Wang, J., 2013a. Landscape framework and global stability for stochastic reaction diffusion and general spatially extended systems with intrinsic fluctuations. J. Phys. Chem. B 117 (42), 12908–12934.

Wu, W., Wang, J., 2013b. Potential and flux field landscape theory. i. global stability and dynamics of spatially dependent non-equilibrium systems. J. Chem. Phys. 139 (12), 121920.

Wu, W., Wang, J., 2014. Potential and flux field landscape theory. ii. non-equilibrium thermodynamics of spatially inhomogeneous stochastic dynamical systems. J. Chem. Phys. 141 (10), 105104.

Wu, W., Zhang, F., Wang, J., 2018. Landscape and flux theory of turbulence. Annals of Physics 389, 63–101.

Xavier, J., 2011. Social interaction in synthetic and natural microbial communities. Mol. Syst. Biol. 7 (1), 483.

Xie, X., 2013. Enzyme kinetics, past and present. Science 342, 1457–1459.

Xing, J., 2010. Mapping between dissipative and hamiltonian systems. J Phys a-Math Theor 43 (37), 37500.

Xu, D.and Schulten, K., 1992. The Photosynthetic Bacterial Reaction Center : II. Structure, Spectroscopy and Dynamics, NATO Science Series A : Life Sciences. Plenum Press, New York.

Xu, L., Shi, H., Feng, H., Wang, J., 2012. The energy pump and the origin of the non-equilibrium flux of the dynamical systems and the networks. J. Chem. Phys. 136 (16), 165102.

Xu, L., Wang, J., 2017a. Quantifying the landscape and flux of game theory. PLoS One 13, e0201130.

Xu, L., Wang, J., 2017b. Quantifying the landscape and flux of multi-locus multi-allele evolution. J. Theo. Biol. 422, 31–49.

Xu, L., Zhang, F., Wang, E., Wang, J., 2013. The potential and flux landscape, lyapunov function and non-equilibrium thermodynamics for dynamic systems and networks with an application to signal-induced ca2+ oscillation. Nonlinearity 26 (2), R69–R84.

Xu, L., Zhang, F., Zhang, K., Wang, E., Wang, J., 2014a. The potential and flux landscape theory of ecology. PloS one 9 (1), e86746.

Xu, L., Zhang, K., Wang, J., 2014b. Exploring the mechanisms of differentiation, dedifferentiation, reprogramming and transdifferentiation. PloS one 9 (8), e105216.

Yan, H., Zhang, K., Wang, J., 2016. Physical mechanism of mind changes and tradeoffs among speed, accuracy, and energy cost in brain decision making: Landscape, flux, and path perspectives. Chin. Phys. B. 25 (7), 078702.

Yan, H., Zhao, L., Hu, L., Wang, X., Wang, E., Wang, J., 2013. Nonequilibrium landscape theory of neural networks. Proc. Natl. Acad. Sci. USA 110 (45), E4185–E4194.

Yang, Q., Ferrell, J., 2013. The cdk1-apc/c cell cycle oscillator circuit functions as a time-delayed, ultrasensitive switch. Nat Cell Biol 15 (5), 519.

Yasuda, K., Shindo, Y., Ishiwata, S., Apr. 1996. Synchronous behavior of spontaneous oscillations of sarcomeres in skeletal myofibrils under isotonic conditions. Biophys J 70 (4), 1823–1829.

Yu, C., Wang, J., 2016. A physical mechanism and global quantification of breast cancer. PloS one 11 (7), e0157422.

Yu, J., Xiao, J., Ren, X., Lao, K., Xie, X., 2006. Probing gene expression in live cells, one protein molecule at a time. Science 311 (5767), 1600–1603.

Yurtsev, E., Chao, H., Datta, M., Artemova, T., Gore, J., 2013. Bacterial cheating drives the population dynamics of cooperative antibiotic resistance plasmids molecular systems biology 9:683 (2013). Mol. Sys. Biol. 9, 683.

Zeng, Q., Wang, J., 2017. Landscape and flux of information flows. Entropy 19, 678.

Zhang, B., Wolynes, P., 2015. Topology, structures, and energy landscapes of human chromosomes. Proc. Natl. Acad. Sci.USA 112, 6062–6067.

Zhang, B., Wolynes, P. G., 2014. Stem cell differentiation as a many-body problem. P Natl Acad Sci USA 111 (28), 10185.

Zhang, F., Xu, L., Zhang, K., Wang, E., Wang, J., 2012. The potential and flux landscape theory of evolution. J. Chem. Phys. 137 (6), 065102.

Zhang, K., Sasai, M., Wang, J., 2013. Eddy current and coupled landscapes for nonadiabatic and nonequilibrium complex system dynamics. Proc. Natl. Acad. Sci. USA 110 (37), 14930–14935.

Zhang, K., Wang, J., 2017. Landscape and flux theory of non-equilibrium open economy. Physica A 482, 189–208.

Zhang, K., Wang, J., 2018. Exploring the underlying mechanisms of the xenopus laevis embryonic cell cycle. J. Phys. Chem. B 122, 5487–5499.

Zhang, Y., Tan, Y., Stormer, H., Kim, P., 2005. Experimental observation of the quantum hall effect and berry's phase in graphene. Nature 438 (7065), 201–204.

Zhang, Z., Wang, J., 2014. Curl flux, coherence, and population landscape of molecular systems: Nonequilibrium quantum steady state, energy (charge) transport, and thermodynamics. J. Chem. Phys. 140 (24), 245101.

Zhang, Z., Wang, J., 2015a. Landscape, kinetics, paths and statistics of curl flux, coherence, entanglement and energy transfer in non-equilibrium quantum systems. New J Phys 17, 043053.

Zhang, Z., Wang, J., 2015b. Shape, orientation and magnitude of the curl quantum flux, the coherence and the statistical correlations in energy transport at nonequilibrium steady state. New J Phys 17, 093021.

Zhang, Z., Wang, J., 2015c. Vibrational and coherence dynamics of molecules. Phys Chem Chem Phys 17 (37), 23754–23760.

Zhang, Z., Wang, J., 2016. Origin of long-lived quantum coherence and excitation dynamics in pigment-protein complexes. Sci. Rep. 6, 37629.

Zhang, Z. D., Fu, H. C., Wang, J., 2017. Nonequilibrium-induced enhancement of dynamical quantum coherence and entanglement of spin arrays. Phys. Rev. B. 95, 144306.

Zhao, L., Wang, J., 2016. Uncovering the mechanisms of caenorhabditis elegans ageing from global quantification of the underlying landscape. J R Soc Interface 13 (124), 20160421.

Zhou, J., Aliyu, M., Aurell, E., Huang, S., 2012. Quasi-potential landscape in complex multi-stable systems. J R Soc Interface 9 (77), 3539–3553.

Zhou, P., Li, T., 2016. Construction of the landscape for multi-stable systems: Potential landscape, quasi-potential, a-type integral and beyond. J. Chem. Phys. 144 (9), 094109.

Zhu, Z., Marcus, R., 2008. On collisional energy transfer in recombination and dissociation reactions: A wienerhopf problem and the effect of a near elastic peak. J. Chem. Phys. 129, 214106.

Zia, R., Schmittmann, B., 2007. Probability currents as principal characteristics in the statistical mechanics of non-equilibrium steady states. J Stat Mech-Theory E 7, 07012.

Ziebert, F., Aranson, I., 2013. Effects of adhesion dynamics and substrate compliance on the shape and motility of crawling cells. PLoS ONE 8 (5), e64511.

Ziebert, F., Swaminathan, S., Aranson, I., May 2012. Model for self-polarization and motility of keratocyte fragments. J R Soc Interface 9 (70), 1084–1092.

Zieske, K., Schwille, P., Jan. 2013. Reconstitution of pole-to-pole oscillations of min proteins in microengineered polydimethylsiloxane compartments. Angew. Chem. Int. Ed. Engl. 52 (1), 459–462.

Zimmermann, J., Enculescu, M., Falcke, M., 2010. Leading-edge-gel coupling in lamellipodium motion. Phys Rev E Stat Nonlin Soft Matter Phys 82 (5).

Ziv, E., Nemenman, I., Wiggins, C., 2007. Optimal signal processing in small stochastic biochemical networks. PLoS One 2 (10), e1077.

Zliobaite, I., Fortelius, M., Stenseth, N., 2017. Reconciling taxon senescence with the red queens hypothesis. Nature

552, 92–95.

Zumdieck, A., Kruse, K., Bringmann, H., Hyman, A. A., Jülicher, F., 2007. Stress generation and filament turnover during actin ring constriction. PLoS ONE 2 (1), e696.

Zusman, D. R., Scott, A. E., Yang, Z., Kirby, J., 2007. Chemosensory pathways, motility and development in myxococcus xanthus. Nature Reviews Microbiology 5 (11), 862–872.

Zwicker, D., Decker, M., Jaensch, S., Hyman, A. A., Jülicher, F., 2014. Centrosomes are autocatalytic droplets of pericentriolar material organized by centrioles. Proc. Natl. Acad. Sci. USA 111 (26), E2636–E2645.

Zwicker, D., Lubensky, D. K., ten Wolde, P. R., 2010. Robust circadian clocks from coupled protein-modification and transcription-translation cycles. Proc Natl Acad Sci U S A 107 (52), 22540–22545.

Zyczkowski, K., Horodecki, P., Sanpera, A., Lewenstein, M., 1998. Volume of the set of separable states. Phys. Rev. A 58, 883–892.